A UNITED STATES
DEPARTMENT OF
COMMERCE
PUBLICATION

NBS MONOGRAPH 119

A High-Dispersion Spectral Analysis Of the Ba II Star HD 204075 (ζ Capricorni)

U.S.
DEPARTMENT
OF
COMMERCE
National
Bureau
of
Standards

UNITED STATES DEPARTMENT OF COMMERCE Maurice H. Stans, *Secretary*
NATIONAL BUREAU OF STANDARDS Lewis M. Branscomb, *Director*

A High-Dispersion Spectral Analysis of the Ba II Star HD 204075 (ζ Capricorni)

Jack L. Tech

Institute for Basic Standards
National Bureau of Standards
Washington, D.C. 20234

U.S. National Bureau of Standards, Monograph 119

Nat. Bur. Stand. (U.S.), Monogr. 119, 174 pages (March 1971)
CODEN: NBSMA
Issued March 1971

For sale by the Superintendent of Documents, U.S. Government Printing Office, Washington, D.C. 20402
(Order by SD Catalog No. C13.44:119), Price $ 3.25

Library of Congress Catalog Card No.: 70-607151

Acknowledgments

This investigation could not have been completed without the continued guidance and encouragement of my teacher and friend, Prof. C. H. Payne-Gaposchkin. I only hope that the work adequately reflects the benefits I have derived from my frequent appeals to her experience and good counsel in matters of scientific judgment and stellar spectroscopy.

I am indebted to Prof. Leo Goldberg not only for his active interest and frequent advice throughout this investigation, but also for arousing my interest in stellar abundances and for introducing me to the theory of the curve of growth through his supervision of my earlier study of the solar chromium abundance.

I am grateful to Prof. J. L. Greenstein for suggesting the problem and for lending me the high-dispersion plates of ζ Capricorni on which the analysis is based. His hospitality at the California Institute of Technology and his instructing me in the use of the direct-intensity microphotometer are very much appreciated.

My colleagues in the spectroscopy laboratory at the National Bureau of Standards, especially Dr. Karl G. Kessler, were unstinting in their support of this work. I am greatly indebted to Dr. William C. Martin for such support, for many useful discussions, and for constructively criticizing parts of the manuscript. Charles H. Corliss has patiently endured my constant demands on his wide experience in the field of laboratory f-values. His contributions are gratefully acknowledged.

My training in the critical identification of spectral lines has been provided by Dr. Charlotte Moore-Sitterly. Her generosity in critically reading the manuscript and in helping to resolve a number of problems that arose in this work is deeply appreciated. Her great interest in the analysis of ζ Capricorni led to many fruitful discussions and to a corresponding improvement of the work.

I would like to thank Drs. A. A. Nikitin and N. P. Penkin for valuable conversations and helpful instruction during my stay in the Astronomy Department of the State University of Leningrad under the auspices of the cultural exchange program with the Soviet Union.

Many lively discussions with Drs. Gerald Newsom, Andrea Dupree, Roger Kopp, Paul Blanchard, and Frances Wright were also of great help to me.

Finally, I should like to acknowledge the careful typing of the original manuscript by Miss Judith Grabusnik and the meticulous assistance given by Mrs. Ruth Peterson in many phases of the technical clerical work.

This NBS Monograph is a partially revised and updated version of a doctoral thesis presented earlier to the Department of Astronomy at Harvard University. The work was supported in part by fellowship grants from the National Science Foundation.

Contents

	Page
Acknowledgments	III
1. Introduction	1
1.1. General remarks	1
1.2. The barium stars	2
1.3. The problem	3
2. Observational material and measurements	4
2.1. Basic data for ζ Capricorni	4
2.2. The plates	4
2.2.1. Description	4
2.2.2. Wavelength measurements	4
2.2.3. Microphotometry	5
2.3. Equivalent widths	5
2.3.1. The primary equivalent widths	5
2.3.2. Derivation of equivalent widths from the measured central depths	8
2.3.3. The treatment of weak lines	10
2.4. Comparison with other measurements	11
2.5. Estimation of the error	11
3. Line identifications and *gf*-values	18
3.1. The identification of spectral lines	18
3.1.1. General principles	18
3.1.2. Literature sources used in making line identifications	19
3.1.3. The identification of λ 4608.74	19
3.1.4. A nonsense curve of growth for tantalum (Ta I)	22
3.2. The *gf*-values	23
3.2.1. The use of *gf*-values in this study	23
3.2.2. Sources of *gf*-values	23
3.2.3. Wavelength-dependent corrections to the *gf*-values of NBS Monograph 53	24
3.2.4. Comparison of the NBS intensity estimates for neodymium with those of King (1936)	27
3.3. A relation for converting NBS intensities of unclassified lines to *gf*-values	29
4. Curve of growth analysis	31
4.1. The differential method	31
4.2. The stellar line strengths	34
4.3. Conversion of NBS *gf*-values to line strengths in ε Virginis	35
4.4. Theoretical curve of growth for ζ Capricorni	46
5. Comments on individual spectra	48
5.1. Introduction	48
5.2. The spectra	48
5.2.1. Aluminum	48
5.2.2. Barium (Ba I)	48
5.2.3 Barium (Ba II)	48
5.2.4. Cadmium	49
5.2.5. Cerium	49
5.2.6. Dysprosium	49
5.2.7. Europium	52
5.2.8. Iron (Fe I)	52
5.2.9. Lanthanum	52
5.2.10. Lithium	52
5.2.11. Magnesium	53
5.2.12. Molybdenum	53
5.2.13. Neodymium	53
5.2.14. Nickel	53
5.2.15. Oxygen	53
5.2.16. Praseodymium	53

5.2.17. Ruthenium........ 53
5.2.18. Samarium........ 54
5.2.19. Scandium........ 56
5.2.20. Silicon........ 56
5.2.21. Strontium........ 56
5.2.22. Sulfur........ 56
5.2.23. Technetium........ 56
5.2.24. Titanium (Ti II)........ 56
5.2.25. Vanadium........ 56
6. Atmospheric parameters for ζ Capricorni........ 57
6.1. The excitation temperatures........ 57
6.2. The ionization equilibrium........ 68
6.3. The Carter effect........ 68
6.4. Gas velocities in the atmosphere of ζ Capricorni........ 73
6.4.1. Thermal velocity........ 73
6.4.2. Microturbulence........ 76
6.4.3. Macroturbulence........ 77
7. The chemical composition of ζ Capricorni........ 79
7.1. The abundances........ 79
7.2. Use of ζ Capricorni as a comparison star........ 82
8. Discussion and summary........ 86
8.1. The accuracy of the abundances........ 86
8.2. Discussion........ 86
8.3. Summary........ 88
Appendix
A.1. Sample differential curves of growth........ 89
A.2. Sample absolute curves of growth........ 107
A.3. Table A, the line list arranged by wavelength........ 123
A.4. Table B, the line list arranged alphabetically by spectrum........ 146
A.5. References........ 169

List of Tables

Table	*Description*	Page
2.1.	Fundamental data for HD 204075	4
2.2.	Observational material for ζ Capricorni	4
3.1.	Sources of *gf*-values	24
3.2.	Mean ratios of original NBS intensity estimates for lines observed in each of two different exposures	26
3.3.	Comparison of NBS intensity estimates for neodymium with those of A. S. King	27
4.1.	Coefficients for the polynomials representing the normalized stellar curves of growth	35
4.2.	Conversion of NBS *gf*-values to line strengths in ϵ Virginis	35
5.1.	NBS *gf*-values for recently classified lines of Ce II	49
5.2.	NBS *gf*-values for recently classified lines of Nd II	53
5.3.	Suggested revision of Warner's Sm II identifications > 5000 Å	54
6.1.	Differential excitation temperatures of ζ Cap relative to the sun and to ϵ Vir	58
6.2.	Adopted excitation temperatures	61
6.3.	Determination of differential electron pressures for ζ Cap relative to the sun and to ϵ Vir	68
6.4.	Mean excitation potentials for Fe I lines used in the construction of the solar curve of growth shown in figure 6.10	73
6.5.	Doppler velocities derived from individual curves of growth	76
7.1.	Parameters used in the determination of relative ionization equilibria	79
7.2.	First ionization potentials and partition functions used in the calculation of ionization corrections to the relative abundances	80
7.3.	Logarithmic abundance ratios	81
7.4.	Abundances derived from NBS *gf*-values converted to line strengths in ϵ Virginis	81
7.5.	Logarithmic abundances in ζ Capricorni relative to iron	81
8.1.	Physical parameters for ζ Capricorni	88
A	The line list arranged by wavelength	123
B	The line list arranged alphabetically by spectrum	146

A High-Dispersion Spectral Analysis of the Ba II Star HD 204075 (ζ Capricorni)

Jack L. Tech

A double differential curve of growth analysis, using both the sun and ϵ Virginis (G9 II–III) as comparison stars, has been performed for the Ba II star ζ Capricorni. The observational material consists of equivalent widths, central depths, and half-widths for 1100 spectral lines measured on direct-intensity tracings of plates obtained by J. L. Greenstein at the coudé focus of the 200-in telescope. The plates cover the spectral regions 3880–4825 Å and 5100–6720 Å at reciprocal dispersions of 2.3 and 3.4 Å/mm, respectively. Line identifications given in earlier lists for barium stars have been critically re-examined. Three lines have been attributed with reasonable certainty to dysprosium, which has not previously been observed in barium stars.

The atmospheric parameters derived for ζ Cap are:

θ_{exc} :	1.13	$[P_e]_{\zeta-\odot}$:	−1.28
θ_{ion} :	0.99	$[P_e]_{\zeta-\epsilon}$:	+0.13
$\log 2\alpha$:	−2.5	$[k]_{\zeta-\odot}$:	−1.10
v_{micro} :	3.5 km/s	$[k]_{\zeta-\epsilon}$:	−0.03
v_{macro} :	5.5 km/s		

Atmospheric abundances have been derived for 37 elements. The results obtained with respect to the two comparison stars are in good agreement. The barium star exhibits essentially solar abundances for most elements lighter than germanium, but overabundances by factors of about two are indicated for carbon and lithium. With the exception of europium, all observed elements heavier than germanium are found to be overabundant in ζ Cap. Improved NBS *gf*-values, converted to the system of line strengths in ϵ Vir, have yielded exceptionally well-defined curves of growth for several rare earths. Overabundances by factors of about eight or nine have been found for the *s*-processed rare earths, as well as for dysprosium, which is generally considered to be *r*-processed. The abundances derived for the rare earths are greater by about a factor of three than those derived for the same star by Warner (Mon. Not. Roy. Astron. Soc. **129**, 263 (1965)).

Key words: Abundances of elements in stars; Ba II stars (ζ Capricorni); curve of growth; equivalent widths; identification of spectral lines; ionization in stars; oscillator strengths; temperature in stars; turbulence in stars.

1. Introduction

1.1. General Remarks

In recent years considerable importance has been attached to obtaining accurate determinations of chemical abundances in the atmospheres of stars of abnormal composition. Abnormality in this context is ordinarily defined in terms of the solar composition taken as standard. The atmospheres of the great majority of cool dwarfs like the sun are found to exhibit more or less solar abundances, which suggests that their composition is essentially that of the interstellar medium from which the stars were formed. The development of theories of stellar evolution and of the formation of chemical elements through nucleosynthesis has relied heavily upon the characteristics of stars departing from the normal (Burbidge et al., 1957; Burbidge and Burbidge, 1957; Seeger et al., 1965).

There are several widely studied classes of stars for which striking abundance anomalies have been reliably established. Extreme metal deficiencies characterize the older stars of Population II (Aller and Greenstein, 1960) and certain high-velocity stars (Koelbloed, 1967). The magnetic Ap stars separate into subgroups distinguished by different types of compositional anomalies. Among the elements most affected are Sr, Y, Zr, Cr, Fe, Mn, O, and the rare earths, especially Eu. The origin of the abnormal abundances in these stars is not well understood, but has been related to the loss of angular momentum during pre-main-sequence contraction, and to surface nuclear processes generated by strong magnetic fields (Cameron, 1967).

The CH stars (Wallerstein and Greenstein, 1964) show multiple characteristics that also appear individually in other groups of stars—high carbon abundance, metal deficiencies, and enhancement of certain rare earths. The occurrence of nuclear activity has been spectroscopically verified in the case of S-type stars, in which Merrill (1952) identified lines of technetium, whose longest-lived isotope thus far detected has a half-life of only about 200,000 years.

1.2. The Barium Stars

The barium stars form one of the most important groups of abnormal stars. They are distinguished by the unusual strength of the Ba II resonance doublet at λλ4554 and 4934 Å. These stars played a central role in the early development of theories of element synthesis (Burbidge and Burbidge, 1957). Bidelman and Keenan (1951) first recognized the Ba II stars as forming a special class and pointed out their characteristic spectroscopic features. They are giants of spectral types G and K and spectroscopically resemble stars of type S in showing extraordinarily strong lines of ionized barium and certain other heavy elements, but technetium has not yet been identified in these stars. For their spectral type, the Ba II stars also exhibit unusually strong lines of Sr II (λ4077 and λ4215) and a striking enhancement of the G band (due to CH). Miss Maury (1897) very early recognized the unusual strength of Sr II and Ba II in the star ζ Capricorni.

Intermediate-band photometry by Bond and Neff (1969) reveals a broad absorption centered near λ4000 Å in the spectra of Ba II stars. The similarity of this opacity feature to that observed in the carbon stars of type N strengthens Mrs. Gorden's (1968) argument that the barium and N-type stars are related, perhaps differing from each other only in surface temperature.

The most notable characteristic of the Ba II stars from the point of view of element formation is the great enhancement of lines in the spectra of elements such as strontium, barium, zirconium, samarium, cerium, lanthanum, neodymium, and yttrium, whose most abundant isotopes are formed predominantly by slow neutron capture (*s*-process). Garstang (1952) was the first to call attention to the great richness of lines of the singly ionized rare earths in the spectrum of ζ Capricorni. The overabundances found for these elements in the atmospheres of Ba II stars is interpreted as strong evidence that products of interior nuclear reactions have been brought up to the surface through convective mixing. The determination of accurate chemical abundances in these stars, therefore, is of great importance to the further refinement of current ideas concerning element formation.

Warner has listed the basic data for twenty known Ba II stars. In addition to the five stars reported in the original announcement by Bidelman and Keenan, fifteen other Ba II stars have been identified, chiefly by Bidelman, the Cowleys, Warner, and Wallerstein (Warner, 1965a) More recently, Bidelman identified the G8 II star ζ Cygni as also belonging to this group, but its Ba II star characteristics are comparatively mild (Chromey et al., 1969).

The small number of stars now definitely established as Ba II stars may considerably misrepresent their actual frequency and evolutionary importance. H. E. Bond, for example, has informed the writer that he has tentatively identified about 75 stars showing Ba II characteristics on his set of objective prism plates taken at the Cerro Tololo Observatory in Chile.

Several workers have studied the chemical composition of Ba II stars, the most extensive investigation being that by Warner (1965a), who has derived relative abundances for nine southern Ba II stars. The star HD 46407 was studied differentially with respect to κ Geminorum in the classic work by the Burbidges (1957). This star was also included in the work of Warner, who found smaller overabundances of the *s*-process elements than found by the Burbidges. Warner traced the discrepancy to underestimated equivalent widths in the earlier work.

Cowley (1968) derived differential abundances for HR 774 relative to the standard star π^6 Orionis that are in good agreement with those derived by Nishimura (1967) for the same star relative to ϵ Virginis. Danziger (1965), from a differential study of HD 116713 and HD 83548 relative to α Boötis, found significantly larger overabundances for the rare earths than those obtained by Warner for the same stars. Unsöld (1969) compares in detail the results of these two investigations and emphasizes how easily systematic differences in abundance determinations can result from the use of slightly different values for the general atmospheric parameters.

Chromey et al. (1969) have analyzed the mild Ba II star ζ Cygni differentially with respect to ϵ Virginis. Relatively small enhancements were found in the abundances of the *s*-processed elements. From evidence that the enhancement of heavy elements occurs earlier in the main-sequence phase of these giants, the authors conclude that the Ba II stars do not form a discrete group, but that the development of the typical Ba II star features progresses in a continuous fashion for stars evolving along this path.

1.3. The Problem

The brightest known barium star ($m_v=3.9$), ζ Capricorni (HD 204075), is also the earliest in spectral type, listed as G5–Ba2 in the scheme proposed by Warner (1965a). This star was studied qualitatively by Garstang (1952) and Greenstein (1954) and quantitatively for the first time by Warner.

Because of the great interest in the barium stars, it was considered of some importance to make an accurate study of one of them at higher dispersions than heretofore available. This would eliminate some of the problems caused by the severe blending that results from their spectroscopic richness in lines of the singly ionized rare earths. J. L. Greenstein emphasized to the writer the importance of such an analysis of ζ Capricorni and generously offered the loan of high-dispersion spectrograms of this star taken by him at the coudé focus of the 200-in Palomar telescope.

It is the purpose of the present investigation to derive the physical parameters and chemical composition of the atmosphere of ζ Capricorni from this observational material.

2. Observational Material and Measurements

2.1. Basic Data for ζ Capricorni

The basic data for HD 204075, as given in the comprehensive summary of Ba II stars by Warner (1965a), are listed in table 2.1. The UBV photometric indices obtained after applying his estimated correction for CN absorption to the original values are given in parentheses.

TABLE 2.1. *Fundamental data for HD 204075*

α (1950):	$21^h\ 23.8^m$	Rad. Vel. (km/s):	+3.3
δ (1950):	−22° 38′	V:	3.74
m_v:	3.9	B−V:	1.00 (0.92)
Spectral type:	G5–Ba2	U−B:	0.57 (0.67)
μ (″/yr):	0.024		

As with all the known barium stars, the proper motion and velocity of HD 204075 indicate that it belongs to intermediate Population I. Bidelman assigned ζ Cap to luminosity class II–III, but Warner concluded that it is closer to II. From a study of H and K emission, Warner also derived an absolute magnitude of $M_v = -3.4$ for the star and estimated its mass to be about $4M_\odot$.

TABLE 2.2. *Observational material for ζ Capricorni*

Plate number	Date	Emulsion (Eastman Kodak)	Wavelength range	Reciprocal dispersion
			(Å)	*(Å/mm)*
Pc 3469	9–19–57	IIa–O	3700–5100	9.2
Pb 4768a	9–23–59	I–N	6430–8150	6.8
Pb 4768b	9–23–59	I–N	8150–8800	6.8
Pc 4775	9–24–59	I–N	6250–8650	13.6
Pc 6001	6–30–61	IIa–O	3700–5100	9.2
Pa 5994a	6–29–61	IIa–O	3880–4300	2.3
Pa 5994b	6–29–61	IIa–O	4300–4825	2.3
Pa 6000a	6–30–61	103a–F	5100–5850	3.4
Pa 6000b	6–30–61	103a–D	5850–6720	3.4

2.2. The Plates

2.2.1. Description

As stated earlier, the high-dispersion spectrograms of ζ Capricorni were obtained by J. L. Greenstein at the coudé focus of the 200-in telescope. A summary of the plates is given in table 2.2.

2.2.2. Wavelength Measurements

All the spectrograms were measured by hand on the comparators in the Spectroscopy Section of the National Bureau of Standards. A total of 10,000 individual settings were made on lines in the spectral range 3880 to 8700 Å. This figure includes at least two measurements for each line. A versatile computer program, CWLT5, was written to aid in the reduction of these measurements. This double-precision program for polynomial fitting by least squares has also been used repeatedly in other phases of reduction and analysis of the data. As applied to wavelength determinations in stellar spectra, input to CWLT5 consists of three sets of data cards: (1) comparator readings and standard wavelengths for lines measured in the iron comparison spectra on each plate; (2) comparator settings and laboratory wavelengths for a few identified lines in the stellar exposure; and (3) comparator settings for the remaining, unidentified, lines in the stellar exposure. For sets (1) and (2), the program finds the least-squares polynomial of lowest degree that adequately fits the input wavelengths as a function of the corresponding comparator readings. When CWLT5 is used as a general $X-Y$ fitting program, set (2) is omitted. The *difference* in the wavelengths calculated by the two polynomials for the lines in set (2) represents the Doppler shift of the stellar spectrum. The mean Doppler shift is calculated and used in the determination of the "laboratory" wavelength for each stellar line of set (3) after its "observed" wavelength has been calculated by the polynomial representing the iron comparison spectrum. In the calculation of the polynomials and the value of the correction for radial velocity, the program automatically rejects any lines that depart by more than a prescribed number of standard deviations from the mean fit, presumably as a result of poor measurement or incorrect identification. As a final check, the program plots the residuals of the fit for a visual appraisal of the quality of the measurements.

A comprehensive line list including identifications and estimated visual intensities for ζ Cap is being prepared from this material. The final list will probably contain about 3500 discrete absorption lines. A need has long been felt for such a reference description for Ba II stars (Cowley, 1968). In the present investigation the complete line list was used only to resolve questions associated with the identification of those lines for which equivalent widths were measured.

2.2.3. Microphotometry

Only plates Pc 3469, Pa 5994a–b, and Pa 6000a–b are of photometric quality. The calibration plates were obtained by Greenstein with a wedge-slit grating spectrograph. Using the wedge-silt calibrations, the writer made tracings of these five plates by use of the direct-intensity recording microphotometer at the California Institute of Technology. Several important regions of the plates were traced twice under different conditions. The scale of the charts ranges from 0.6 to 1.2 angstroms per inch. A sample region, reduced, is shown in figure 5.3.

2.3. Equivalent Widths

2.3.1. The Primary Equivalent Widths

Line crowding and strong absorption by the CH and CN molecules make it extremely difficult to find unblended lines or to locate the continuum level shortward of 4300 Å. Except for a few lines considered of great importance to the analysis, therefore, the measurements have been restricted to the spectral regions 4316 to 4819 Å and 5102 to 6710 Å. For brevity, spectral lines measured in these two regions are distinguished by referring to them as "blue" and "red" lines, respectively. Although the gap between 4800 and 5100 Å is covered by the charts for plate Pc 3469, this region has been omitted from the abundance analysis because of the considerably lower dispersion.

The charts were divided into 32 sections corresponding to the several pieces of broken plate Pa 6000a and to the natural stopping points in the tracing process caused by (1) occasional checking of the clear plate reading, (2) changes in the photographic calibration of the plate, and (3) periodic adjustment of the vertical scale of the tracings. For each succeeding section, the plate was backed up to provide a region of overlap with the preceding section.

The continuum was located on the tracings by drawing a straight line through the high points found in regions about 20 Å wide. A comparison of these tracings with those in the Utrecht Solar Atlas (Minnaert et al., 1940) helped to identify windows in the spectrum. The continuum level for each chart section was drawn independently without reference to that of the preceding section for the overlap region. Special care was also given to avoid the underestimation of continuum level that Unsöld (1955) warns is a common mistake of beginners.

After the continuum had been established over the entire chart coverage, the lines to be measured were selected by marking a point in their profiles to serve as a starting point for the tracer point of the planimeter. Lines whose profiles were incomplete because of partial blending with adjacent lines were sketched in at this time. Only lines that had the appearance of being relatively unblended were selected.

A few good lines in each chart section were then identified to serve as the standards required by the computer program CWLT5 in calculating wavelengths for the remaining lines.

The equivalent widths of all selected lines were measured by use of a precision polar planimeter in the usual way. Equivalent widths measured by planimeter are called the "primary" widths to distinguish them from equivalent widths derived later from measurement of central depth alone. The data recorded for each line included (a) an indication Q of the quality of the line on a scale from 1 (poor) to 5 (excellent); (b) the width in millimeters of the profile at half-intensity; (c) the positions of the continuum and vertex of the line on the chart scale; and (d) the chart section number. The judgment of quality index was based on the extent to which the profile had to be completed by hand, on the suspicion of any blending, and on the general appearance of the line.

The information for each line was punched on cards as input to a special adaptation of CWLT5 whose output for each line consisted of the wavelength (in Å), half-width (in mÅ), central depth (R_c), and equivalent width (in both mÅ and the form log W/λ). At the same time, the ratio of measured equivalent width to that estimated by the product of half-width and central depth was calculated for each line. Every line for which this

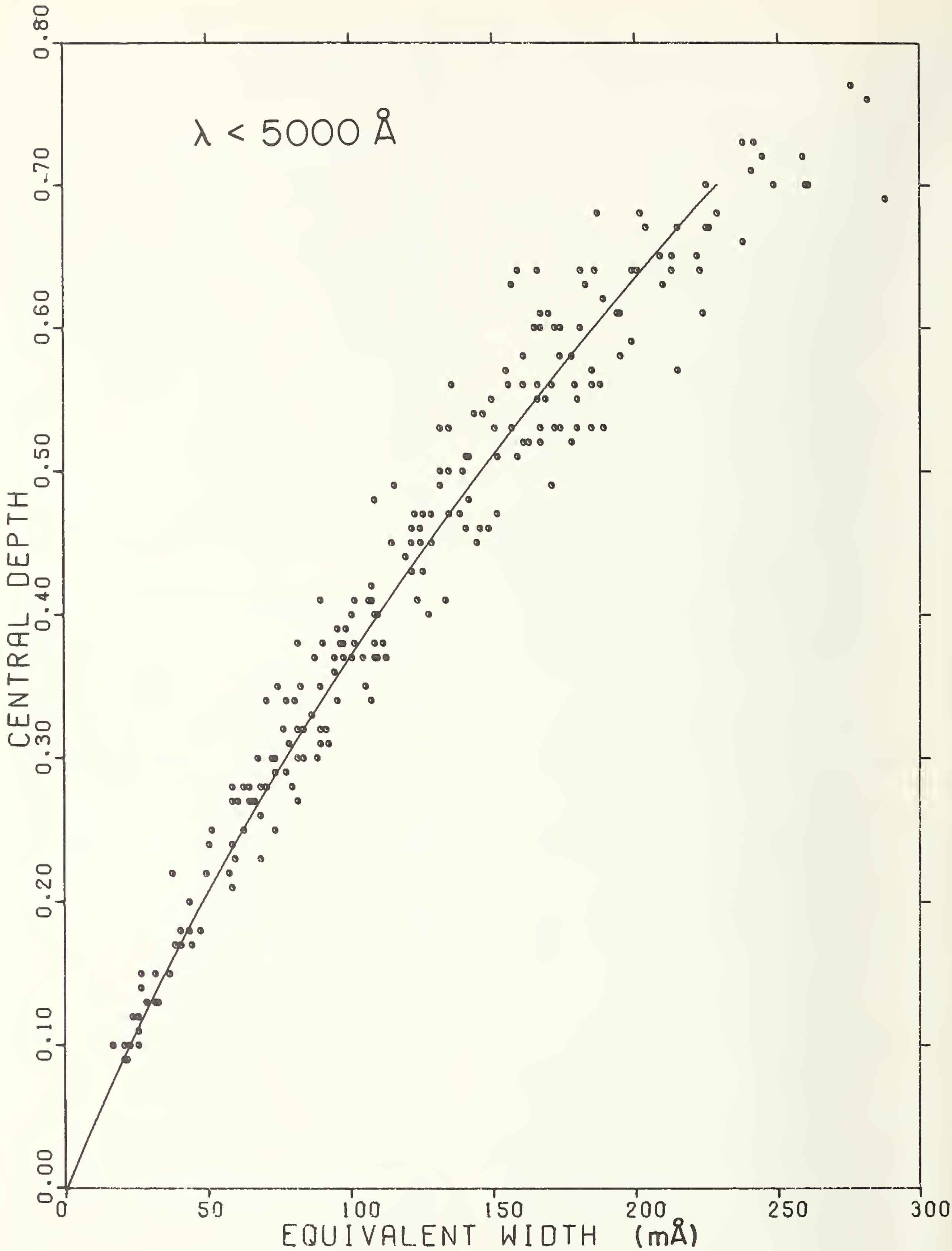

FIGURE 2.1. *Relation between equivalent width and central depth for lines with wavelengths shorter than 5000 Å.*

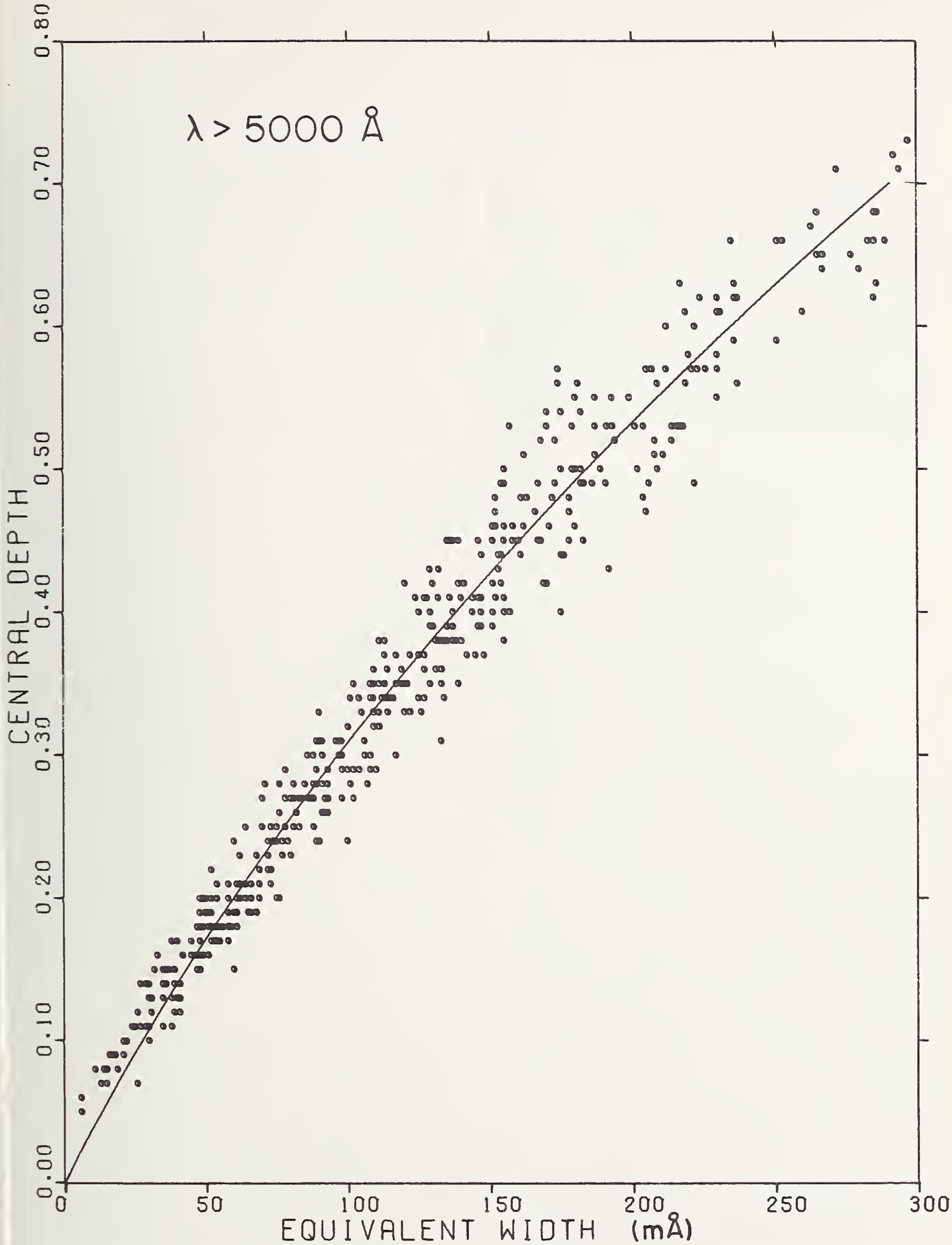

FIGURE 2.2. *Relation between equivalent width and central depth for lines with wavelengths longer than 5000 Å.*

ratio departed greatly from unity was remeasured as a check. A number of errors in recording or keypunching were thus detected. The residuals of a polynomial fit of measured half-widths to the central depths were also plotted. All lines falling far off the mean curve were later checked for the possibility of being broad blends.

To avoid any bias in line selection, only at this stage of the reduction was a comparison made with the line identification lists as described in section 3.1.2. About 50 of the measured lines turned out to be unusable because it was not possible to identify their chemical origin. Also, more than 100 lines had to be rejected as being unresolved strong blends. Table A in the Appendix lists the measured quantities and relevant spectroscopic information for some 1100 lines used in the remainder of this investigation.

2.3.2. Derivation of Equivalent Widths From the Measured Central Depths

After obtaining a reliable set of primary equivalent widths directly from the line profiles by counting squares or, as here, by planimetry, it is possible to augment the number of measurements by abbreviated methods and to improve the primary set by statistical smoothing. Both of these applications have been made to the measurements in ζ Cap.

The method most frequently used for augmenting a primary set of measurements is to establish a functional relationship, often involving the wavelength, between the central depths and equivalent widths of the small primary set to enable the derivation of equivalent widths for additional lines simply by a measurement of central depth alone. Values derived in this way are here called the "R_c-widths." The technique has been used with success (Warner, 1964b) in investigations involving a large number of lines in several stars, where practicality rules out direct planimetry for all lines of interest.

An improved set of equivalent widths can be obtained (Wright, 1948) by averaging the primary widths themselves with the semi-independent values returned through the functional relationship derived between central depth and equivalent width. For certain types of blending the R_c-width of a line may even be a better approximation to the actual line absorption than is the directly measured width. This would be the case, for example, when two lines forming a blend are close enough in wavelength to produce a broadened profile, but not so close as to have completely additive central depths. Thus, an average with the R_c-width can partially eliminate from the original planimeter values any contribution caused by unrecognized blending.

The primary equivalent widths (W) measured in ζ Cap are plotted against central depth (R_c) in figure 2.1 for wavelengths shorter than 5000 Å and in figure 2.2 for those longer than 5000 Å. The relation between the two quantities is well-defined in each of the two regions. The mean curves drawn were derived from a least squares parabolic fit to the points and were constrained to make $W = 0$ when $R_c = 0$. The equations of these curves are

$$\text{blue region: } W = 205\, R_c + 173\, R_c^2 \text{ (mÅ)} \tag{2.1}$$

$$\text{red region: } W = 252\, R_c + 233\, R_c^2 \text{ (mÅ).} \tag{2.2}$$

A slight improvement in the standard deviation of the fit can be made by plotting W/λ, rather than W, against R_c. More importantly, however, it is found that by choosing W/λ the fitted equations describe so nearly the same curve that no significant compromise in the analytical representation is made if both spectral regions are treated together. The combined plot, omitting lines of quality $Q < 2$ for $\lambda > 5000$ Å, is shown in figure 2.3. The mean curve drawn in this figure represents adequately the distribution of points for $R_c \leq 0.60$. Its equation, with both W and λ expressed in angstroms, is

$$(W/\lambda) \times 10^7 = 400\, R_c + 460\, R_c^2. \tag{2.3}$$

For values of R_c in the range $0.10 \leq R_c \leq 0.60$, the semi-independent R_c-widths calculated by this formula have been averaged with the primary equivalent widths listed in column (10) of tables A and B. This average was used in the calculation of the quantity log (W/λ) listed in column (11) of the same tables.

The above formula has been used also to derive equivalent widths for some lines not measured by planimeter. These are distinguished from the planimeter measurements by assigning a value zero to the chart-section number given in column (13) of tables A and B. The lines in this category include (a) those whose importance was recognized only after the original planimeter measurements had been completed, and (b) lines of certain elements represented by an insufficient number of primary measurements to define an accurate curve of growth.

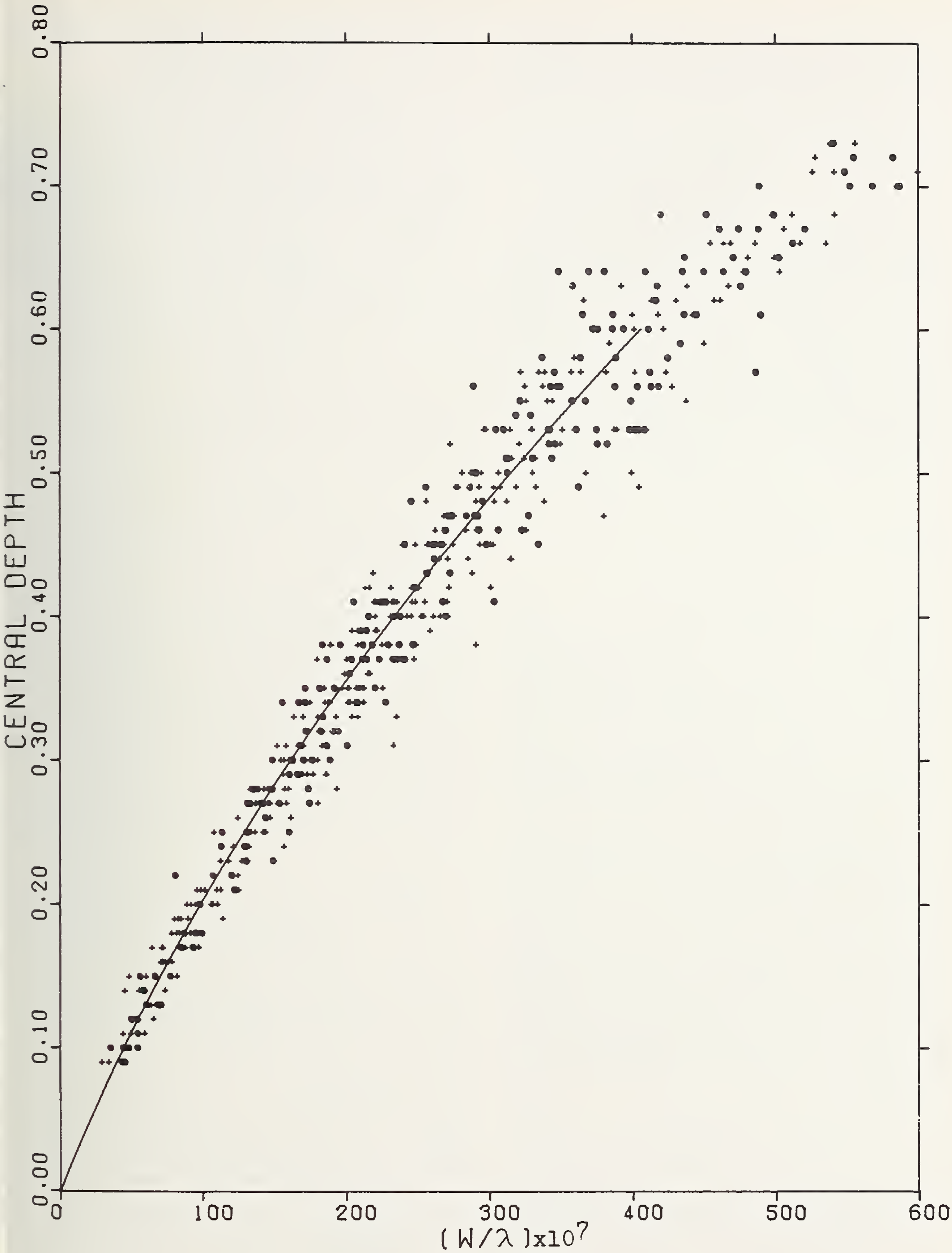

FIGURE 2.3. *Composite relation between equivalent width and central depth for lines < 5000 Å* (circles) *and > 5000 Å* (crosses).

Most of the lines in both these groups failed to have planimeter measurements because their profiles could not be confidently sketched to completion owing to blending with adjacent lines. Their relatively undisturbed central depths, however, could be measured with some assurance.

2.3.3. The Treatment of Weak Lines

Several considerations demonstrate that the primary equivalent widths of weak lines ($R_c < 0.15$) are too small. First, the use of these measurements in curves of growth gives a distinct curvature to the "straight-line" portion. Second, the plots in figures 2.1 and 2.2 show the weak lines falling progressively farther to the left of the mean curve as R_c decreases. Third, the primary values are significantly less than the estimate derived by the "triangle-rule," whose reliability is well established in the literature. One formulation of this rule describes the equivalent width of faint lines in terms of the product between central depth and half-width, namely,

$$W = AR_cH. \tag{2.4}$$

For faint lines, the half-width can be regarded as a constant equal to the limiting Doppler half-width (as $R_c \rightarrow 0$) found below. The factor A partially offsets the inadequacy of the triangular representation of line profiles and is best determined empirically. The need for this factor is caused in part by the inability of a triangle to account for the absorption in the wings of the line and for the rounding at the line center.

As determined from the measurements, the factor A is a function of central depth. Its value ranges from about 1.00 for $R_c < 0.20$ to about 1.10 for $R_c = 0.70$. The average value over the entire range is $A = 1.06$. It is not surprising that A is found to depend upon R_c, because the quadratic expression found above relating R_c and W can be regarded as just an extension of the triangle rule to include stronger lines. For faint lines the quadratic term can be neglected and the formula for the R_c-width reduces to

$$\text{(at 5000 Å)} \qquad W = 0.20\, R_c \qquad \text{(in Å)}. \tag{2.5}$$

The coefficient of R_c in this expression agrees well with the limiting Doppler half-widths found below.

It is noteworthy that our empirically derived factor, $A = 1.06$, corresponds to that predictable for weak lines of Gaussian profile. In the usual notation (Unsöld, 1955), for pure Doppler broadening the equivalent width of a line,

$$\frac{W_\lambda}{2\Delta\lambda_D} = \int_0^\infty \{1 - \exp(-\tau_0 e^{-v^2})\} dv, \tag{2.6}$$

can be approximated for small optical thicknesses by

$$\frac{W_\lambda}{2\Delta\lambda_D} = \frac{\sqrt{\pi}}{2}\tau_0. \tag{2.7}$$

But from the definition of optical depth,

$$I_\lambda = I_\lambda^\circ e^{-\tau_\lambda} \sim I_\lambda^\circ(1 - \tau_\lambda) \tag{2.8}$$

or

$$\tau_0 \sim \frac{I^\circ - I_\lambda}{I^\circ} \equiv R_c. \tag{2.9}$$

Hence, using eq (6.19), we obtain

$$W_\lambda = \frac{\sqrt{\pi}}{2\sqrt{\ln 2}} HR_c = 1.064\, HR_c. \tag{2.10}$$

As further justification for preferring the triangle values, it is well known that the measurement of small areas by planimeter is inherently imprecise. Also, a check of the tracings reveals a consistent underestimation of the limiting half-width when filling in incomplete profiles for faint lines. For weak lines having $R_c < 0.15$, therefore, the planimeter measurements have not been averaged with the R_c-widths, which alone were used in the calculation of log (W/λ).

To summarize, the equivalent widths used in the calculation of log (W/λ) are derived in four different ways:

	Type	*Value taken for* W
(a)	$R_c > 0.60$	the original planimeter measurement
(b)	$0.15 \leq R_c \leq 0.60$	the unweighted average of the planimeter measurement and the R_c-width
(c)	$R_c < 0.15$	the R_c-width.
and		
(d)	lines not measured by planimeter	the R_c-width.

2.4. Comparison With Other Measurements

The only other measurements in the spectrum of ζ Cap with which a comparison can be made are those published in Warner's study of southern barium stars (1964b). His measurements were made at reciprocal dispersions of 6.8 Å/mm (blue) and 13.6 Å/mm (red). The equivalent widths measured in the present investigation are plotted against those of Warner in figure 2.4 for $\lambda < 5000$ Å and in figure 2.5 for $\lambda > 5000$ Å. The comparison is restricted to those lines judged in the present work to be least blended. In the blue spectral region the agreement between the two sets of measurements is quite good, at least for these selected lines. There is no evidence of any serious systematic difference over the range of equivalent widths shown, but the present measurements tend to be smaller than Warner's for weak lines. This may be related to his choice of the wing factor $A = 1.15$, which is perhaps too large for weak lines, or to a difference in the choice of continuum.

In the red region, the two sets of measurements are in poor agreement. Besides the sizable scatter revealed in figure 2.5, there is also a striking systematic difference. On the average, Warner's values are almost 50 percent larger, but individual lines have equivalent widths differing by factors up to 6. Apart from this single comparison, there is no evidence for a systematic discrepancy in the present data between the two spectral regions. For example, such a systematic error should give rise to a relative displacement of lines from the two wavelength regions when plotted together on a curve of growth. Warner was led to treat the two spectral regions independently because of such an apparent discrepancy in their absolute scales.

A test has been made to ascertain whether an important residual difference in scale between the two regions exists in the present data. Figure 2.6 shows an absolute curve of growth for iron based on the *gf*-values tabulated by Corliss and Tech (1968). A differential curve of growth based on solar line strengths obtained by reading the Utrecht equivalent widths into the Pierce-Aller solar curve of growth is shown in figure 2.7. In neither figure is an appreciable systematic difference observed between measurements made in the blue (< 5000 Å, circles) and the red (> 5000 Å, crosses) spectral regions. In these curves of growth the values used for the absolute and differential excitation temperatures are those derived in section 6.1. Warner's measurements for the same lines are similarly plotted in figures 2.8 and 2.9. On the basis of the scatter shown in these plots, it appears that the origin of the unsatisfactory comparison in figure 2.5 lies chiefly in Warner's data.

It is difficult to attribute the disagreement in equivalent widths solely to the well-known dispersion effect (Unsöld, 1955), which predicts that larger equivalent widths will be derived from lower-dispersion plates because of greater chances for unrecognized blending. This may explain the more widely scattered points in the plots, but it is improbable that nearly *all* lines would be affected in this manner, especially in the red where the line crowding is not great. A difference in calibration and in the choice of continuum must play a large role.

2.5. Estimation of the Error

It is virtually impossible in a work of this kind to formulate a quantitative measure of error. The greatest error is probably associated with the location of the continuum, but for reasons cited later, the choice of continuum level is considered to have been physically realistic. Duplicate measurements of the equivalent widths for lines in the regions of overlap between sections of the tracings were usually in agreement to within about 5 percent and rarely differed by more than 10 percent. Values of the central depths and half-widths for these lines always agreed to within 0.02 in R_c and about 15 percent in *HW*. The individual measurements for these lines were averaged and assigned the section number of the longer wavelength section to the line. The half-widths of the lines could not be measured to better than 1 mm, which corresponds to about 30 mÅ on the average chart scale.

Averaging the primary equivalent widths with the semi-independent values calculated from the relation established above between R_c and W has probably improved the measurements. From the consistency of the data, the small scatter of many of the curves of growth, and the comparison made in section 2.4 with the independent measurements by Warner, an estimate can be made with some assurance that the probable error in the values tabulated here for log (W/λ) is less than about ± 0.10.

398-978 O - 71 - 2

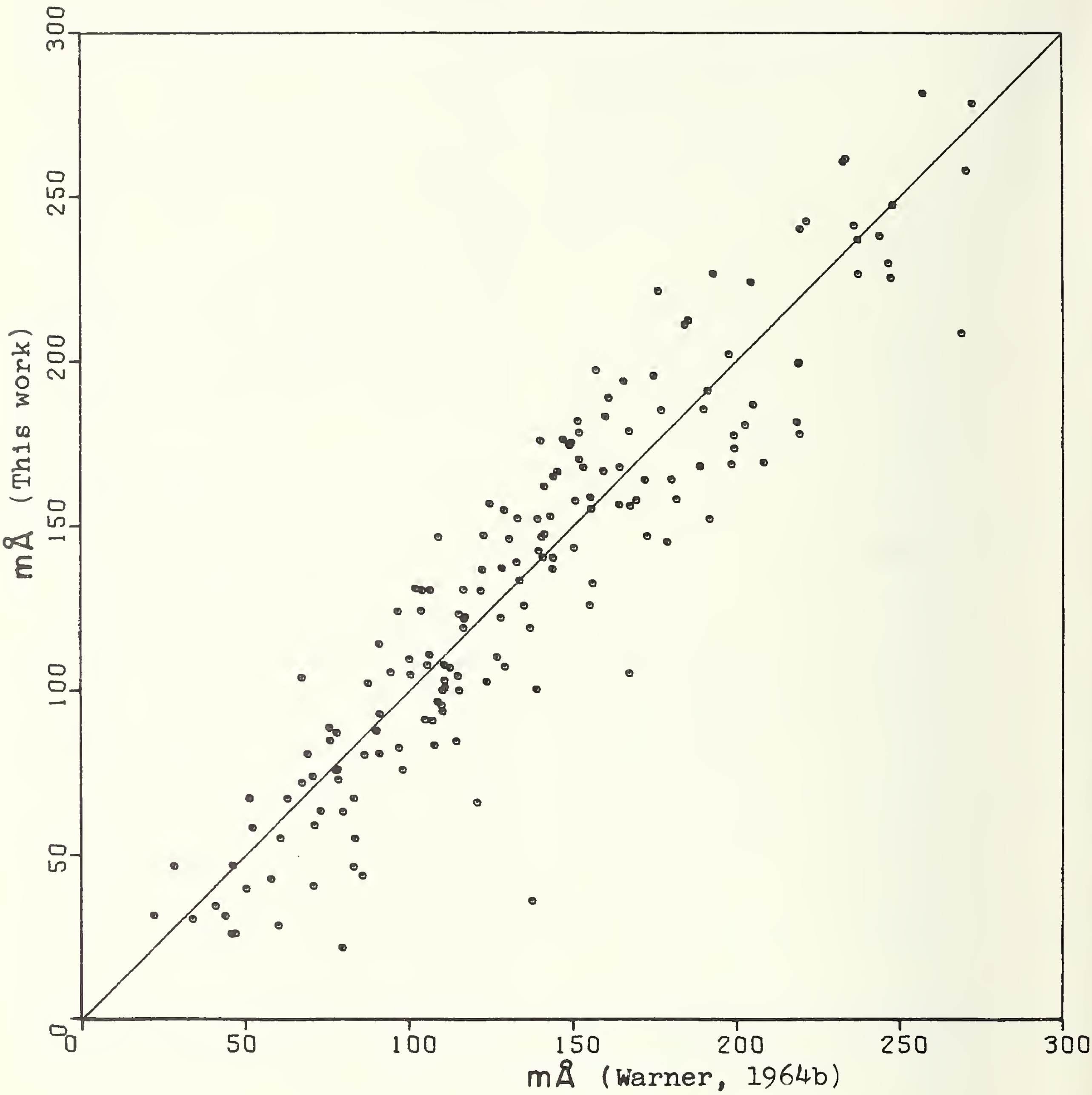

FIGURE 2.4. *Comparison of equivalent widths measured in this investigation with those of Warner for lines with wavelengths < 5000 Å.*

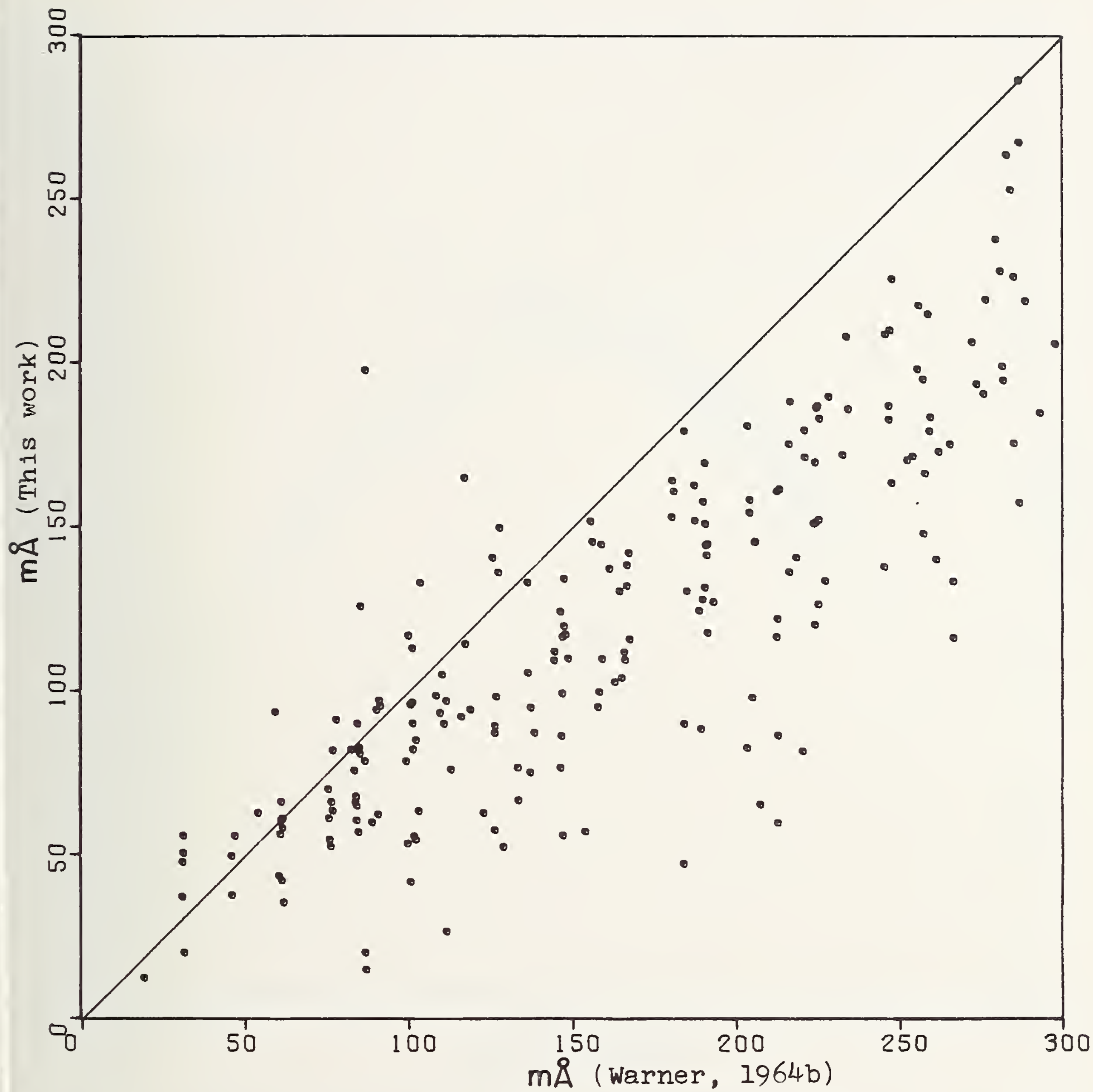

FIGURE 2.5. *Comparison of equivalent widths measured in this investigation with those of Warner for lines with wavelengths > 5000 Å.*

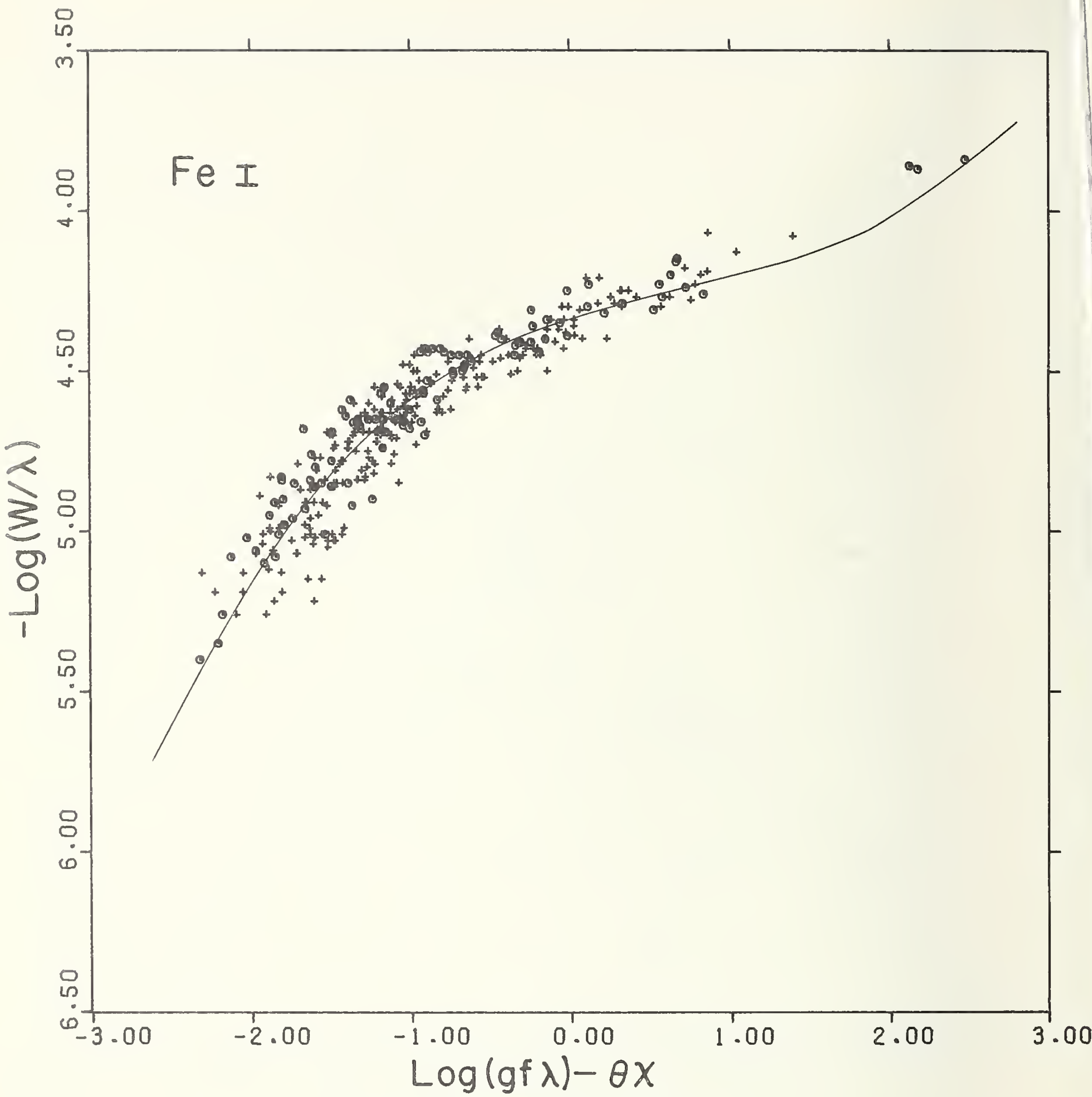

FIGURE 2.6. *Absolute curve of growth for iron.*

Circles, $\lambda < 5000$ Å; *crosses*, $\lambda > 5000$ Å.

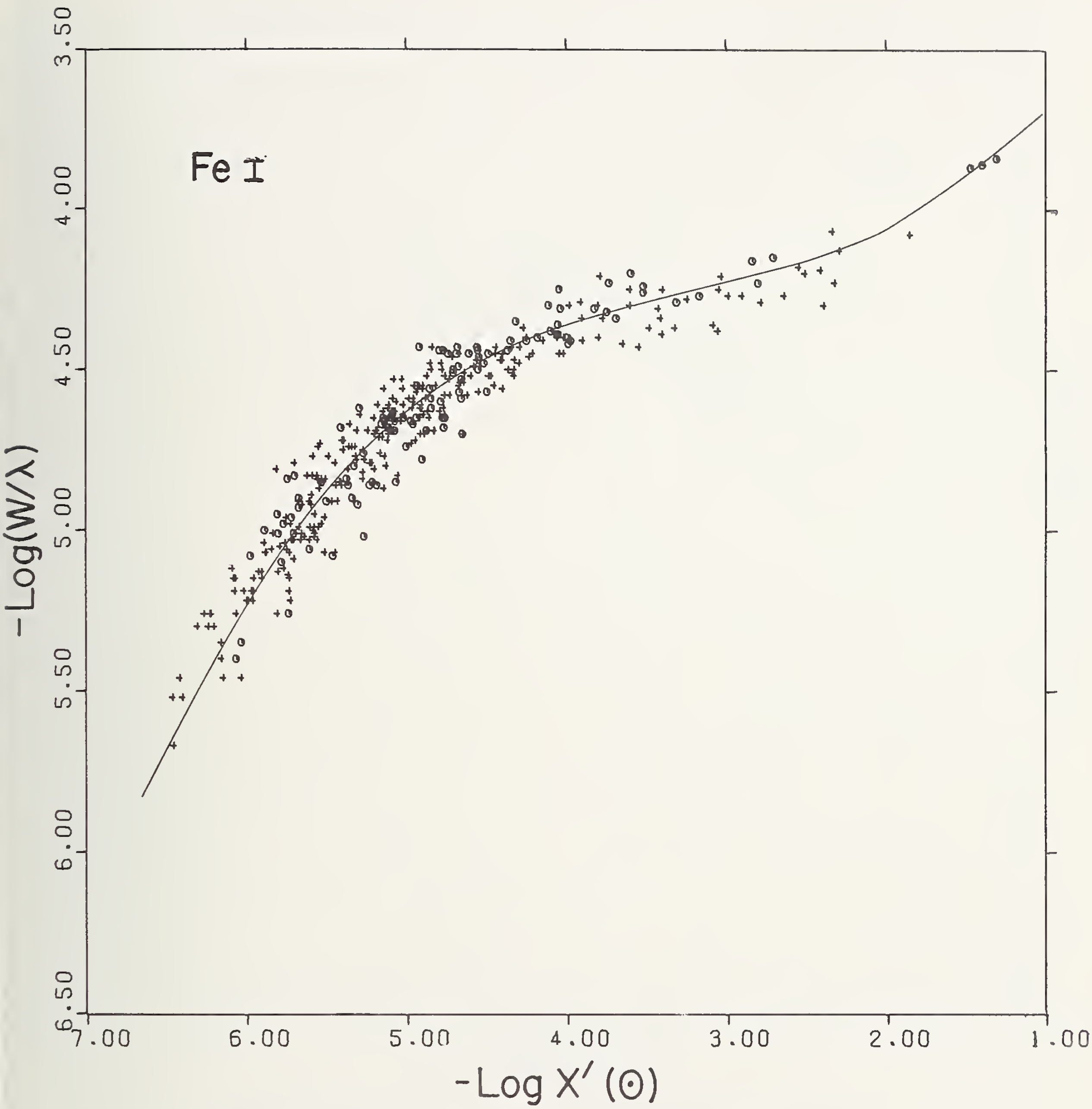

FIGURE 2.7. *Differential curve of growth for iron based on solar line strengths.*
Circles, $\lambda < 5000$ Å; *crosses*, $\lambda > 5000$ Å.

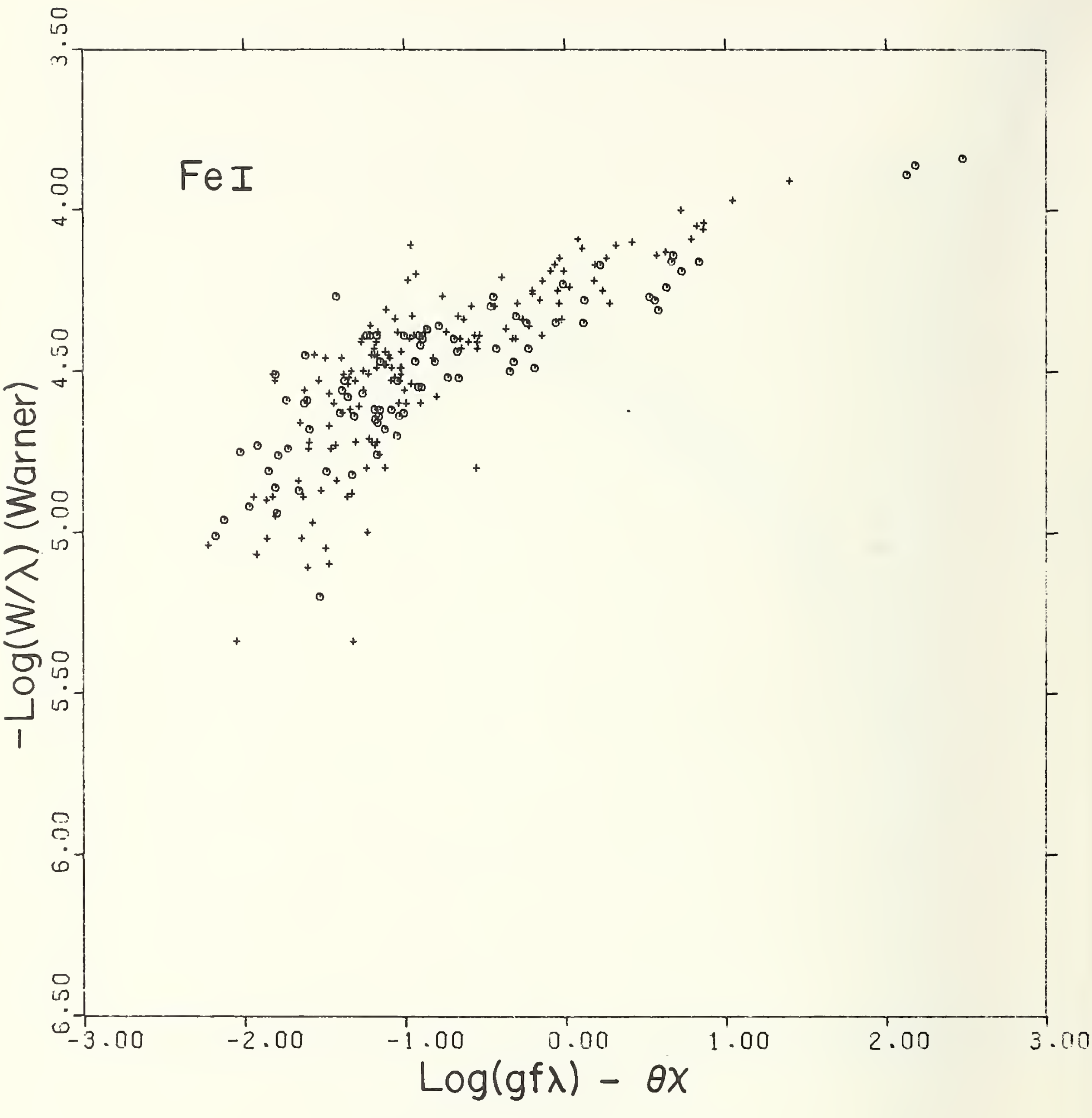

FIGURE 2.8. *Absolute curve of growth for iron.*

The equivalent widths used in this plot are taken from the work by Warner (1964b). *Circles*, λ < 5000 Å; *crosses*, λ > 5000 Å.

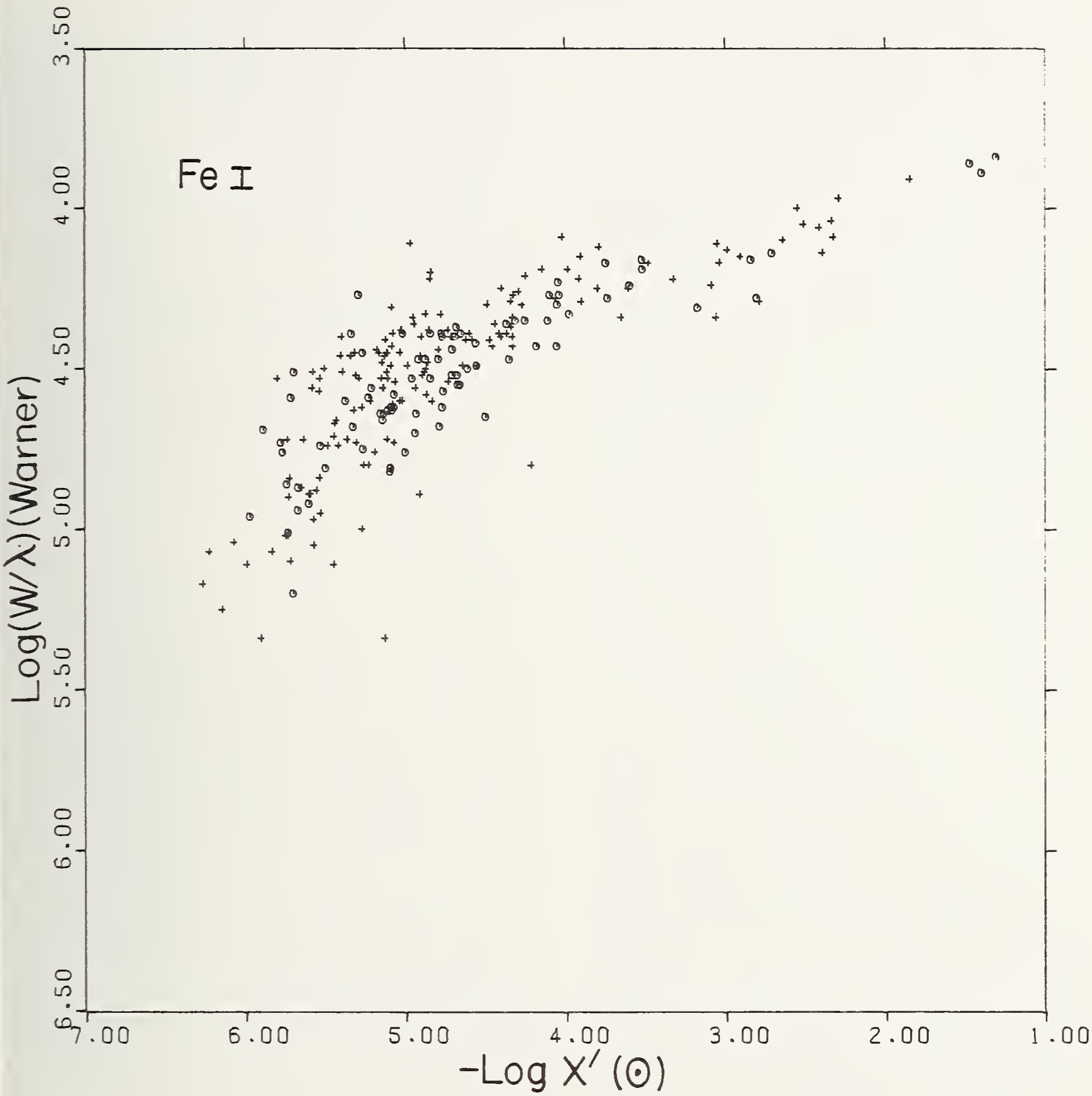

FIGURE 2.9. *Differential curve of growth for iron using solar line strengths.*

The equivalent widths are taken from the work by Warner (1964b). *Circles*, $\lambda < 5000$ Å; *crosses*, $\lambda > 5000$ Å.

3. Line Identifications and *gf*-Values

3.1. The Identification of Spectral Lines

3.1.1. General Principles

No matter how sophisticated the method used, it is evident that a determination of chemical abundances in a stellar atmosphere can have physical meaning only to the extent that the spectral lines used in the determination are correctly identified as to chemical origin and spectrum. The importance of meaningful line identifications is being stressed throughout this study.

The starting point in any attempt at line identification is always the observed wavelength, adjusted to compensate for the Doppler shift and other physical effects, if necessary. Wavelength coincidence within a realistic tolerance between the observed line and the postulated identification must be common to *all* identifications but in itself does not provide a conclusive criterion as to the origin of the observed line. This point is often overlooked. The observed stellar wavelength serves basically as *negative* evidence that simplifies the problem by allowing the investigator to exclude from consideration the vast majority of spectral lines known from independent laboratory investigations.

A stellar spectrum generally represents a superposition of a variety of atomic and molecular spectra. In the present analysis of ζ Capricorni, for example, the spectra of about 50 different chemical species have been identified. If reference cannot be made to a list of accurate line identifications for a similar star, the intelligent approach to unraveling such a superposition of spectra is to compare element by element the laboratory wavelengths of pertinent spectra with the stellar line list. This procedure is less susceptible to errors than the alternative one of comparing the stellar lines individually with some comprehensive collection of laboratory wavelengths of many spectra. The latter approach has led to many errors of line identification in the literature. To be reliably productive, this approach requires that a sound enough familiarity with the stellar spectrum and the physical conditions in the star has already been acquired to permit a refined judgment. It may also be useful in the identification of those lines remaining unexplained after the first method has been exhausted.

In comparing a simple laboratory spectrum with that of the star, it is necessary first to account for the behavior of the resonance lines. If the resonance lines, or the strongest and most sensitive lines in the range of the stellar observations, are unaccountably absent in the stellar spectrum, any coincidences between stellar lines and the subordinate lines of the laboratory spectrum are very likely to be accidental. In the case of very complex spectra, whose total intensity is distributed among many lines of similar intensities, the probability of accidental coincidence of a stellar and laboratory wavelength becomes quite large, and other factors must be considered along with wavelength agreement. These include the excitation potentials, the results of comparisons of relative line intensities in the stellar and laboratory spectra, the wavelength tolerance, the line shape, and the general quality of the line lists.

Implicit in the eventual judgment about the chemical origin of a given absorption feature in a stellar spectrum is the reservation, of course, that the judgment may be incorrect. Even when the investigator is confronted with conflicting evidence, however, the probability can ordinarily be considered high that the assigned origin of a line is actually the physically correct one provided the *weight* of the evidence favors it. In certain cases, as in the identification of $H\alpha$ in many stars, this probability of correctness can approach unity. In other cases, when the evidence is ambiguous or when the line for some reason cannot be compared for consistency with a group of related lines, for example with other lines of the same multiplet, the process of line identification will often be quite subjective. For weaker lines especially, there always remains the possibility that the stellar line may be a blend.

Under such circumstances, the acceptance of abundance results from any atmospheric analysis must necessarily be cautious. For example, an independent study of sources of data now available for hafnium spectra raises some doubt as to whether hafnium contributes significantly to any of the lines assigned to Hf II and used to derive a hafnium abundance in a recent analysis of ϵ Virginis. The same is true in the case of Cd I and, to a lesser extent, of Gd II, Pr II, and some other spectra in that work. It is admitted, however, that some other observer might be able to marshal evidence in persuasive support of those identifications. The purpose of this argument is only to stress the important point that the reliability of derived chemical abundances can never be greater than the reliability of the line identifications, and that errors in this phase of the analysis severely compete in magnitude with other sources of error. This is especially true when the number of stellar lines observed for a given chemical species is small. The point is well illustrated in connection with the later discussion of ruthenium in ζ Cap.

3.1.2. Literature Sources Used in Making Line Identifications

In the main, only two important sources have been used to assist in the identification of spectral lines observed in ζ Capricorni. These are the Second Revision of the Rowland Table (Nat. Bur. Stand. (U.S.), Monogr. 61, 1966) and the Tables of Spectral Line Intensities (Nat. Bur. Stand. (U.S.), Monogr. 32, 1961). The first of these is probably the most useful single reference for line identifications in stars near spectral type G. The authoritative solar identifications contained in that work document the results of critical evaluations by C. E. Moore and others and are appropriately conservative. The severe deficiency of the solar spectrum in lines of the rare earths, however, represents a crucial limitation to the application of the Rowland Table to line identifications in barium stars, where the enhancement of lines of certain rare earths is a feature that helps to define the class. In this respect, the NBS Intensity Tables, currently one of the best sources for wavelengths in the first and second spectra of the rare earths, offer a most useful and necessary supplement to the Rowland Table. The Intensity Tables are correspondingly deficient in lines of the lighter elements and the iron group, but in the case of only one rare earth spectrum (Ce II) does it appear that the spectrum of ζ Cap has *exceeded* the sensitivity limit of those tables.

The usefulness of NBS Monograph 32 in analyzing a stellar spectrum is significantly increased by the inclusion of line classifications and of relative intensities on a fairly uniform scale. Since the arc temperature to which these intensity measurements correspond is 5100 K, the stated relative intensities (at least over limited spectral ranges and within a single spectrum) serve as a rough guide to those observed in the spectra of stars having reciprocal excitation temperatures ($5040/T_{\mathrm{exc}}$) near the typical value $\theta^*_{\mathrm{exc}}=1.00$. If the stellar temperature departs appreciably from this value, a rough mental conversion of the intensities can be made by paying attention to the excitation potential of the line. This feature was an enormous aid in the treatment of the rare earths in the barium star ($\theta_{\mathrm{exc}}=1.13$). It often provided the only additional evidence required beyond simple wavelength coincidence to confirm a line identification or to recognize a blend. It is possible that too much reliance has been placed on these intensities, but their general utility in this respect has been amply proven.

In general, the intensity estimates included in most laboratory analyses of atomic spectra must be used with great caution in making identifications in stellar spectra. The rough intensity estimates listed in the MIT Wavelength Tables (Harrison et al., 1939), for example, are not homogeneous and can be very misleading. The best criterion for relative intensity comparisons is to be had from laboratory estimates by a single experienced observer, such as those contained in the many contributions by A. S. King or the NBS Intensity Tables.

Several other references used extensively in making line identifications in ζ Cap include the Revised Multiplet Table (Nat. Bur. Stand. (U.S.), Tech. Note 36, 1959), the line lists for ϵ Virginis by Cayrel and Cayrel (1963) and for barium stars by Warner (1964b), the MIT Wavelength Tables, individual papers in the literature, and some unpublished laboratory line lists.

3.1.3. The Identification of λ 4608.74

The identification of a line measured at 4608.74 Å on the tracings of ζ Cap has been selected as an illustration of the procedure. The line is well isolated and is of good quality. Its observed central depth and equivalent width are $R_c = 0.20$ and $W = 47$ mÅ, respectively. The Revised Multiplet Table contains no line sufficiently near the observed wavelength to provide an identification. The Rowland Table lists an unidentified weak line ($W=4$ mÅ) at 4608.71 Å, but since the line observed in ζ Cap is ten times stronger, the coincidence in wavelength is tentatively assumed to be fortuitous. Experience with other lines has shown generally closer agreement in equivalent widths between corresponding unidentifiable features in ζ Cap and the sun. The only possibility found in NBS Monograph 32 is a Mo I line with intensity 2.5 at 4608.71 Å having a low excitation potential of 2.50 eV. This identifica-

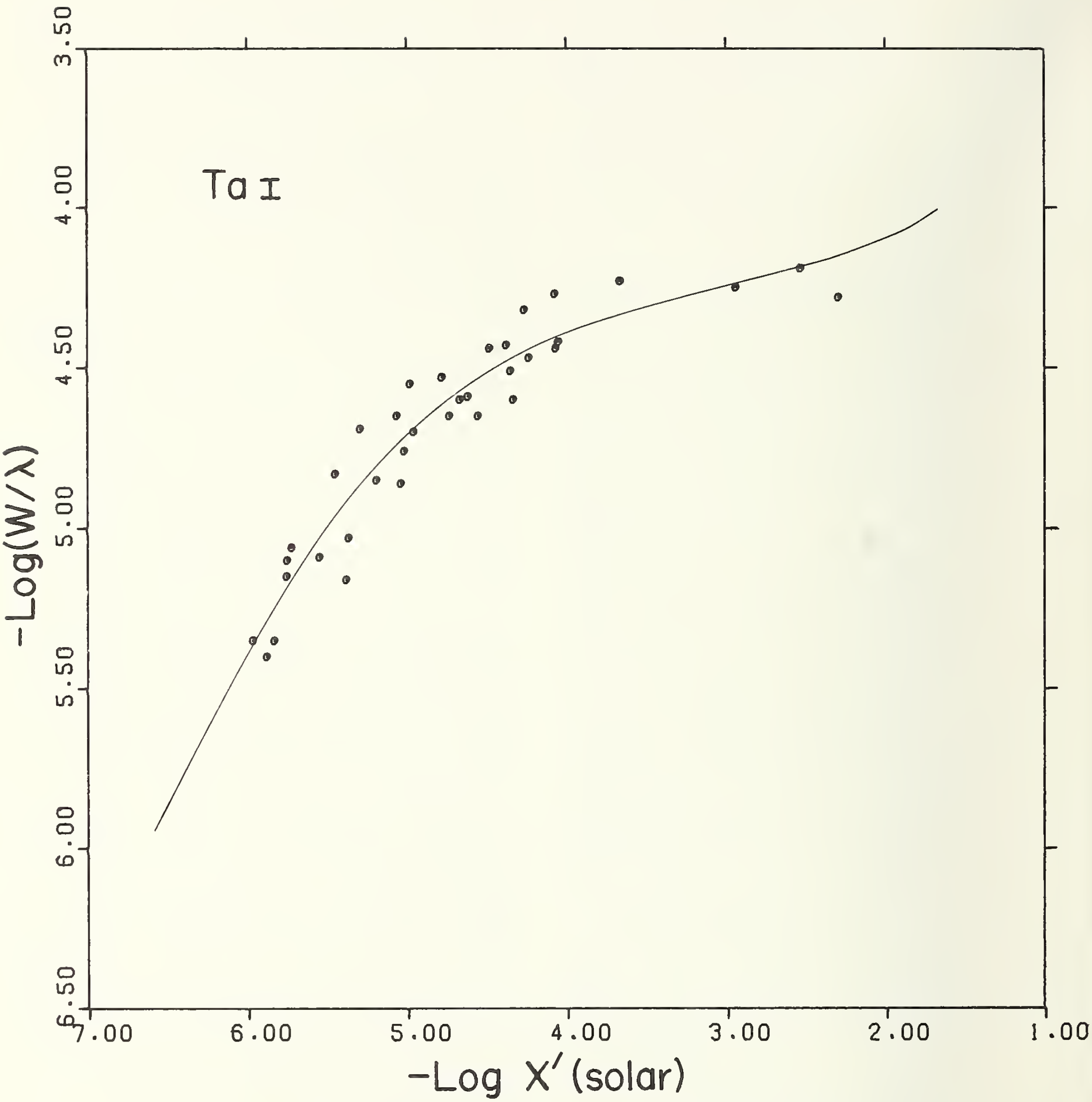

FIGURE 3.1. *A nonsense differential curve of growth for "tantalum" in ζ Capricorni.*

As explained in the text, the lines used actually belong to ten different spectra but approximately coincide in wavelength with known Ta I lines. Note the reasonable fit of these points to the theoretical curve of growth adopted for the star. This plot should be compared with that of figure 3.2.

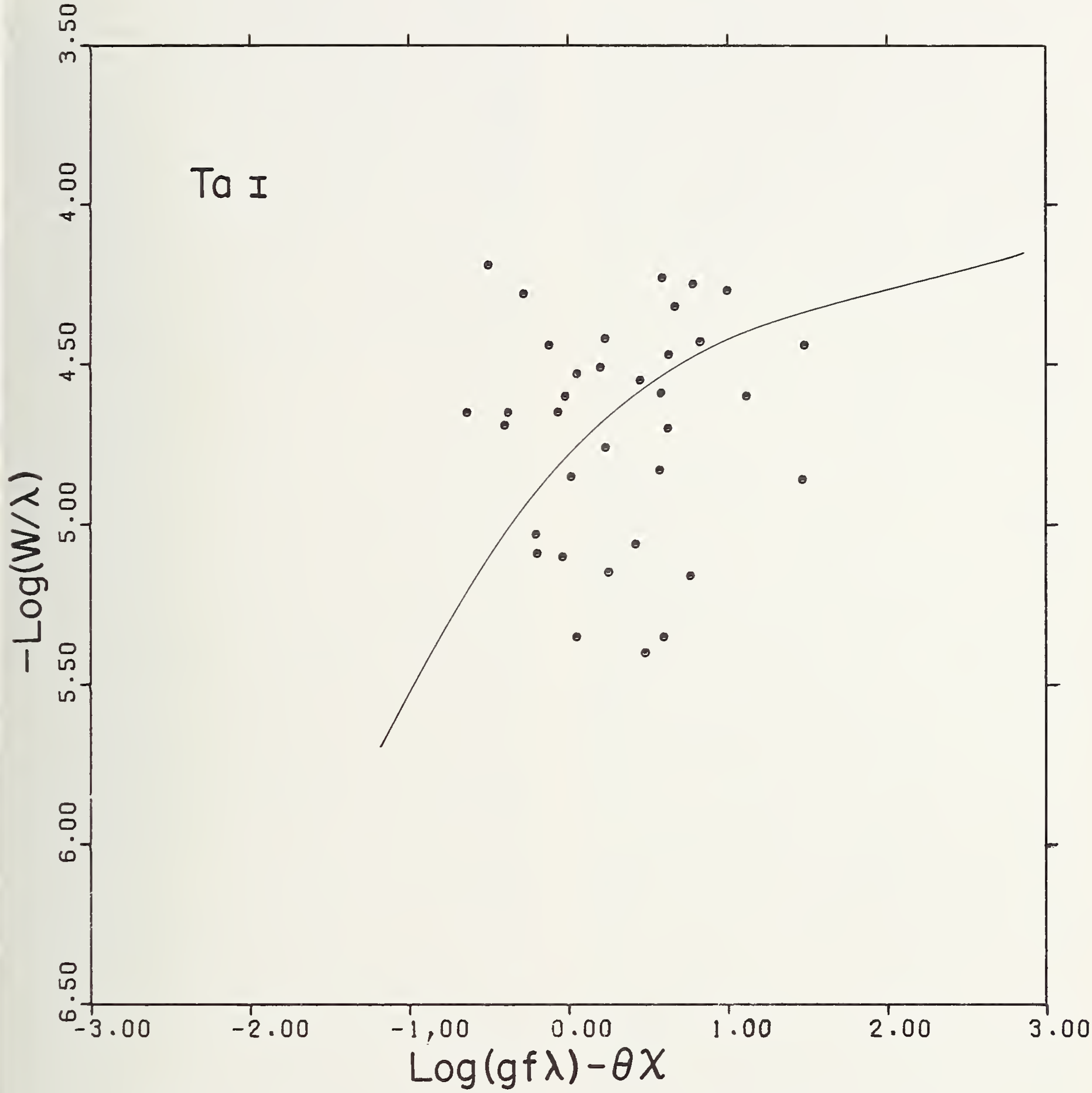

FIGURE 3.2. *An absolute curve of growth constructed by use of the same "tantalum" lines as in figure 3.1.*

The *gf*-values are taken from the work of Corliss and Bozman (1962). The scatter caused by bad line identifications is considerably more pronounced than in the differential curve of growth.

tion for the line is given in Warner's list for ζ Cap, but a rough check for intensity consistency casts doubt upon its correctness. The strongest lines of Mo I near this wavelength in Monograph 32 are masked in ζ Cap by lines of different chemical origin, but the line at 4621.38 Å with intensity 8 provides a good test, because its excitation potential (2.28 eV) is comparable with that of the line under discussion. On the basis of the relative laboratory intensities its central depth would be expected to be about 0.40, but no line absorption is present at that wavelength on the tracings. Several other nearby Mo I lines to be expected on the assumption of the above identification are also absent. The identification of the observed stellar line as Mo I must, therefore, be rejected.

Unless such a line for some reason were considered of strategic importance, the expenditure of additional effort to identify it would probably not be justifiable, except as an example.

An examination of this wavelength region on the tracings of η Pegasi (G2 II–III) suggests that the line might belong to the spectrum of one of the rare earths enhanced in ζ Cap. The line is not present in η Peg, even though the spectra of the two stars apart from these rare earths are quite similar. The MIT Tables, listing a cerium line of unknown ionization stage (I or II) at 4608.75 Å, offers some support for this conclusion, but the absence of this line from NBS Monograph 32 raises serious doubt. The strength of the observed stellar line would definitely require it to be above the sensitivity threshold of the cerium list in that work. An appeal to the unpublished cerium lists of Martin and Corliss, and of Albertson, confirms the Ce II identification, however, and the contradictory evidence of Monograph 32 is resolved by a check of the original spectrograms used for that work—the line is present with intensity 4 on those plates, but was accidentally omitted from the measurements. Finally, from the list of Ce II energy levels provided by Goldschmidt (1968) the classification of the line has been determined, and a *gf*-value calculated for it. The identification as Ce II appears to be correct, and the line has been included in the curve of growth for Ce II.

3.1.4. A Nonsense Curve of Growth for Tantalum (Ta I)

A forceful demonstration that even random line identifications can lead to apparently reasonable results is provided by the following example, which illustrates, also, one of the major hazards in applying the method of differential analysis to stellar atmospheres.

A nonsense curve of growth has been constructed for tantalum in ζ Cap by selecting from the final list of observed lines all those that approximately correspond in wavelength to known tantalum lines (Ta I). The coincidences in wavelength are fortuitous, and the observed lines are properly attributed to *ten* different spectra in table A. In associating these lines with tantalum, general intensity considerations were also taken into account in the sense that wavelength coincidences with very weak Ta I lines were disregarded. Differential excitation corrections depending on the actual tantalum excitation potentials were made in the usual way to solar line strengths. The latter were obtained by reading the Utrecht equivalent widths for the corresponding solar lines at those "tantalum" wavelengths into the Pierce-Aller curve of growth. It is emphasized again that these are *not* tantalum lines, either in the sun or in the barium star. But the resultant differential curve of growth, shown in figure 3.1, has little scatter and appears to be quite well established. By fitting to the points the theoretical curve adopted later for ζ Cap, one might conclude that the tantalum abundance in the barium star differs very little from that in the sun. The predicted shift for equal abundances with respect to hydrogen in the two objects is 0.75. The observed horizontal shift of the observed curve to the theoretical one is 0.69.

The curve of growth for the same lines, constructed by using the *gf*-values given for Ta I in NBS Monograph 53, is shown in figure 3.2. A comparison of the two curves leaves little doubt that the differential abundance derived above for "tantalum" has no physical meaning.

It is a well-known observation, commonly attributed to poor laboratory *f*-values, that curves of growth constructed by use of stellar line strengths tend to show less scatter than those constructed by use of laboratory oscillator strengths. In view of the above curves for "tantalum," this result is not entirely surprising. In fact, several of the differential curves of growth constructed here for ζ Cap show noticeably *more* scatter than do the corresponding absolute curves. Misidentified lines will ordinarily not stand out in differential curves of growth because the differential curves of many spectroscopically conspicuous elements fall quite close on the horizontal axis if the excitation temperatures and relative chemical abundances in the two objects are nearly the same. The more prominent scatter of misidentified lines on absolute curves of growth is caused partly by the greater involvement of (a) the absolute abundances of the individual elements in the star, (b) the relative partition functions of the elements, and (c) the excitation potentials of the individual lines plotted, the latter being virtually suppressed in a differential analysis because of the commonly small differential excitation temperatures. This is clearly shown by table 7.3, giving the predicted horizontal shifts of differential curves of growth for equal chemical abundances in the barium and comparison stars studied here. For example, the predicted shifts for the neutral elements in the iron group are essentially identical, as are the shifts for all the singly ionized atoms. Some elements having ionization potentials significantly different from the average depart from this rule—neutral zinc, for example.

For equal abundances, then, the differential curves of many elements will actually coincide within the error of observation, as can be seen by superimposing the sample curves of growth shown in section A.1 of the Appendix. In such circumstances, the correctness of the line identifications becomes almost irrelevant to the appearance of the empirical curves of growth, as demonstrated above for tantalum. It is a great weakness of the differential method that mistakes in spectral line identifications are often inconspicuous.

A good example in this connection is offered by the work of Cowley (1968), who examined point by point all those lines that showed a wide scatter from the absolute (but not the differential) curve of growth that he constructed for Fe I in the Ba II star HR 774. He demonstrated that in nearly every case the dominant contributor to the line had very likely not been properly chosen.

This discussion argues strongly that even in a differential analysis the use of relative or absolute *gf*-values is very desirable whenever possible, if only as an additional check on the line identifications. Such recourse undermines one of the important advantages often cited for the differential method, namely its independence from laboratory *f*-values, but its many other advantages remain intact and persuasive.

3.2. The *gf*-Values

3.2.1. The Use of *gf*-Values in This Study

As explained in section 3.1.4, the use of absolute *gf*-values in this differential study has been confined for the most part to the resolution of questions connected with spectral line identifications and to the recognition of blends. But in certain instances *gf*-values have been used also as a means to improve abundances determined from inadequately populated differential curves of growth. For several spectra, in particular those of the rare earths, the total number of good lines observed in the barium star greatly exceeds the number in common with the line lists of the comparison stars. Only two of the 61 lines of neodymium measured in ζ Cap appear also in the list for ϵ Virginis, for example. The situation with respect to the sun is somewhat more favorable, but the rare earth lines used in the analysis are generally quite weak in the solar spectrum because of the differences in opacity, electron pressure, and chemical abundance. The difficulty in accurately measuring such weak solar lines greatly increases the scatter in the differential curves of growth for these elements with respect to the sun.

Under such circumstances, more reliable differential abundances can be obtained by a suitable conversion of the available *gf*-values to the system of line strengths in the comparison star. The details of this conversion are given in section 4.3. This procedure obviously permits a better utilization of the experimental material. A similar approach was used by Wallerstein and Greenstein (1964) in their differential study of two CH stars with respect to ϵ Virginis. With the exception of Nd II, however, the present results for the conversion of several spectra to the system of ϵ Vir do not agree entirely with those obtained by Wallerstein and Greenstein. This discrepancy has been discussed privately with Wallerstein, but joint efforts to pinpoint its origin were not successful.

3.2.2. Sources of *gf*-Values

The *gf*-values used in this investigation are listed in column (7) of the main table A; they were taken from the sources given in table 3.1. In the few cases (except Fe II) where *gf*-values for a single spectrum were taken from more than one tabulation, a comparison of values in common showed the data to be very nearly on the same scale, and no corrections for scale were applied. The small corrections suggested by Warner (1967) to the *gf*-values for Sc II and Ti II given by Corliss and Bozman (1962) are, however, included. For Fe II, a correction $+0.75 \pm 0.18$ (std. dev.) was required to bring the values of log (gf λ) of Groth (1961) onto the same scale as those of Warner (1967). This correction was derived from 53 good lines common to both tabulations. No significant dependence on wavelength or line intensity was noted.

TABLE 3.1. *Sources of* gf-*values*

Sp.	Ref.	Sp.	Ref.	Sp.	Ref.
Al I	[1]	Ge I	[4]	Sc I	[4]
Ba I	[2]	La II	[4]	Sc II	[4]
Ba II	[2]	Li I	[1]	Si I	[3, 9]
C I	[1]	Mg I	[3]	Si II	[3]
Ca I	[3]	Mn I	[4]	Sm II	[4]
Ce II	[4]	Mo I	[4]	Sr I	[8, 4]
Co I	[4]	Na I	[3]	Ti I	[4]
Cr I	[4]	Nb I	[4]	Ti II	[4, 10, 11]
Cr II	[10, 11, 12]	Nd II	[4]	V I	[4]
Cu I	[5]	Ni I	[7]	W I	[4]
Dy II	[4]	O I	[1]	Y I	[4]
Eu II	[4]	Pb I	[4]	Y II	[4]
Fe I	[6]	Pr II	[4]	Zn I	[4]
Fe II	[11, 12]	Ru I	[4]	Zr I	[4]
Gd II	[4]	S I	[3]	Zr II	[4]

References

[1] Wiese, W. L., Smith, M. W., and Glennon, B. M., Atomic Transition Probabilities, Vol. I, Nat. Bur. Stand. (U.S.), Nat. Stand. Ref. Data Ser., 4 (1966).
[2] Miles, B. M., and Wiese, W. L., Nat. Bur. Stand. (U.S.), Tech. Note. 474 (1969).
[3] Wiese, W. L., Smith, M. W., and Glennon, B. M., Atomic Transition Probabilities, Vol. II, Nat. Bur. Stand. (U.S.), Nat. Stand. Ref. Data Ser., 22 (1969).
[4] Corliss, C. H., and Bozman, W. R., Nat. Bur. Stand. (U.S.), Monogr. 53 (1962).
[5] Kock, M., and Richter, J., Z. Astrophys. **69**, 180 (1968).
[6] Corliss, C. H., and Tech, J. L., Nat. Bur. Stand. (U.S.), Monogr. 108 (1968).
[7] Corliss, C. H., J. Res. Nat. Bur. Stand. (U.S.), **69A** (Phys. and Chem.), 87 (1965).
[8] Eberhagen, A., Z. Phys. **143**, 392 (1955).
[9] Miller, M. H., and Bengston, R. D., Astrophys. J. **156**, 393 (1969).
[10] Yamashita, Y., Publ. Domin. Astrophys. Obs. **12**, 455 (1967).
[11] Warner, B., Mem. Roy. Astron. Soc. **70**, 165 (1967).
[12] Groth, H. G., Z. Astrophys. **51**, 231 (1961).

3.2.3. Wavelength-Dependent Corrections to the *gf*-Values of NBS Monograph 53

It has been necessary to make wavelength-dependent corrections to the gf-values for some spectra given in the compilation by Corliss and Bozman (1962). Despite a number of well-known shortcomings, this work remains the only source of experimental gf-values for many spectra. As pointed out in the discussion of samarium in section 5.2.18 and as shown in figure 3.3, a horizontal shift between the blue and the red lines appeared in the absolute curve of growth constructed for Sm II in ζ Cap. The possible causes of such a systematic discrepancy are many and complex. The observed shift may yet be attributable to the identifications or to the measured equivalent widths, but it appeared important to start by examining the gf-values themselves. A possible cause for the observed discrepancy emerged.

The gf-values given by Corliss and Bozman in NBS Monograph 53 are based on relative emission intensities measured for 39,000 spectral lines of 70 elements by Meggers, Corliss, and Scribner (Nat. Bur. Stand. (U.S.), Monogr. 32, 1961). C. H. Corliss has generously put at the disposal of the author the original record books containing these intensity estimates. The intensities represent visual estimates on spectrograms exposed to an arc fired between copper electrodes diluted with 0.1 atomic percent of the element under investigation. They were calibrated against the simultaneously exposed copper lines and are claimed to be on a uniform scale. Because of the spectrograph design and the varying sensititivity of the photographic emulsions used, it was necessary to make five different sets of exposures in order to cover the wavelength region from 2000 to 9000 Å. The breaks, or overlap regions, between the various exposures occur on the average at 2800, 3800, 4800, and 6800 Å. In reducing the measurements, duplicate intensity estimates for lines observed on both exposures in the regions of overlap were simply averaged, but an examination of the original data reveals in some cases a systematic, not a random, variation between the two sets of spectrograms. These systematic effects are probably related to a variability in the burning of the arc and in the vaporization of the elements from the copper electrodes from one exposure to the next. In any case, it would seem more appropriate to correct for these systematic variations not by averaging the overlap regions but by adjusting the different sets of exposures either to the intensity scale of an arbitrarily selected one or to some average scale.

In table 3.2 the intensity ratios found between exposures for a number of spectra of immediate interest in this investigation are tabulated. Only the overlap regions at 4800 and 6800 Å are important for this study. No difference was found between the calculated intensity ratios for the first and second spectra of the elements considered. In some cases, however, the ratio appears to be dependent upon the line intensity. For example, the ratio for lanthanum

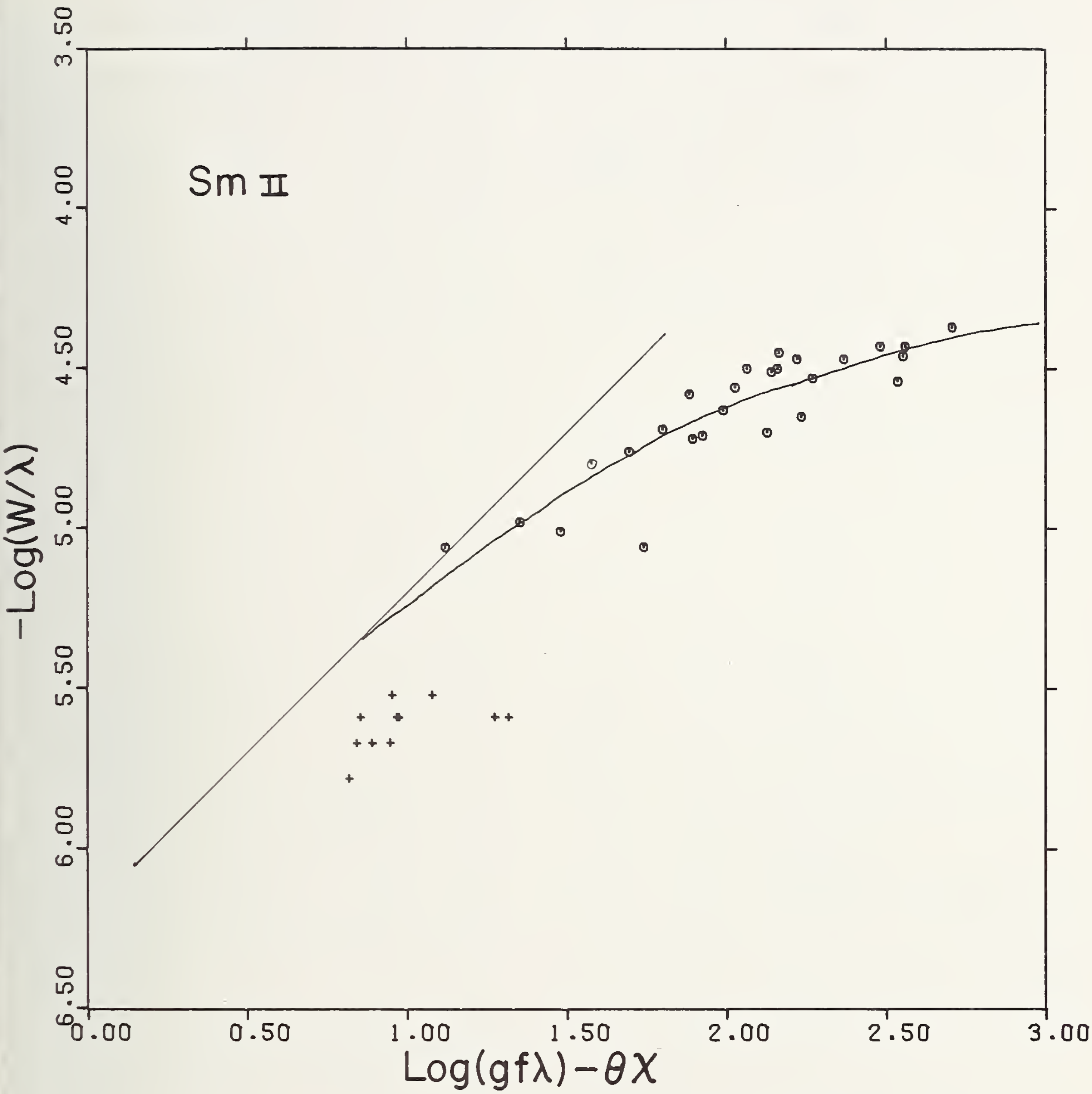

FIGURE 3.3. *Absolute curve of growth for* Sm II *in ζ Capricorni.*

As explained in the text, a systematic error in the *gf*-values of Corliss and Bozman is believed to contribute to the systematic horizontal shift between lines with wavelengths greater than 5000 Å (*crosses*) and less than 5000 Å (*circles*).

TABLE 3.2. *Mean ratios of original NBS intensity estimates for lines observed in each of two different exposures*

Element	Range of overlap	No. of lines	Intensity ratio	Standard deviation	Intensity range	Intensity dependence	Correction to log $(gf\lambda)$
	(Å)						
Ce	4680–4931	72	1.79	0.40	1–28	Y	−0.18
	6612–7000	37	1.74	.45	0.3–6	N	−.42
Co	4663–4843	9	2.83	.61	0.6–4	N	(−.30)
	6678–6873	4	1.64	.27	0.4–2	N	(−.50)
Cr	4646–4923	24	0.98	.25	3–100	Y	.00
	6661–6979	5	1.34	.33	1–2.5	N	
Dy	4698–4894	18	1.50	.30	3–19	N	−.15
	6639–6930	24	1.16	.19	0.6–22	N	−.21
Eu	4840–4912	4	1.00	.27	5–12	N	.00
	6645–6915	13	2.74	.45	0.6–100	N	−.40
Gd	4728–4894	34	0.97	.14	2–45	N	.00
	6568–6887	28	1.44	.20	0.7–8	N	−.15
La	4602–4861	40	0.81	.17	2–60	Y	+.12
	6650–6959	11	1.20	.18	1–13	N	+.04
Mn	4701–4845	10	1.15	.14	2–90	N	−.05
	6942–6943	1	3.00		0.4–0.4		
Mo	4595–4869	44	0.60	.14	1.6–90	Y	+.30
	6650–6992	32	2.18	.78	0.2–7	Y	−.13
Nd	4670–4945	71	1.88	.45	1.2–26	N	−.30
	6650–6907	28	1.83	.31	0.8–5	N	−.56
Ni	4714–4919	8	0.66	.16	1.8–12	N	(+.18)
	6643–6915	4	2.34	.89	0.5–1.6	N	
Pr	4687–4785	16	0.75	.12	5–30	N	
	4785–4926	25	1.70	.39	1.2–13	Y	
	6595–7021	19	1.67	.45	0.6–7	Y	
Sc	4670–4910	18	1.41	.31	2.5–110	Y	−.15
	6737–6836	5	1.10	.09	3.5–7	N	.00
Sm	4674–4930	53	1.98	.29	1.4–65	N	−.30
	6569–6910	42	1.11	.23	1.4–22	N	−.35
Ti	4722–4886	27	1.10	.20	1.6–40	Y	−.05
	6575–6944	13	1.46	.20	1–8	N	−.20
V	4670–4905	33	0.92	.19	1.4–50	N	.00
	6605–6871	12	1.33	.31	0.5–5	Y	.00
Zr	4627–4894	39	1.02	.17	2–200	Y	.00
	6678–6855	17	1.31	.25	0.6–9	N	−.10

at the 4800 Å break varies from about 1.0 at $I=2$ to 0.6 at $I=60$. Also, the ratio found for praseodymium changes abruptly from less than 1.0 to greater than 1.0 in the middle of the 4800 Å overlap region. A thorough analysis of these additional complexities is beyond the scope of this investigation, but is being pursued in connection with the revision of NBS Monograph 32 now in progress by C. H. Corliss and the writer.

The successive columns of table 3.2 give the relevant chemical element, the exact spectral region of overlap, the number of lines common to the different exposures in the overlap region, the mean intensity ratio at the break in the sense intensity-longward/intensity-shortward, the standard deviation from the mean, the range of (shortward) intensities in the region of overlap, an indication of any intensity dependence (Y = yes, N = no), and the correction to log ($gf\,\lambda$) recommended to place all values *between* the breaks on a scale consistent with that at 4500 Å. The intensities in NBS Monograph 32 for most lines *within* the stated overlap ranges represent averages from two exposures and the indicated correction must be suitably adjusted. The recommended corrections do not exactly correspond to the observed intensity ratios. When a dependence upon intensity is indicated, the adopted correction was weighted toward the stronger lines. Also, the corrections for some spectra are absent or given with reservations (in parentheses) because of insufficient data.

The effect of the wavelength-dependent error as it propagates to the NBS gf-values is particularly apparent in the absolute curve of growth constructed for Nd II in ζ Cap (fig. 3.4). The average shift required to bring the red lines into unsystematic scatter about the curve defined by the blue lines is -0.22, in good agreement with the correction found in table 3.2.

3.2.4. Comparison of the NBS Intensity Estimates for Neodymium With Those of King (1936)

A possible consistency check on the above results was obtained by comparing for neodymium the arc intensity estimates of Meggers et al. (1961) with those of King (1933). Because of the somewhat unequal excitation conditions in the two experiments, the first and second spectra are treated separately, and the range of excitation potentials for lines used has been restricted. The average value of the ratio $R=I_{\mathrm{NBS}}/I_{\mathrm{King}}^{0.65}$ was calculated from selected lines on each side of the break at 4800 Å. The empirical exponent 0.65, derived in a preliminary analysis, compensates for the nonlinearity of King's intensity estimates and eliminates the intensity dependence of the ratio R. The value found for this exponent is in good agreement with Russell's (1925) observation that in many multiplets the square roots of King's intensities are proportional to the LS theoretical intensities. The results for neodymium spectra are given in table 3.3.

TABLE 3.3. *Comparison of NBS intensity estimates for neodymium with those of A. S. King*

$$R=\frac{I_{\mathrm{NBS}}}{I_{\mathrm{King}}^{0.65}}$$

Range	Spectrum	No. of lines	$\langle R\rangle$	Std. Dev.
(Å)				
4350–4670	Nd I	20	0.85	0.13
	Nd II	67	1.29	.27
4910–5320	Nd I	29	1.91	.37
	Nd II	39	4.29	.55

It is seen that the NBS intensities tend to become larger with respect to King's intensities as the 4800 Å overlap region is crossed. This is in general agreement with the results given above, but it is emphasized that no firm conclusions can be drawn owing to a lack of knowledge about the photographic details in the King experiment.

It is noteworthy that among the rare earths only lanthanum shows an intensity ratio less than unity at the 4800 Å break. The discrepancy discussed by Wallerstein (1966) in the solar La/Ce abundance ratio appears to be related to this fact. Using NBS gf-values, Wallerstein found that the La/Ce ratio in the sun was anomalously high in comparison with that observed in chondritic meteorites. A partial re-analysis of Wallerstein's data carried out in the light of the above results resulted in an appreciable reduction of that discrepancy.

The validity of applying the stated corrections outside the overlap regions in which they are explicitly found cannot be easily established. Judging from the available evidence and from the manner in which the original intensity estimates were calibrated, it appears that the extrapolation is required. But until a more definitive analysis of these sys-

398-978 O - 71 - 3

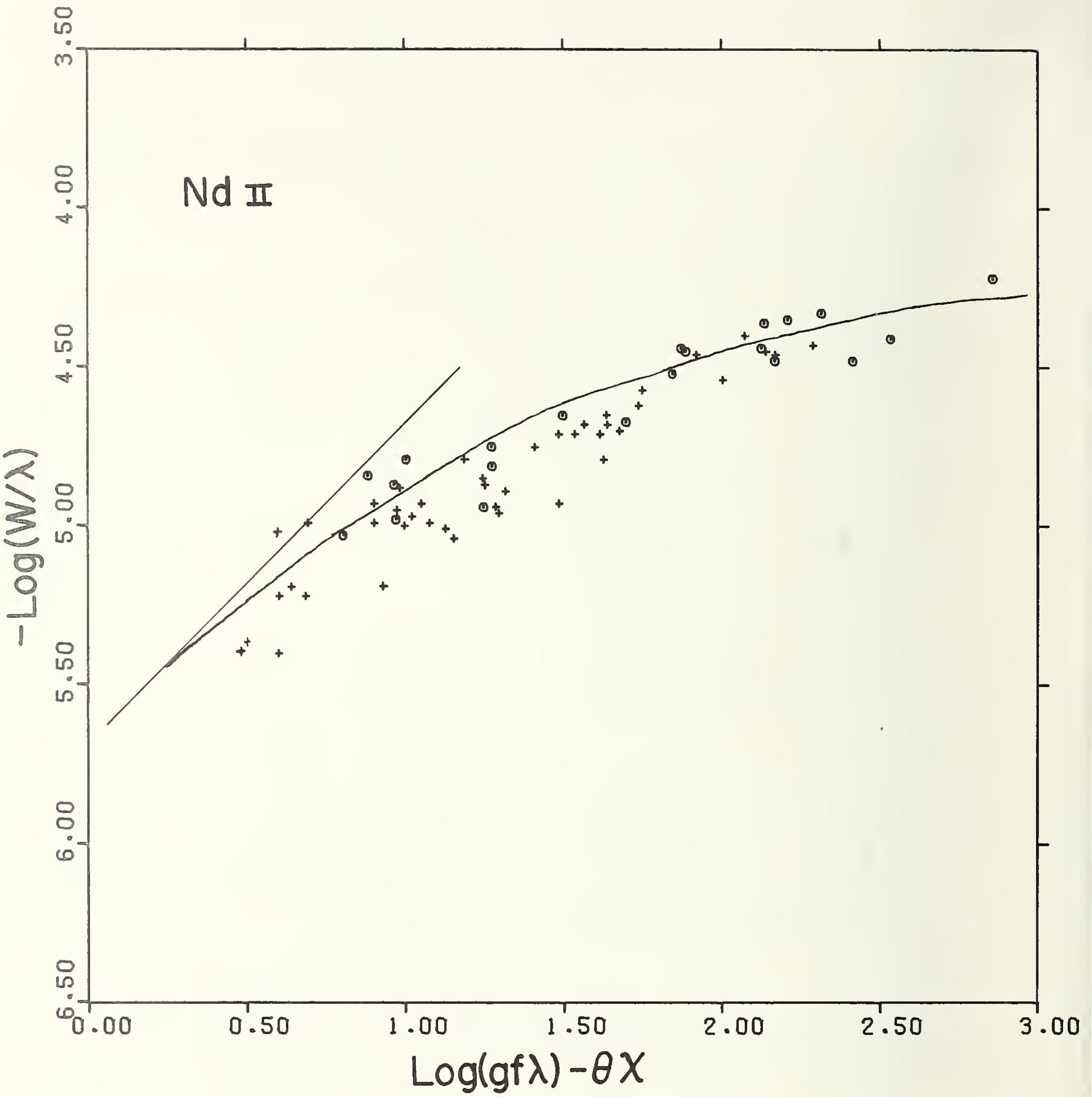

FIGURE 3.4. *The curve of growth for* Nd II *defined by the blue lines* (*< 5000 Å*, circles) *lies to the left of that defined by the red lines* (*> 5000 Å*, crosses).

This has been tentatively attributed to a systematic error in the *gf*-values of Corliss and Bozman, but a systematic error in the measured equivalent widths may also contribute.

matic effects can be made, the indicated corrections have been adopted only for Eu, Dy, Nd, Sm, La, and Ce, which seem well established and are of greatest importance in the present study. In the meantime, it is important to call the attention of other users of the NBS *gf*-values to the above results and suggest that, for greatest accuracy, astrophysical usage of these *gf*-values be restricted as far as possible to lines whose original intensities lie in the range $3 < I < 200$, and whose range of wavelength does not cross one of the overlap regions noted above (at least for those elements exhibiting abnormal behavior in those regions).

3.3. A Relation for Converting NBS Intensities of Unclassified Lines to *gf*-Values

As a final remark on the line intensities given in NBS Monograph 32, we derive a useful relation that appears not yet to have been recognized, but that is extremely useful in constructing absolute curves of growth for stars whose excitation temperature θ^*_{exc} $(5040/T^*_{\mathrm{exc}})$ is near unity. We have found this relation to be very helpful in identifying rare earth lines in ζ Cap.

The collection of *gf*-values by Corliss and Bozman, although based on the NBS Intensity Tables, included only those lines from the latter tables whose energy classifications were known, roughly 60 percent of the total. But in many cases the remaining 40 percent of the lines become available for constructing stellar curves of growth, because attention is focused not so much on *gf* as on the quantity $\log\,(gf\lambda) - \theta^*_{\mathrm{exc}}\chi$, for which a reasonable approximation can be found even without knowing the line classification. Here χ is the lower excitation potential of the line expressed in electron volts.

The NBS arc intensities provide *gf*-values through the expression

$$gf = C(u/Np)I\lambda^3 e^{E_u/kT^{\mathrm{arc}}_{\mathrm{exc}}} \qquad (3.1)$$

where C is an empirical normalizing function that converts relative values of *gf* to absolute values, u is the partition function, N is the percentage of atoms of the element in the given stage of ionization, and p is the persistence of the atoms in the arc stream. The other symbols have their usual meanings. The values of C, N, p, and T can be found in the introduction to the work of Corliss and Bozman.

After multiplying both sides of eq (3.1) by the wavelength, converting to logarithms, and subtracting $\theta^*_{\mathrm{exc}}\chi$, we find

$$\log\,(gf\lambda) - \theta^*\chi = 4\log\lambda + \log I + C' + \alpha\theta^{\mathrm{arc}}E_u - \theta^*\chi \qquad (3.2)$$

where $\alpha = 1.2398 \times 10^{-4}$ eV/cm^{-1}. The wavelength is here expressed in angstrom units and the upper energy level E_u in cm^{-1}. We have also set

$$C' = \log\,(u/Np) + \log C. \qquad (3.3)$$

In the original reduction, Corliss and Bozman adopted for $\log C$ an empirically determined function that was the same for all spectra and that depended on E_u. A detailed investigation by Warner and Cowley (1967) indicates that the function varies from spectrum to spectrum, however. In the case of Fe I, for example, the constant value $\log C = -16.61$ appears to be most appropriate.

The last two terms of eq (3.2) can be put into a more convenient form by setting

$$\theta^* = \theta^{\mathrm{arc}} + \Delta\theta. \qquad (3.4)$$

and by using the relations

$$\chi = \alpha E_l, \qquad (3.5)$$

$$n = 1.0003$$

and

$$(E_u - E_l) \cong \frac{10^8}{n\lambda} \qquad (3.6)$$

where E_l is the energy of the lower level of the transition, and n is the approximate dispersion of air. We then have

$$\begin{aligned}\alpha\theta^{\mathrm{arc}}E_u - \theta^*\chi &= \alpha\theta^{\mathrm{arc}}E_u - \alpha(\theta^{\mathrm{arc}} + \Delta\theta)E_l \\ &= \alpha\theta^{\mathrm{arc}}(E_u - E_l) - \Delta\theta\chi \qquad (3.7) \\ &= \frac{\alpha\theta^{\mathrm{arc}}}{n\lambda} \times 10^8 - \Delta\theta\chi.\end{aligned}$$

Since the temperature of the NBS arc is 5100 K, we have $\theta^{\mathrm{arc}} = 0.99$, and eq (3.1) becomes, finally,

$$\log\,(gf\lambda) - \theta^*\chi = 4\log\lambda + \log I + \frac{12300}{\lambda} + C' - \Delta\theta\chi \qquad (3.8)$$

where the difference $\Delta\theta$ is just

$$\Delta\theta = \theta^*_{\text{exc}} - 0.99. \tag{3.9}$$

For unclassified lines, the unknown correction term $-\Delta\theta\chi$ can be reasonably approximated by adopting for χ a value most suitable to the given wavelength and element. For the sun, where $\Delta\theta = 0.03$ ($\theta^{\odot}_{\text{exc}} = 1.02$) one might arbitrarily choose $\chi = 2$ eV for unclassified lines. The maximum error in calculating $\log (gf\lambda) - \theta^{\odot}\chi$ by the above formula is then only 0.09 over a range of 5 eV, well within the accuracy of the NBS intensities themselves. As a practical matter, those workers who use the NBS *f*-values from magnetic tape in computer applications might consider the advantages of having the NBS Intensity Tables on tape instead. Equation (3.8) not only makes the unclassified lines available in many cases for constructing curves of growth, but also reproduces the NBS *gf*-values themselves (by setting $\theta^* = 0.00$). Unlike the *gf*-values, moreover, the line intensities are not subject to revision as the partition functions are improved or as the normalizing function C of eq (3.1) becomes better understood. Also, evidence is accumulating that the temperature of the NBS arc may actually be closer to 7000 K than to the adopted value 5100 K (Corliss, private communication). If this should prove to be the case, the above analysis remains intact, of course, but some modification would be necessary. For example, the value of the quantity C' in eq (3.8) would require an adjustment to reflect the different degree of ionization corresponding to the higher arc temperature, and the application of the equation to unclassified lines would have to be restricted to stars having excitation temperatures near $\theta^*_{\text{exc}} = 0.72$.

Note Added In Proof:

The recent, very important measurements of Fe I *f*-values at the Kiel Institut für Experimentalphysik[1,2], the National Bureau of Standards[3], and elsewhere leave little doubt that a temperature error was present in the early measurements of King and King[4,5]. This temperature error has been propagated to a number of other collections of experimental *f*-values that directly or indirectly used the data of King and King for purposes of calibration. Such a propagated temperature error occurs also in NBS Monographs 53 and 108, which have served as sources of *f*-values for several spectra in the work presented here.

It must be explicitly pointed out that the stellar analysis given in the present work is a differential one, and the results do not significantly depend on the *f*-values. The restricted use of *f*-values here—mainly to assist in line identifications—has been explained in sections 3.1.4 and 3.2.1. As a test of the effect the temperature error has on our absolute curves of growth, we have reconstructed the curve of growth for Ce II shown in figure 4.4 after applying the temperature correction derived below. The shape of the curve was negligibly affected; it is merely shifted in the direction of smaller abscissae by −0.97.

It is apparent from eq (3.1) and the subsequent analysis that

$$\Delta \log (gf) = \Delta\theta\chi_u + \Delta C' \tag{3.10}$$

where $\Delta \log (gf)$ is the error in $\log (gf)$ resulting from an error $\Delta\theta$ in the adopted arc temperature. Not for all lines, but for the vast majority of them, the temperature error present in the aforementioned NBS monographs unquestionably dominates any systematic errors owing to departures from LTE and other causes. Monograph 108 is a tabulation of *f*-values from several sources and any assumed temperature error would, of course, be that of a "fictitious" arc. Since the values in this compilation were calibrated against the NBS arc used in the preparation of Monograph 53, the temperature error in the two works should be approximately the same, however.

From a least-squares comparison of Monograph 108 with the Kiel *f*-values only, we find $\Delta\theta = -0.25$, corresponding to a temperature for the NBS arc of 6810 K, compared with the previously adopted value 5100 K. Application of this correction to the NBS values gives a standard deviation of ± 0.16 between the two sets of $\log (gf)$-values. Even without a knowledge of the element-dependent quantity $\Delta C'$ in eq. (3.10), it would seem that useful *relative* *f*-values, for statistical purposes only, could still be obtained by applying eq (3.10) to the data of Monograph 53. We cannot here give further study to this recommendation, but such an investigation, including the relationship to the temperature error of the so-called normalization function C, might be worthwhile because of the likelihood that many spectra included in that monograph, especially those of the rare earths, will not be re-observed in more precise experiments in the near future.

[1] Garz, T., and Kock, M., Astron. & Astrophys. **2**, 274 (1969).
[2] Richter, J., and Wulff, P., Astron. & Astrophys. **9**, 37 (1970).
[3] Bridges, J. M., and Wiese, W. L., Astrophys. J. **161**, L71 (1970).
[4] King, R. B., and King, A. S., Astrophys. J. **82**, 371 (1935).
[5] King, R. B., and King, A. S., Astrophys. J. **87**, 24 (1938).

4. Curve of Growth Analysis

4.1. The Differential Method

The atmosphere of ζ Capricorni has been studied differentially with respect both to the sun and to the G9 II–III giant ϵ Virginis, analyzed in detail by Cayrel and Cayrel (1963). The method of differential analysis used here, implicit in the pioneering work of Adams and Russell (1928), has been extensively developed by Greenstein (1948, 1949) and by Pagel (1964).

The theory of stellar atmospheres has now reached such a successful stage of development that the analysis of a stellar spectrum should, ideally, be based on a reliable model atmosphere calculated for the star. The widespread availability and use of electronic computers has essentially eliminated any computational objections to such a refined depth-dependent analysis. But, as pointed out by Cowley and Cowley (1964), the difficulty is not merely computational. Uncertainties in the experimental data (the equivalent widths, the laboratory f-values), and in the stellar parameters (effective temperatures, surface gravities), as well as the theoretical problems associated with the treatment of blanketing, turbulent atmospheres, and departures from local thermodynamic equilibrium, make it doubtful whether a calculated model offers accuracy in abundance determinations as great as the complexity and labor of such a treatment would suggest.

In particular, for the rare earths that are of great interest in Ba II stars, there is considerable uncertainty both in the absolute scale of the one set of available f-values and in the relevant partition functions. Also, in an atmosphere with high macroturbulent velocity (as in ζ Cap) there is some doubt whether a physically meaningful temperature distribution with depth can be assigned. In any case, experience has shown for several stars—ϵ Virginis, for example—that the results of analysis in the single-layer approximation are in very good agreement with those obtained for the same stars by detailed analyses based on model atmospheres.

For comparison with the results derived in the present monograph, the writer is currently carrying out a depth-dependent analysis of ζ Capricorni. A model atmosphere was developed for this purpose from the grid maintained by Gingerich and his coworkers at the Smithsonian Astrophysical Observatory. The analysis is not yet completed, but the preliminary results indicate only minor differences with the differential study presented here.

The curve of growth for spectral lines can be viewed quite generally as a saturation curve giving the equivalent width as a function of total oscillator strength. In the Milne-Eddington formulation, the abscissa of the curve of growth is defined by the line strength parameter η_0, where (Unsöld, 1955; Aller, 1963)

$$\log \eta_0 = \log N_r + \log (gf\lambda) - \theta\chi_{r,s} - \log u(T) - \log v - \log k_\lambda + \text{const.} \qquad (4.1)$$

Here N_r is the abundance of the element in the rth stage of ionization, $\chi_{r,s}$ is the excitation potential of the lower level s of the transition, g is the statistical weight of the level, $\theta = 5040/T_{\text{exc}}$, $u(T)$ is the partition function, and k_λ is the continuous absorption coefficient. In the analysis, the small variation of the opacity over the wavelength range of the observational material can be ignored. Differentially, for two stars of similar temperature, the small differences in values for the partition functions are not important, and one may write

$$[\eta_0] = [N_r] - \Delta\theta\chi_{r,s} - [v] - [k] \qquad (4.2)$$

where the bracket notation introduced by Helfer et al. (1959) is used. By this convention the bracket $[Q]$ is defined as the logarithmic difference in any physical quantity Q between the star under study and the comparison star. That is,

$$[Q] = \log Q(\text{star}) - \log Q(\text{standard}) = \log \frac{Q(\text{star})}{Q(\text{standard})}. \qquad (4.3)$$

By normalizing the theoretical curves of growth such that the values of abscissa $\log X = \log \eta_0 + \text{const.}$ and ordinate $\log (W/\lambda)$ coincide for weak lines, the microturbulent parameter v is eliminated from the analysis (Cayrel and Jugaku, 1963), and one may write

$$[X] = [N_r] - \Delta\theta\chi_{r,s} - [k]. \qquad (4.4)$$

In the differential curves of growth given here for ζ Cap, values of $\log (W_\zeta/\lambda)$ are plotted against

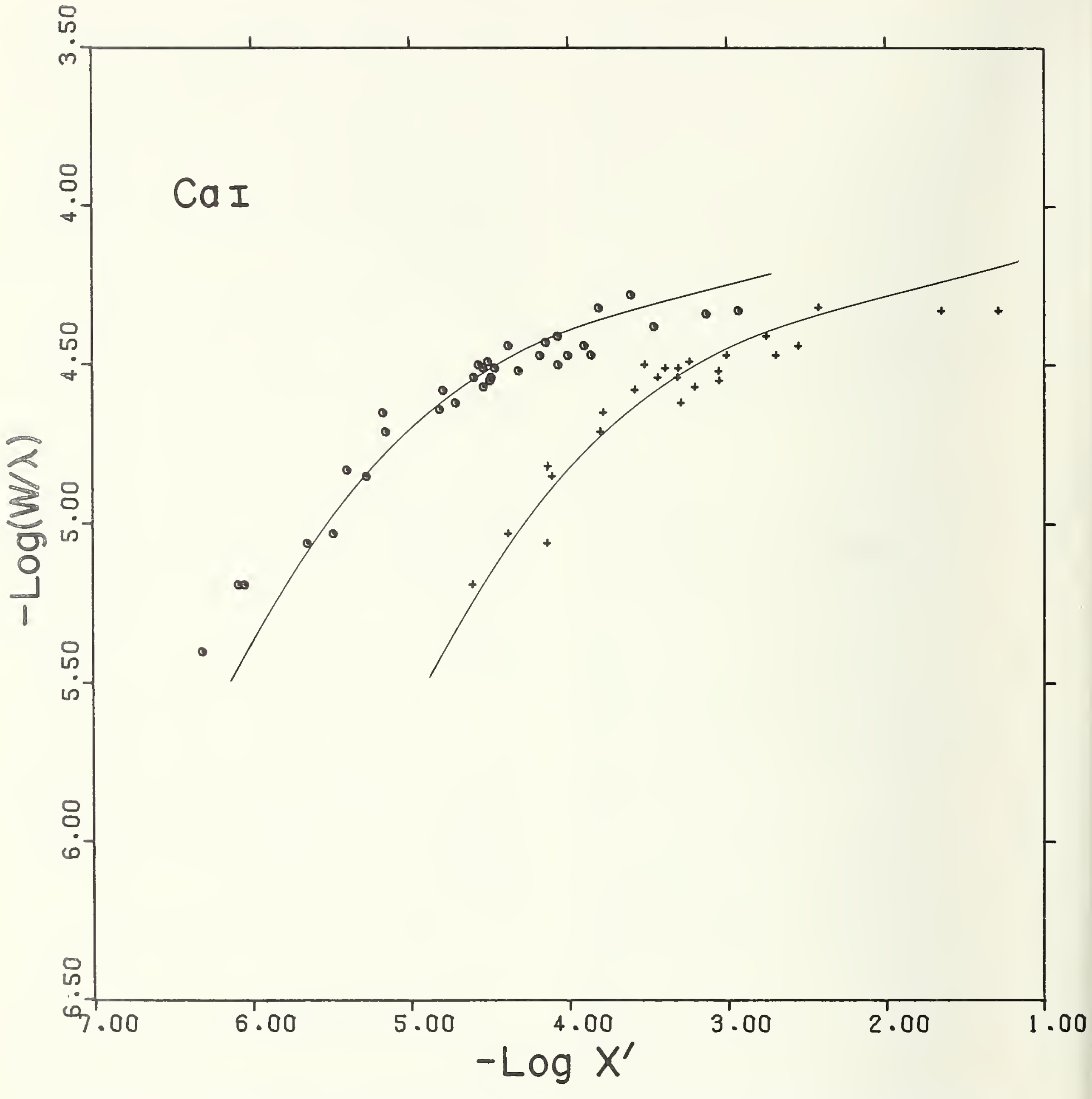

FIGURE 4.1. *Differential curves of growth for calcium with respect to the sun* (circles) *and to ε Virginis* (crosses).

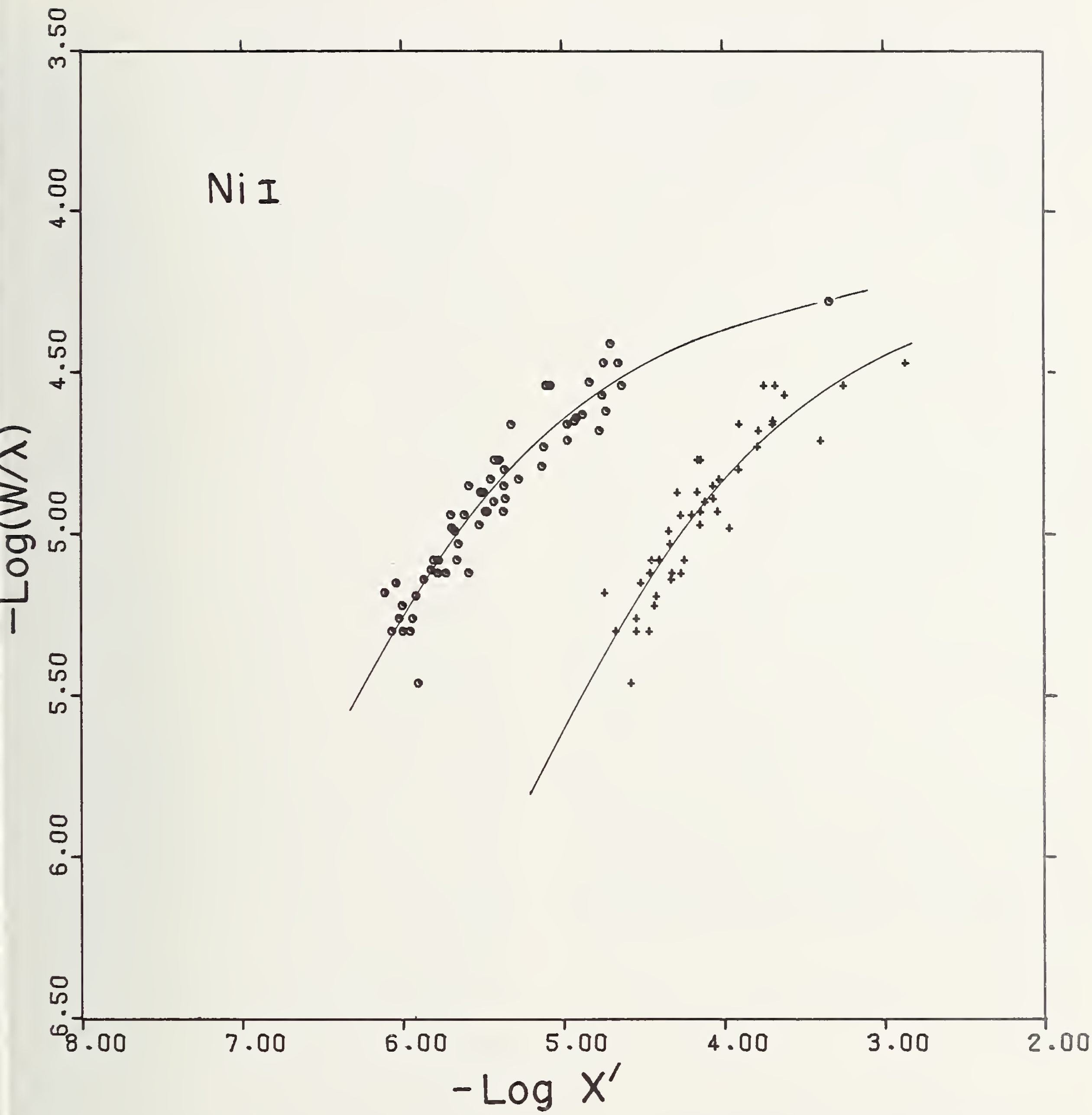

FIGURE 4.2. *Differential curves of growth for nickel with respect to the sun* (circles) *and to ε Virginis* (crosses).

$\log X_* - \Delta\theta(\zeta - *)\chi_{r,s}$ where X_* is the normalized stellar line strength obtained from the theoretical curve for the comparison star (sun or ϵ Vir) and

$$\Delta\theta(\zeta - *) = \theta^{\zeta}_{\text{exc}} - \theta^{*}_{\text{exc}}. \tag{4.5}$$

By eq (4.4), the horizontal displacement required to shift the empirical curve into coincidence with the adopted theoretical curve immediately gives the logarithmic abundance ratio of the element for the given stage of ionization in the stars in terms of the difference in opacity,

$$[X] = [N_r/k]. \tag{4.6}$$

Finally, the application of corrections to be discussed later for differences in opacity and ionization equilibrium between the two stars gives the total ratio of stellar abundances for the given element.

There are several advantages to performing a double differential analysis by using two comparison stars. Comparison of two differential curves derived from the same spectral lines helps in the recognition of bad blends or poor measurements. For example, a widely discrepant point in *both* empirical curves can usually be traced to blending in the barium star. Also, many lines measured in ζ Cap do not appear in the line list for ϵ Vir, but are available for use in the differential curve relative to the sun. The double analysis thus permits a fuller exploitation of the observational data for the barium star.

In accordance with the analysis of the Cayrels, the chemical composition of ϵ Virginis is assumed to be identical to that of the sun. As a byproduct of the double differential analysis, however, one can in fact derive the relative abundances also for ϵ Virginis. The horizontal shift between any two differential curves plotted for some spectrum in ζ Cap is simply

$$\Delta \log X = [X]_{\zeta-\odot} - [X]_{\zeta-\epsilon} = [N_r/k]_{\zeta-\odot} - [N_r/k]_{\zeta-\epsilon}. \tag{4.7}$$

By expanding the brackets, it is seen that the parameters for the barium star cancel out, and

$$\Delta \log X = [N_r/k]_{\epsilon-\odot}. \tag{4.8}$$

The differential curves of growth for Ca I and Ni I in ζ Cap using the stellar line strengths discussed in the next section are shown in figures (4.1) and (4.2). The observed values of $\Delta \log X$ are 1.37 and 1.23 for Ni I and Ca I, respectively. The corresponding values predicted in the detailed analysis by the Cayrels on the assumption of equal abundances for ϵ Vir and the sun are 1.38 and 1.12.

4.2. The Stellar Line Strengths

The solar line strengths, $\log X(\odot)$, used in constructing the differential curves of growth for ζ Cap were obtained by entering the Pierce-Aller curve of growth with solar equivalent widths from the Second Revision of the Rowland Table (Nat. Bur. Stand. (U.S.), Monogr. 61, 1966) and reading off the corresponding value of the abscissa. Similarly, the line strengths $\log X(\epsilon)$ for differential curves relative to ϵ Virginis were obtained by use of the equivalent widths and theoretical curve of growth for ϵ Virginis given by Cayrel and Cayrel (1963). In both cases, the theoretical curves were normalized to have equal ordinate ($\log (W/\lambda)$) and abscissa ($\log X(*)$) for weak lines.

To avoid the errors and the labor of evaluating graphically both sets of comparison line strengths for the 1100 spectral lines measured in ζ Cap, computer-oriented polynomials have been calculated to represent each theoretical curve in the form $\log X = f(\log W/\lambda)$. Since the values of $\log (W_{\odot}/\lambda)$ and $\log (W_{\epsilon}/\lambda)$ were included on the punched cards containing the measurements in ζ Cap, the evaluation of the corresponding $\log X(*)$ could be rapidly accomplished.

The theoretical curves of growth for the two comparison stars were indirectly reconstructed. The Pierce-Aller curve of growth was obtained by using the solar equivalent widths and solar line strengths listed by the Cayrels in their line list for ϵ Vir. The curve for ϵ Vir was similarly reconstructed from the values of $\log X(\epsilon)$ given by Wallerstein and Greenstein (1964) in their line list for two CH stars.

The analytical representation for each curve was obtained by fitting the corresponding set of points to a polynomial by means of the general least-squares program CWLT5 mentioned earlier. It was necessary to divide each curve into three sections, because a simple polynomial representation for the entire curve is not possible to the desired precision. Table 4.1 lists the coefficients of fifth-degree polynomials describing each section. The coefficients are stated in exponential format, in which the sign and integer following each number represent the exponent of the power of ten by which the preceding number is to be multiplied. (In this convention, for example, $1.2345+3 = 1.2345 \times 10^3$). Nowhere does the error in the calculation of $\log X$ exceed 0.02 by use of these expressions.

TABLE 4.1. *Coefficients for the polynomials representing the normalized stellar curves of growth*

$$\log X(*) = \sum_{i=0}^{5} a_i y^i$$

$$y = \log\ (W_*/\lambda)$$

	Sun	ϵ Virginis	ζ Capricorni
	$-6.50 \leqslant y \leqslant 4.85$	$-6.50 \leqslant y \leqslant -4.85$	$-6.50 \leqslant y \leqslant -4.60$
a_0	+9.054776210 +2	+7.592728450 +2	+1.500322741 +3
a_1	+7.295101356 +2	+6.216381693 +2	+1.325361840 +3
a_2	+2.343845144 +2	+2.032155776 +2	+4.674737809 +2
a_3	+3.769455460 +1	+3.330008853 +1	+8.244279540 +1
a_4	+3.030168531 +0	+2.729582146 +0	+7.261594589 +0
a_5	+9.739678650 −2	+8.949677628 −2	+2.554781086 −1
	$-4.85 \leqslant y \leqslant -4.45$	$-4.85 \leqslant y \leqslant -4.45$	$-4.60 \leqslant y \leqslant -4.20$
a_0	−2.969210028 +5	+7.322789597 +5	−2.269867716 +5
a_1	−3.157713154 +5	+7.829199288 +5	−2.528140610 +5
a_2	−1.342551273 +5	+3.348216960 +5	−1.125246254 +5
a_3	−2.852608896 +4	+7.159176686 +4	−2.501961990 +4
a_4	−3.029173506 +3	+7.653391012 +3	−2.779276587 +3
a_5	−1.286112672 +2	+3.272402327 +2	−1.233999502 +2
	$-4.45 \leqslant y \leqslant -3.50$	$-4.45 \leqslant y \leqslant -3.50$	$-4.20 \leqslant y \leqslant -3.50$
a_0	+1.722082789 +4	+1.782950880 +4	−1.411797999 +4
a_1	+2.152726622 +4	+2.311731158 +4	−1.773508229 +4
a_2	+1.075557085 +4	+1.197860158 +4	−8.874656647 +3
a_3	+2.684783907 +3	+3.100207120 +3	−2.210547953 +3
a_4	+3.348264877 +2	+4.007339284 +2	−2.739442329 +2
a_5	+1.669141190 +1	+2.069643167 +1	−1.350177854 +1

We stress that no physical significance is attached to these analytical expressions, which were used solely as an expedient labor-saving device. Although the adopted polynomial representations yield the desired accuracy, no claim is made that the best representations for the curves have been found.

For later use, the coefficients representing the normalized curve of growth for ζ Capricorni as described in section 4.4 are also listed in table 4.1.

4.3. Conversion of NBS *gf*-Values to Line Strengths in ϵ Virginis

As pointed out in section 3.2.1, the spectra of certain rare earths are more completely developed in ζ Cap than in ϵ Vir as a result of the greater abundances in the barium star. For example, only two of more than 60 Nd II lines measured in ζ Cap are also contained in the line list for ϵ Vir. Some other lines of Nd II that were in fact observed in the comparison star could not be used in the differential curves of growth, either because the degree of blending was different in the two objects or because the spectral range of the present observations did not include them.

In order to use the extensive observational material to better advantage, therefore, the NBS *gf*-values for several spectra have been converted to the system of ϵ Virginis by a method that is essentially a reversal of the familiar one by which estimates of *f*-values are obtained from observed stellar line strengths. This indirect procedure gives fairly reliable differential abundances from the *gf*-values without making any demands on the correctness or consistency of their absolute scales.

If the curve of growth constructed for ϵ Vir by use of *gf*-values has the same shape as the theoretical curve derived by the Cayrels (1963), one can write with sufficient accuracy

$$\log X(\epsilon) = \log\ (gf\lambda) - \theta(\epsilon)\chi + \delta \tag{4.9}$$

where δ is a constant that differs from spectrum to spectrum and effectively shifts the corresponding $gf\lambda$ curves of growth to the normalized theoretical curve for the comparison star. Values of the quantity δ have been determined that are appropriate to six rare-earth spectra for which the differential curves of growth for ζ Cap are not sufficiently populated to yield reliable abundances. Within each spectrum, an unweighted average was taken of the δ-values obtained by applying eq (4.9) to all but a few badly blended lines in the list given for ϵ Vir. A slightly different treatment of the Pr II spectrum was required, because the Pr II lines measured in ϵ Vir are so badly blended that little confidence can be accorded a δ-value derived from those lines. The δ-value cited for Pr II in table 4.2 was therefore obtained by first applying eq (4.9) to the more numerous solar Pr II lines and then adding the shift +1.06 predicted from the model atmosphere analysis by the Cayrels. The individual residuals indicate the probable error in the determination of the δ-values to be less than about ±0.20. The results are given in table 4.2.

TABLE 4.2. *Conversion of NBS* gf*-values to line strengths in ϵ Virginis*

$$\text{lof } X(\epsilon) = \log\ (gf\lambda) - \theta(\epsilon)\chi + \delta$$

Spectrum	δ
Ce II...........	−7.00
La II...........	−6.26
Nd II...........	−6.53
Pr II...........	−7.43
Sm II...........	−6.95
Y II.............	−5.46

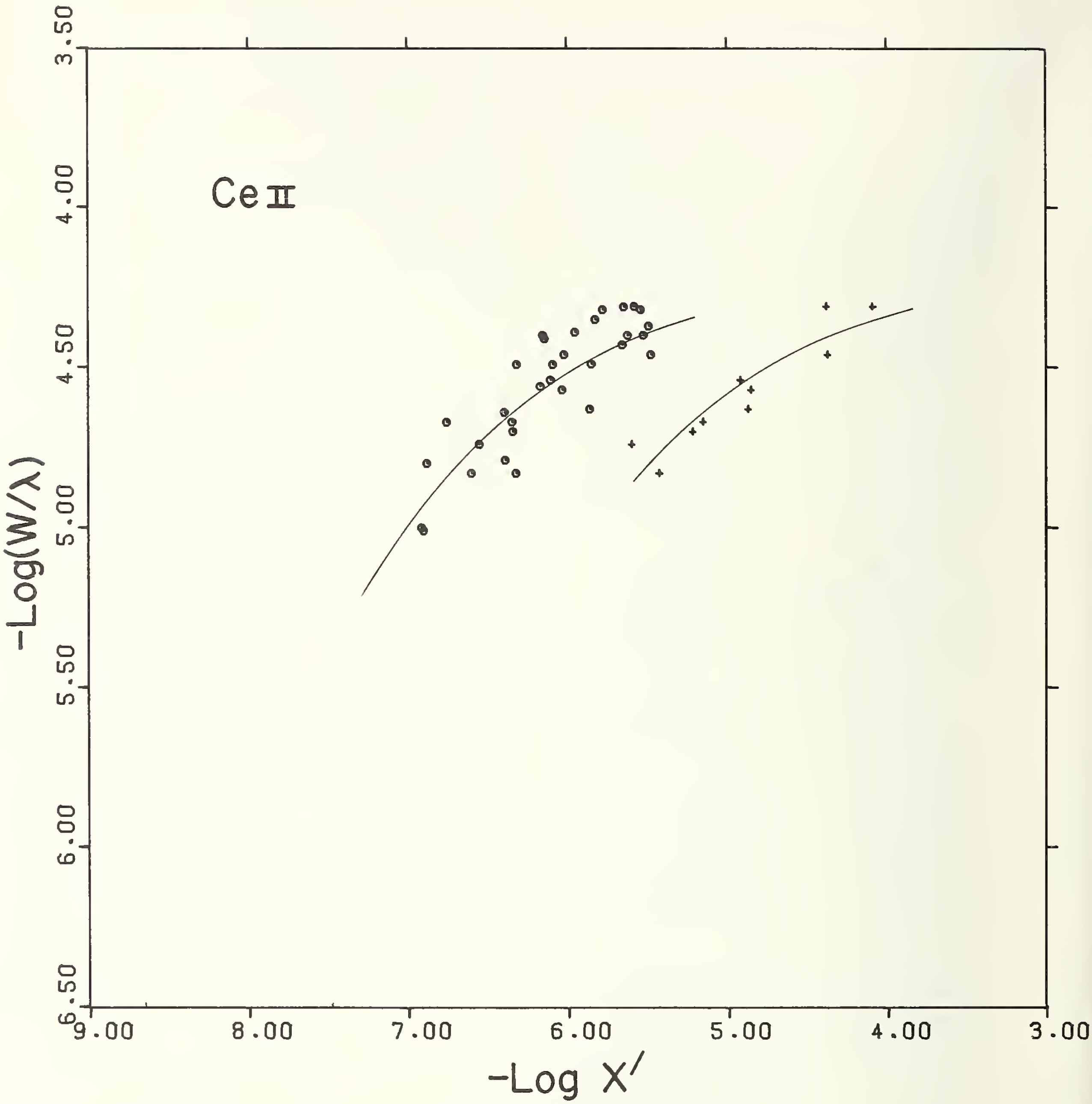

FIGURE 4.3. *Differential curves of growth for singly ionized cerium relative to the sun* (circles) *and to ε Virginis* (crosses).

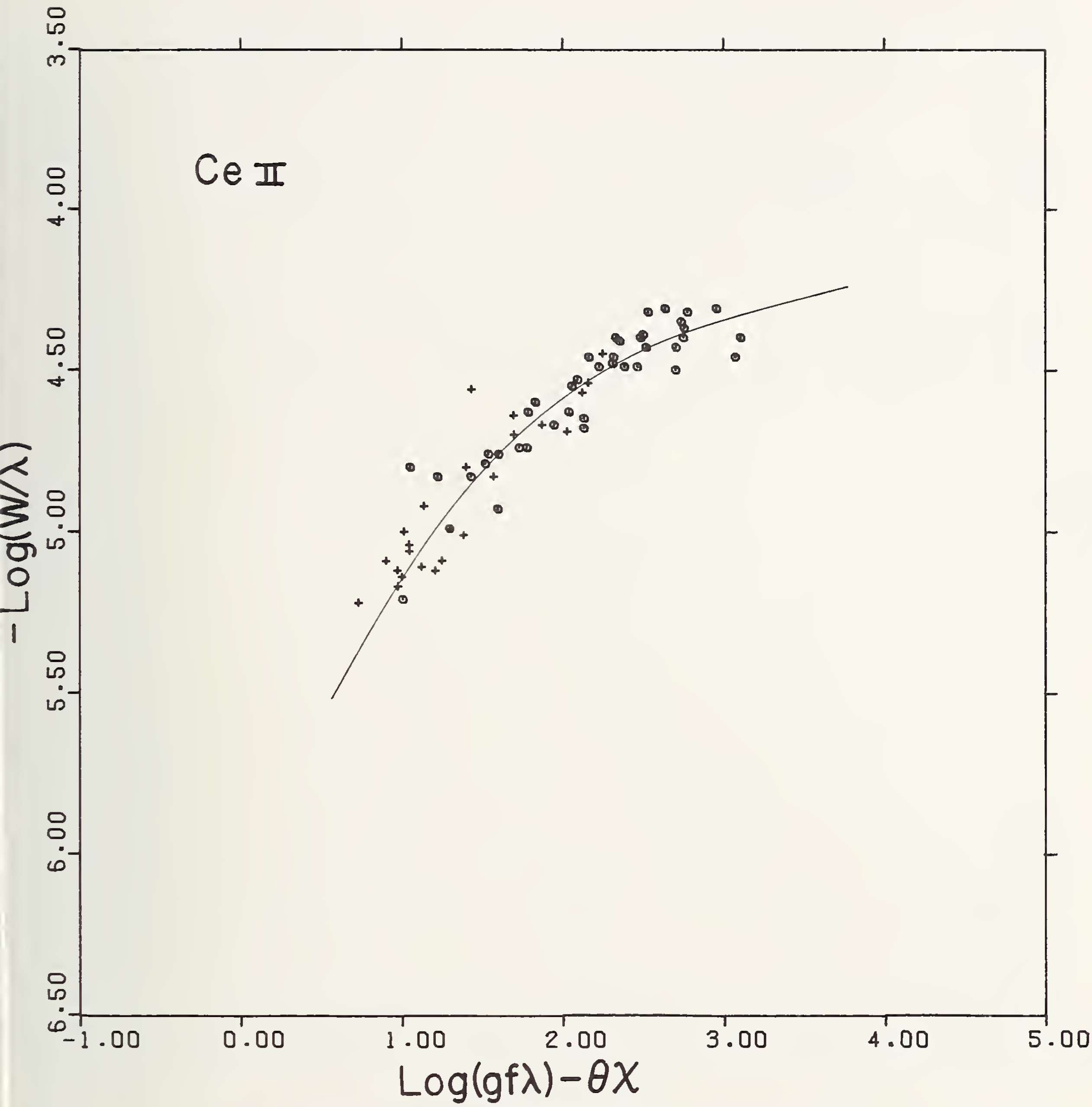

FIGURE 4.4. *Absolute curve of growth for singly ionized cerium.*

(*Circles*, λ < 5000 Å; *crosses*, λ > 5000 Å.)

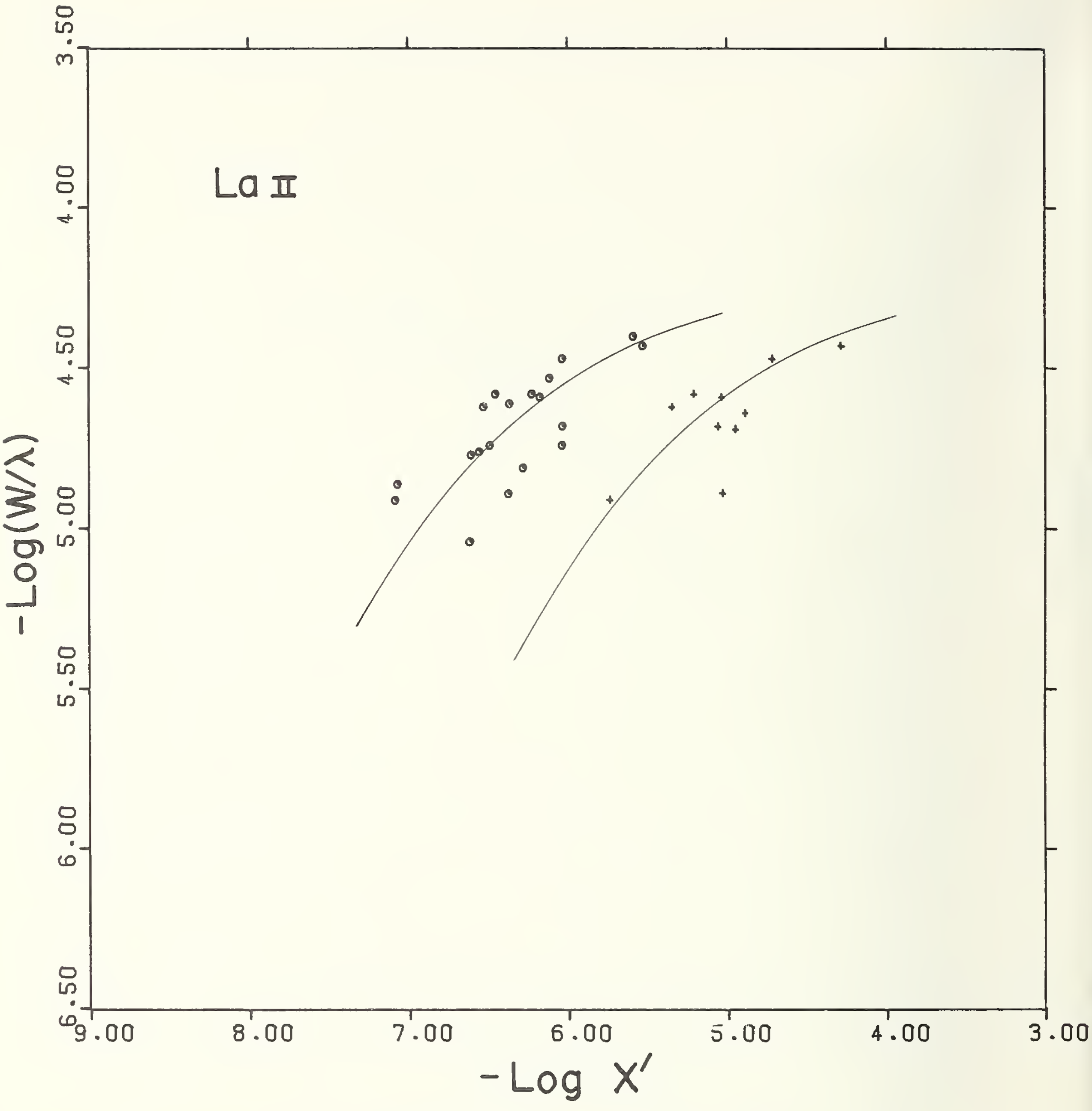

FIGURE 4.5. *Differential curves of growth for singly ionized lanthanum relative to the sun* (circles) *and to* ϵ *Virginis* (crosses).

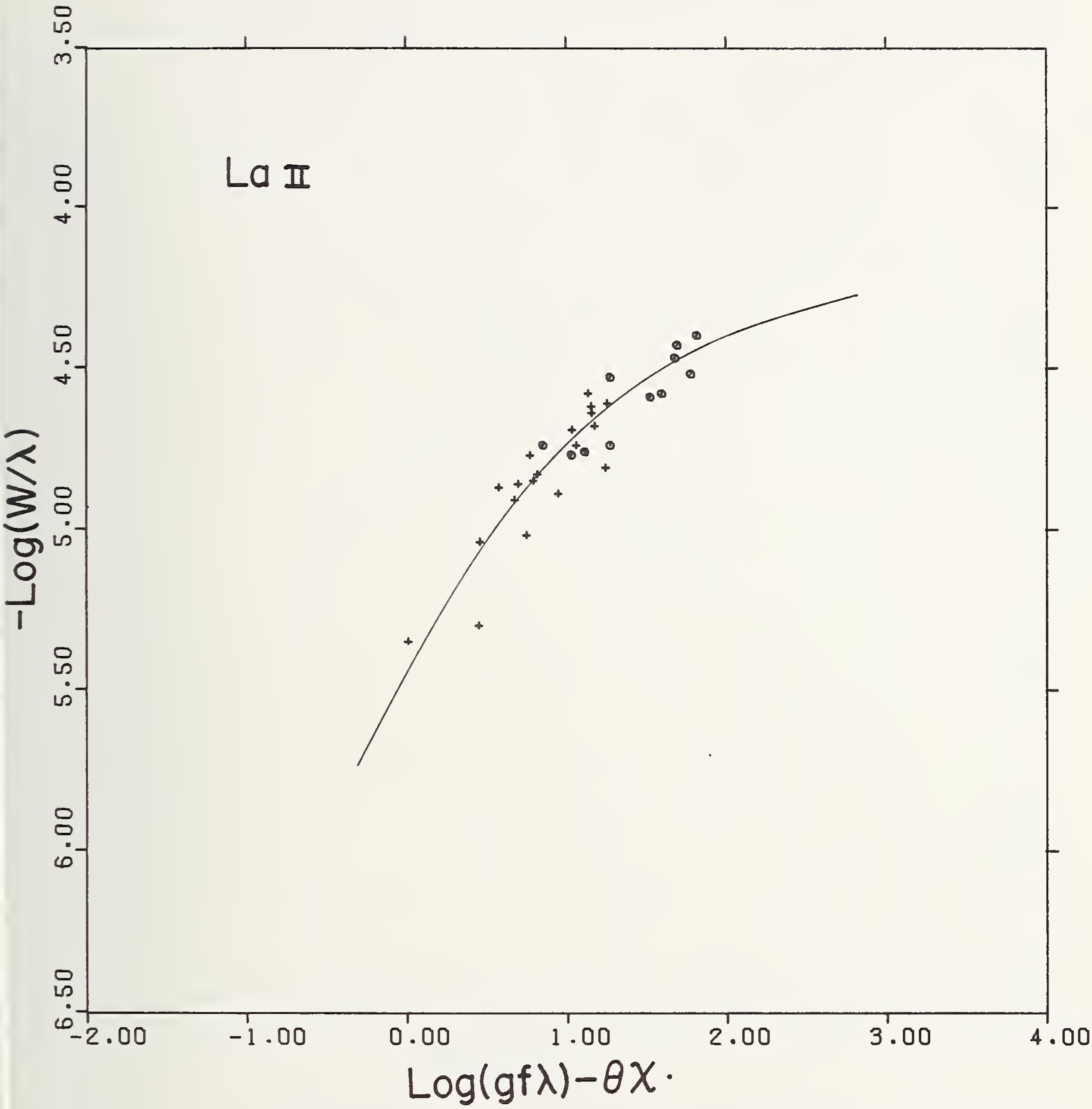

FIGURE 4.6. *Absolute curve of growth for singly ionized lanthanum.*

(*Circles*, λ < 5000 Å; *crosses*, λ > 5000 Å.)

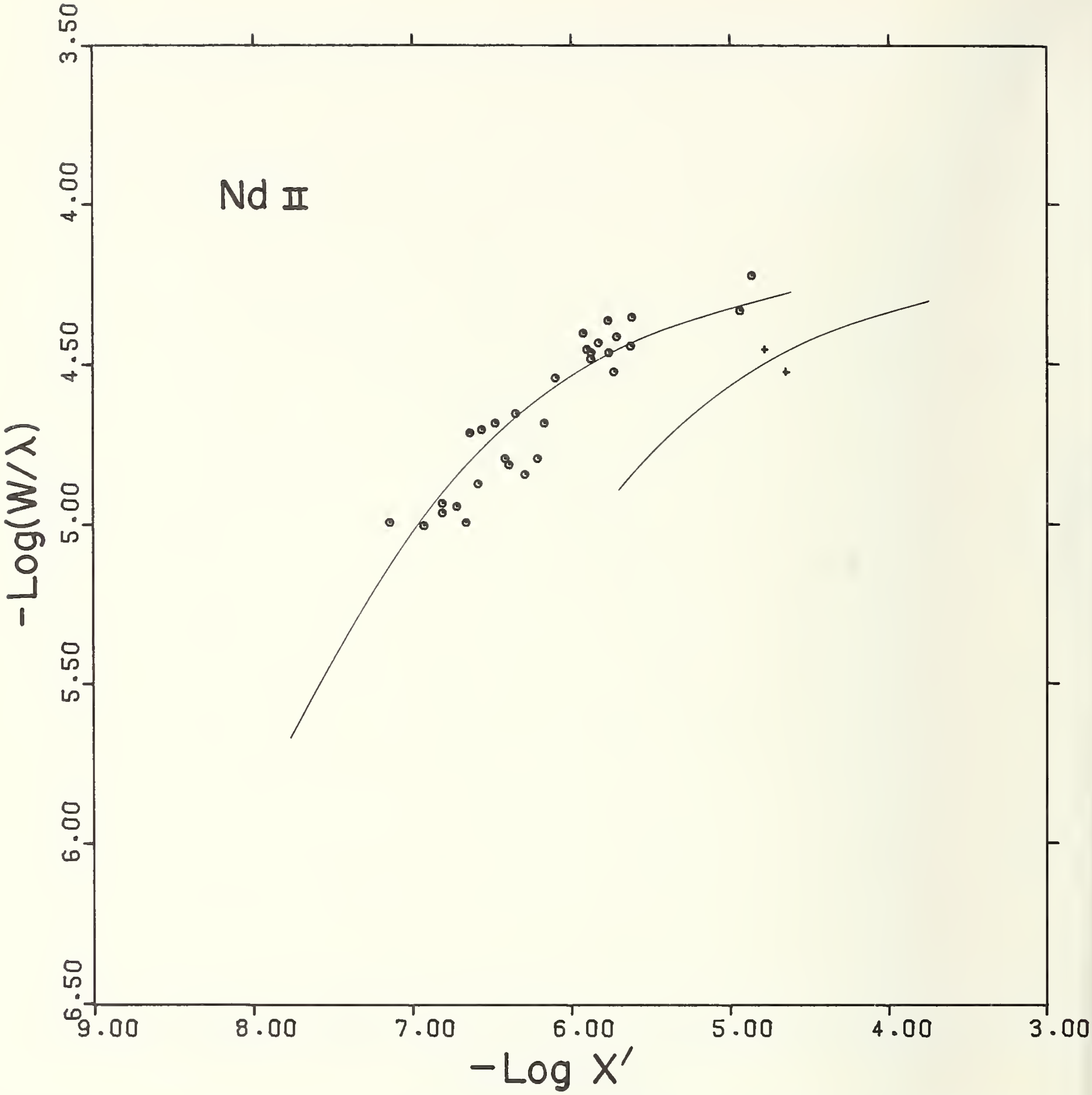

FIGURE 4.7. *Differential curves of growth for singly ionized neodymium relative to the sun* (circles) *and to ϵ Virginis* (crosses).

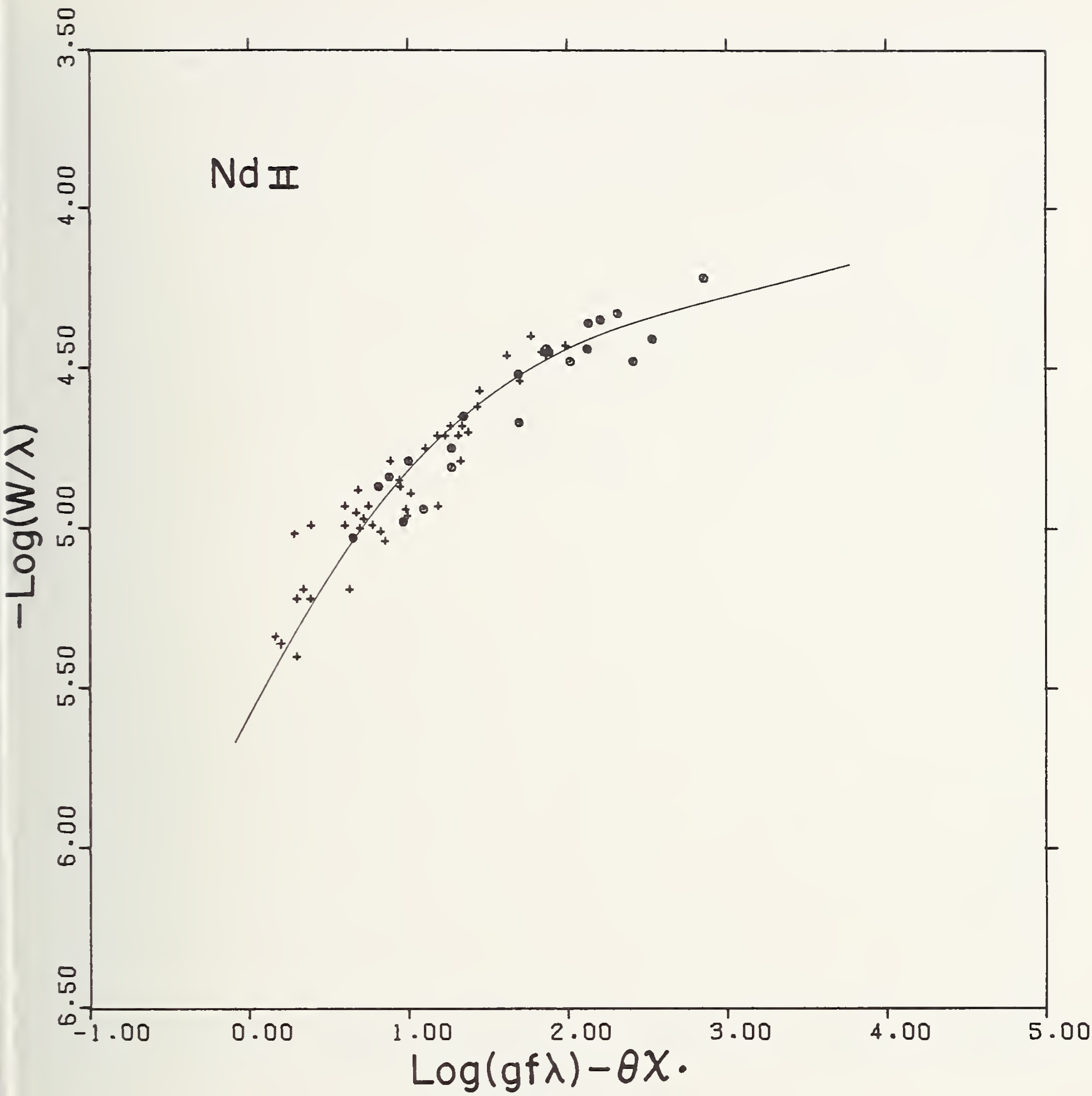

FIGURE 4.8. *Absolute curve of growth for singly ionized neodymium.*

(Circles, $\lambda < 5000$ Å; *crosses*, $\lambda > 5000$ Å.)

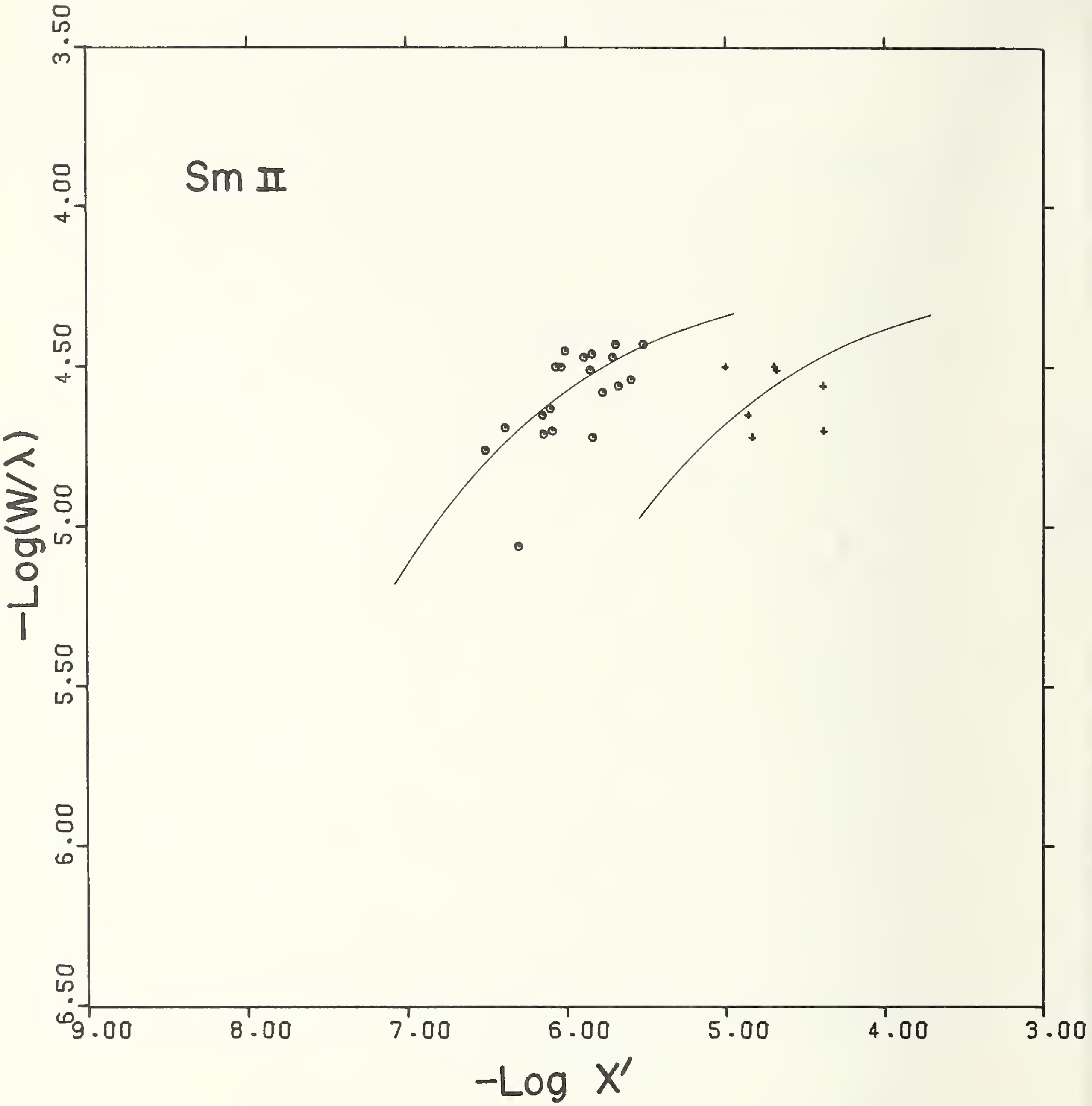

FIGURE 4.9. *Differential curves of growth for singly ionized samarium relative to the sun* (circles) *and to ε Virginis* (crosses).

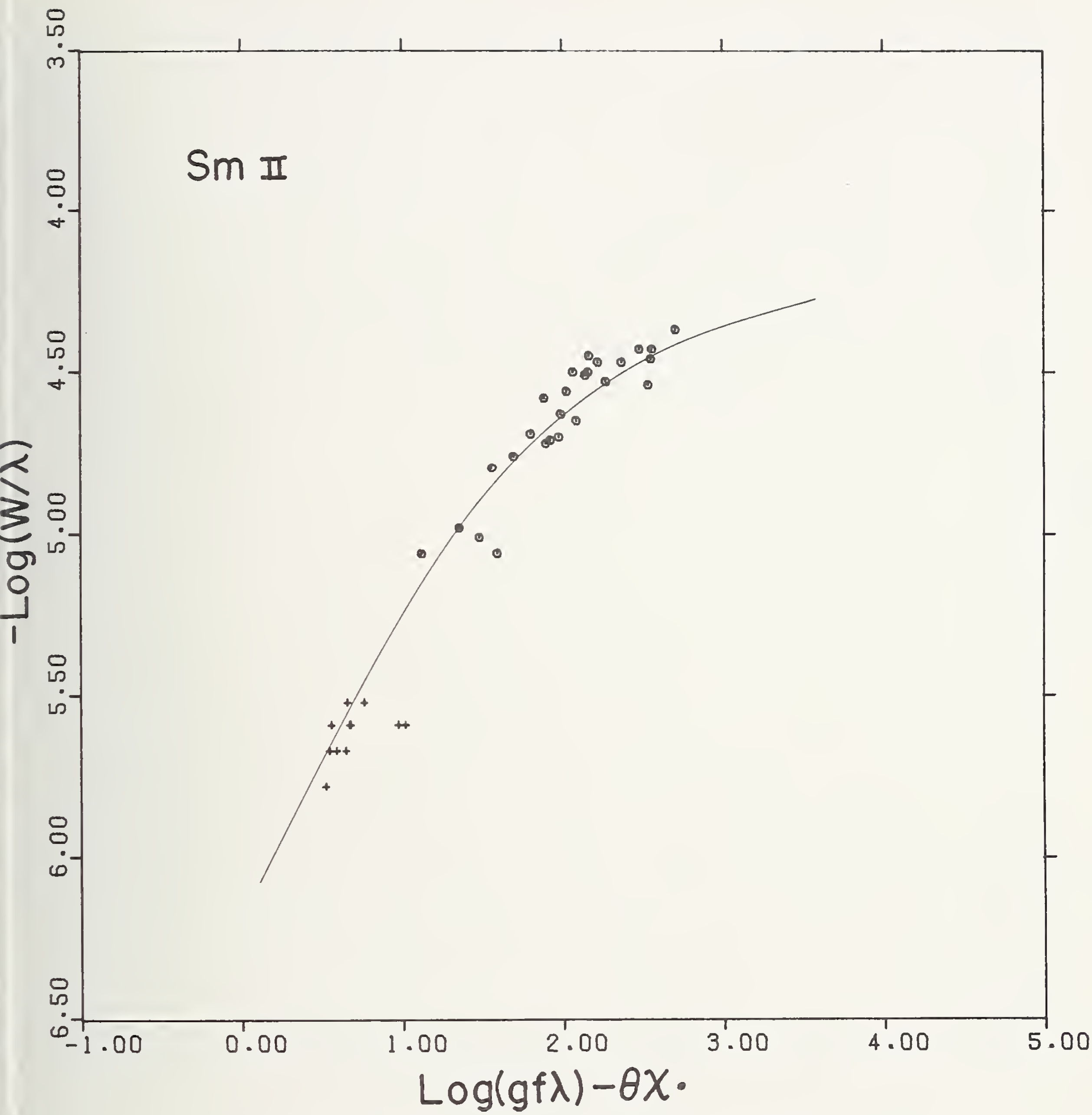

FIGURE 4.10. *Absolute curve of growth for singly ionized samarium.*

(*Circles*, $\lambda < 5000$ Å; *crosses*, $\lambda > 5000$ Å.)

398-978 O - 71 - 4

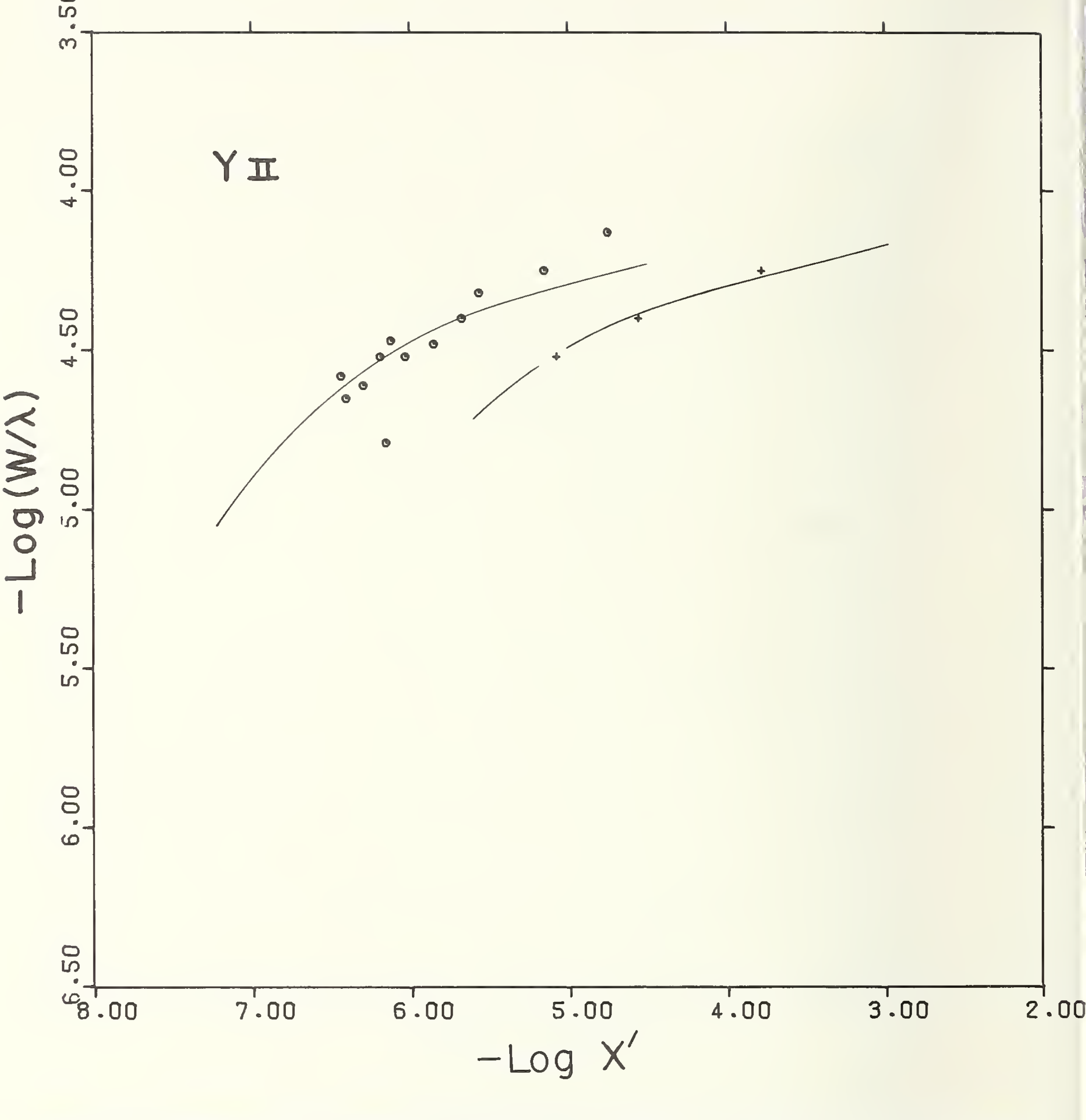

FIGURE 4.11. *Differential curves of growth for singly ionized yttrium relative to the sun* (circles) *and to* ϵ *Virginis* (crosses).

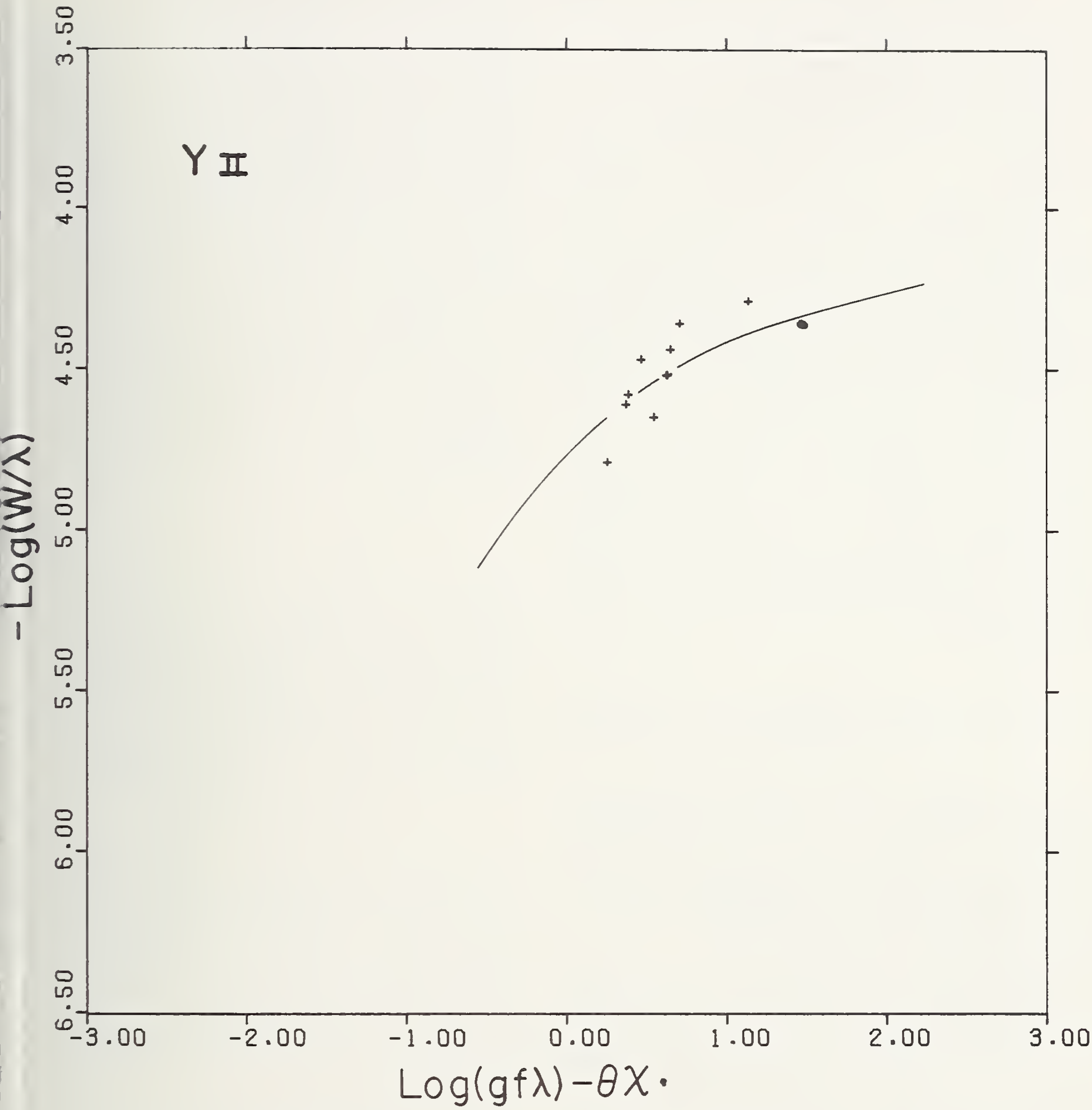

FIGURE 4.12. *Absolute curve of growth for singly ionized yttrium.*

(*Circles*, $\lambda < 5000$ Å; *crosses*, $\lambda > 5000$ Å.)

Now, in the differential curve of growth, the abscissa is

$$\log X'(\epsilon) = \log X(\epsilon) - \Delta\theta(\zeta - \epsilon)\chi. \quad (4.10)$$

But by eq (4.9), this is equivalent to

$$\log X'(\epsilon) = \log (gf\lambda) - \theta(\epsilon)\chi + \delta - \Delta\theta(\zeta - \epsilon)\chi \quad (4.11)$$

or

$$\log X'(\epsilon) = \log (gf\lambda) - \theta(\zeta)\chi + \delta. \quad (4.12)$$

The absolute curves of growth constructed for ζ Cap can, therefore, be treated in the same way as the differential curves in the derivation of relative abundances, provided the correction factors δ are applied to the relative abundances obtained from the observed shifts of the absolute curves. Since these absolute curves of growth tend to be very well defined, the determination of the abundance shifts can be accomplished with exceptional reliability. The analysis is carried out in section 7.1. The absolute and differential curves of growth for five of these spectra are shown in figures 4.3 to 4.12. The absolute curve of growth for praseodymium can be found in the Appendix.

4.4. Theoretical Curve of Growth for ζ Capricorni

Fundamentally, every line of every atom in a stellar atmosphere has a unique curve of growth—there is no "universal" curve. To simplify the analysis of ζ Cap, some one theoretical curve of growth must be selected that most nearly describes the shape of the many empirical curves constructed here for this star.

Hunger (1956) has examined the most common theoretical curves of growth based on simple stellar models (Milne-Eddington, and Schuster-Schwarzschild) and on simple mechanisms for line formation (pure scattering, pure absorption). He concludes that the differences between these curves are so small, i.e., comparable with the errors in the physical data to which they are applied, that the choice of one curve over another matters little in the analysis of a stellar atmosphere in this approximation. As a mean theoretical curve, Hunger recommended the use of that for pure absorption in the M–E approximation or of that for coherent scattering and the S–S model.

With various values assumed for the damping constant, all the major theoretical curves based on simple models (Wrubel, 1949; Hunger, 1956; van der Held, 1931) have been compared with the empirical curves of growth for ζ Cap. The best-fitting curve was not the same for all spectra. Some of this variation could, however, be traced to the effects of blends or to the influence of systematic errors in the stellar line strengths (sec. 6.3) on the shape of the empirical curves. The theoretical curve that offers the best fit to the majority of the empirical curves of growth for ζ Cap, and the one that has been adopted, is that for pure absorption in a Milne-Eddington atmosphere (Hunger, 1956). The quantity R_c, the limiting central depth for strong lines in a given spectral region, appears in the expression for both the ordinate and abscissa of this curve. In most of the following it can be assumed without significant error that $R_c = 1$. For example, the ordinate of the theoretical curve is $\log (W/2R_c b)$, where b, the Doppler width, is given by

$$b = \frac{v_0 \lambda}{c}. \quad (4.13)$$

Since the ordinate is $\log (W/\lambda)$ in the empirical curves, the vertical shift between the empirical and theoretical curves of growth immediately gives the velocity parameter v discussed in section 6.4.2.

The shape of the upper part of the curve of growth is governed by the choice of damping parameter. For ζ Cap, the value of the damping parameter

$$\log 2\alpha = \log (\Gamma/\Delta\omega_D) \quad (4.14)$$

was empirically found to be $\log (2\alpha) = -2.5$ from a comparison of the theoretical curve with those of the empirical curves for which the damping region is reasonably well defined. At 5000 Å the classical radiation damping constant is $\gamma_{cl} = 0.889 \times 10^8$ s^{-1}. (Aller, 1963). The observed damping $\Gamma = 1.4 \times 10^8$ s^{-1} in ζ Cap is thus about 60 percent larger than the classical value.

The normalized theoretical curves of growth for both ζ Capricorni and ϵ Virginis are shown in figure 4.13. The shapes of the two curves are practically identical and can be made nearly to coincide by sliding the curve of ζ Cap down the linear portion to compensate for the difference in velocity parameters for the two stars.

The curve shown in figure 4.13 for ζ Capricorni has been drawn on all the empirical curves plotted in this study.

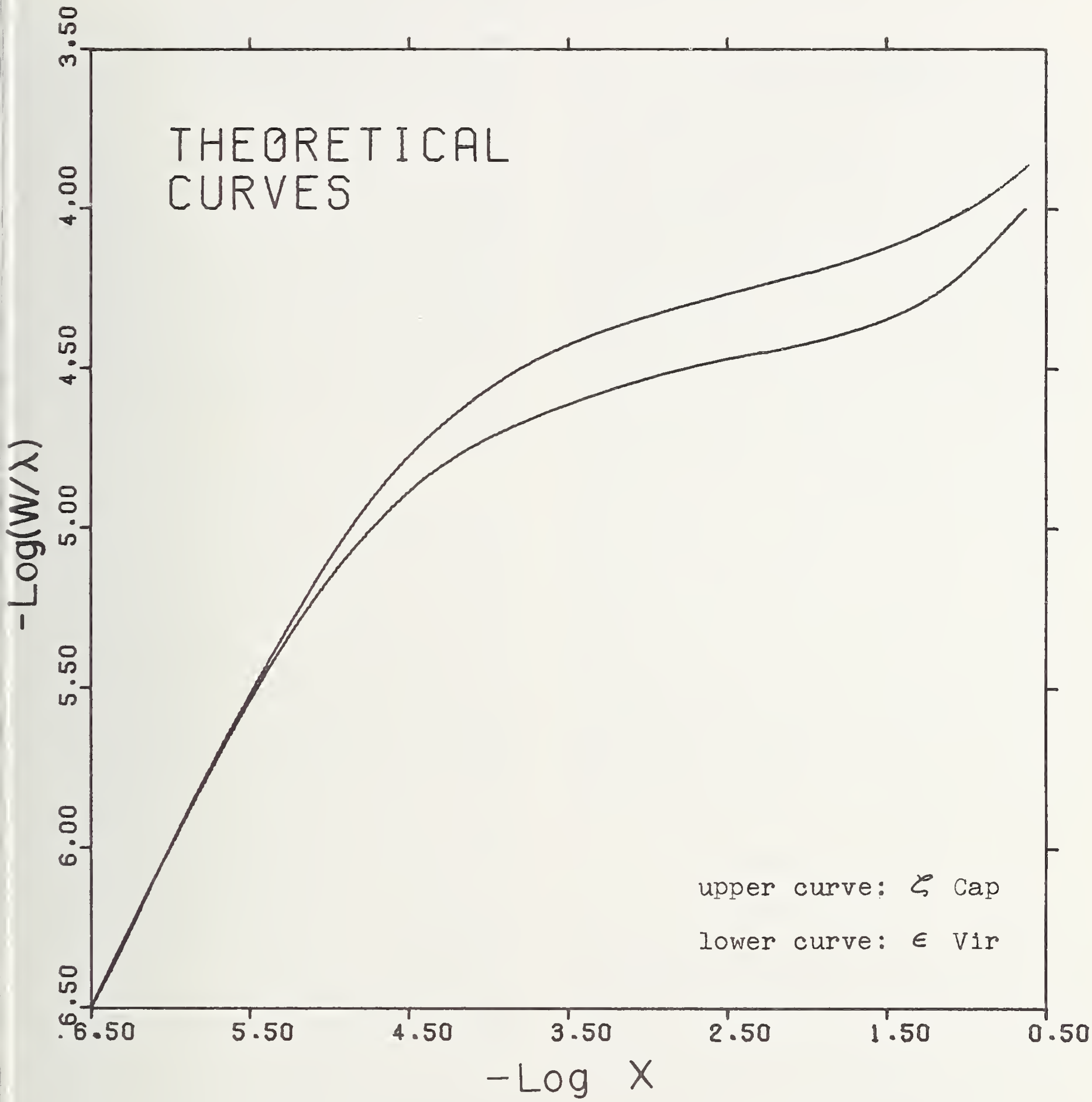

FIGURE 4.13. *Normalized theoretical curves of growth for ζ Capricorni and ϵ Virginis.*

The curve for ζ Cap is that calculated by Hunger (1956) for pure absorption in a Milne-Eddington atmosphere ($\log 2\alpha = -2.5$). The curve for ϵ Vir is taken from the study by Cayrel and Cayrel (1963).

5. Comments on Individual Spectra

5.1. Introduction

Some of the results derived later in this investigation of HD 204075 are closely associated with certain early judgments and spectroscopic details about the individual spectra studied. The writer has, for example, proposed energy transitions for a number of previously unclassified lines of the singly ionized rare earths and has derived new *gf*-values for them from the arc emission intensities given by Meggers et al. (1961). Further, the identifications adopted for many lines differ from those as assigned by Warner (1964b) for this star and, in a few cases, differ also from the solar identifications for the corresponding lines as given in the Second Revision of the Rowland Table (Moore et al., 1966). The interpretation of Sm II in ζ Cap has a bearing on a possible systematic error in the measurement of equivalent widths and also leads to a major revision of some of the *gf*-values in the work by Corliss and Bozman (1962).

Some of the above considerations require explanation or justification and ultimately affect the derivation of chemical abundances and physical parameters for ζ Capricorni. In the next section the most important individual comments are given for the various spectra, arranged alphabetically by element. To avoid unnecessary repetition, certain other results not derived until later in the study are freely quoted in the presentation of this basic background analysis.

5.2. The Spectra

5.2.1. Aluminum

The Al I $4s-5p$ doublet at 6697 Å offers the only lines suitable for an abundance determination. Although the $4s-6p$ doublet at 5558 Å falls within the range of the observational material, it must be excluded from the analysis; one of its members is a severe blend with three Fe I transitions, and the other is masked by a Ce II line.

5.2.2. Barium (Ba I)

Since the primary measurements in ζ Cap revealed no lines of Ba I, the tracings were subsequently examined at the predicted positions of about 20 strong Ba I lines. Most of the lines in the list were either not present or were masked by lines otherwise identified. For example, the strong line of Ba I at 5535.5 Å is masked by a hopeless blend of Nd II, Ce II, and Fe I. Also, the moderately strong line at 5826 Å attributed to Ba I by Warner almost certainly belongs to Nd II.

Central depths have been measured for several remaining features, most of which appear not as distinct lines but only as parts of broader continuum depressions. At two of the measured wavelengths (5971.70 and 6595.33 Å), unidentified weak lines appear also in the solar spectrum. It may be unsafe to attribute any of these features in ζ Cap to Ba I, but the measured equivalent widths can be regarded as useful upper bounds. In any case, the presence of Ba I in ζ Cap has *not* been unambiguously established.

5.2.3. Barium (Ba II)

Only four Ba II lines occurred in the primary list. Since they are all strong lines falling on the damping portion of the curve of growth, an effort was made to locate fainter lines that might help to define the weak portion of the curve of growth more positively. An examination of the microphotometer tracings at the positions of all Ba II lines listed in the Revised Multiplet Table yielded only two additional lines. One of them, at 4524.93 Å, occurs as one of three dips in a broad profile caused by blending with adjacent lines of Ti II (4524.73 Å) and Fe I (4525.15 Å). By using the correlation between central depth and equivalent width discussed in section 2.3.2, equivalent widths were derived for all three lines. The reliability of the Ba II measurement was then tested by demonstrating that the Fe I and Ti II lines, measured in the same way, fit acceptably onto their already well-populated curves of growth.

The second line, a weak feature at 6379.94 Å, probably corresponds to a similar line observed in the solar spectrum. The measurement of this line in ζ Cap yielded an equivalent width of 19 mÅ. No identification is attached to the line in the Revised Rowland Table, but Warner has provisionally identified it in ζ Cap as belonging to Ba II. On the basis of a new compilation of oscillator strengths for Ba II (Miles and Wiese, 1969) the line would be roughly 30 times too strong to be attributed to Ba II. The line may be a blend having Mn I as a contributor.

5.2.4. Cadmium

If present in ζ Cap, the strong red line of cadmium at 6438 Å would fall in a portion of the tracings very favorable for its detection, but the continuum at that position is undisturbed. A line with equivalent width 101 mÅ was measured at 4678.16 Å, but it probably corresponds to a moderately strong unidentified feature at the same wavelength in the solar spectrum rather than to Cd I.

5.2.5. Cerium

Twelve Ce II lines for which *f*-values were previously unavailable have been measured in ζ Cap. Recent progress in the analysis of Ce II by Z. Goldschmidt (1968) has made it possible to calculate new *gf*-values for these lines by using her new level values in conjunction with the line intensities given in NBS Monograph 32. A new *gf*-value has also been calculated for the line at 5359.50 Å, in accordance with its revised classification by Goldschmidt. By using her level values, tentative classifications have been found for three additional lines not included in her list. The results are given in table 5.1. The values cited for the quantity log $(gf\lambda)$ do not incorporate the corrections suggested in section 3.2.3 of the present study.

The Ce II curve of growth constructed by use of the NBS *gf*-values (fig. 4.4) shows little scatter and provides evidence that the Ce II lines measured in ζ Cap are relatively unblended. Only the lines at 4604 and 5610 Å depart significantly from the mean curve. The large half-width measured for the latter line suggests that it is a blend, probably with C_2. According to the Pr II curve of growth, the Pr II line of the same wavelength would not significantly contribute to the observed line. The line at 4604.18 Å appears to belong predominantly to Sm II.

TABLE 5.1. *NBS gf-values for recently classified lines of* Ce II

Wavelength	Intensity (NBS)	Energy levels	Low EP	log $(gf\lambda)$
(Å)		(cm^{-1})	(eV)	
4413.19	8	9198–31851	1.14	3.01
4484.83	12	9054–31345	1.12	3.15
4608.76	3	11388–33080*	1.41	2.81
4659.40	4	9779–31235	1.21	2.73
4686.81	6	8804–30135	1.09	2.78
4702.01	6	6550–27812	0.81	2.50
4753.65	2	10314–31345*	1.28	2.47
5347.81	3.5	5969–24663*	0.74	2.10
5359.50	2.5	14387–33040	1.78	2.99
5468.37	15	11310–29592	1.40	3.38
5556.97	6	14517–32508	1.80	3.36
5959.69	3.5	13118–29893	1.63	2.93
6143.36	4	13676–29949	1.70	3.05

*Tentative classification suggested by the writer.

5.2.6. Dysprosium

The three Dy II lines measured on the tracings of ζ Cap have provided the first abundance determination for dysprosium in a barium star. Surprisingly, a large overabundance is indicated. Dysprosium is a predominantly *r*-processed rare earth and had been expected to show (like europium) a relatively normal abundance in these stars. Even though the dysprosium abundance has been derived from only three lines, the determination is regarded as fairly reliable.

Unfortunately, two of the measured Dy II lines occur in the unfavorable spectral region below 4300 Å, where line crowding is severe. To establish the general correctness of the adopted continuum in the vicinity of the Dy II lines, several nearby lines belonging to other spectra were also measured and shown to fit reasonably on their already well-populated curves of growth.

Figure 5.1 shows a comparison of the microphotometer tracing of ζ Cap (solid line) with that of η Pegasi (dashed line) in the spectral region near 4070 Å. As already mentioned, the spectrum of η Peg (G2 II–III) is quite similar to that of ζ Cap except for the enhancement of lines arising from elements such as cerium and neodymium, for which definite overabundances in the barium star have been derived. It is seen that the Fe I lines are of comparable intensity in the two objects, but those of W I, Nd II, Ce II, Zr I, Zr II, and Dy II are all enhanced in ζ Cap. The second Dy II line in this region, at 4103.34 Å, is similarly enhanced with respect to the corresponding line in η Peg. The fact that Dy II behaves like Ce II and Nd II in this respect is interpreted as qualitative evidence that the overabundance derived for dysprosium in ζ Cap is real.

The third Dy II line, at 5169.71 Å, falls in the wing of an adjacent strong blend of Fe I and Fe II. The measured equivalent width is therefore not very accurate but is considered to be a good upper limit. The location of this line on the differential curve of growth with respect to the sun (fig. 5.2) is not consistent with the two other Dy II lines and adds considerable uncertainty to the abundance determination. This line alone suggests an almost normal

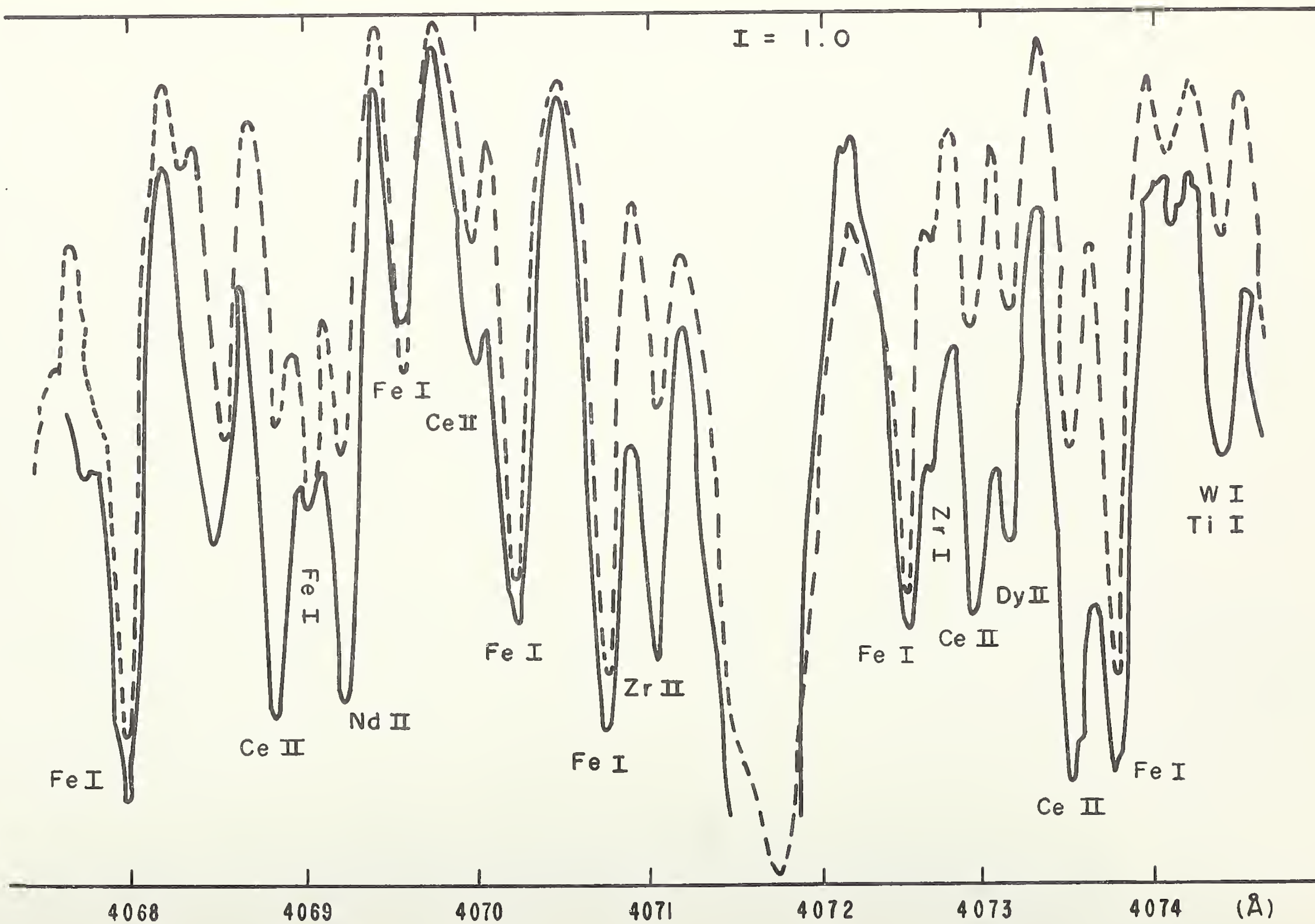

Figure 5.1. *Intensity tracings of the spectra of ζ Capricorni* (solid line) *and η Pegasi* (dashed line) *in the vicinity of* Dy II λ *4073.12.*

Note that the Dy II line is enhanced in ζ Cap relative to the comparison star. The same behavior is exhibited for lines arising from elements for which definite overabundances have been established in ζ Cap. The zero-intensity levels of the two tracings fall off the page but coincide within 10 percent.

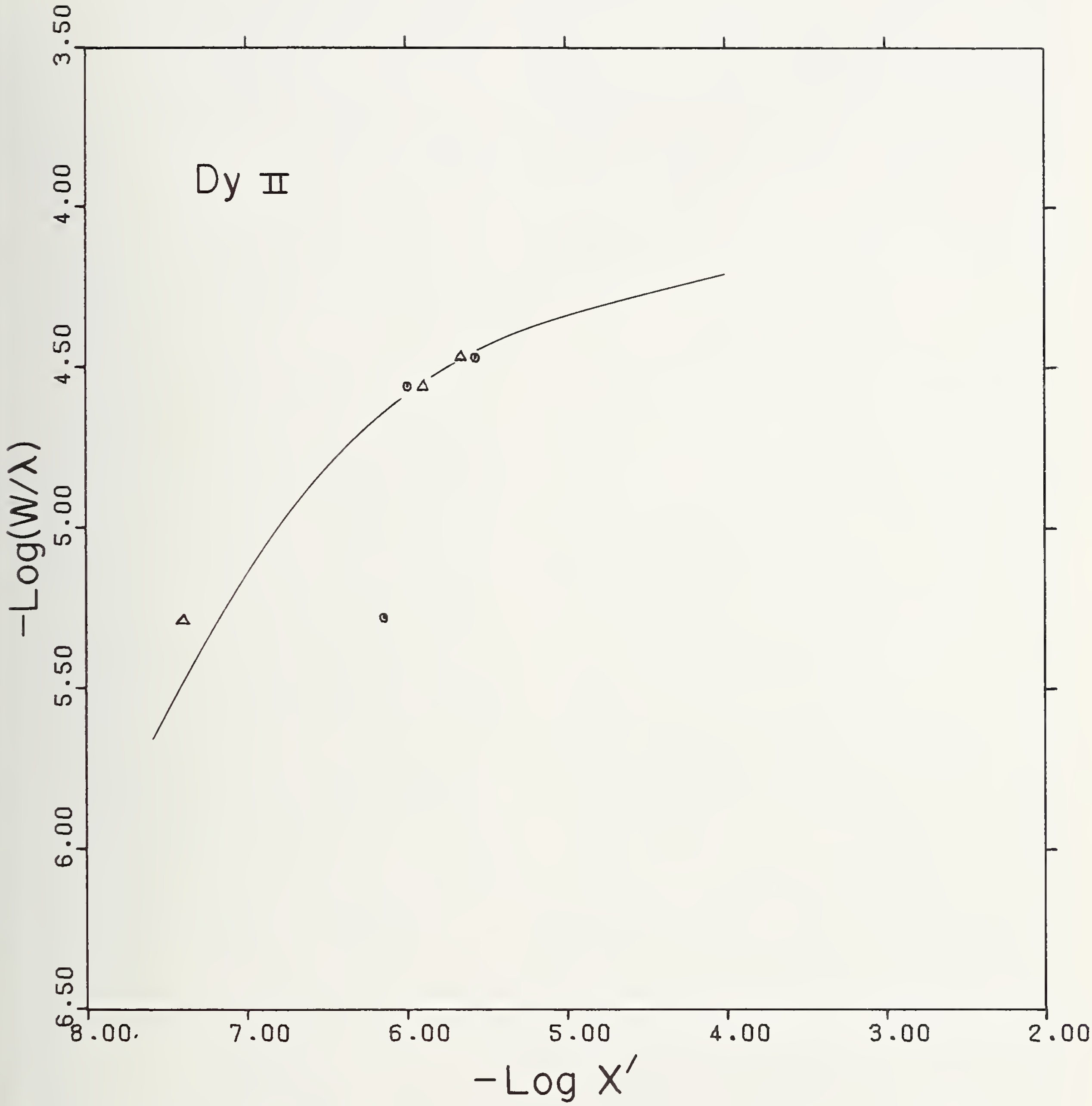

FIGURE 5.2. *Differential curve of growth for dysprosium relative to the sun* (circles).

The absolute curve of growth (*triangles*) constructed by use of *gf*-values has been superimposed on this figure.

dysprosium abundance in ζ Cap. However, a more detailed examination has shown that the Dy II identification given in the Revised Rowland Table for this line is almost certainly incorrect. By use of *gf*-values, it was found that λ 5169 is an order of magnitude too strong to fit the mean solar curve of growth defined by nine other Dy II lines. C. E. Moore has pointed out to the writer that she earlier regarded this line as a blend with Fe II. In figure 5.2 the absolute curve of growth for Dy II in ζ Cap has been superimposed on the differential curve. It is seen that, when *gf*-values are used, the line at 5169 Å does not depart significantly from the theoretical curve fitted to the stronger lines.

5.2.7. Europium

Only three europium lines, all belonging to Eu II, have been measured in the spectrum of ζ Cap. In deriving the europium abundance from the differential curve of growth with respect to the sun, greatest weight has been assigned the unblended line at 6645 Å. The equivalent width of the line at 4129 Å in ζ Cap is somewhat uncertain because of the difficulty in making accurate measurements in that part of the spectrum. Slight blending with a weak Ce II line is also suspected.

The solar line strength for the remaining Eu II line, at 6437 Å, is definitely too large. According to the Revised Rowland Table, the solar line has an unidentified contributor on its long wavelength side. This is confirmed also by the ratio of the *gf*-values for $\lambda\lambda$ 6645 and 6437. Both lines fall on the linear part of the curve of growth and have essentially the same excitation potential.

5.2.8. Iron (Fe I)

Because of the large number of iron lines measured in ζ Cap, it is unnecessary to examine all the identifications in detail. A few undetected blends or misidentifications will not significantly affect the curve of growth or the resultant relative abundance for iron. However, several lines originally identified with iron have been reassigned to other spectra on the basis of their wide divergences from the iron curve of growth. In this category are the lines at 5804 Å (Nd II), 5680 Å (Ce II), and 5805 Å (La II).

5.2.9. Lanthanum

The La II line at 6526 Å offers a good example of a case where an equivalent width derived from central depth is more reliable than that measured by planimetry. The half-width (469 mÅ) of this line is far in excess of that expected from its central depth (0.50). The reason for this is that the line is flanked on each side of its profile by somewhat weaker lines of Si I. The Si I contributions broaden the line, but are sufficiently separated in wavelength that they do not seriously affect its central depth. The equivalent width derived from its central depth is 184 mÅ, whereas that found by direct planimetry is 260 mÅ.

5.2.10. Lithium

Weak absorption at the position of the Li I resonance doublet was measured in ζ Cap to have an equivalent width of 29 mÅ, which is about 25 percent the value obtained by Warner. At lower dispersions, blending with an unidentified feature at λ6707.45 (Fe?) often interferes with the accurate measurement of the lithium absorption (Bonsack, 1959; Rodgers and Bell, 1968), but on the tracings of ζ Cap the broad lithium doublet is well separated from that feature. In the light of the discussion of samarium below, Warner's identification of λ6707.45 as belonging to Sm II (Rodgers and Bell, 1968) is subject to serious doubt.

In table A the Utrecht measurement is quoted for the equivalent width of the lithium doublet in the sun, but in the derivation of the differential abundance of lithium in ζ Cap preference has been given to the value $\log (W_{\odot}/\lambda) = -6.15$, as found by Greenstein and Richardson (1951).

Warner (1965) has derived a useful relation giving the abundance of lithium relative to the sun when the line is unsaturated and H^- is the dominant source of opacity. He shows that

$$\log \frac{N^*(\mathrm{Li})}{N^{\odot}(\mathrm{Li})} = \log \frac{W^*(\mathrm{Li})}{W^{\odot}(\mathrm{Li})} - 4.93(\gamma - 1) \qquad (5.1)$$

where $\gamma = \theta^*_{\mathrm{eff}}/\theta^{\odot}_{\mathrm{eff}}$. By assuming that

$$\frac{\theta^{\zeta}_{\mathrm{eff}}}{\theta^{\odot}_{\mathrm{eff}}} = \frac{\theta^{\zeta}_{\mathrm{ion}}}{\theta^{\odot}_{\mathrm{ion}}}, \qquad (5.2)$$

and using the values obtained below, it follows that

$$\log \frac{N^{\zeta}(\mathrm{Li})}{N^{\odot}(\mathrm{Li})} = +0.24 \qquad (5.3)$$

which, as expected for the reasons cited by Warner, is somewhat smaller than the value $+0.33$ derived below on the assumption of an isothermal atmosphere.

5.2.11. Magnesium

The weaker Mg I lines at 6318.72 and 6319.22 Å have fairly good profiles on the tracings. Since the other unblended Mg I lines are so strong, these two fainter lines are quite valuable in fixing the shoulder of the Mg I curve of growth.

5.2.12. Molybdenum

Although five lines have been attributed to Mo I in table B, these identifications must be considered as tentative. Only the line at 6030.66 Å shows an undisturbed profile. The measured equivalent widths for the lines at 4411 and 5506 Å, which appear as side distortions on the profiles of adjacent strong lines, are not entirely trustworthy.

5.2.13. Neodymium

The recent analysis of Nd II by Wyart (1968) has made it possible to calculate *gf*-values for 13 previously unclassified lines of Nd II that have been observed in ζ Cap. Also, the *gf*-value and excitation potential of the line at 5745 Å have been changed from the NBS values to conform with Wyart's revised classification for this line. Tentative classifications have been found for two lines not included in the work by Wyart. The new data are summarized in table 5.2. The values cited for the quantity log (*gf*λ) do not reflect the corrections suggested in section 3.2.3 of the present study.

TABLE 5.2. *NBS* gf-*values for recently classified lines of* Nd II

Wavelength	Intensity (NBS)	Energy Levels	Low EP	log (*gf*λ)
(*Å*)		(cm^{-1})	(*eV*)	
4563.22	20	1470–23378*	0.18	2.08
4817.18	3.0	5986–26739	.74	1.76
4818.96	2.0	3802–24547	.47	1.31
5385.88	12	5986–24547	.74	2.28
5744.76	5	10883–28286	1.35	2.47
5753.51	3.0	1650–19026	0.20	1.12
5769.86	4	10887–28214	1.35	2.38
6009.30	1.6	3067–19703	0.38	1.01
6382.06	2.5	11581–27246	1.44	2.23
6385.20	7	9358–25014*	1.16	2.40
6428.64	2.0	1650–17201	0.20	0.91
6549.52	1.6	513–15777	.06	.67
6550.19	1.6	2585–17848	.32	.93
6591.43	1.2	1650–16817	.20	.69

*Tentative classification suggested by the writer.

5.2.14. Nickel

A line measured at 5347.79 Å was initially attributed to Ni I, but the nickel curve of growth for ζ Cap does not permit this identification. The line is too strong by about 400 percent to fit on the curve of growth. A line at 5347.81 Å is listed as Ce I in NBS Monograph 32, but an examination of the unpublished cerium line lists of Martin and of Albertson reveals a peculiarity in the behavior of this line that suggests it may be a blend of Ce I and Ce II. Its strength in the spectrum of ζ Cap supports that conclusion. The measured equivalent width of 42 mÅ, as well as the line intensity given in NBS Monograph 32, must represent the Ce II component of this line.

5.2.15. Oxygen

Weak lines observed at 6300.32 and 6363.80 Å have been identified as the forbidden $2p^4\,{}^3P_{2,1} - 2p^4\,{}^1D_2$ transitions of [O I]. The first of these is badly blended on the longer wavelength side of its profile, but the line at 6363 Å is well isolated on the tracings. The solar equivalent widths for these lines are taken from the work of Goldberg, Müller, and Aller (1960). Unfortunately, the green forbidden line at 5577 Å is masked by strong C_2 absorption in ζ Capricorni.

5.2.16. Praseodymium

Unfortunately, praseodymium is a very difficult element in barium stars. Many of the available Pr II lines are badly blended, often with lines belonging to other enhanced spectra, including CH. Even at high dispersion such blending inflates the measured equivalent widths of most of the Pr II lines available in the blue region. Each of the three moderately strong lines that would help to establish the shoulder of the Pr II curve of growth is a blend with Ce II. These lines, at 4408, 4413, and 4510 Å, have here been given less weight in the determination of the praseodymium abundance. The solar line strengths obtained for the lines at 4570.61 and 4612.07 Å have also been given less weight, because it is doubtful whether these lines in the solar spectrum actually belong to Pr II.

5.2.17. Ruthenium

The Ru I lines most likely to be present with any intensity in the range 4000 to 4800 Å all coincide with strong lines otherwise identified. The strongest expected line falls exactly on the 4554 line of Ba II. If ruthenium were sufficiently abundant, the lines at

4584 Å and 4709 Å would seem to have the best chance of detection on the tracings. These wavelengths place them in relatively isolated positions on the tracing, but still in the wings of adjacent lines. Figure 5.3 shows that there are slight dips in the continuum at these wavelengths, but these may not be real. Although the identifications are relatively insecure, the derived equivalent widths would at least represent maximum values for these lines. When plotted on a $gf\lambda$-curve of growth, the points for these lines appear reasonably situated, but this may be fortuitous. The abundance obtained for ruthenium is not markedly different from that obtained by Warner. Of the three lines used by Warner in deriving a ruthenium abundance, however, we feel that one is a strong Fe II line, one is an unblended CH line, and the third is a Cr II line blended with C_2. The final derived ruthenium abundances, therefore, cannot be directly compared.

5.2.18. Samarium

It is obviously impractical and undesirable to set forth at length the individual complexities that each of the more than 40 spectra observed in ζ Cap has presented. It is perhaps justifiable, however, to explore in some detail the problems encountered in the treatment of Sm II, mainly because of its bearing on the need suggested earlier for a recalibration of the extensive collection of f-values by Corliss and Bozman (1962).

The original measurements included Sm II lines only shortward of 5000 Å, many of which are seriously blended. It was expected that the determination of the samarium abundance could be improved by finding some other suitable lines in the red. Although Warner (1964b) includes six red lines in his samarium analysis, it now appears doubtful whether any of those lines contains a significant Sm II contribution. This group of lines is summarized in table 5.3.

A survey of the tracings yielded eleven weak lines in the range 5300 to 6700 Å that may belong to Sm II. The measured central depths and derived equivalent widths must be considered as upper limits, because most of the lines are weak features without distinct profiles. When plotted on an absolute curve of growth with gf-values from NBS Monograph 53, these lines fall very much below the mean curve defined by the blue lines, as shown in figure 3.3. The samarium abundances implied by the lines in the two spectral regions differ by a factor of more than two. Efforts to improve the data have thus made matters even worse, but fortunately this dilemma can be resolved and leads to consequences of some importance, as described below.

TABLE 5.3. *Suggested revision of Warner's (1964b) Sm II identifications > 5000 Å*

Wavelength	$-\log (W/\lambda)$ (Warner)	Probable identification	Note
5719.12	4.88	Pr II + Nd II	
5779.25	4.84	Fe I	1
5867.79	4.98	Ca I	2
6389.87	5.02	Nd II	3
6628.88	5.34	Ce II	4
6754.68	5.25	Sm II?	5

Notes

1. No line is present at this wavelength on the higher dispersion tracings used here. The measurement must refer to the Fe I line at 5778.78 Å.
2. The samarium line of this wavelength belongs to Sm I.
3. On our plates a line was measured at 6390.00 Å, which agrees with a laboratory wavelength of Nd II. The samarium line at 6389.87 Å would have been partially resolved, if present.
4. Although a Ce I line is listed at this position in several laboratory sources, a check with the unpublished cerium observations of Martin leaves little doubt that there is a Ce II line of nearly the same wavelength, thus explaining its appearance in ζ Cap.
5. This line falls beyond the range of the present measurements.

The possibility emerges, then, that there does indeed exist a systematic error in the present material that has resulted in underestimated equivalent widths for the red, as previosuly indicated by the comparison with Warner's measurements in figure 2.5. However, this argument would still not be consistent with the differential curves of growth, which show no conclusive wavelength dependence. In any case, the extent of the shift observed in Sm II considerably exceeds that suggested by the comparison with Warner or that allowable by an alteration of the adopted continuum. A second possibility is that the blue section of the curve of growth is substantially raised by the effects of blending. Some of these lines are severely blended, but it is regarded as unlikely that *all* of them are thus affected.

Further attempts to resolve this discrepancy in Sm II led to an examination of the f-values themselves and to the conclusion that they contain a calibration error. The nature of this error has already been discussed in section 3.2.3. In particular, application of the correction suggested by that discussion brings the results for Sm II in the two wavelength regions into satisfactory agreement.

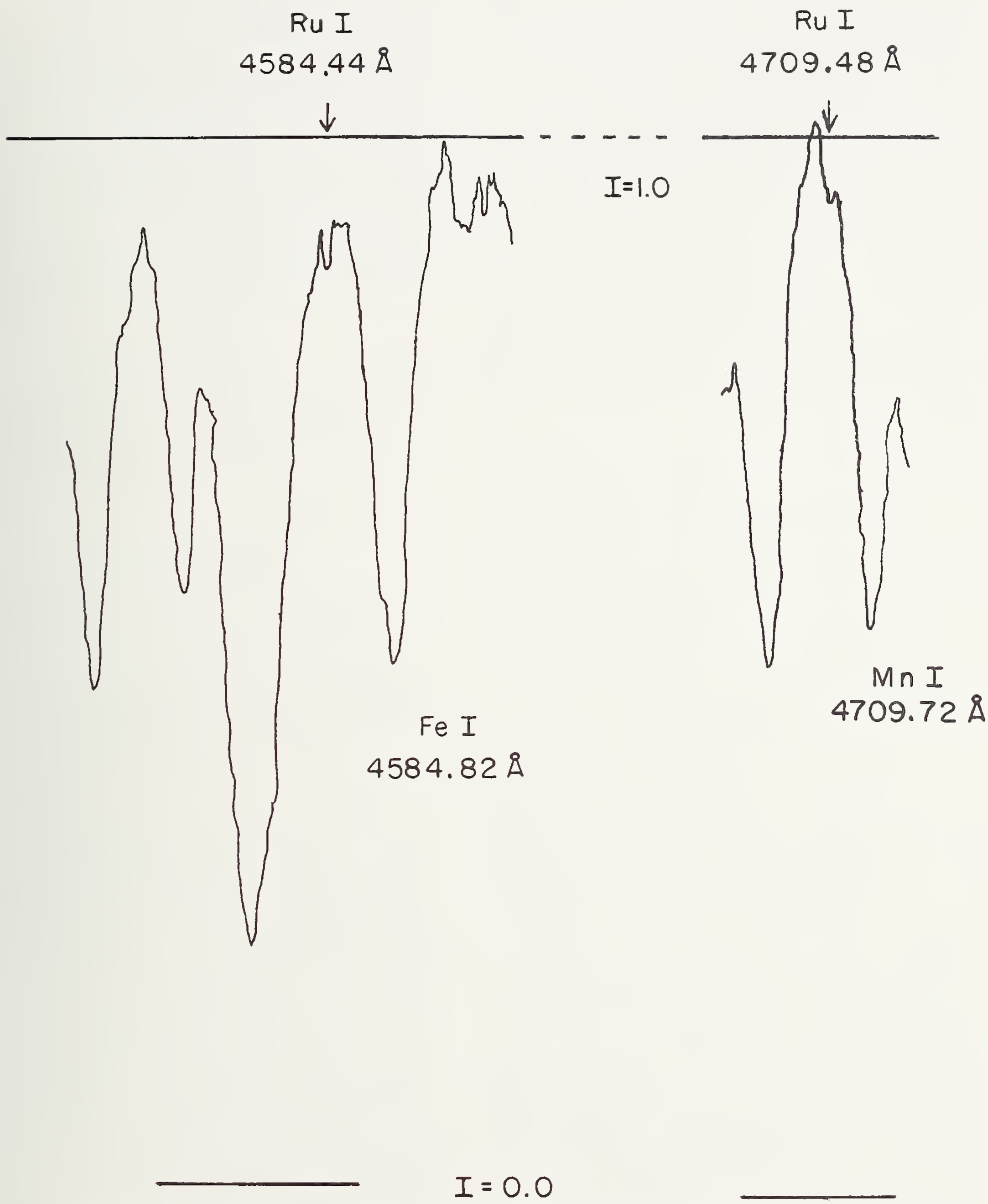

FIGURE 5.3. *Microphotometer tracing of the spectrum of ζ Capricorni in the vicinity of two* Ru I *lines.*

5.2.19. Scandium

The first spectrum of scandium is represented in ζ Cap by a very unsatisfactory group of weak lines whose equivalent widths could be only poorly measured. The Sc I line at 5700 Å is strongly blended with Cu I. The observed line is assigned to both spectra, but Cu I appears to be the dominant component. Certain intensity anomalies indicate the presence of blending in some of the remaining lines. For example, both in the sun and in ζ Cap (but not in ε Vir) the pair of lines 6210/6239 Å show an intensity relation opposite to that observed in laboratory sources, even though the lines have the same excitation potential. The same situation is observed for the pair 5355/5356 Å, the second member of which is not present on the tracings of ζ Cap.

5.2.20. Silicon

A weak line appearing at 5675.73 Å in the spectra of both ζ Cap and the sun is considered likely to have the same chemical origin in the two objects. Charlotte Moore tentatively identifies it in the Revised Rowland Table as belonging to Si I. Since this line departs significantly from the mean silicon curve of growth for ζ Cap, the correctness of the identification becomes more doubtful, but the line has been retained in our list.

5.2.21. Strontium

Although sparsely populated curves of growth cannot be expected to yield trustworthy stellar abundances, a consistent result from a double differential analysis of the type used here gives slightly increased confidence in abundances derived from just a few lines.

The strontium abundance in ζ Capricorni is based solely on the resonance line of Sr I at 4607.33 Å. The solar line strengths for the three remaining lines measured in the barium star must be given low weight because of the inherent difficulty in measuring such faint lines in the solar spectrum. The Sr I line lists for ε Vir and ζ Cap have only three lines in common, the two weaker of which appear to be blends in ε Vir.

Apart from these considerations, the three weak lines given in the Sr I list for ζ Cap are themselves so seriously blended as to be unsatisfactory for use in the determination of the strontium abundance. The intensities of other nearby lines of CN indicate that a significant fraction of the measured Sr I λ6508 absorption is due to a coincident CN line. The line at 6550 Å belongs predominantly to Sm II, and that at 6504 Å is a broad blend of Sr I with V I and Pr II. Other lines from Sr I and Sr II were considered too strong to be of any use or too hopelessly blended to yield even approximately reliable equivalent widths.

5.2.22. Sulfur

The relative intensities observed in ζ Cap for the S I pair of lines 6046/6052 Å are in the same order as those given in the Revised Multiplet Table, but are reversed in comparison with those observed in the sun or in ε Vir.

5.2.23. Technetium

From the new Tc I analysis by Bozman, Corliss, and Tech (1968), a group of about 25 lines judged most likely to be present in the spectrum of ζ Cap was selected. A careful examination of the complete line list for ζ Cap (3883–8700 Å) did not yield any positive evidence for the presence of Tc I in this spectrum.

5.2.24. Titanium (Ti II)

Unfortunately, the stronger lines of Ti II in the list are all affected by blending, mainly with lines of Ce II. We have given less weight to these lines in fitting the curve of growth.

5.2.25. Vanadium

Among the lines of V I measured are some rather bad blends with Gd II, Nd II, and CH. Less weight was given to these recognized blends in fitting the curve of growth and deriving the vanadium abundance.

6. Atmospheric Parameters for ζ Capricorni

6.1. The Excitation Temperatures

Measurements in the line spectrum of ζ Cap permit a direct spectroscopic determination of the mean excitation temperature. In the approximation used here, a Boltzmann correction accounting for the differing populations of the atomic energy levels appears as an additive term in the expression for the abscissa of the curve of growth and effectively reduces all curves to that for resonance lines. In absolute curves of growth the quantity plotted along the abscissa is

$$\log X' = \log\,(gf\lambda) - \theta_{\mathrm{exc}}\chi \tag{6.1}$$

and in differential curves,

$$\log X' = \log X - \Delta\theta_{\mathrm{exc}}\chi. \tag{6.2}$$

The stellar line strength, log X, is obtained by reading the equivalent width observed in the standard comparison star into its empirical or theoretical curve of growth. The quantity $\Delta\theta_{\mathrm{exc}}$ is given by

$$\Delta\theta_{\mathrm{exc}} = \theta_{\mathrm{exc}}\,(\zeta\ \mathrm{Cap}) - \theta_{\mathrm{exc}}(\mathrm{standard}) \tag{6.3}$$

and χ is the excitation potential of the lower level of the transition.

If the range of excitation of the lines plotted is sufficiently restricted, as by using lines belonging to the same multiplet, the Boltzmann correction remains effectively constant. The quantities θ_{exc} or $\Delta\theta_{\mathrm{exc}}$ can therefore be determined in the following way (Aller, 1963). Separate curves of growth are prepared for lines in each of several small excitation ranges. The horizontal shifts required to bring the separate curves into best coincidence or onto an average fit with some theoretical curve will, according to the above expressions for log X', be linearly related to the mean excitation potential of the lines used in the separate curves. The gradient of this linear function is taken as defining the mean excitation temperature.

The procedure just described has several important drawbacks. To obtain an accurate mean temperature, it is necessary to have measurements of high quality for a large number of unblended lines covering a sizable range of excitation. Using such observational material for Arcturus, for example, Griffin and Griffin (1967) constructed numerous partial curves of growth whose relative shifts yielded remarkably well-defined excitation temperatures for Ti I and Fe I. More commonly, it is necessary to take rather large (~ 1 eV) ranges of excitation in order to populate the individual curves of growth satisfactorily. This is true even for neutral iron, which has a well-developed spectrum in many stars of interest. In a star with $\theta_{\mathrm{exc}} = 1.00$, this leads to a horizontal spread due to temperature alone of 1 dex in the individual absolute curves of growth.

The derived temperature can also depend markedly both on the way in which the available lines are separated into excitation ranges and also on the way in which the horizontal shifts are made to bring the curves into "best" visual coincidence. Using the same observational material for Fe I in ϵ Vir, Griffin and Griffin (1967) and Cayrel and Cayrel (1963) obtained $\Delta\theta_{\mathrm{exc}} = 0.13$ and $\Delta\theta_{\mathrm{exc}} = 0.18$, respectively, for the differential excitation temperature of ϵ Vir relative to the sun.

In an attempt to overcome these difficulties, the following method has been adopted for obtaining spectroscopic temperatures. A preliminary estimate of θ_{exc} or $\Delta\theta_{\mathrm{exc}}$ is chosen and the quantity $\log X'$ is computed for each of the observed lines of a given element. A least-squares cubic or quartic polynomial is then calculated to give the best representation of log X' as a function of log (W/λ). The standard deviation σ of the points from this mean curve in a direction parallel to the $\log X'$-axis is affected by the choice of temperature. By iterating the calculation for several values of θ_{exc} around the initial estimate, a series of σ-values is obtained that describes the variation in the scatter of the curve of growth as a function of assumed temperature. A graph of this function is found to be a smooth one with a unique minimum. The mean temperature is taken to be that value for which σ is least. Virtues of this method are as follows: (a) each line is treated separately with its correct excitation potential rather than in a group with other lines covering a finite range of excitation; (b) the method gives dispassionately reproducible results; (c) a system of weights can be applied to the lines with little additional effort. For example, Unsöld (1955) recommends that higher excitation lines should be more heavily weighted, because any error in the choice of temperature will have more effect on the positions of these lines in the curve of growth than on lines of lower excitation. In the application of the minimum-sigma method this was approximately achieved because, in general, there are more medium and high excitation lines than low. Trial calculations with a system of weights equal to the excitation potentials did not produce significantly different results.

A major disadvantage of this method is that great care must be exercised in assuring that no widely discordant lines are used in the analysis. In general, lines on the flat or damping portions of the curve of growth should also be excluded. Such lines will dominate the value of the standard deviation and mask the smaller excess caused by using a slightly incorrect temperature. In addition, it must be established that the mean curve from which the deviations are calculated really does represent the distribution of points adequately.

As a test of this procedure, the mean excitation temperature for iron in ϵ Vir has been determined with a rather different group of lines from that used by the Cayrels in their determination of the temperature. The lines used are those measured in ζ Cap that also appear in the Cayrels' line list for ϵ Vir, about 180 in all. The use of solar line strengths obtained from the Pierce-Aller curve of growth gave a differential temperature of 0.19, as shown in figure 6.1. By use of the f-values given by Corliss and Tech (1968), an absolute temperature of 1.21 was also derived (fig. 6.1). The differential temperature relative to the sun is in good agreement with the value 0.18 derived by the Cayrels and 0.17 by Nishimura (1967) for ϵ Vir.

For later use, an absolute temperature determination based on about 300 Fe I lines observed in ζ Cap was similarly made for the sun. The solar equivalent widths used are those taken from the Revised Rowland Table and listed in Table A. The analysis, shown in figure 6.2, yields the value $\theta_{\mathrm{exc}}(\odot)=1.02$, which is in agreement with a value predictable from the above results for ϵ Vir, namely,

$$\theta_{\mathrm{exc}}(\odot)=\theta_{\mathrm{exc}}(\epsilon)-\Delta\theta_{\mathrm{exc}}(\epsilon-\odot)=1.21-0.19=1.02. \tag{6.4}$$

Values for $\theta_{\mathrm{exc}}(\odot)$ currently quoted in the astrophysical literature range from about 0.98 (Cowley and Cowley, 1964) to 1.06 (Warner, 1964a).

The absolute temperature of ζ Cap has been derived from about 300 Fe I lines for which f-values were available. The minimum-sigma criterion yields $\theta_{\mathrm{exc}}(\zeta)=1.13$, as shown in figure 6.2. Since the same group of lines was used in deriving the solar temperature, the vertical separation in this figure between the plots for the sun and for ζ Cap reflects the difference in the contributions of the equivalent widths and of the length of the transition portions of the respective curves of growth to the total scatter.

Differential temperatures for ζ Cap with respect to both the sun and to ϵ Vir have been similarly determined from lines of Fe I, Ni I, Ti I, and Cr I. These are the only spectra with a sufficient number of measured lines and wide enough range of excitation potentials to be useful for this purpose. The value obtained for $\Delta\theta_{\mathrm{exc}}(\zeta-\epsilon)$ may be poor in the case of Cr I because the requirements just stated are only marginally satisfied. The V I curve of growth is sufficiently populated, but the lines differ very little in excitation. A summary of the results is presented in the following table.

TABLE 6.1. *Differential excitation temperatures of ζ Cap relative to the sun and to ϵ Vir*

Spectrum	$\Delta\theta_{\mathrm{exc}}(\zeta-\odot)$	No. of lines	$\Delta\theta_{\mathrm{exc}}(\zeta-\epsilon)$	No. of lines
Fe I	0.10	328	−0.09	189
Ni I	.09	45	−.09	24
Ti I	.09	45	−.08	34
Cr I	−.01	35	−.14	21

As has been discovered in other stellar analyses (Cayrel and Cayrel, 1963), the lines of Cr I require a significantly different excitation temperature from that of other neutral spectra in the iron group. A satisfactory explanation has not yet been proposed for the effect. It seems improbable that chromium should be excited in different layers of the atmosphere from other elements of similar ionization potential. The *ad hoc* appeal to such selective stratification of elements remains unconvincing in the absence of a reasonable mechanism to produce it. A nonequilibrium population of the low odd levels near 3.00 eV, or differential damping effects (Sandage and Hill, 1951) between lines from lower odd and lower even levels would also influence the determination of the excitation temperatures. It may be relevant in this connection that the term structure in Cr I is such that there is an unusually large number of level differences that very nearly repeat and lead to doubly or triply classified lines. This problem does not, in general, affect the low-level lines.

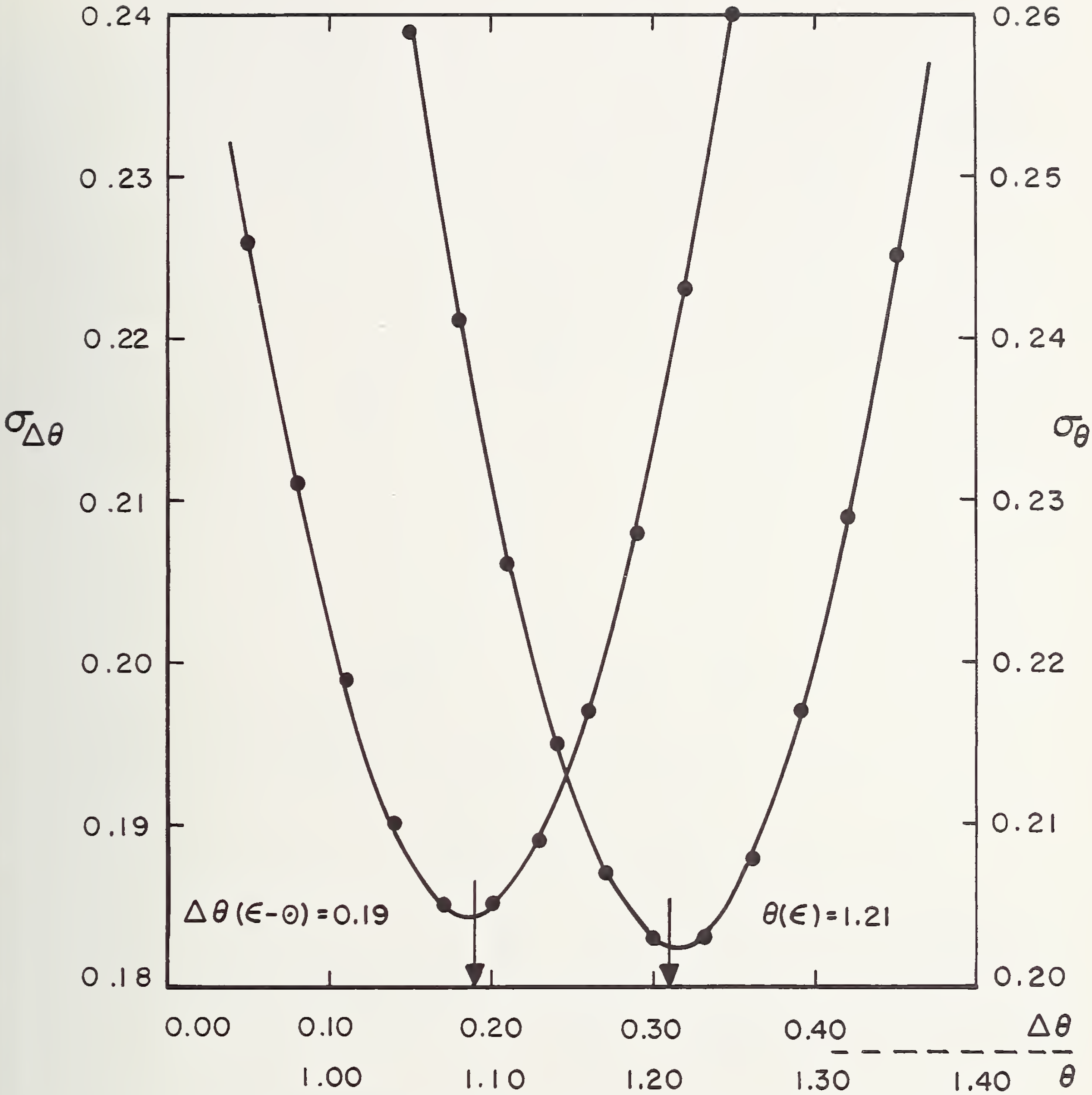

FIGURE 6.1. *Determination of absolute and differential excitation temperatures for ε Virginis.*

(*Abscissa*, assumed temperature; *ordinate*, standard deviation of horizontal scatter in the curve of growth for neutral iron.)

398-978 O - 71 - 6

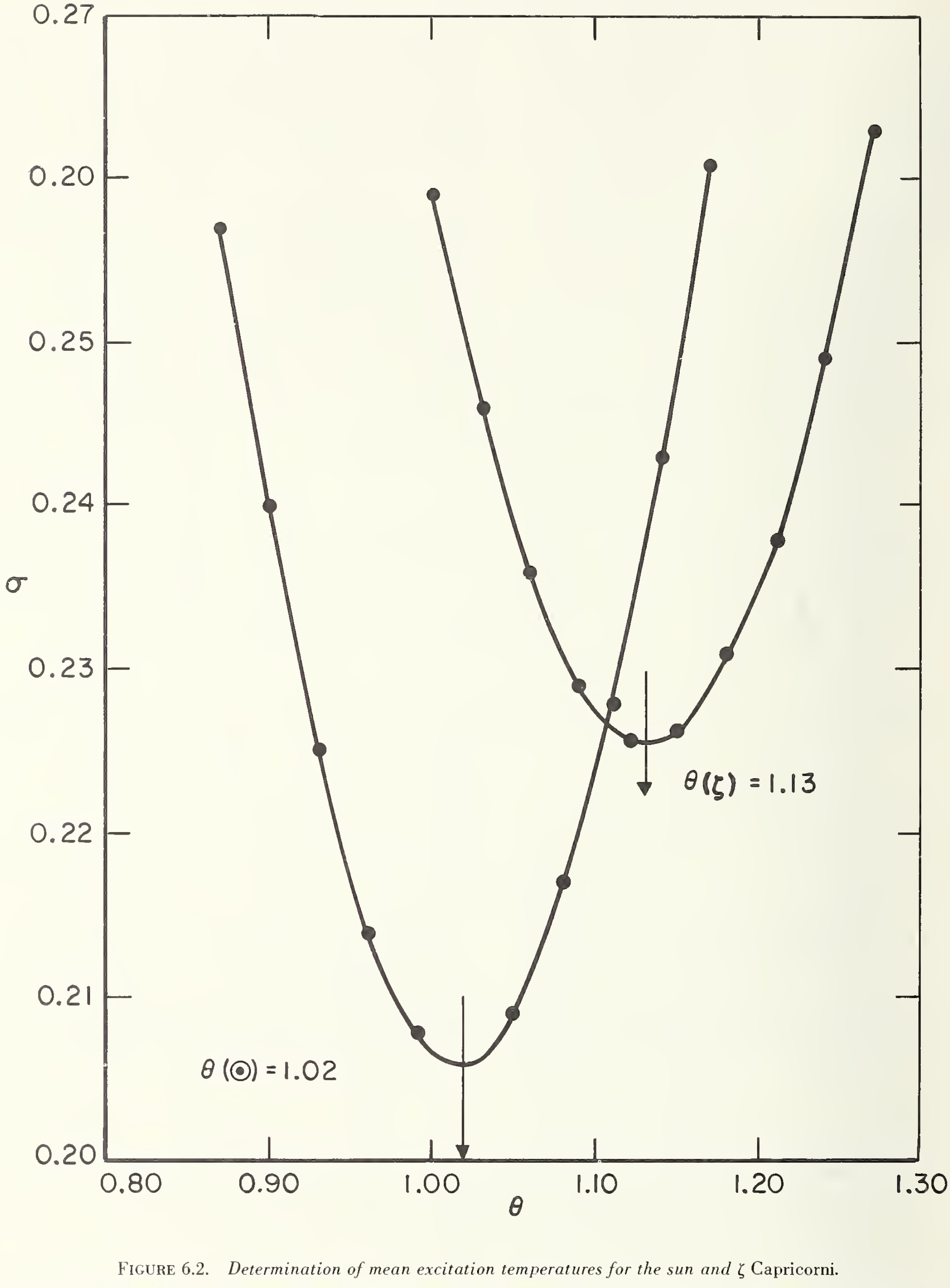

FIGURE 6.2. *Determination of mean excitation temperatures for the sun and* ζ Capricorni.

(*Abscissa*, assumed temperature; *ordinate*, standard deviation of the horizontal scatter in the curve of growth for neutral iron constructed by use of NBS *gf*-values.)

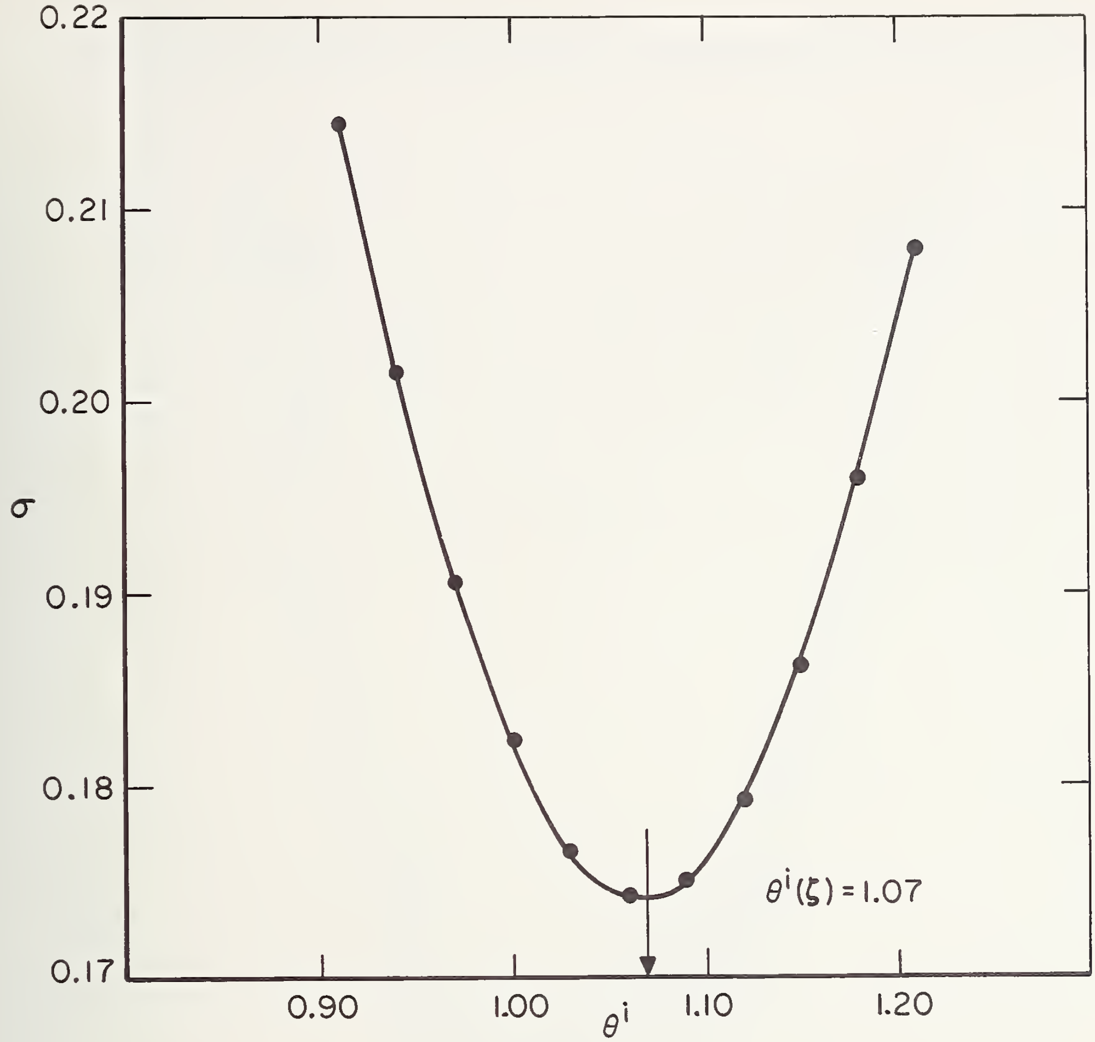

FIGURE 6.3. *Determination of mean excitation temperature from ion lines observed in ζ Capricorni.*

(*Abscissa*, assumed temperature; *ordinate*, standard deviation of the horizontal scatter in the composite curve of growth.)

The mean excitation temperature obtained from spectra of singly ionized atoms ($\theta^i_{\rm exc}$) was found to be slightly higher than that from neutral spectra ($\theta^n_{\rm exc}$). The determination was made in the following way. About 200 lines representing 14 singly ionized elements were combined into a single curve of growth using an estimated $\theta^i_{\rm exc}=\theta^n_{\rm exc}$. Differential shifts related to their respective abundances were then applied to the individual elements in such a way that the sum of the deviations of the points for each element from the mean multi-elemental curve was zero. The procedure was iterated through a succession of mean calculated curves and sets of shifts to the point where the shifts remained constant. Having thus applied individual shifts to bring all ion spectra onto a single curve of growth, only the value of $\theta^i_{\rm exc}$ was then varied to provide a minimum-sigma test. The result using *gf*-values is shown in figure 6.3.

The above analysis fixes the temperature of ζ Cap almost exactly midway between those of the sun and ϵ Vir. The finally adopted values are as follows, each with an estimated error of ±0.03. The differential excitation temperatures are assumed to be the same for both neutral (n) and ion (i) spectra.

TABLE 6.2. *Adopted excitation temperatures*

$\theta_{\rm exc}(\odot)=1.02$	$T_{\rm exc}(\odot)=4940°\pm140$
$\theta^n_{\rm exc}(\zeta)=1.13$	$T^n_{\rm exc}(\zeta)=4460°\pm120$
$\theta^i_{\rm exc}(\zeta)=1.07$	$T^i_{\rm exc}(\zeta)=4710°\pm130$
$\theta_{\rm exc}(\epsilon)=1.21$	$T_{\rm exc}(\epsilon)=4165°\pm100$

$$\Delta\theta_{\rm exc}(\zeta-\odot)=+0.10$$

$$\Delta\theta_{\rm exc}(\zeta-\epsilon)=-0.09$$

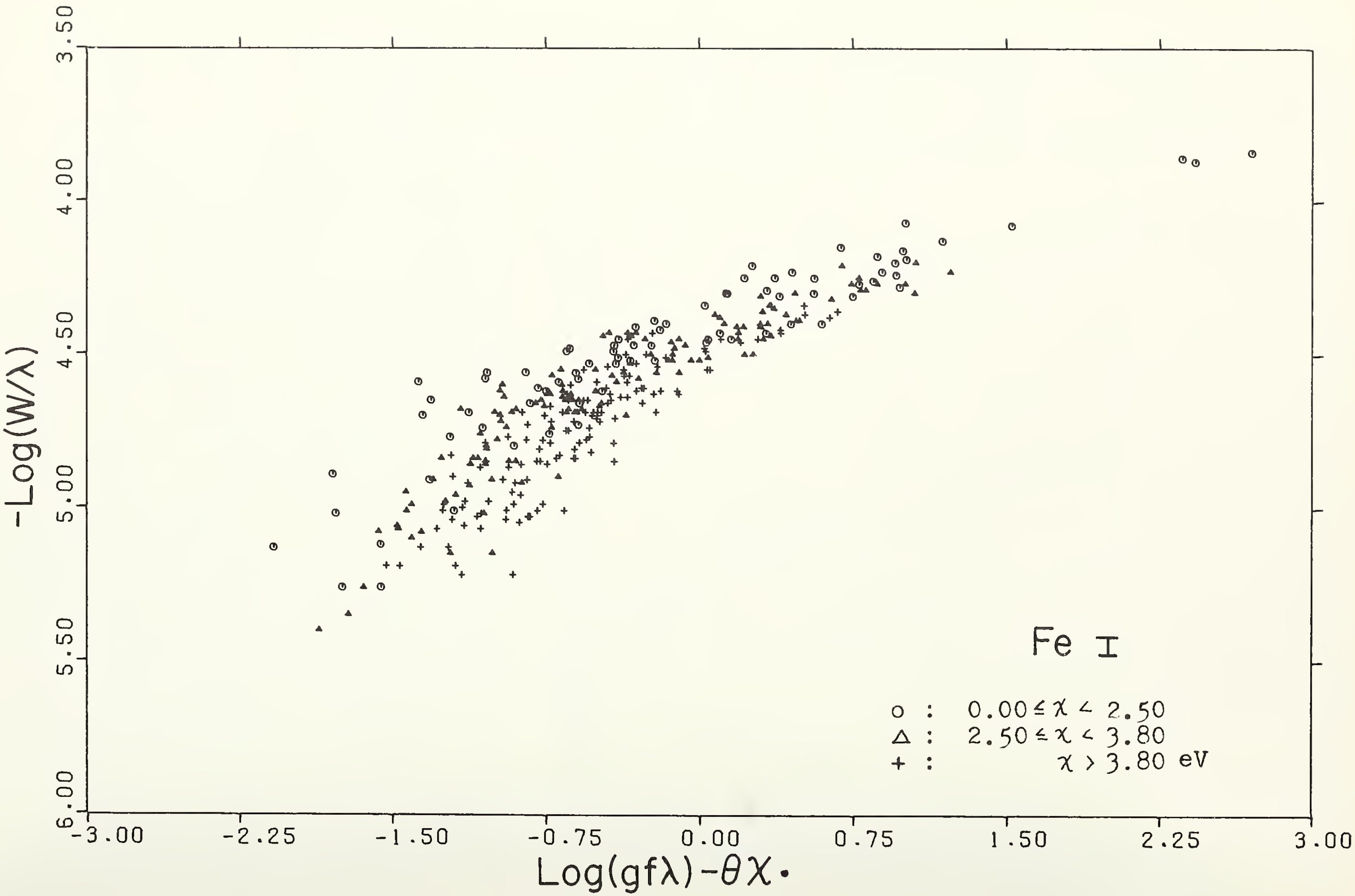

FIGURE 6.4. *Absolute curve of growth for iron.*

The grouping of lines by excitation potential is caused by use of an incorrect temperature ($\theta = \theta_{adopted} - 0.15$).

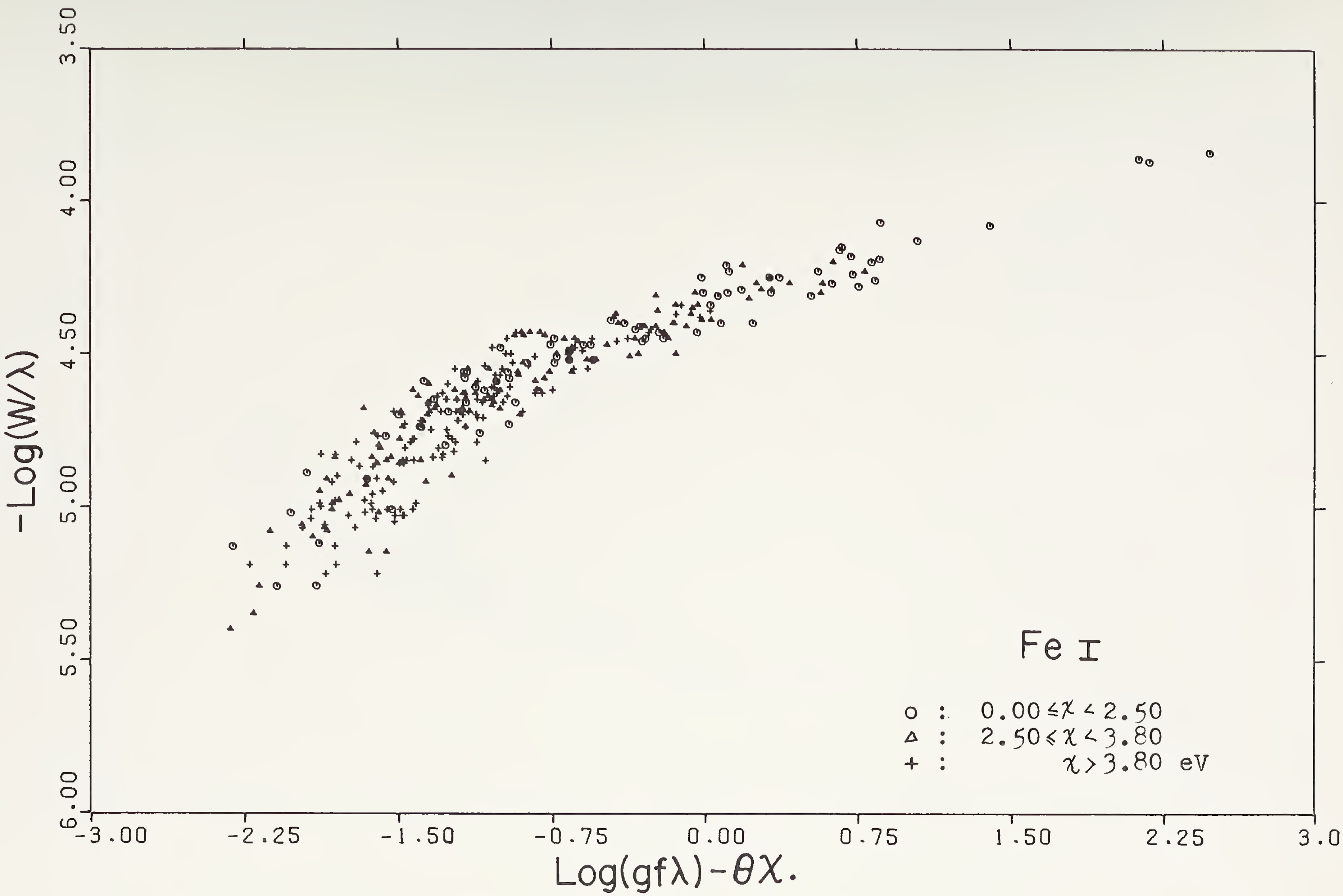

FIGURE 6.5. *Absolute curve of growth for iron* ($\theta = \theta_{adopted}$).

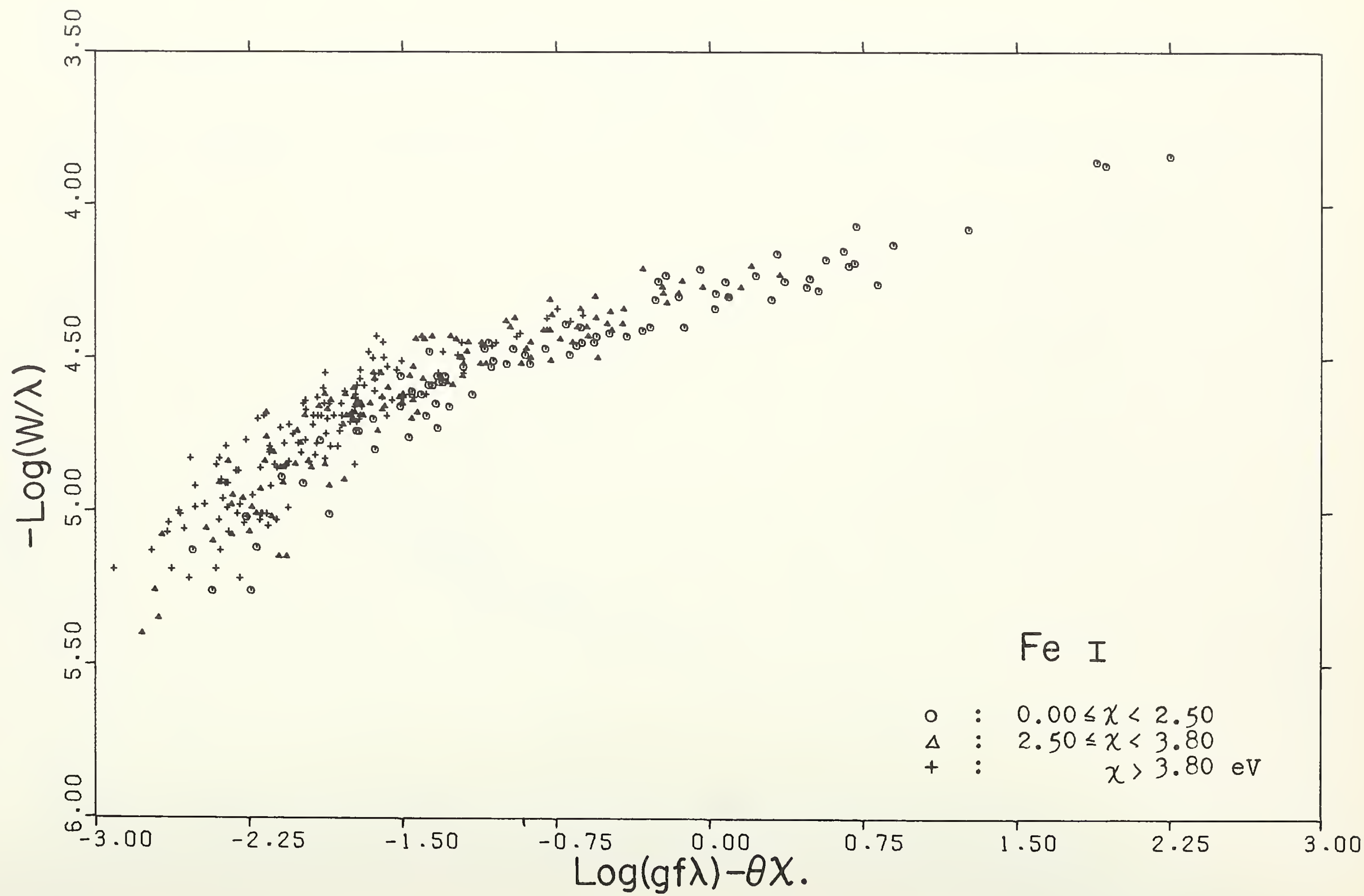

FIGURE 6.6. *Absolute curve of growth for iron.*

The grouping of lines by excitation potential is caused by use of an incorrect temperature ($\theta = \theta_{\mathrm{adopted}} + 0.15$).

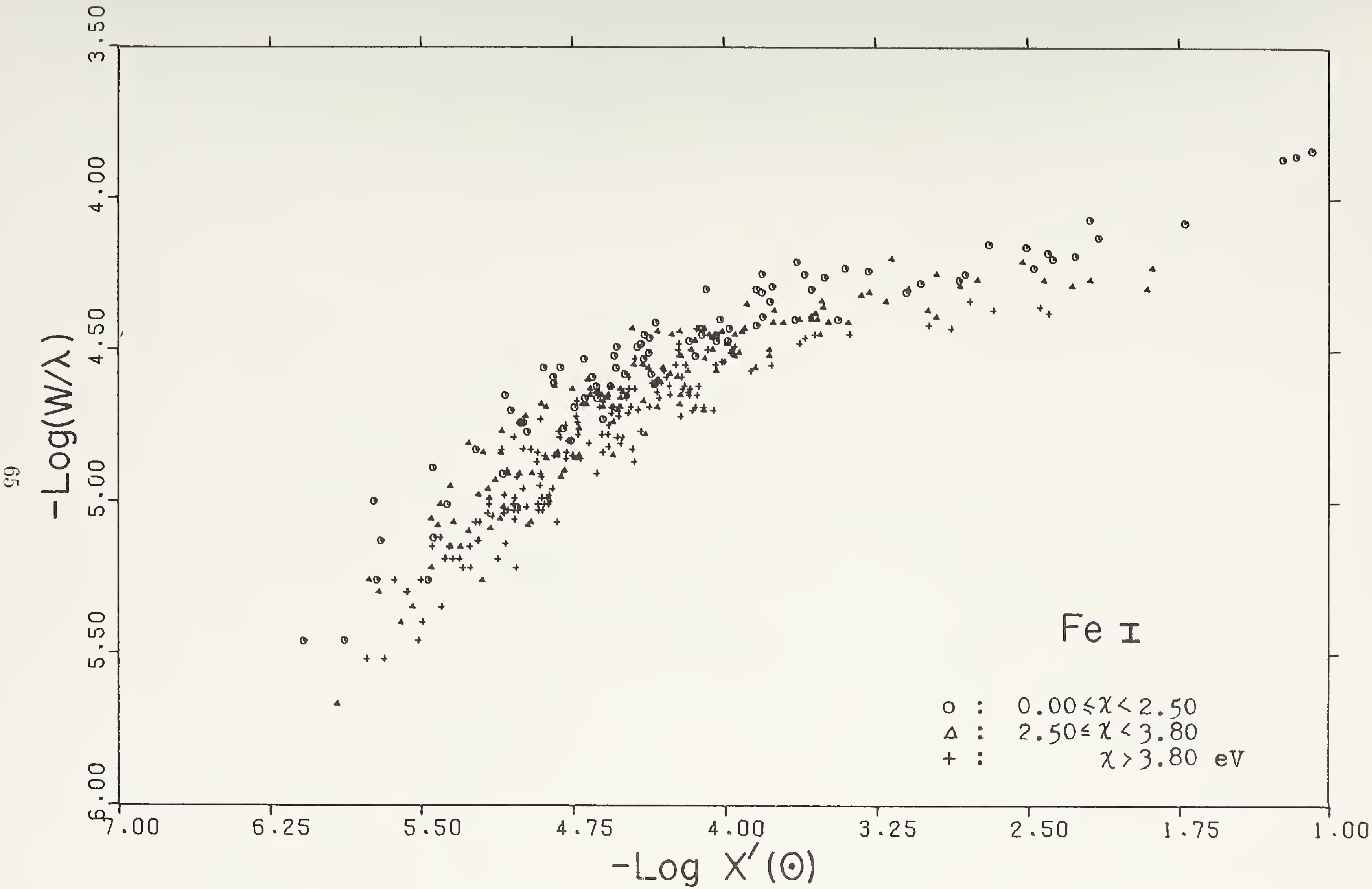

FIGURE 6.7. *Differential curve of growth for iron.*

Use of an incorrect excitation temperature causes the systematic grouping of lines by excitation potential. ($\Delta\theta = \Delta\theta_{\text{adopted}} - 0.15$).

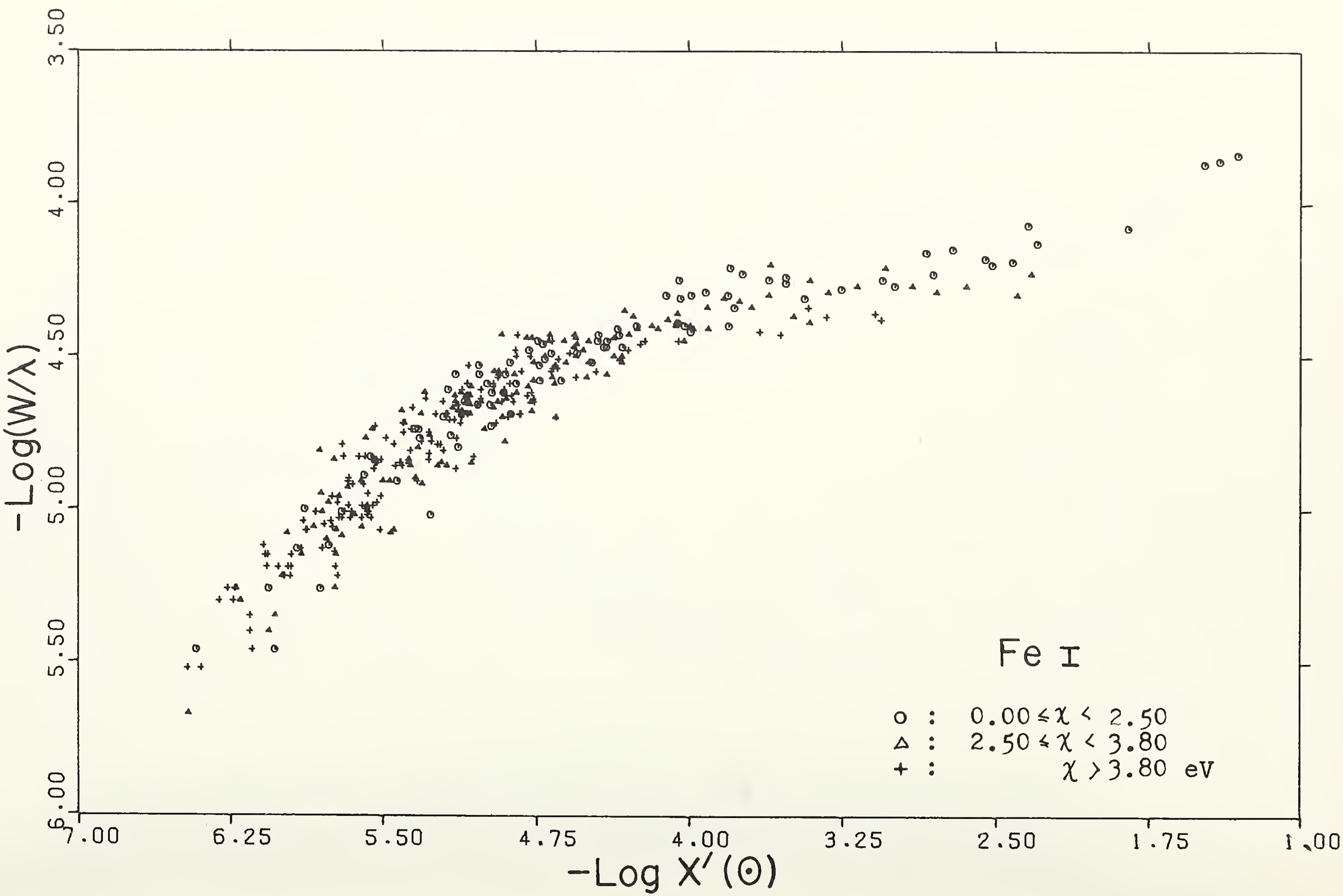

FIGURE 6.8. *Differential curve of growth for neutral iron* ($\Delta\theta = \Delta\theta_{adopted}$).

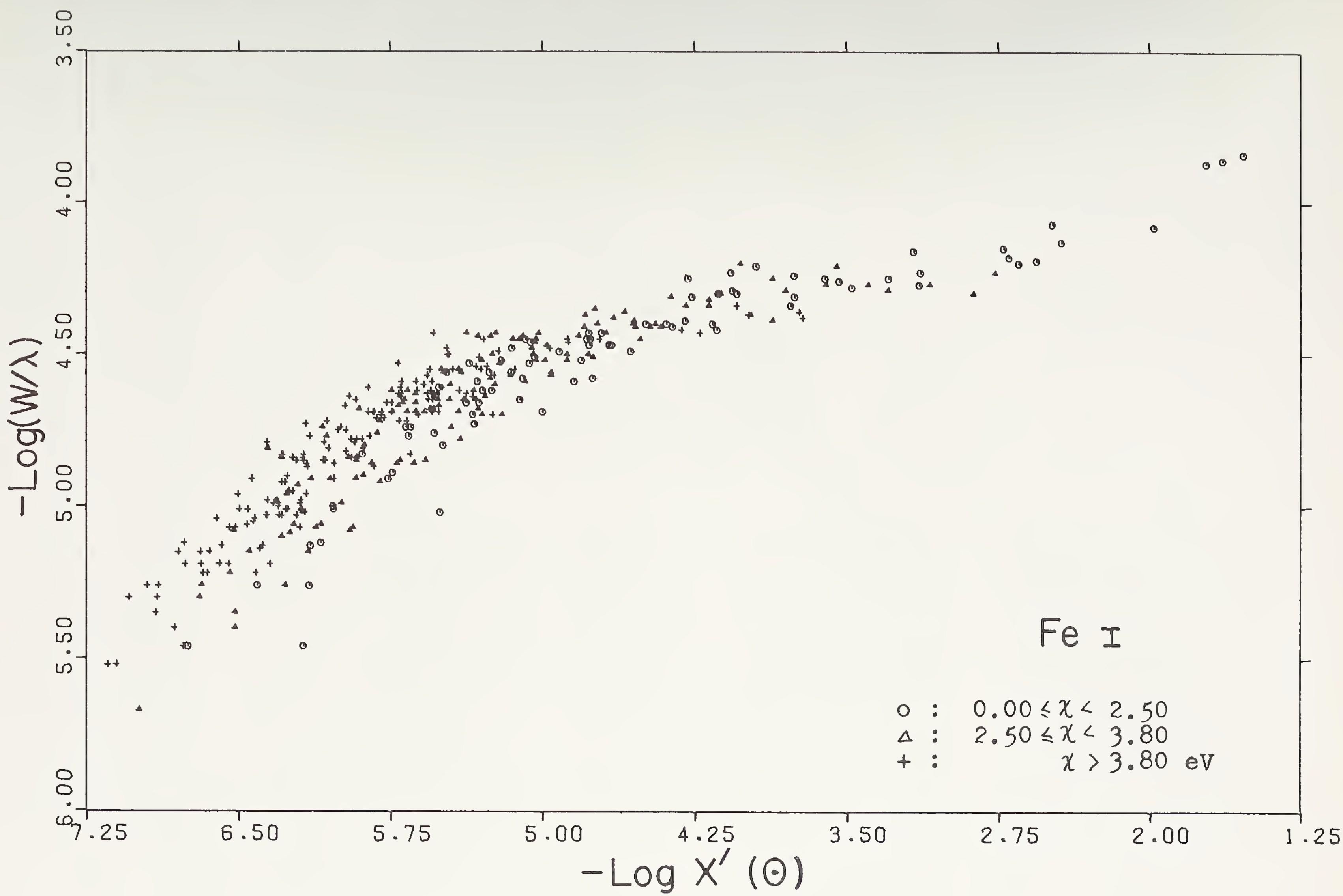

FIGURE 6.9. *Differential curve of growth for iron.*

Use of an incorrect excitation temperature causes the systematic grouping of lines by excitation potential ($\Delta\theta = \Delta\theta_{\text{adopted}} + 0.15$).

The effect that the choice of temperature has on the scatter in the curves of growth for iron is shown in figures 6.4 to 6.9, which compare absolute and differential curves using the excitation temperatures derived above with those using temperatures differing by ± 0.15 from the adopted values. As the temperature departs from the adopted values, the scatter becomes worse, and a clear separation of the points according to excitation potential emerges. It is important to note that the scatter in the *damping* portion of the differential curve relative to the sun is less for $\Delta\theta = +0.25$ than for the adopted differential temperature. This is related to the Carter effect discussed in section 6.3.

6.2. The Ionization Equilibrium

To obtain the total abundance of an element from the observed differential shifts in the curves of growth, the differential ionization equilibrium must be known. Writing the Saha equation for both the barium star and the comparison star, and subtracting, gives in the bracket notation of section 4.1

$$[N_{r+1}/N_r] = -[P_e] - \Delta\theta_{\mathrm{ion}}\chi_r - \frac{5}{2}[\theta_{\mathrm{ion}}] \qquad (6.5)$$

where χ_r is the ionization potential, θ_{ion} is the ionization temperature, P_e is the electron pressure, and $[N_{r+1}/N_r]$ is the horizontal shift between curves of growth drawn for some element observed in two stages of ionization.

Ideally, $\Delta\theta_{\mathrm{ion}}$ and $[P_e] = \Delta \log P_e$ would be determined simultaneously by plotting against ionization potential the relative shifts found for several spectra observed in two stages of ionization. The range of ionization potentials is so small for such spectra observed in ζ Cap, however, that a meaningful simultaneous determination is not possible. The usual assumption was therefore made that $\Delta\theta_{\mathrm{ion}} = \Delta\theta_{\mathrm{exc}}$, and the value of $[P_e]$ was derived from the observed shifts between differential curves of growth for the neutral and singly ionized stages of the six elements given in table 6.3.

Although only the differential values are important in the determination of relative chemical abundances, the absolute values of P_e^{ζ} and $\theta_{\mathrm{ion}}^{\zeta}$ can be estimated by taking $\theta_{\mathrm{ion}}^{\odot} = 0.89$ and $\log P_e^{\odot} = 1.30$ at a representative optical depth of 0.35 (Aller and Pierce, 1952). This gives $\log P_e^{\zeta} = +0.02$ and $\theta_{\mathrm{ion}}^{\zeta} = 0.99$. A value of $\theta_{\mathrm{ion}}^{\zeta} = 0.98$ would be obtained if $\theta_{\mathrm{ion}}^{\zeta}$ were approximated by taking $\theta_{\mathrm{ion}}^{\zeta} = \theta_{\mathrm{exc}}^{\zeta} - 0.15$, as has been suggested by the work of Preston (1961) and others.

TABLE 6.3. *Determination of differential electron pressures for ζ Cap relative to the Sun and to ϵ Vir*

Element	Wt.	χ	Sun		ϵ Vir	
			$[N^+/N^0]$	$[P_e]$	$[N^+/N^0]$	$[P_e]$
		eV				
Fe	3	7.87	0.37	−1.26	0.68	0.12
Ti	1	6.82	.52	−1.30	.44	.26
Cr	1	6.76	.33	−1.11	.45	.15
Sc	1	6.54	.40	−1.15	.54	.14
Zr	1	6.84	.62	−1.40	.50	.21
Y	1	6.38	.81	−1.55	.75	−.09

Adopted: $[P_e]_{\zeta-\odot} = -1.28$

$[P_e]_{\zeta-\epsilon} = +0.13$

6.3. The Carter Effect

The differential curve of growth shown in figure 2.7 for Fe I in ζ Cap relative to the sun shows on the damping portion of the curve a systematic displacement between the blue and the red lines. This displacement can be traced to the solar line strengths.

In his study of Fe I in the sun, Carter (1949) found that lines absorbed from odd energy levels ("odd" lines, for brevity) were systematically stronger on the damping portion of the solar curve of growth than were lines having the same *f*-value but absorbed from lower even levels. He attributed this separation by parity to differential damping in the solar atmosphere or to a preferential population of odd states during recombination from Fe II. Sandage and Hill (1951) noted a similar effect for Cr I in the sun. The process is still not well understood.

The Carter effect is shown in figure 6.10, which is a solar curve of growth based on *gf*-values taken from NBS Monograph 108. The separation of the odd and even lines is quite striking for values of $\log (W/\lambda)$ greater than about -4.80. The strong separation does not continue into the linear portion of the curve. It is apparent that solar line strengths obtained for odd lines on the damping portion of the curve will be overestimated relative to those for even lines. This overestimation will be transmitted to differential curves of growth constructed with solar line strengths as a *reversed* Carter effect. That is, the odd lines will fall to the right of the even lines on the damping portion of the differential curve. This is clearly seen

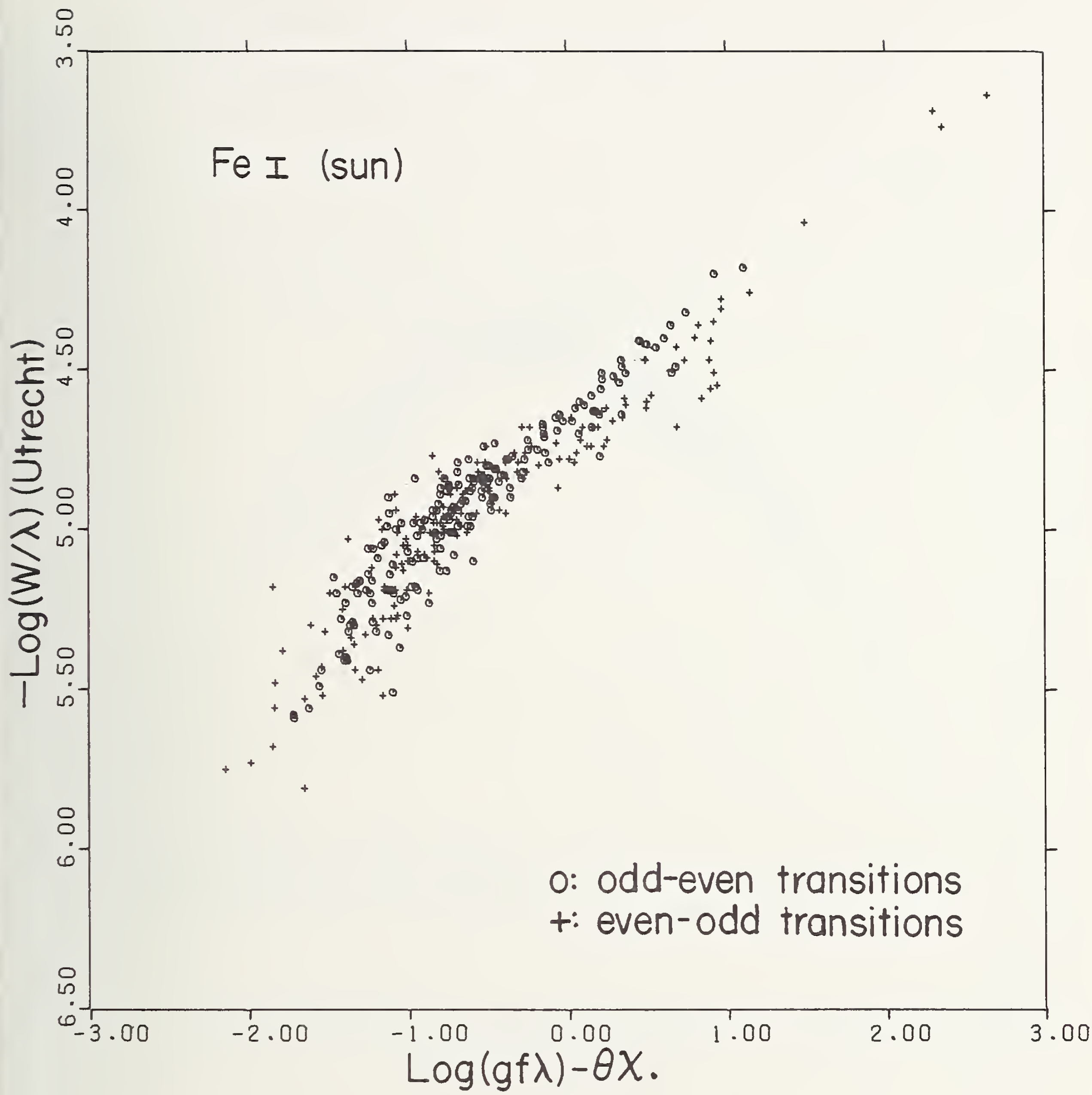

FIGURE 6.10. *Absolute curve of growth for neutral iron in the sun.*

A distinction is made between odd-even transitions (*circles*) and even-odd transitions (*crosses*). $\theta = 1.02$.

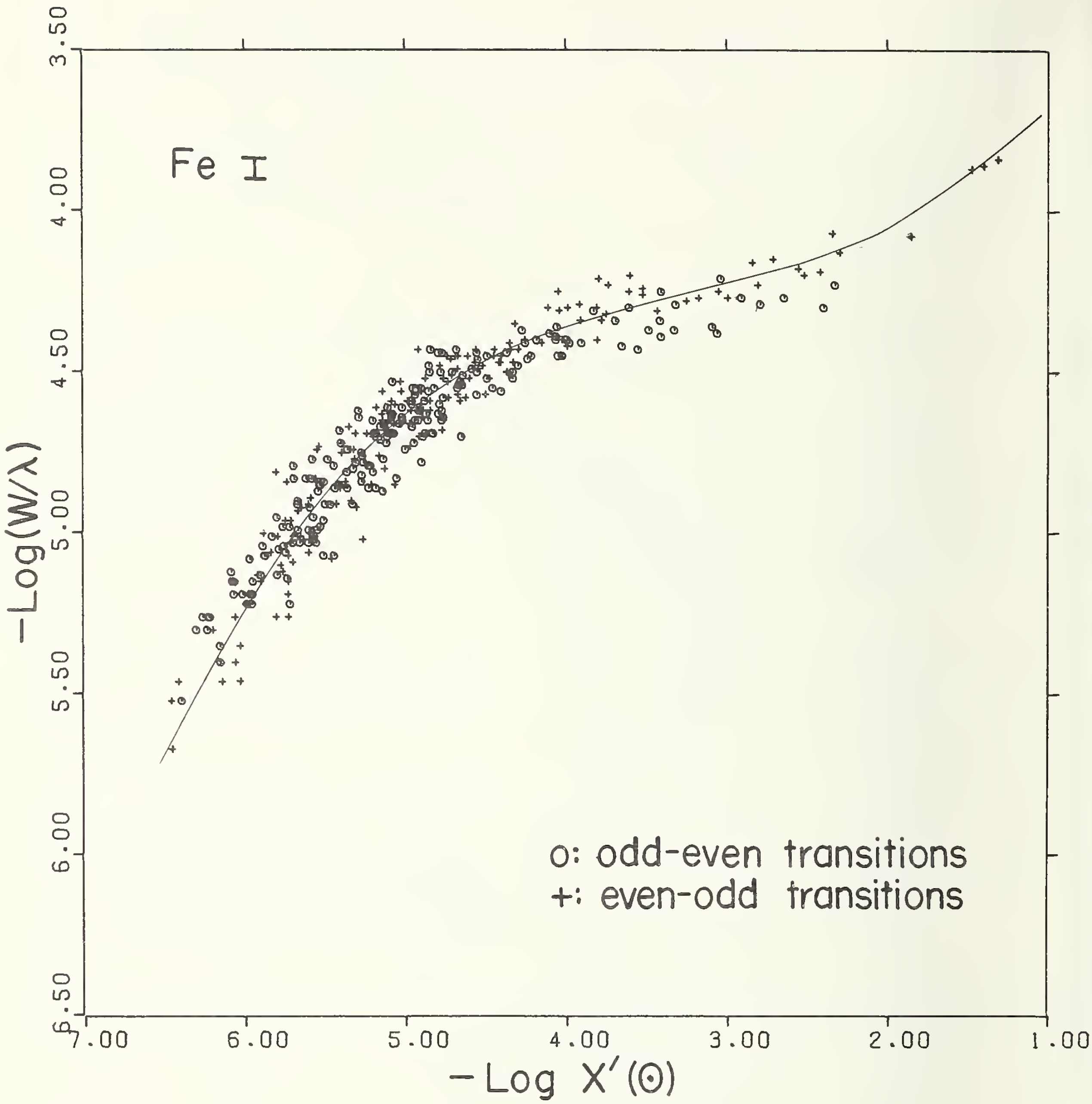

FIGURE 6.11. *Differential curve of growth for neutral iron in ζ Capricorni.*

A distinction is made in this plot between odd-even (*circles*) and even-odd (*crosses*) transitions. Notice the reversed Carter effect on the damping portion of the curve.

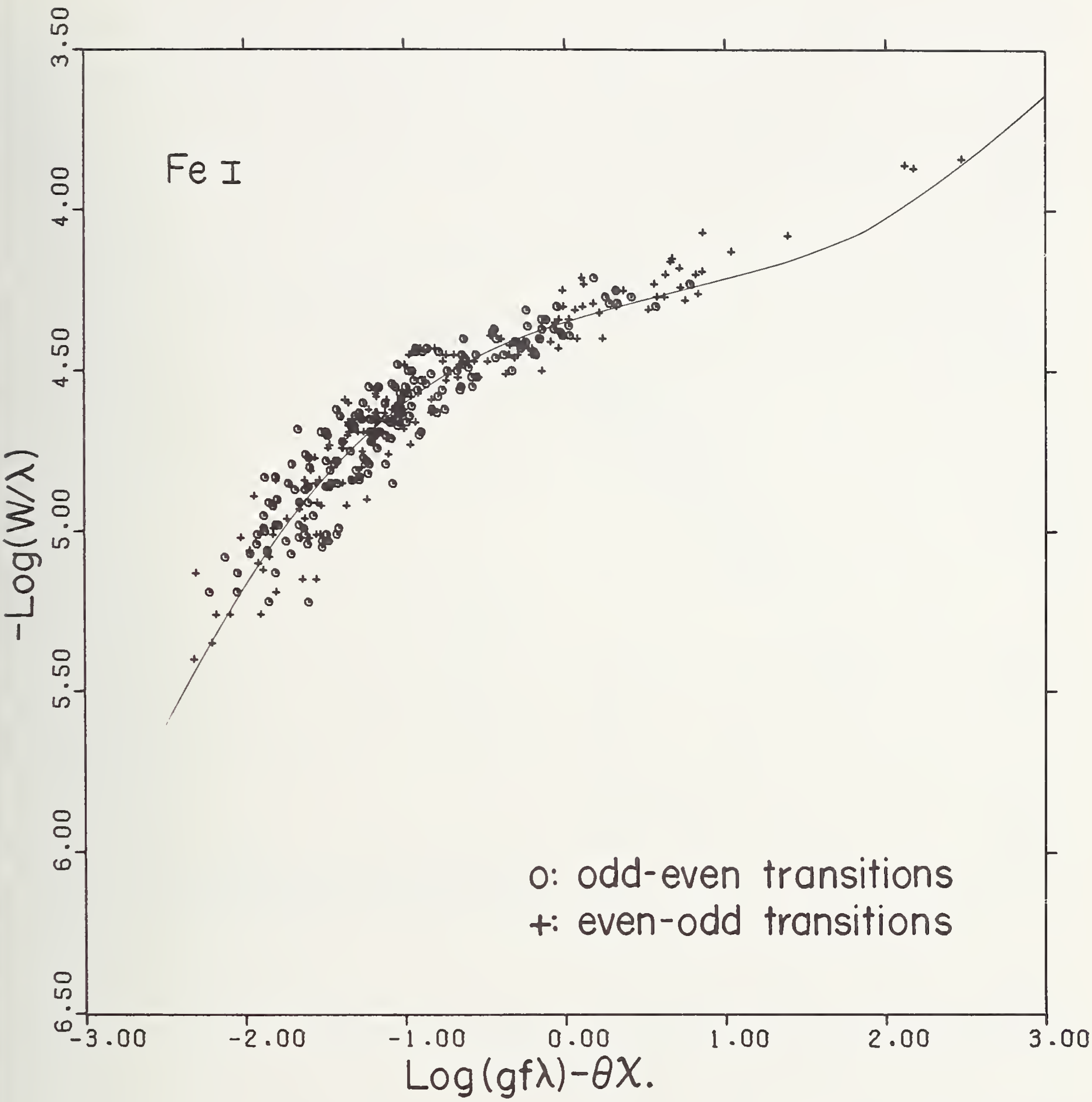

FIGURE 6.12. *Absolute curve of growth for neutral iron in ζ Capricorni.*

Notice the absence of any significant Carter effect. (*Circles,* odd-even transitions; *crosses,* even-odd transitions.)

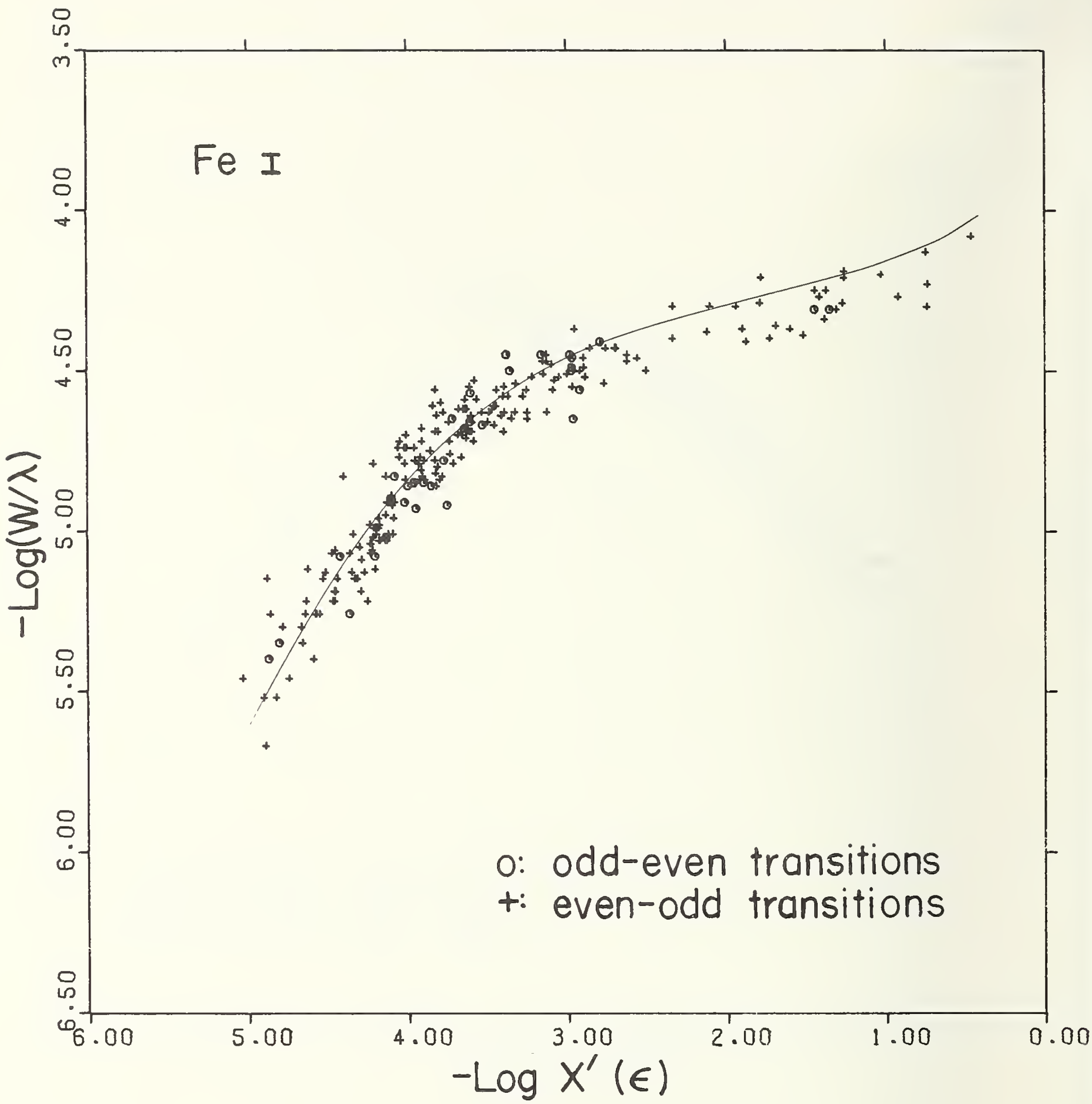

FIGURE 6.13. *Differential curve of growth for neutral iron relative to ϵ Virginis.*

Circles, odd-even transitions; *crosses*, even-odd transitions.

in figure 6.11, where the differential curve for ζ Cap is now constructed with a distinction made between odd and even lines. Comparison of this plot with that of figure 2.7 shows, moreover, that the odd lines generally have wavelengths greater than 5000 Å, thus explaining the apparent wavelength separation in figure 2.7. That no significant internal Carter effect is present in ζ Cap itself is apparent from figure 6.12 and figure 6.13, in which the even-odd distinction is made in plots using *gf*-values and line strengths from ε Vir, respectively.

The curve shown in figure 6.10 differs considerably from those obtained for Fe I by Kuli-Zade (1968), who also used NBS *gf*-values. In that investigation the bifurcation of the lines according to parity was present not only on the damping portion but was found to extend over the entire solar curve of growth. That result can, however, be traced to the use of an inappropriate mean solar excitation temperature. The effect the selection of excitation temperature has on the parity distribution in the solar curve of growth is indicated by the following argument.

Let us examine the mean excitation potentials for lines of each parity in the damping and Doppler regions of the solar curve of growth. The mean level of line formation for higher excitation lines will be at greater optical depths than for lower excitation lines. The effects of pressure and collisional damping will also be correspondingly greater. Averaging the excitation potentials for just the Fe I lines used in our figure 6.10 yields the results shown in table 6.4.

TABLE 6.4. *Mean excitation potentials for* Fe I *lines used in the construction of solar curve of growth shown in figure 6.10.*

The number of lines used in forming the individual averages is given in parentheses.

Region	$\langle\chi\rangle$ odd	$\langle\chi\rangle$ even	$\Delta\langle\chi\rangle$ odd-even
	eV	*eV*	*eV*
Entire curve...........	4.07 (173)	2.53 (143)	1.54
Damping portion log $(W/\lambda)>-4.90$.....	3.91 (76)	1.96 (65)	1.95
linear portion and shoulder log $(W/\lambda)<-4.90$.....	4.18 (101)	2.99 (78)	1.19

On the damping part of the curve there is a 2 eV difference in the mean excitation potentials for even and odd lines, almost twice that for the remainder of the curve. From the point of view of line excitation, table 6.4 suggests that the damping portion defined by the odd lines, rather than by the even lines, corresponds more closely to the linear portion of the curve when a mean excitation temperature is used because of the more equivalent average excitation energies.

The mean excitation temperature would normally be derived by minimizing the scatter for the fainter lines on the curve of growth, as this is the more useful region for abundance work. If a temperature so derived were decreased (θ_{exc} increased), the odd lines on the average would be shifted farther to the left than the even lines (owing to the excitation differential), the odd-even displacement being greater on the damping portion. The effect is shown in figure 6.14, which has the appearance of the curves reported by Kuli-Zade. The odd-even separation can be reversed, however, simply by adopting a mean excitation temperature that is too high (fig. 6.15). In general, if a mean excitation temperature θ produces minimum parity separation, a temperature $\theta'=\theta+\Delta\theta$ will yield an average parity displacement of 1.5 $\Delta\theta$ along the abscissa of the curve of growth. On the damping portion of the curve, the corresponding displacement will be about 2 $\Delta\theta$.

In one sense, then, the Carter effect can be interpreted as simply a manifestation of the Adams-Russell effect (Adams and Russell, 1928), which describes the observation that in some stars θ_{exc} (or $\Delta\theta_{exc}$) is a function of excitation potential. The phenomenon appears as a curvature in the plot (see sec. 6.1) of relative shifts of partial curves of growth against excitation potential, or as a grouping of points by excitation potential in a curve of growth constructed by use of some mean temperature. On this basis, it would be expected that a star showing the one effect would also show the other.

We note, finally, that the tendency in ε Vir for the low-level lines to indicate a greater microturbulent velocity than the high-level lines (Cayrel and Cayrel, 1963, figs. 7–9) is intimately related to the reversed Carter effect transmitted by the solar line strengths and to the distribution of excitation energies cited in table 6.4.

6.4. Gas Velocities in the Atmosphere of ζ Capricorni

6.4.1. Thermal Velocity

On the assumption that the gas kinetic temperature in the atmosphere of ζ Capricorni is equal to the

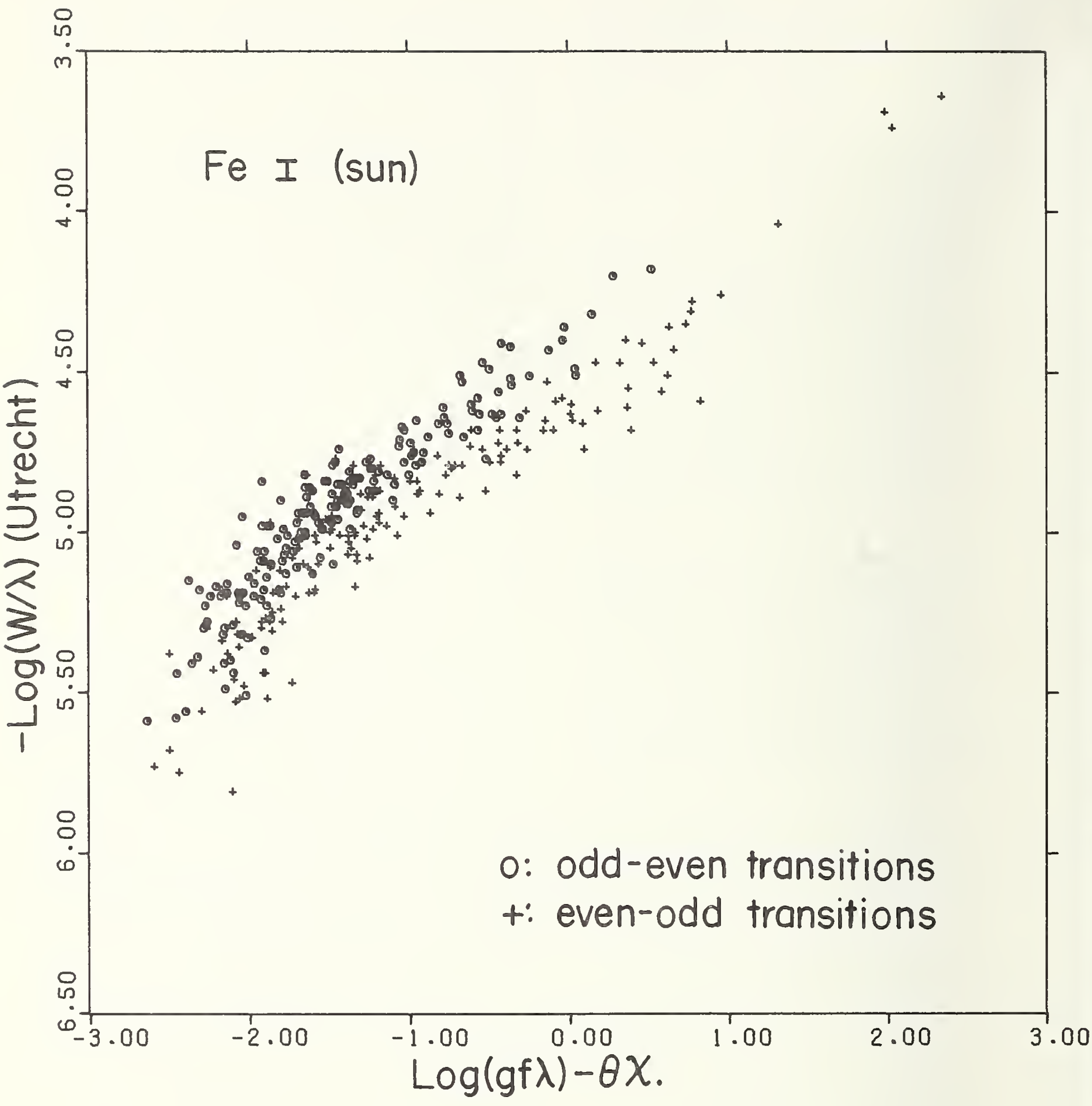

FIGURE 6.14. *Enhancement of the Carter effect in the solar curve of growth by use of an incorrect mean excitation temperature* ($\theta = 1.22$). *Circles*, odd-even transitions; *crosses*, even-odd transitions.

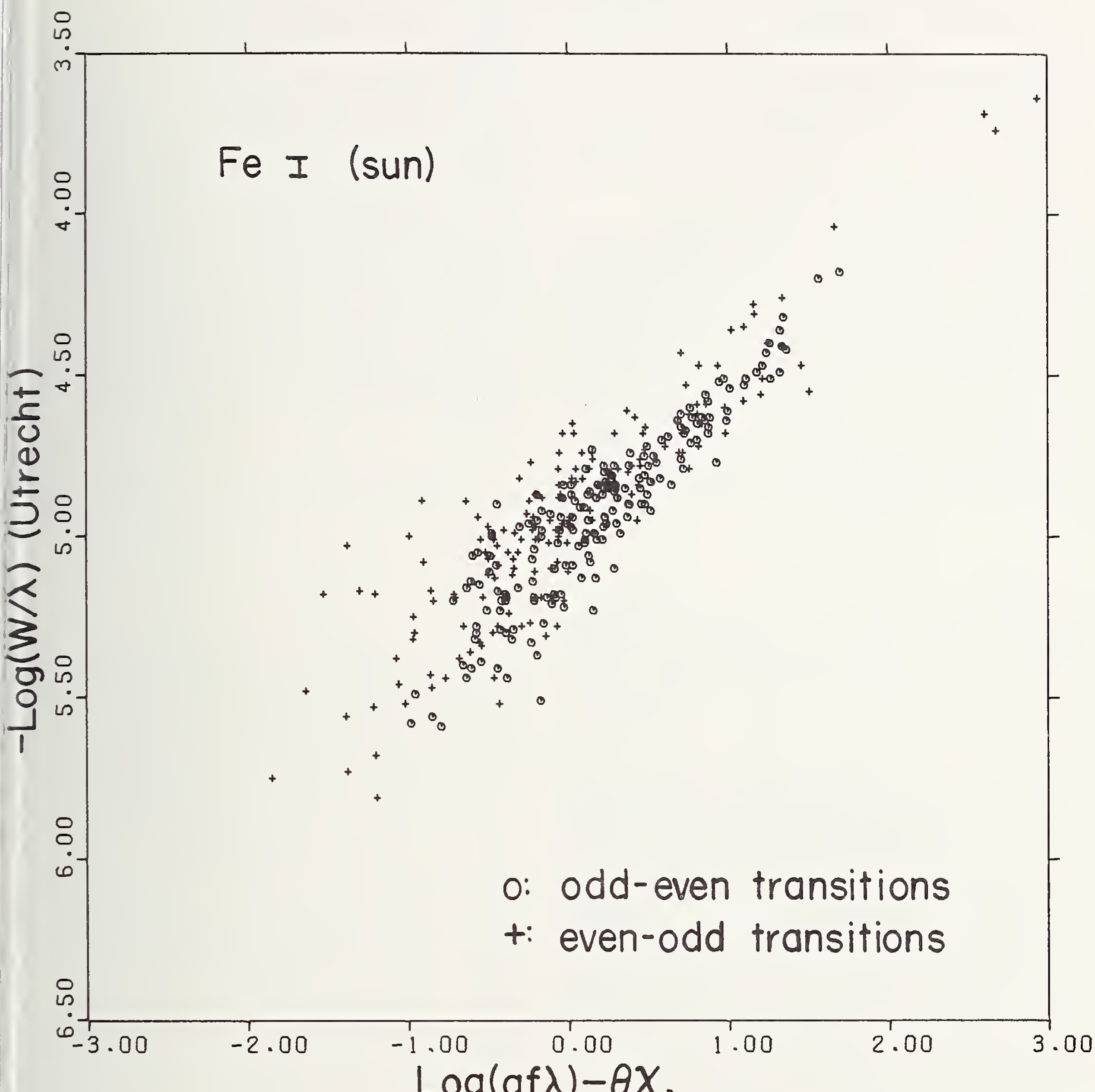

FIGURE 6.15. *Reversed Carter effect in the solar curve of growth caused by use of an inappropriate excitation temperature* ($\theta = 0.82$).
Circles, odd-even transitions; *crosses*, even-odd transitions.

398-978 O - 71 - 5

excitation temperature derived in section 6.1, the purely thermal velocity is given by the relation

$$v_t = \sqrt{\frac{2kT}{M}}. \qquad (6.6)$$

For the iron group, this gives

$$v_t \sim 1.2 \text{ km/s}. \qquad (6.7)$$

6.4.2. Microturbulence

From the theoretical curves of growth for simple stellar models, the curve for pure absorption in the Milne-Eddington approximation has been found to represent most satisfactorily the empirical curves of growth for ζ Capricorni. As discussed in section 4.4., the theoretical curve with damping constant log $(2\alpha) = -2.5$ has been used. The ordinate of the theoretical curve (Hunger, 1956) is log $(W/2bR_c)$, where R_c is the limiting central depth for strong lines, and b, the "Doppler width," is given by

$$b = \Delta\lambda_D = v_0\lambda/c. \qquad (6.8)$$

The rms Doppler speed v_0, or velocity parameter, includes purely thermal gas motions and small-scale turbulence (microturbulence) according to the relation

$$v_0^2 = v_t^2 + v_{\text{micro}}^2. \qquad (6.9)$$

The quantity v_0 was determined from the observations by shifting the empirical curves of growth both vertically and horizontally until the best fit to the theoretical curve was achieved. The value derived for v_0 depends to some extent upon the theoretical curve with which the observations are compared, but the differences are small (Hunger, 1956).

Since the quantity log (W/λ) is plotted along the ordinate in the empirical curves of growth, the velocity parameter v_0 is obtained from the vertical shift Δ log (W/λ) according to the relation

$$\Delta \log (W/\lambda) = \log (W/\lambda) - \log (W/2bR_c) \qquad (6.10)$$

or

$$\log v_0 = \Delta \log (W/\lambda) + 10.20 \qquad (6.11)$$

where the value R_c=0.95 observed for Mg I λ5183.60 has been taken as a representative limiting central depth. The variation of R_c with wavelength is not significant in comparison with the errors inherent in fitting the empirical curves of growth.

Table 6.5 lists the velocities derived from those spectra whose curves of growth are sufficiently populated to allow reasonably accurate determinations. The average values for v_0 as derived from absolute curves of growth and differential curves with respect to the sun and to ε Vir are in good agreement. There is a tendency for lines of singly ionized spectra to give a higher microturbulent velocity than those of neutral spectra, as in supergiants (Wright, 1948), but Sc II is a notable exception. A more careful examination shows that the higher velocities derived from Ti II and Fe II are probably related to blending in the stronger observed lines. In any case, the variations in the derived velocities amount to only ±0.10 on the ordinate of the curve of growth, which is about the error in making the fit. In view of the marginal significance of the variations, a single value of v_0 has been adopted for all spectra,

$$\Delta \log (W/\lambda) = -4.63 \qquad (6.12)$$

$$\log v_0 = 5.57 \pm 0.05 \qquad (6.13)$$

$$v_0 = 3.7 \pm 0.4 \text{ km/s}. \qquad (6.14)$$

TABLE 6.5. *Doppler velocities derived from individual curves of growth*

Spectrum	Source of Line Strengths					
	$gf\lambda$		ε Vir		Sun	
	$-\Delta$ log (W/λ)	v_0	$-\Delta$ log (W/λ)	v_0	$-\Delta$ log (W/λ)	v_0
		km/s		*km/s*		*km/s*
Fe I	4.63	3.7	4.67	3.4	4.65	3.5
Ca I	4.70	3.2	4.68	3.3	4.71	3.1
Cr I	4.62	3.8	4.68	3.3	4.63	3.7
Mn I	4.63	3.7	4.70	3.2	4.65	3.5
Ni I	4.74	2.9	4.58	4.2	4.66	3.5
Ti I	4.59	4.1	4.66	3.5	4.60	4.0
Na I	4.66	3.5	.....	.....	.....	.....
Ce II	4.61	3.9	4.52	4.8	4.48	5.2
Fe II	4.49	5.1	4.60	4.0	4.52	4.8
Nd II	4.58	4.2	.....	.....	4.56	4.4
Sm II	4.55	4.5	.....	.....	.....	.....
Ti II	4.54	4.6	4.65	3.5	4.51	4.9
Sc II	.....	.....	4.65	3.5	4.61	3.9
(Average)	4.61	3.9	4.64	3.6	4.60	4.0

Adopted: Δ log $(W/\lambda) = -4.63$
$v_0 = 3.7$ km/s.

Using eq (6.9), we finally obtain

$$v_{\text{micro}} = \sqrt{[(3.7)^2 - (1.2)^2]} \qquad (6.15)$$

or

$$v_{\text{micro}} = 3.5 \pm 0.5 \text{ km/s}. \qquad (6.15)$$

The microturbulent velocity in ζ Cap is therefore about twice that observed in the sun or in ϵ Vir Cayrel and Cayrel, 1963).

6.4.3. Macroturbulence

As is characteristic of giant stars, the lines in the spectrum of ζ Cap are quite broad. The measured half-widths amount typically to 0.20–0.40 Å. Doppler broadening is almost wholly responsible for the half-widths of weak and moderately strong lines. Since half-widths were measured for nearly all lines used in this investigation, it is possible to obtain a very good determination of the Doppler width, and hence the macroturbulent speed.

If a Maxwellian distribution of velocities is assumed, the relative intensity in a line broadened only by the Doppler effect is

$$\frac{dI}{I} = \frac{1}{\sqrt{\pi}} e^{-\left(\frac{\Delta\lambda}{\Delta\lambda_D}\right)^2} \frac{d\lambda}{\Delta\lambda_D} \qquad (6.17)$$

where $(\Delta\lambda/\Delta\lambda_D)$ is the Doppler shift in units of the shift corresponding to the most probable speed v_D. The exponential term reaches its maximum value, unity, at the line center and decreases to one-half this maximum value at a distance $\Delta\lambda_H$ from the line center, where $\Delta\lambda_H$ is defined by

$$e^{-\left(\frac{\Delta\lambda_H}{\Delta\lambda_D}\right)^2} = \frac{1}{2}. \qquad (6.18)$$

The Doppler half-width, D_λ, of the line (total width at half-intensity) is therefore given by

$$D_\lambda = 2\Delta\lambda_H = 2 \cdot \sqrt{\ln 2}\, \Delta\lambda_D = 1.665\, \Delta\lambda_D. \qquad (6.19)$$

After substitution in the Doppler formula, the total Doppler velocity is found to be

$$v_D \equiv \frac{c\Delta\lambda_D}{\lambda} = 0.60\, D_\lambda \frac{c}{\lambda}. \qquad (6.20)$$

The Doppler half-width, D_λ, is deduced from the experimental data by extrapolating the observed half-widths to very weak lines. The ratio H/λ, where H is the observed half-width, is plotted against central depth in figure 6.16. The correlation is not strong. To reduce the number of points to be plotted, all lines with a quality $Q < 2$ have been omitted for wavelengths greater than 5000 Å and $R_c > 0.12$. The weak lines of poor quality have been retained in order to demonstrate a possible underestimation of half-widths for such lines. In general such weak lines had incomplete profiles that were approximately sketched in to allow measurement by planimeter.

With H and λ expressed in angstroms, the result for both regions is

$$\frac{H}{\lambda} \times 10^7 = 415 + 350 R_c \pm 35 \text{ (p.e.)}. \qquad (6.21)$$

The extrapolation to $R_c = 0$ gives the Doppler half-width and Doppler width

$$\text{at } 4500 \text{ Å} \quad D_\lambda = 0.19 \pm 0.02 \text{ Å}, \quad \Delta\lambda_D = 0.11 \pm 0.01 \text{ Å} \qquad (6.22)$$

$$\text{at } 6000 \text{ Å} \quad D_\lambda = 0.25 \pm 0.02 \text{ Å}, \quad \Delta\lambda_D = 0.15 \pm 0.01 \text{ Å}$$

The corresponding Doppler velocity from eq (6.20) is

$$v_D = 7.4 \pm 0.6 \text{ km/s}. \qquad (6.23)$$

In deriving this velocity, the contribution of the apparatus profile to the total line width has been neglected. The results of measurement of a dozen lines on the tracings near 6300 Å caused by O_2 absorption in the earth's atmosphere suggests an upper limit of 0.15 Å for the instrumental half-width of these lines. On the assumption that both the Doppler and the instrumental profiles are Gaussian, the squares of their respective half-widths must be added to give the square of the half-width of the folded profile. A partial instrumental correction to the above velocity can be made with only a small residual error by adopting $H_{\text{instr}} = 0.10$ Å as a mean value for the entire range of wavelengths. The final Doppler velocity then becomes

$$v_D = 6.6 \pm 0.6 \text{ km/s}. \qquad (6.24)$$

The total Doppler velocity is related to the thermal (v_t) and the turbulent (ξ) velocities by

$$v_D^2 = v_t^2 + \xi^2. \qquad (6.25)$$

If the assumption is made that

$$\xi^2 = v_{\text{micro}}^2 + v_{\text{macro}}^2, \qquad (6.26)$$

the macroturbulent velocity is found to be

$$v_{\text{macro}} = 5.5 \pm 1 \text{ km/s}. \qquad (6.27)$$

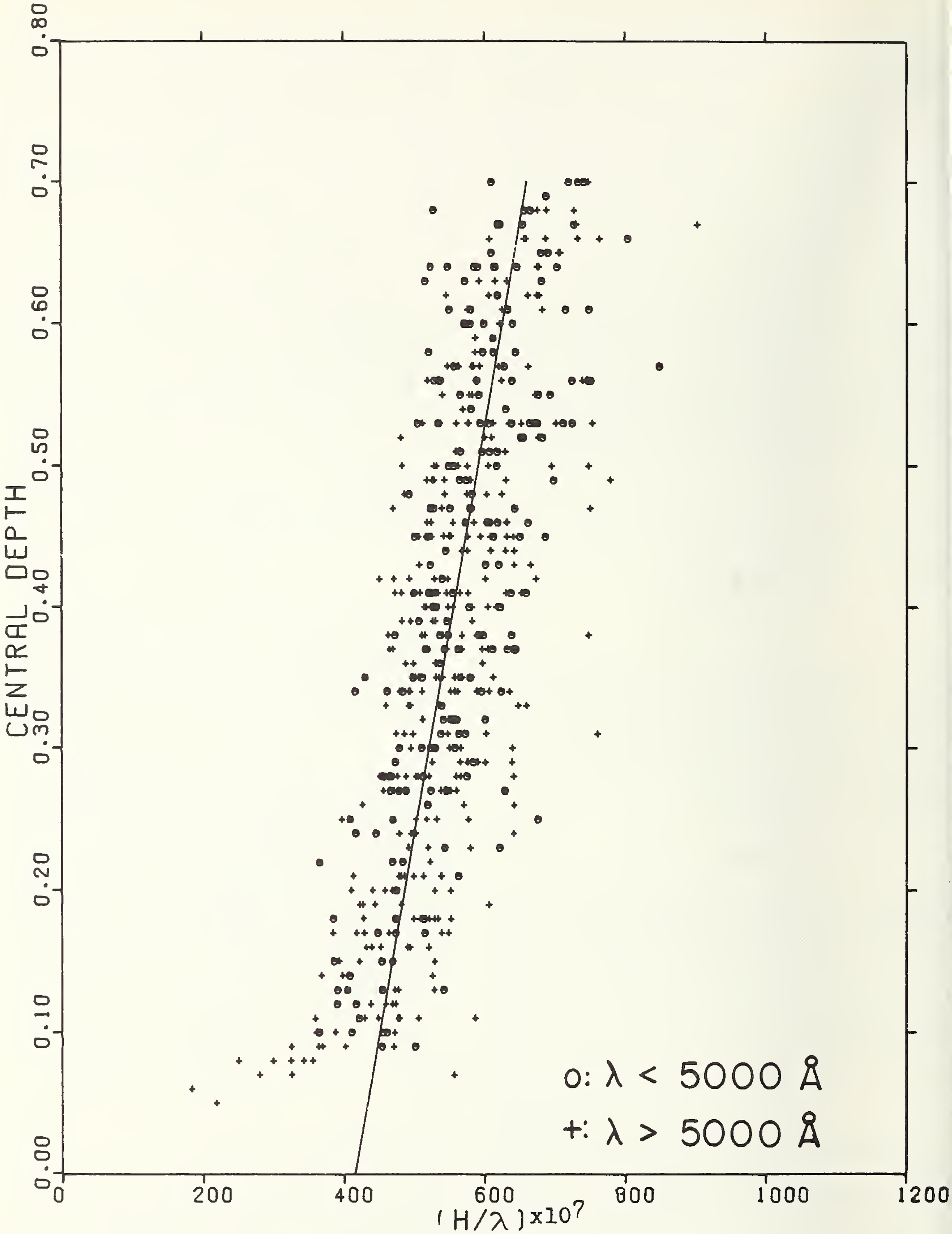

FIGURE 6.16. *Relation between half-width and central depth.*

Circles, $\lambda < 5000$ Å; *crosses,* $\lambda > 5000$ Å.

7. The Chemical Composition of ζ Capricorni

7.1. The Abundances

Having visually fitted the adopted theoretical curve of growth as well as possible to each of the empirical curves, and thereby found the relative horizontal shifts, the determination of differential chemical abundances in ζ Cap with respect to the sun and to ϵ Vir is straightforward. In none of these stars is second ionization important. Attention can therefore be confined to the neutral and singly ionized stages.

Now, for a given element in ζ Cap and one of the comparison stars (*) we can write

$$\log \frac{N_r^\zeta}{N^\zeta} - \log \frac{N_r^*}{N^*} = \log \frac{N_r^\zeta}{N_r^*} - \log \frac{N^\zeta}{N^*} \tag{7.1}$$

or

$$\log \frac{N^\zeta}{N^*} = \log \frac{N_r^\zeta}{N_r^*} - \log \frac{N_r^\zeta}{N^\zeta} + \log \frac{N_r^*}{N^*}. \tag{7.2}$$

In the bracket notation, this becomes

$$[N] = [N_r] - [N_r/N]. \tag{7.3}$$

In this expression, N is the *total* number of atoms per gram of stellar material, and N_r is the number of them in the rth stage of ionization. The last term is the logarithmic ratio of the fraction of atoms found in the rth stage of ionization in the two stars and is calculated directly from the ionization equation by using the appropriate known values of T_{ion} and P_e. We seek the quantity $[N]$.

By eq (4.6), the first term on the right side of eq (7.3) is given by the difference in opacities and the horizontal shift of the empirical curve of growth onto the theoretical one. That is,

$$[N_r] = [X] + [k]. \tag{7.4}$$

Combining eqs (7.3) and (7.4), we obtain

$$[N] = [X] + [k] - [N_r/N]. \tag{7.5}$$

This is the basic relation by which the relative total abundances $[N]$ in ζ Capricorni have been determined.

The reasonable assumption is made that absorption by H^- represents the dominant opacity source in these stars. The formula given by Koelbloed (1953) can then be used for the calculation of the logarithmic difference $[k]$:

$$[k] = 1.75\Delta\theta_{\text{ion}} + [P_e]. \tag{7.6}$$

Using the values for $\Delta\theta_{\text{ion}}$ and $[P_e]$ found in section 6.2 we obtain

$$[k]_{\zeta-\odot} = 0.18 - 1.28 = -1.10 \tag{7.7}$$

and

$$[k]_{\zeta-\epsilon} = -0.16 + 0.13 = -0.03. \tag{7.8}$$

The absolute parameters necessary to evaluate $[N_r/N]$ by the Saha equation can be obtained by adding the differential parameters derived earlier to the solar values adopted in section 6.2 for a representative optical depth of 0.35. These parameters are listed in table 7.1. The values derived for $[N_r/N]$ depend primarily on the differential parameters and are not sensitive to the absolute values used in the Saha equation.

TABLE 7.1. *Parameters used in the determination of relative ionization equilibria*

	Sun	$\Delta(\zeta-\odot)$	ζ Cap	$\Delta(\zeta-\epsilon)$	ϵ Vir
θ_{ion}	0.89	+0.10	0.99	−0.09	1.08
$\log P_e$	1.30	−1.28	+.02	+.13	−0.11

To solve Saha's equation,

$$\log \frac{N_+}{N_0} = -\theta I + 2.5 \log T - 0.48 + \log \frac{2u^+(T)}{u^\circ(T)} - \log P_e, \tag{7.9}$$

it is also necessary to know the partition functions $u(T)$. The same values were used for all three stars and were taken mainly from the tabulation by de Galan (1968) for an average temperature $T=5200$ K. The partition functions for some rare earths are not well known because of the fragmentary state of the spectral analyses. The values estimated by Corliss and Bozman (1962) for some of these ions have been adopted here, but for Ce I, Ce II, Nd I, Nd II, Sm I, and Sm II the new energy levels from unpublished analyses in progress by W. C. Martin, Z. Goldschmidt, J. F. Wyart, and others have been used to calculate new partition functions according to the relation

$$u(T)=\sum_{s=0}^{n} g_s e^{-E_s/kT}, \qquad (7.10)$$

TABLE 7.2. *First Ionization Potentials and Partition Functions Used in the Calculation of Ionization Corrections to the Relative Abundances*

($T=5200$ K)

Element	I. P.	$u°(T)$	$u^+(T)$
	(eV)		
Li	5.39	2.1	1.0
C	11.26	9.2	5.9
O	13.61	8.9	4.0
Na	5.14	2.1	1.0
S	10.36	8.9	4.2
Mg	7.64	1.0	2.0
Al	5.98	5.9	1.0
Si	8.15	9.5	5.7
Ca	6.11	1.2	2.2
Sc	6.54	12.2	23.2
Ti	6.82	30.9	56.5
V	6.74	49.0	44.5
Cr	6.76	10.8	7.3
Mn	7.43	6.5	7.8
Fe	7.87	28.5	44.2
Co	7.86	34.4	30.4
Ni	7.63	31.2	11.1
Cu	7.72	2.4	1.0
Zn	9.39	1.0	2.0
Ge	7.90	7.7	4.5
Sr	5.69	1.3	2.2
Y	6.38	12.1	16.3
Zr	6.84	35.5	46.8
Nb	6.88	54.9	44.8
Mo	7.10	11.6	7.9
Ru	7.36	35.3	24.5
Ba	5.21	2.7	4.3
La	5.58	27.0	30.3
Ce	5.65	188.0	190.0
Pr	5.42	80.0	87.0
Nd	5.49	85.0	103.0
Sm	5.63	37.8	61.6
Eu	5.68	9.2	15.7
Gd	6.16	51.0	78.0
Dy	5.93	90.0	100.0
Ta	7.88	18.0	23.7
W	7.98	13.4	14.6
Pb	7.42	1.6	2.1

where g_s is the statistical weight $2J+1$ of the level whose energy is E_s, k is Boltzmann's constant, and T is the adopted ionization temperature. The values used here for first ionization potentials and partition functions are tabulated in table 7.2.

By setting $[N]=0.00$ in eq (7.5), we calculated for each observed curve of growth the quantity

$$[X]'=[N_r/N]-[k] \qquad (7.11)$$

which represents the predicted horizontal abundance shifts on the assumption of equal total abundances in the barium and comparison star. The actual logarithmic abundance ratios are then given by the difference between the observed and predicted shifts. That is,

$$[N]=[X]-[X] \qquad (7.12)$$

The results are presented in table 7.3. The successive columns give the spectrum from which the abundance was derived, the predicted and observed shifts relative to the sun, the corresponding quantities relative to ϵ Vir, and finally the derived abundance ratios.

The abundances of the elements in the iron group tend to be systematically lower in the barium star than in ϵ Virginis, but the effect is quite small. A similarly small, but now positive, difference is found for the differential abundances relative to the sun. This latter result supports an argument by Warner (1964a), who estimated that a differential analysis of a cool giant relative to the sun will yield abundances systematically too large by ~ 0.05 to 0.10 dex because of differences in the temperature structure of their atmospheres.

The apparent sodium deficiency in ζ Cap relative to ϵ Vir is probably a reflection of the corresponding *excess* of sodium found by the Cayrels in ϵ Vir. In general, the abundances in ζ Cap relative to the sun and to ϵ Vir are in excellent agreement.

The abundances of Ce, La, Nd, Pr, Sm, and Y relative to ϵ Vir have also been determined from the curves of growth constructed by use of NBS gf-values. As discussed in section 4.3, it was necessary to apply correction factors δ to convert the observed shifts of the absolute curves to the system of line strengths in ϵ Vir. The abundance results for these elements, given in table 7.4, tend to be somewhat smaller than those derived directly from the stellar line strengths. The results in table 7.4 have been averaged with the dif-

TABLE 7.3. *Logarithmic abundance ratios*

Spectrum	Pred. shift$_\odot$	Obs. shift$_\odot$	Pred. shift$_\epsilon$	Obs. shift$_\epsilon$	$[N]_\odot$	$[N]_\epsilon$
Li I	0.48	0.81	−0.42	....	+0.33	....
C I	1.10	1.45	.03	−0.05	+.35	(−0.08)
O I	1.10	1.05	.03	....	−.05	....
Na I	0.45	0.63	−.40	−.65	+.18	(−.25)
Mg I	.71	.69	−.60	−.74	−.02	−.14
Al I	.54	.73	−.47	−.50	+.19	−.03
Si I	.82	.92	−.47	−.50	+.10	−.03
Si II	1.17	1.17	.23	....	.00	....
S I	1.10	1.38	.02	−.20	+.28	−.22
Ca I	0.55	0.64	−.48	−.59	+.09	−.11
Sc I	.59	.83	−.52	−.38	+.24	+.14
Sc II	1.10	1.23	.03	.16	+.13	+.13
Ti I	0.62	0.70	−.55	−.48	+.08	+.07
Ti II	1.10	1.22	.03	−.04	+.12	−.07
V I	0.61	0.64	−.54	−.57	+.03	−.03
Cr I	.62	.75	−.54	−.59	+.13	−.05
Cr II	1.11	1.08	.04	−.14	−.03	−.18
Mn I	0.69	0.72	−.58	−.76	+.03	−.18
Fe I	.74	.80	−.59	−.64	+.06	−.05
Fe II	1.12	1.17	.08	.04	+.05	−.04
Co I	0.75	0.79	−.56	−.58	+.04	−.02
Ni I	.75	.79	−.52	−.58	+.04	−.06
Cu I	.76	1.02	−.52	−.71	+.26	−.19
Zn I	.99	0.98	−.24	−.04	−.01	+.20
Ge I	.78	.96	−.52	....	+.18	....
Sr I	.50	1.59	−.45	.49	+1.09	+.94
Y I	.57	1.48	−.51	.49	+0.91	+1.00
Y II	1.10	2.29	.03	1.24	+1.19	+1.21
Zr I	0.62	1.41	−.55	0.36	+0.79	+0.91
Zr II	1.10	2.03	.03	.86	+.93	+.83
Nb I	0.63	0.92	−.55	....	+.29	....
Mo I	.66	1.41	−.56	....	+.75	....
Ru I	.69	1.18	−.57	....	+.49	....
Ba II	1.10	2.50	.03	1.40	+1.40	+1.37
La II	1.10	2.09	.03	0.96	+0.99	+0.93
Ce II	1.10	2.17	.03	.96	+1.07	+.93
Pr II	1.10	1.91	.03	.68	+0.81	(+.65)
Nd II	1.10	2.06	.03	1.01	+.96	+.98
Sm II	1.10	1.99	.03	0.80	+.89	+.77
Eu II	1.10	1.26	.03	....	+.16	....
Gd II	1.10	1.48	.03	....	+.38	....
Dy II	1.10	1.95	.03	....	+.85	....
W I	0.77	1.14	.12	....	+.37	....
Pb I	0.69	1.41	.05	....	+.72	....

TABLE 7.4. *Abundances derived from NBS* gf-*values converted to line strengths in* ϵ *Virginis*

Element	Predicted shift	Observed shift − δ	$[N]_\epsilon$
Ce	+0.03	0.93	0.90
La	+.03	.85	.82
Nd	+.03	.95	.92
Pr	+.03	.98	.95
Sm	+.03	.78	.75
Y	+.03	1.06	1.03

TABLE 7.5. *Logarithmic abundances in* ζ *Capricorni relative to iron*

Element	[N(El)/N(Fe)] This study	Estimated error (see text)	[N(El)/N(Fe)] Warner
Li	+0.27	0.4	+1.05
C	+.29	.3	
O	−.11	.3	
Na	+.12	.3	+0.20
Mg	−.08	.35	+.07
Al	+.07	.35	+.04
Si	.00	.2	
S	+.03	.3	
Ca	−.01	.2	.00
Sc	+.15	.2	−.05
Ti	+.04	.2	+.14
V	.00	.2	+.04
Cr	−.04	.15	+10
Mn	−.08	.15	−.08
Co	.00	.15	−.05
Ni	−.02	.15	+.03
Cu	+.03	.25	
Zn	+.09	.3	−.10
Ge	+.12	.3	−.15
Sr	+1.01	.3	+.18
Y	+1.06	.25	+.70
Zr	+0.86	.35	+.60
Nb	+.23	.4	
Mo	+.69	.2	+.47
Ru	+.43	.3	+.45
Ba	+1.38	.5	+1.00
La	+0.93	.3	+0.36
Ce	+.98	.2	+.55
Pr	+.88	.3	+.57
Nd	+.97	.25	+.26
Sm	+.82	.25	+.31
Eu	+.10	.3	+.10
Gd	+.32	.3	+.05
Dy	+.79	.4	
W	+.31	.5	+.61
Pb	+.66	.5	+.31

ferential results in deriving final values for the relative abundances in ζ Cap.

The final description of the chemical composition of ζ Capricorni is presented in table 7.5. The values given for the abundances have been normalized to iron by taking $[N(\mathrm{Fe})]=0.00$. By giving the abundances relative to iron, the small systematic effects mentioned above are eliminated, and the averages of the results obtained from the two comparison stars become more meaningful. The separate abundances derived for the same element observed in two stages of ionization have also been averaged. In all cases there is excellent agreement between the two determinations.

The assumption has been made, of course, that the atmospheres of ϵ Virginis and the sun have identical compositions. The detailed analysis by the Cayrels has shown this assumption to be correct except possibly for sodium. The abundance derived for sodium relative to ϵ Vir has, therefore, been disregarded in the preparation of the final table. The same is true for carbon and praseodymium, whose abundances relative to ϵ Vir were based on only one and two lines, respectively.

7.2. Use of ζ Capricorni as a Comparison Star

In comparing a barium star with the sun or a normal giant, one encounters the problem, owing to differences in opacity and abundances, that many of the rare earth lines strong enough to have been measured in the comparison star are already so strong in the barium star as to fall on the unfavorable flat portion of the curve of growth. Moreover, the weakness of the solar comparison lines of these elements makes their equivalent widths difficult to measure accurately and undoubtedly contributes to the large scatter in several of the differential curves of growth. The weaker rare earth lines found in ζ Capricorni do not appear in the comparison stars at all.

It might be argued that differences among barium stars themselves could be more reliably established by selecting a member of their own class as the comparison star for a differential analysis. It is not suggested that ζ Capricorni, the brightest known barium star and logical candidate, is at present suitable for this purpose. It is highly desirable that independent measurements of equivalent widths from additional sets of plates, preferably including the spectral region from 4800 Å to 5100 Å, first be obtained and perhaps a detailed depth-dependent analysis performed.

As an example, however, several differential curves of growth have been constructed for the Ba II star HD 116713 relative to ζ Cap. The equivalent widths for HD 116713 are taken from the work of Danziger (1965).

The stellar line strengths were obtained by reading the equivalent widths measured in the present investigation into the normalized curve of growth adopted for ζ Capricorni in section 4.4. The differential excitation temperature was found by the minimum-sigma method discussed in section 6.1 to be $\Delta\theta_{\mathrm{exc}}(\mathrm{HD}\ 116713-\zeta)=0.11\pm0.04$. The results for Fe I, Ca I, and Sm II are shown in figures 7.1 through 7.3. For the illustrations, the blue and red lines have been combined into a single curve of growth by compensating for the logarithmic difference of 0.15 in log v found by Danziger between the two regions. The theoretical curve of growth fitted to these plots is that adopted for ζ Capricorni. Differential curves drawn for several other spectra were not quite so smooth as these, but were completely acceptable. The analysis will not be pursued here, but it is of interest to note that the curve for Sm II is almost normalized, suggesting nearly equal abundances if Warner's result is adopted that the electron pressures in the two stars are essentially the same.

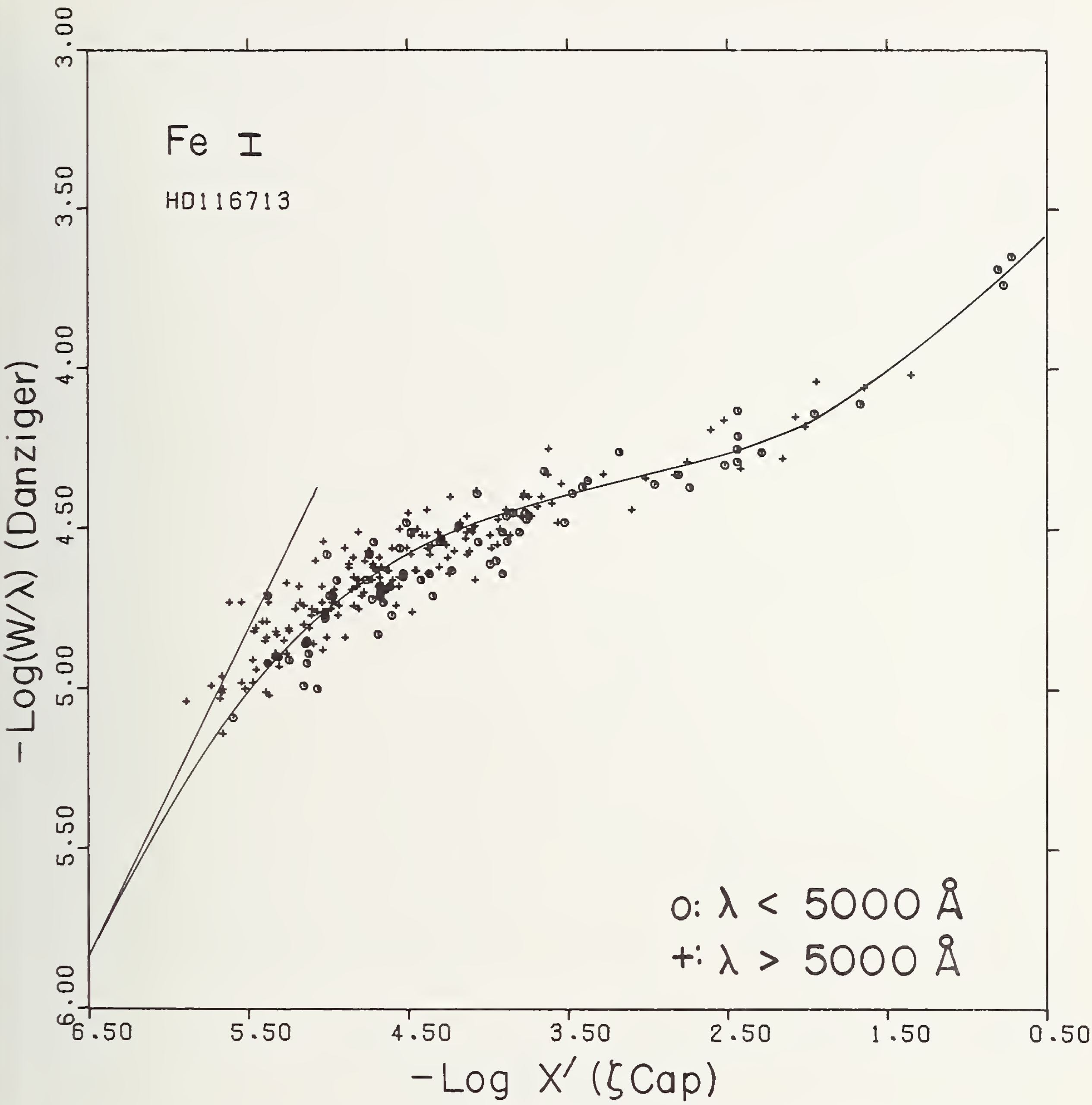

FIGURE 7.1. *Differential curve of growth relative to ζ Capricorni for neutral iron in the barium star HD 116713. Circles,* λ < 5000 Å; *crosses,* λ > 5000 Å.

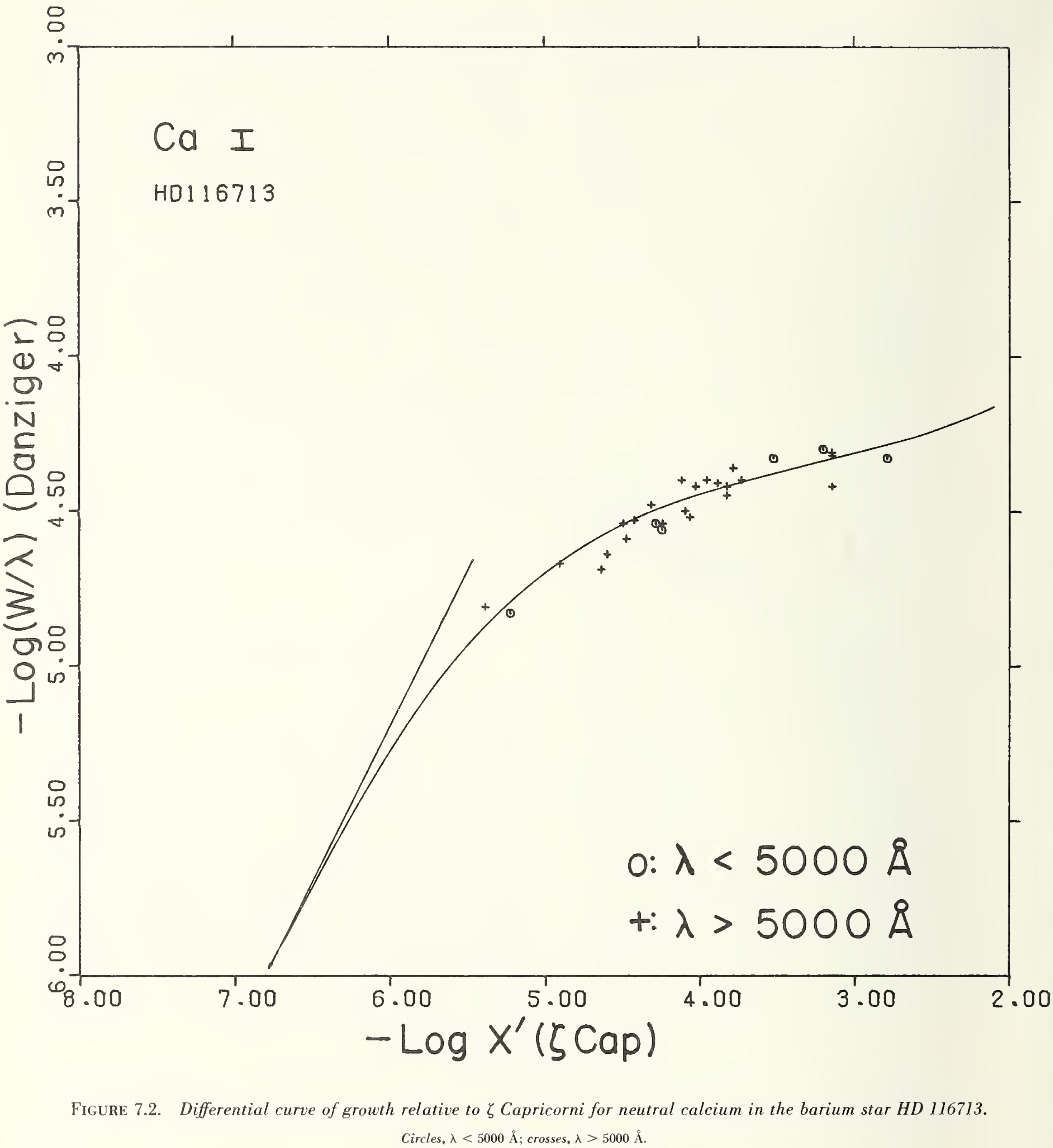

FIGURE 7.2. *Differential curve of growth relative to ζ Capricorni for neutral calcium in the barium star HD 116713. Circles, λ < 5000 Å; crosses, λ > 5000 Å.*

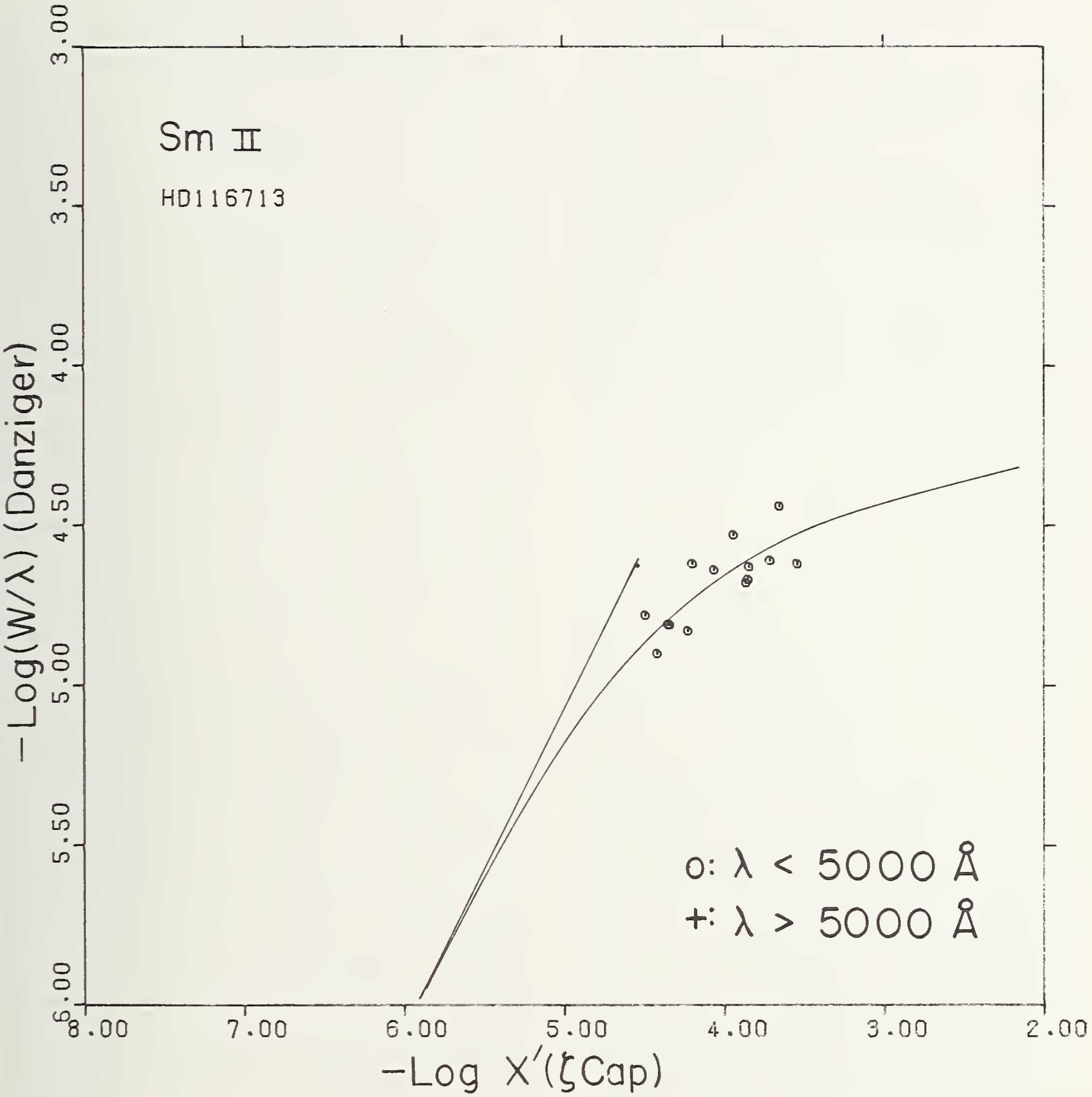

FIGURE 7.3. *Differential curve of growth relative to ζ Capricorni for singly ionized samarium in the barium star HD 116713. Circles, λ < 5000 Å; crosses, λ > 5000 Å.*

8. Discussion and Summary

8.1. The Accuracy of the Abundances

Experience has shown that the errors accumulating in any atmospheric analysis, no matter how carefully performed, usually produce an uncertainty by a factor of about two in the derived abundances. As pointed out by the Burbidges (1957), a quantitative evaluation of the actual error in this kind of work presents difficulties not easily surmounted.

An error in the value adopted for $\Delta\theta_{\text{exc}}$ affects mainly the abundances derived from neutral lines. In the case of ζ Cap, an error of ± 0.01 in the value adopted for $\Delta\theta_{\text{exc}}$ will produce a logarithmic abundance uncertainty of about ± 0.06 for most observed spectra. It is seen from eq. (7.6) that an error in $[P_e]$ is wholly transmitted to the opacity difference $[k]$, which, in turn, is transmitted to the abundances obtained from ions. Since $[P_e]$ depends on the product of $\Delta\theta_{\text{ion}}$ and the average ionization potential for the observed elements (~ 7 eV), an error of ± 0.01 in the value of $\Delta\theta_{\text{ion}}$ will generate uncertainties of about ± 0.07 in abundances derived from ion spectra—all the rare earths, for example. Since neither $\Delta\theta_{\text{exc}}$ nor $\Delta\theta_{\text{ion}}$ can be expected to be correct to better than ± 0.02, the uncertainty in the abundances can easily become ± 0.20 on a logarithmic scale.

Quite apart from errors in the differential parameters, the random errors involved in fitting theoretical curves of growth to the empirical curves severely limit the reliability of the derived abundances. In fact, it has become increasingly the practice in work of this kind to estimate errors in the abundances chiefly by a consideration of the maximum reasonable variation in fitting the curve of growth itself. This variation depends on a number of factors, including the total number of lines used and whether the lines fall on the linear or flat portions of the curve of growth. For spectra with few observed lines, the probable validity of the line identifications assumes dominating importance and must also be taken into account in any error estimate. It is not being overly cautious to distrust any abundance determination based on fewer than five or six good lines.

The estimates of error stated in table 7.5 have been made with all the above considerations in mind. In view of the general consistency of the data and the small scatter in most of the curves of growth, we might reasonably judge the overall accuracy of the abundances to be within the factor of two expected of the method.

8.2. Discussion

The specific abundance abnormalities exhibited by barium stars have been treated in detail by the Burbidges (1957). Their basic account remains essentially unchanged despite the minor modifications required by more recent estimates of neutron capture cross-sections (Seeger et al., 1965). Briefly, it is thought that the originally solar-type material in the interior of the barium star was subjected at some stage in its evolution to a source of neutrons that produced heavy elements from seed nuclei through the process of slow neutron capture. In this *s*-process of element formation, each capture is followed by β-decay to a stable isobar. Some of the *s*-processed stellar material is then brought to the spectroscopically observable surface layers through convective mixing, thus accounting for the abundance anomalies found in these stars relative to the sun, which has undergone a different history.

Among the lighter elements, carbon and lithium show overabundances in ζ Capricorni by about a factor of two. The result here for lithium differs considerably from the factor of ten obtained by Warner (1965a), but the discrepancy is solely attributable to the difference in measurements of equivalent width for the resonance doublet of Li I at 6707.84 Å.

The small overabundance (+ 0.12) obtained for sodium is probably real and appears to be typical of barium stars. Danziger (1965) found somewhat larger overabundances (+ 0.45) for sodium in HD 116713 and HD 83548. It is tempting to interpret the simultaneous excess of carbon and sodium observed in barium stars as evidence of the carbon "flash" discussed by Reeves (1966). Such a flash leads to a very rapid neutron flux that preferentially enhances these two elements. Since this postulated carbon flash almost simulates an *r*-process, the large dysprosium excess found in ζ Cap might also be explained as a product of this stage of the stellar history. However, the normal abundance found for *r*-processed europium would still remain a mystery.

The abundances of the elements from magnesium to germanium do not indicate any important deviations from the normal solar composition. In view of the error estimates, little significance can be attached to the slight overabundances ($\sim +0.10$) obtained for zinc, germanium, and scandium. It is of interest, however, that the result for scandium seems to be more or less typical of barium stars (Burbidge and Burbidge, 1957; Warner, 1965a). The most abundant isotope of scandium is *s*-processed from Ne, but according to the discussion by the Burbidges the production of a great excess of scandium would not be expected owing to the depletion of the neutron supply through the much greater capture cross sections of the iron-peak elements and their products.

The elements strontium, yttrium, and zirconium are similar in that they all have magic-number nuclei and about the same atomic weight. It has been argued (Helfer et al., 1959) that the relative overabundances of these three elements should, therefore, be nearly equal if the *s*-process is the dominant mechanism by which the elements have been formed. Within the experimental uncertainty, the abundances derived for these elements in ζ Capricorni are indeed nearly the same, all of them being overabundant by factors of 8 to 10 relative to the standard solar composition. The abundance for strontium is the most unreliable of these three elements, but the uncertainty is not sufficient to explain the difference by a factor of seven between the present result and that of Warner for the star. In contrast, the abundances derived for yttrium and zirconium in the two investigations are comparable.

The close agreement between the results here and those of Warner for molybdenum, ruthenium, tungsten, and lead is rather encouraging in the light of the paucity of lines observed for these elements and the differences in line identifications for the first two elements. Overabundances of these elements in ζ Cap by about a factor of two are certainly indicated.

The small overabundance obtained for niobium is probably real. There remains some doubt about the line identifications for niobium, but the overabundances found in this investigation and in those of Danziger (1965) and the Burbidges (1957) suggest that the enhancement of niobium is a general characteristic of barium stars.

The result obtained here for the barium abundance should not be taken too seriously, because the measured lines are far too strong to obtain accurate abundance shifts. As expected however, barium is certainly overabundant in ζ Cap—by about a factor of 10 to 30.

The results for the *s*-processed elements confirm the general impression given by a visual inspection of the stellar spectrum and are similar to the results obtained for barium stars by other workers. Among the rare earths, lanthanum, neodymium, praseodymium, cerium, and samarium are overabundant by a factor of eight or nine. The overabundance obtained for gadolinium is much smaller.

It is frustrating that dysprosium has not yet been measured in other barium stars. If the line identifications are correct, a substantial overabundance of this rare earth is indicated in ζ Capricorni. This result is of some interest, because if conflicts with the expectation that the dysprosium abundance in barium stars should be, like that of europium, essentially normal. Neither element is predominantly *s*-processed by current estimates.

In many respects, this independent study of ζ Cap at higher dispersion agrees well with that of Warner for the same star. The most important difference is the relative amounts by which the *s*-processed rare earths in the barium star are found to be overabundant with respect to the solar composition. It is noteworthy that the corresponding abundance ratios found by Danziger (1965)—after compensating for the metal deficiency of Arcturus, his comparison star—are also larger than those derived by Warner for the same two barium stars by about the factor of three found here in the case of ζ Capricorni. As pointed out by Cayrel and Cayrel de Strobel (1966) and by Unsöld (1969), part of this discrepancy might be explained on the basis of the differences in the physical parameters derived for the stars. The temperatures and electron pressures determined by Warner and Danziger for their common stars differ significantly, for example, but that is not the case for ζ Cap. Some of the abundance differences appear too large to be accounted for solely on this basis. Other effects, perhaps of a systematic nature, may be operative. For example, the striking difference of 0.7 dex found in the two investigations for the logarithmic abundance of neodymium relative to iron in ζ Cap appears to be incompatible with the reliability generally claimed for the differential method of abundance analyses. A detailed investigation of this problem is beyond the scope of the present work, but will be discussed further in connection with the model atmosphere analysis of ζ Cap currently in progress by the writer.

8.3. Summary

A differential curve of growth analysis for the barium star ζ Capricorni has been performed. Both the sun and ϵ Virginis have been used as comparison stars. The spectrograms used in the analysis were obtained by J. L. Greenstein at the coudé focus of the 200-in telescope. The reciprocal dispersion was 2.3 Å/mm in the blue and 3.4 Å/m in the red spectral regions. Table A presents identifications, half-widths, central depths, and equivalent widths for the 1100 spectral lines measured in this investigation.

The physical parameters derived for ζ Capricorni are collected in table 8.1.

TABLE 8.1. *Physical parameters for ζ Capricorni*

θ_{exc} : 1.13	$[P_e]_{\zeta-\odot}$: -1.28
θ_{ion} : 0.99	$[P_e]_{\zeta-\epsilon}$: $+0.13$
$\log 2\alpha$: -2.5	$[k]_{\zeta-\odot}$: -1.10
v_{micro} : 3.5 km/s	$[k]_{\zeta-\epsilon}$: -0.03
v_{macro} : 5.5 km/s	

The atmospheric abundances for 37 elements are given in tables 7.3 and 7.5. The results with respect to the sun and to ϵ Virginis are in excellent agreement. The barium star exhibits essentially solar abundances for most elements through germanium. Overabundances by factors of about two are indicated for carbon and lithium, however. The smaller overabundances found for sodium and scandium may be real, but the values are within the estimated error of the determinations. There may be a slight manganese deficiency.

With the exception of europium, all elements heavier than germanium are found to be overabundant in ζ Cap. Large overabundances have been found for the *s*-processed elements, as well as for dysprosium, which is generally considered to be *r*-processed. Although the writer has reasonable confidence in this result for dysprosium, the reliability of the determination is seriously affected by the difficulty in making positive line identifications and by the few lines upon which the determination is based.

The extent by which the rare earths are found to be overabundant—by factors of about eight or nine—is greater than that found by Warner for the same star. Similar results obtained by Danziger for two of the barium stars also studied by Warner suggest that the average scale of Warner's abundances for these elements may be too small.

Appendix

A.1. Sample Differential Curves of Growth

A number of the differential curves of growth constructed for the analysis of ζ Capricorni and not already displayed in connection with discussions in the main text are collected in this section. They are here presented in alphabetic order according to spectrum. Each plot contains differential curves of growth with respect to the sun (*circles*) and to ϵ Virginis (*crosses*).

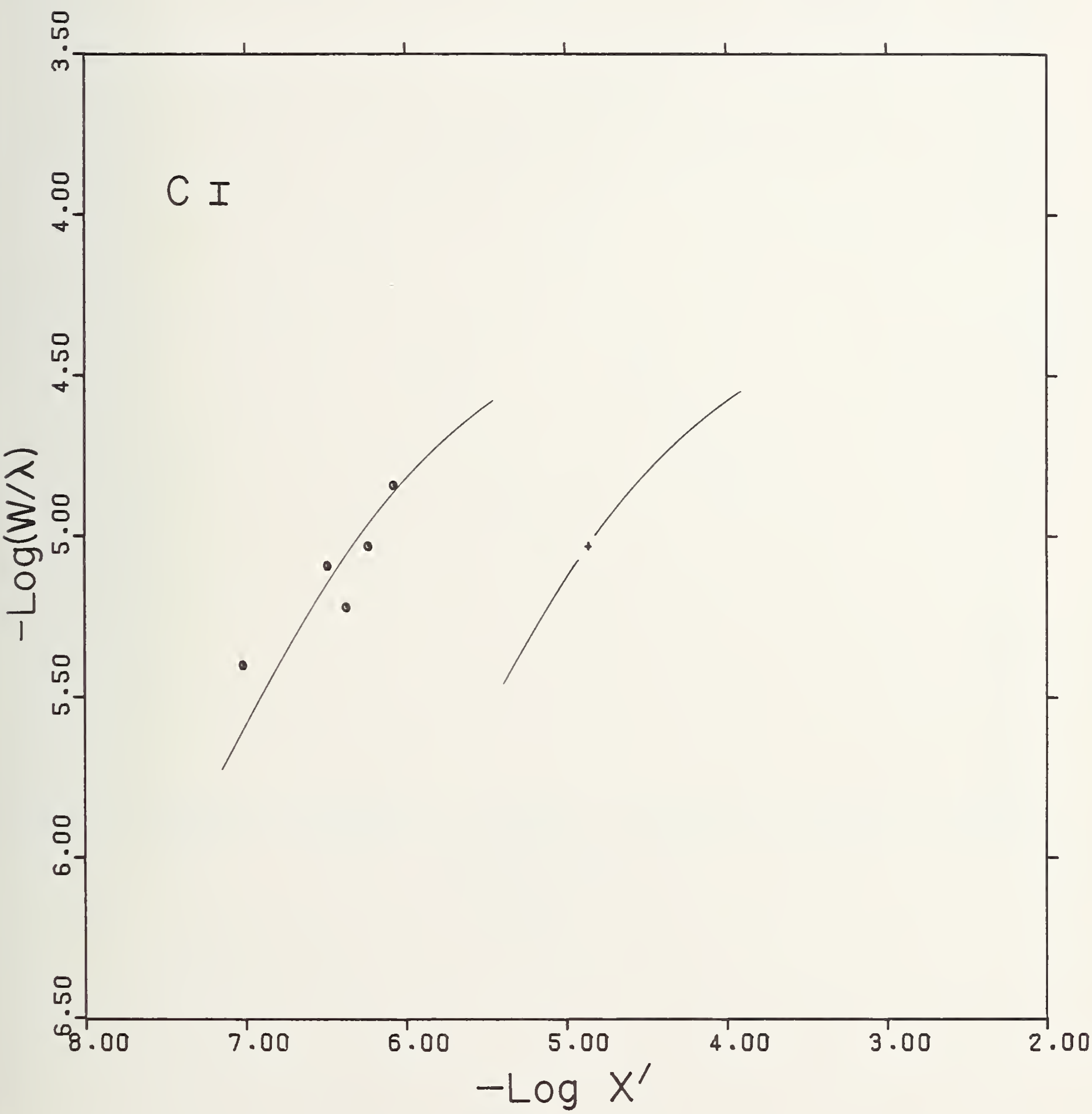

FIGURE A.1–1.

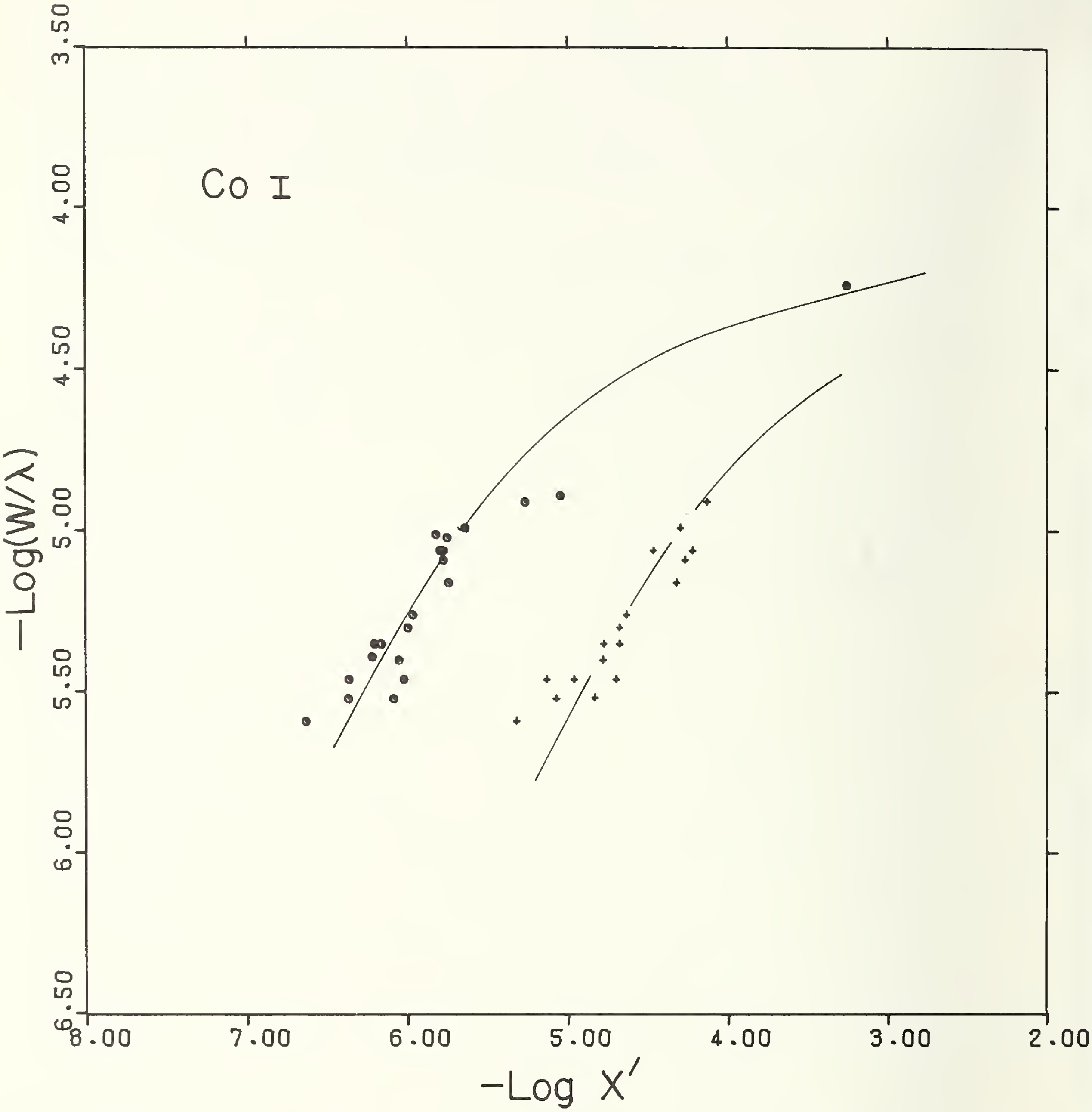
Co I
3.50
4.00
4.50
5.00
5.50
6.00
6.50
−Log(W/λ)
8.00
7.00
6.00
5.00
4.00
3.00
2.00
−Log X′

FIGURE A.1–2.

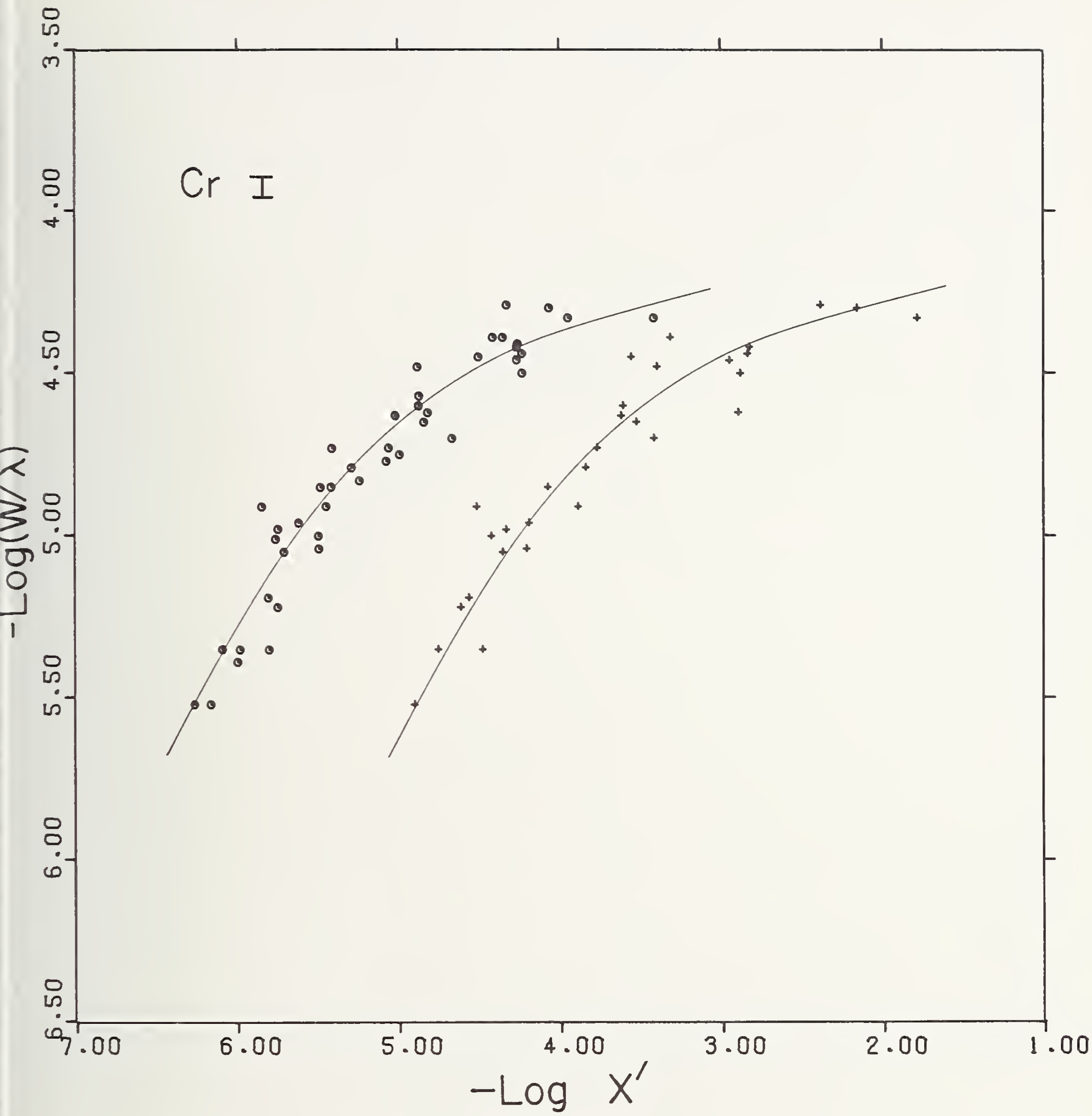

FIGURE A.1–3.

398-978 O - 71 - 7

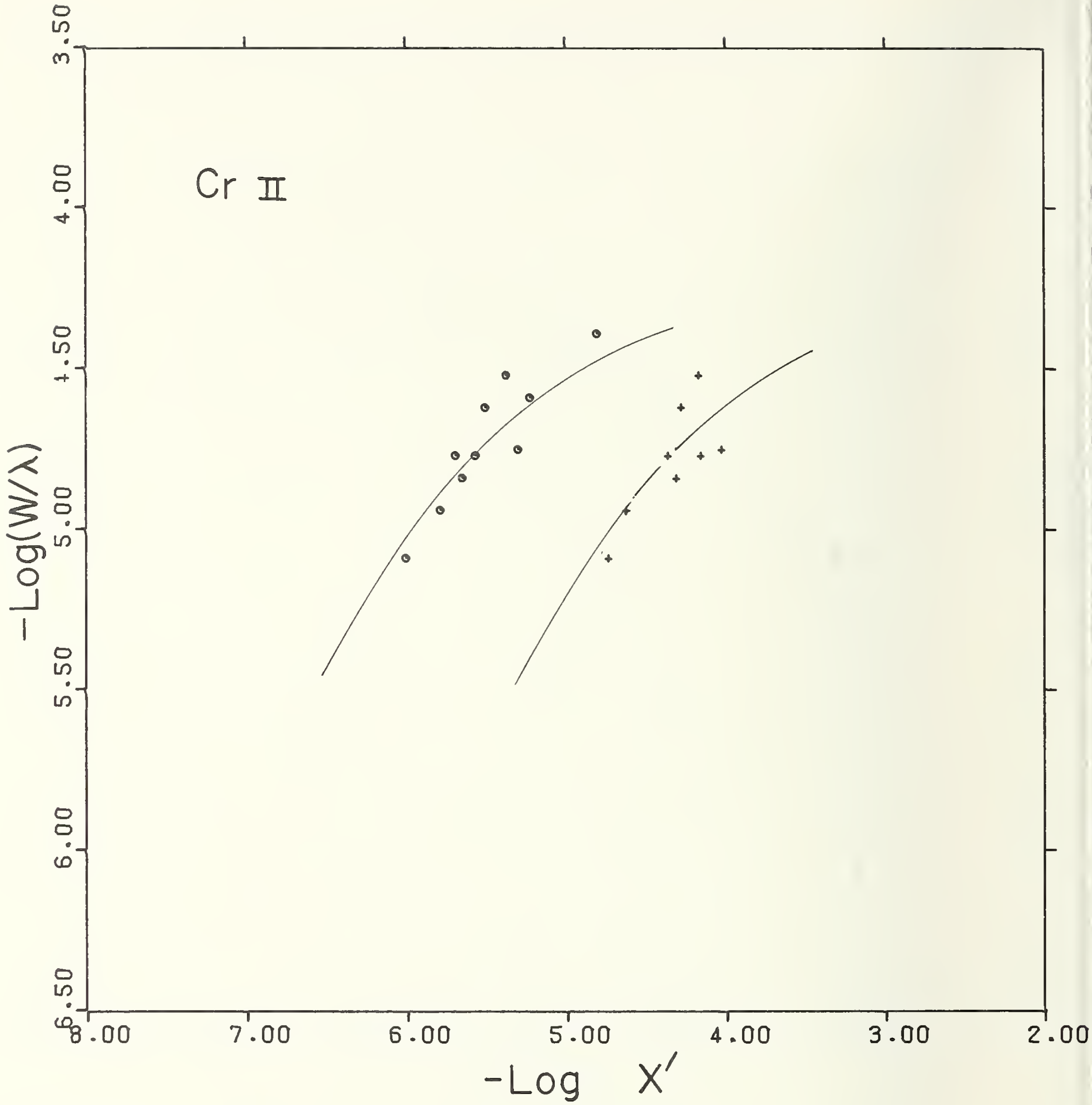

Cr II
3.50
4.00
4.50
5.00
5.50
6.00
6.50
-Log(W/λ)
8.00
7.00
6.00
5.00
4.00
3.00
2.00
-Log X′

FIGURE A.1–4.

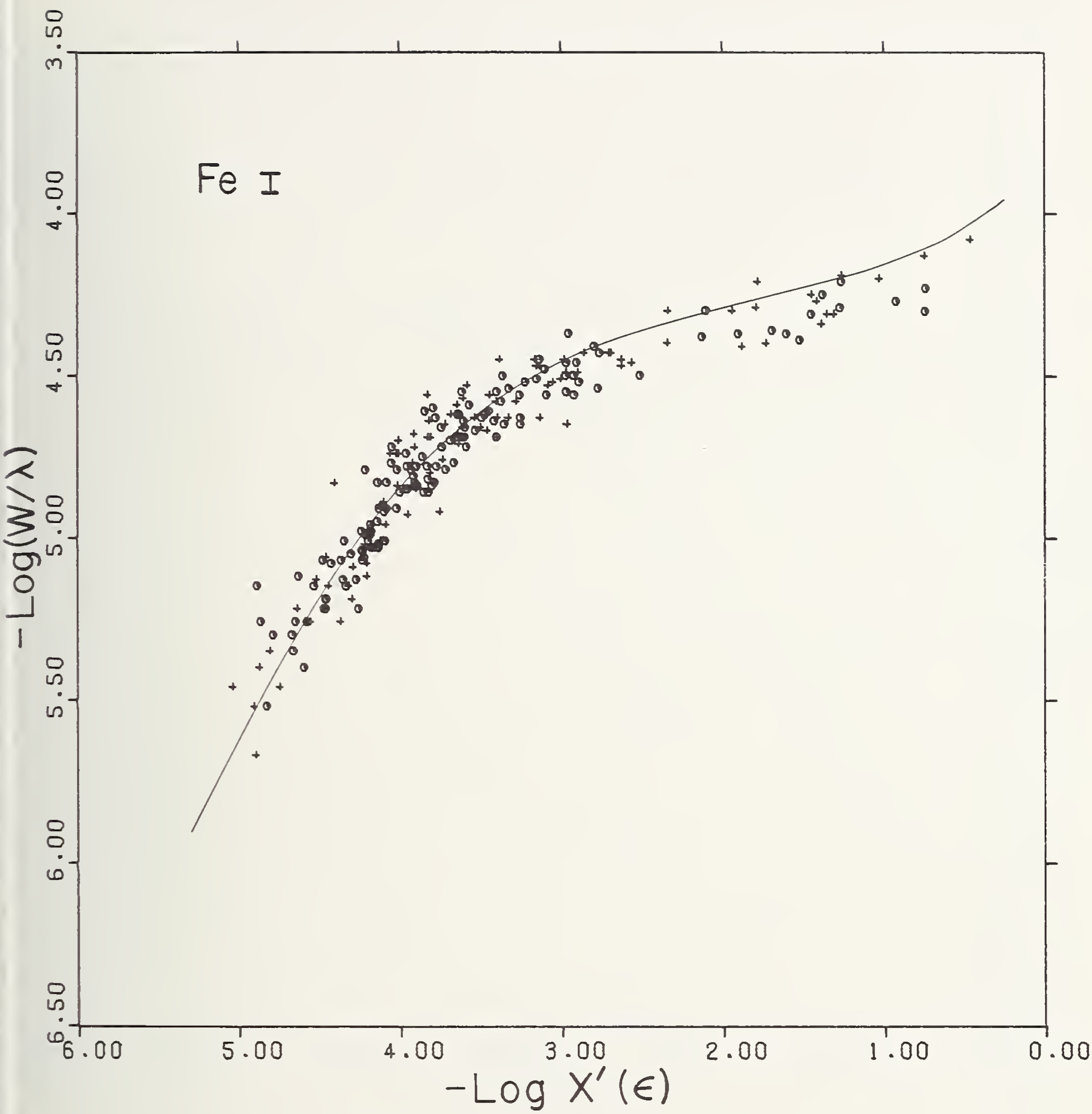

FIGURE A. 1–5. *Differential curve of growth with respect to ε Virginis only.*

Corresponding curves for Fe I with respect to the sun have already been shown and discussed in the main body of the text.

Circles, $\lambda < 5000$ Å; crosses, $\lambda > 5000$ Å.

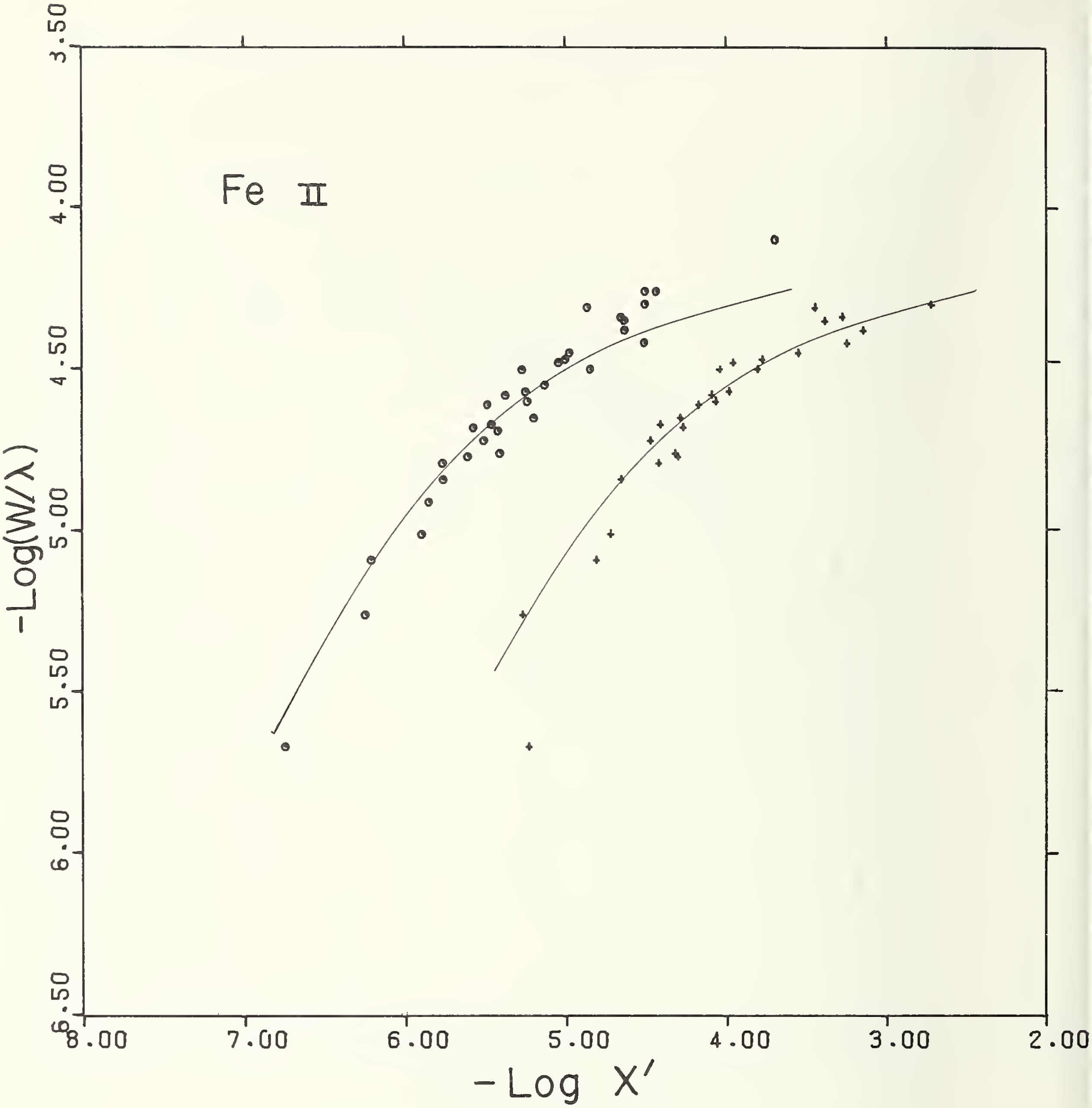

Fe II
3.50
4.00
4.50
5.00
5.50
6.00
6.50
-Log(W/λ)
8.00
7.00
6.00
5.00
4.00
3.00
2.00
-Log X′

FIGURE A.1–6.

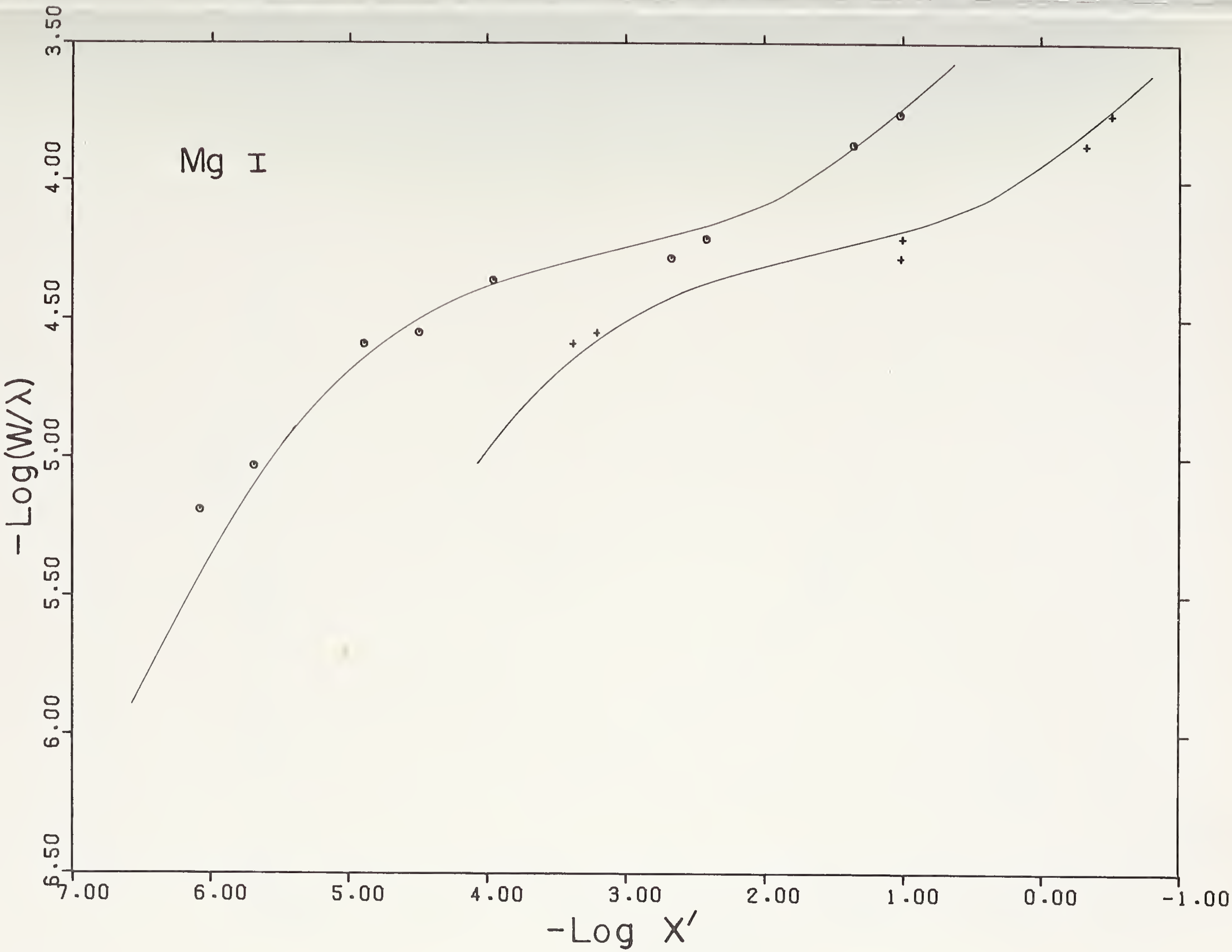

Mg I
3.50
4.00
4.50
5.00
5.50
6.00
6.50
−Log(W/λ)
7.00
6.00
5.00
4.00
3.00
2.00
1.00
0.00
−1.00
−Log X′

Figure A.1–7.

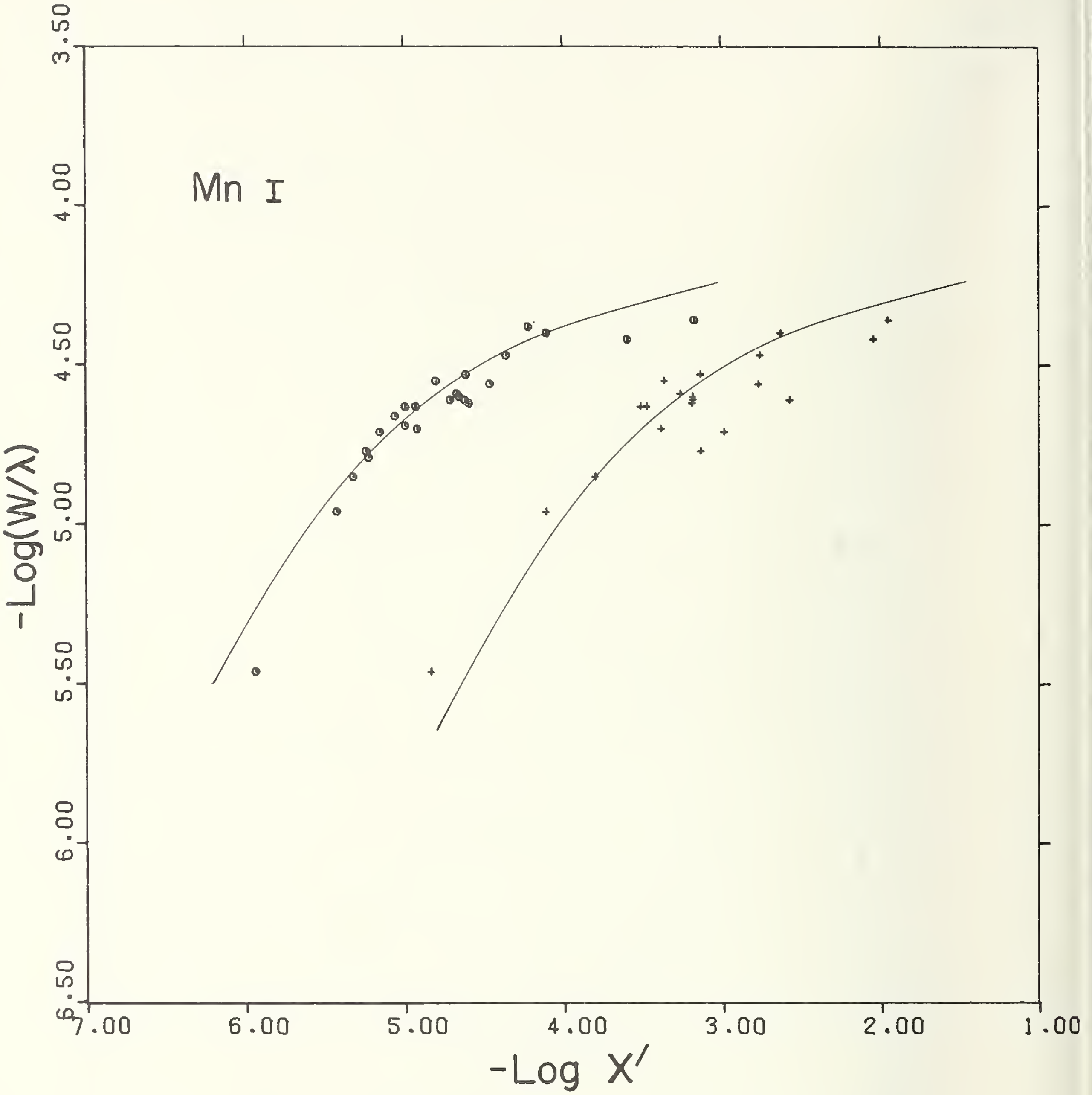

Mn I
-Log(W/λ)
3.50
4.00
4.50
5.00
5.50
6.00
6.50
7.00
6.00
5.00
4.00
3.00
2.00
1.00
-Log X′

FIGURE A.1–8.

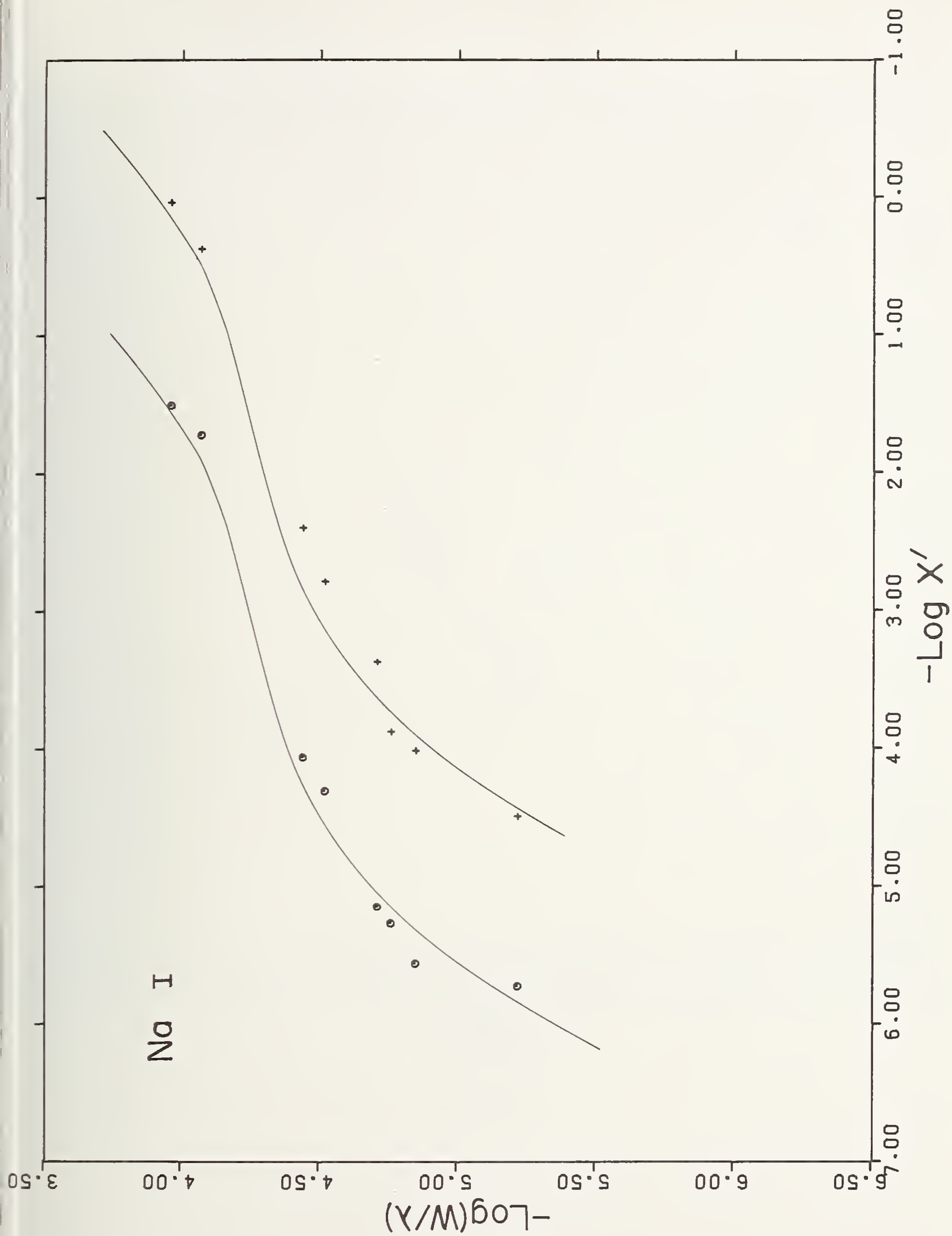

Na I
-Log X'
-Log(W/λ)
-1.00
0.00
1.00
2.00
3.00
4.00
5.00
6.00
7.00
3.50
4.00
4.50
5.00
5.50
6.00
6.50

FIGURE A.1–9.

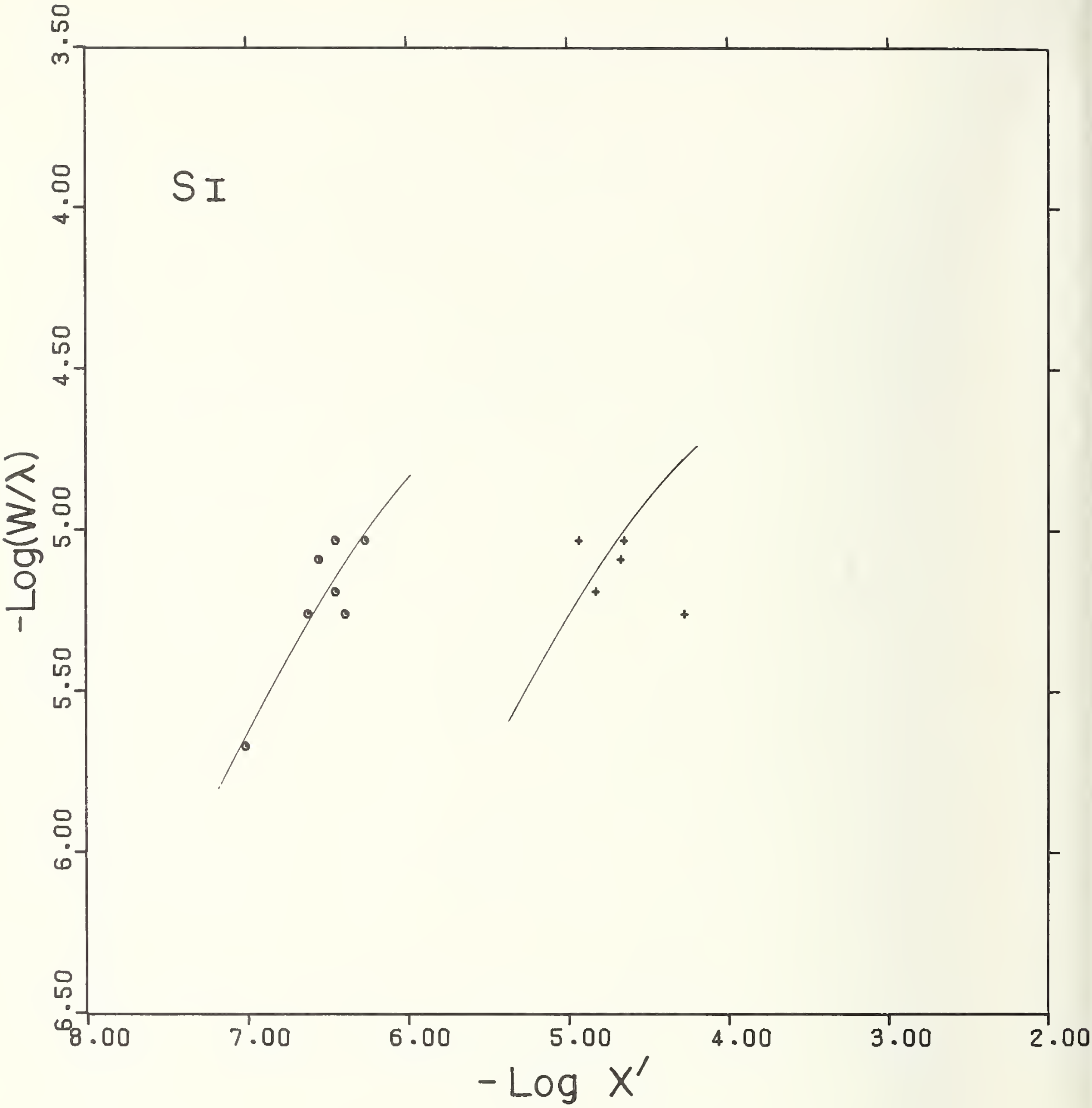
S I
-Log(W/λ)
3.50
4.00
4.50
5.00
5.50
6.00
6.50
8.00
7.00
6.00
5.00
4.00
3.00
2.00
- Log X′

FIGURE A.1–10.

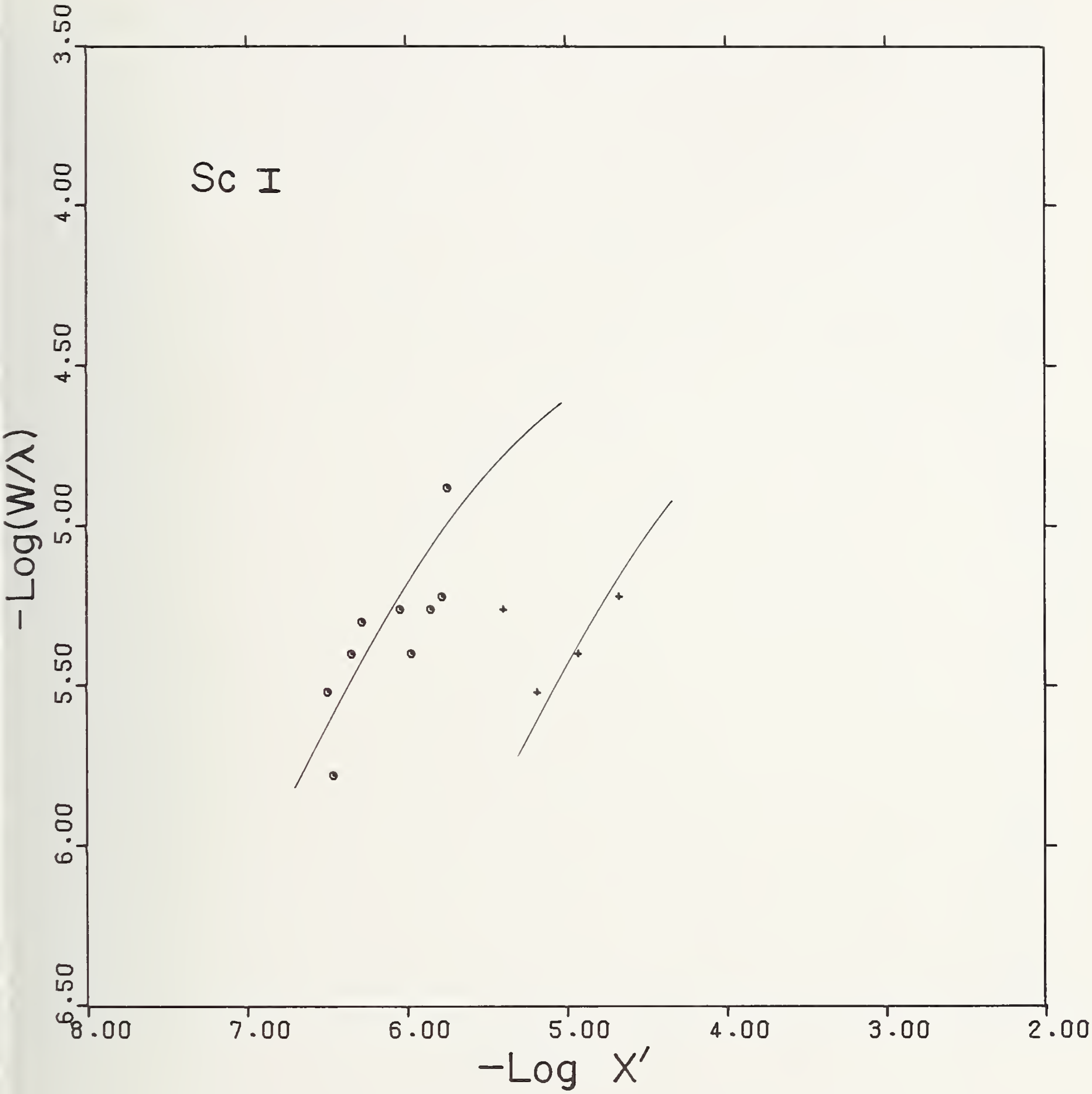

Sc I
3.50
4.00
4.50
5.00
5.50
6.00
6.50
−Log(W/λ)
8.00
7.00
6.00
5.00
4.00
3.00
2.00
−Log X′

Figure A.1–11.

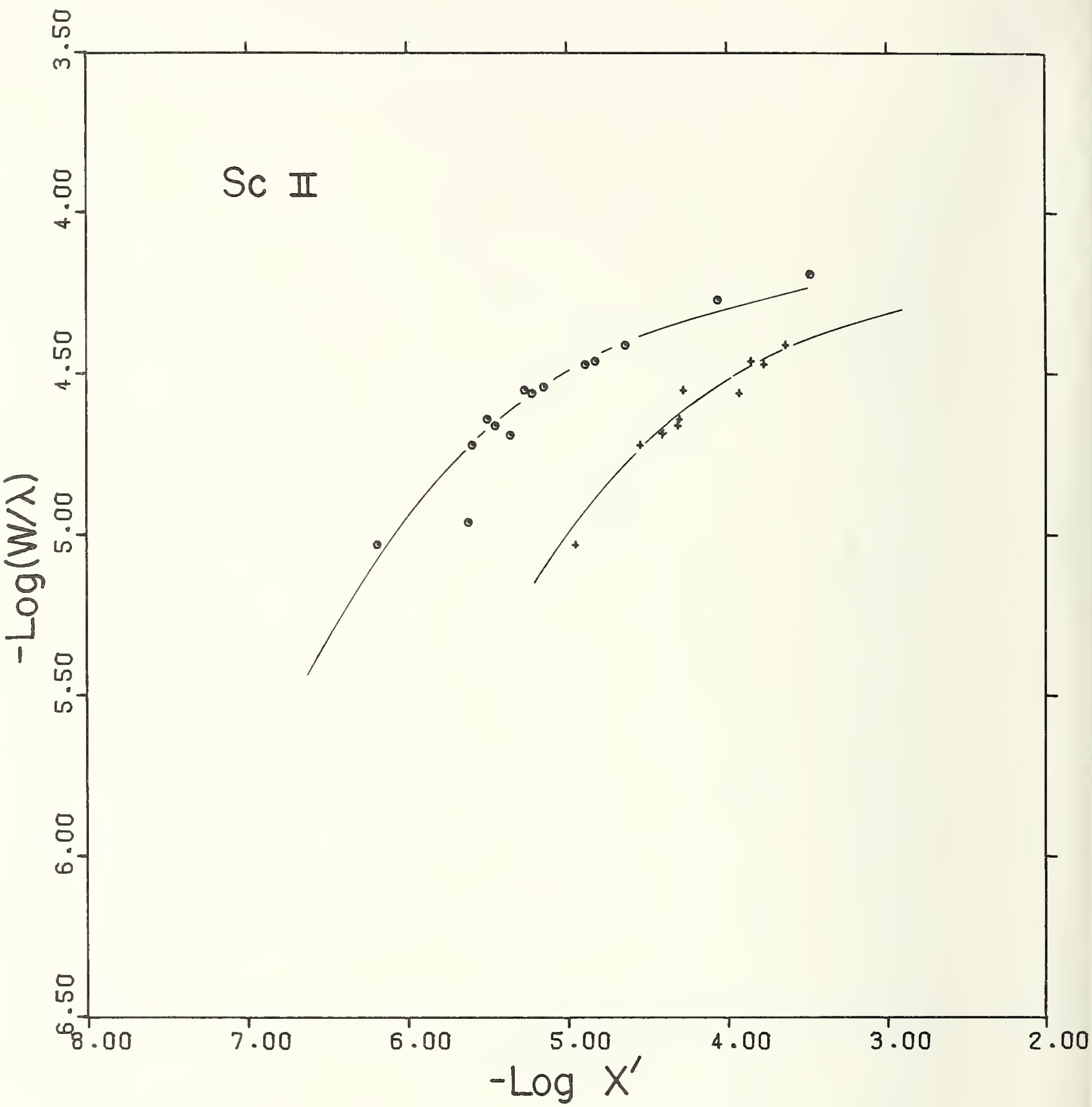
Sc II
-Log(W/λ)
3.50
4.00
4.50
5.00
5.50
6.00
6.50
8.00
7.00
6.00
5.00
4.00
3.00
2.00
-Log X′

FIGURE A.1–12.

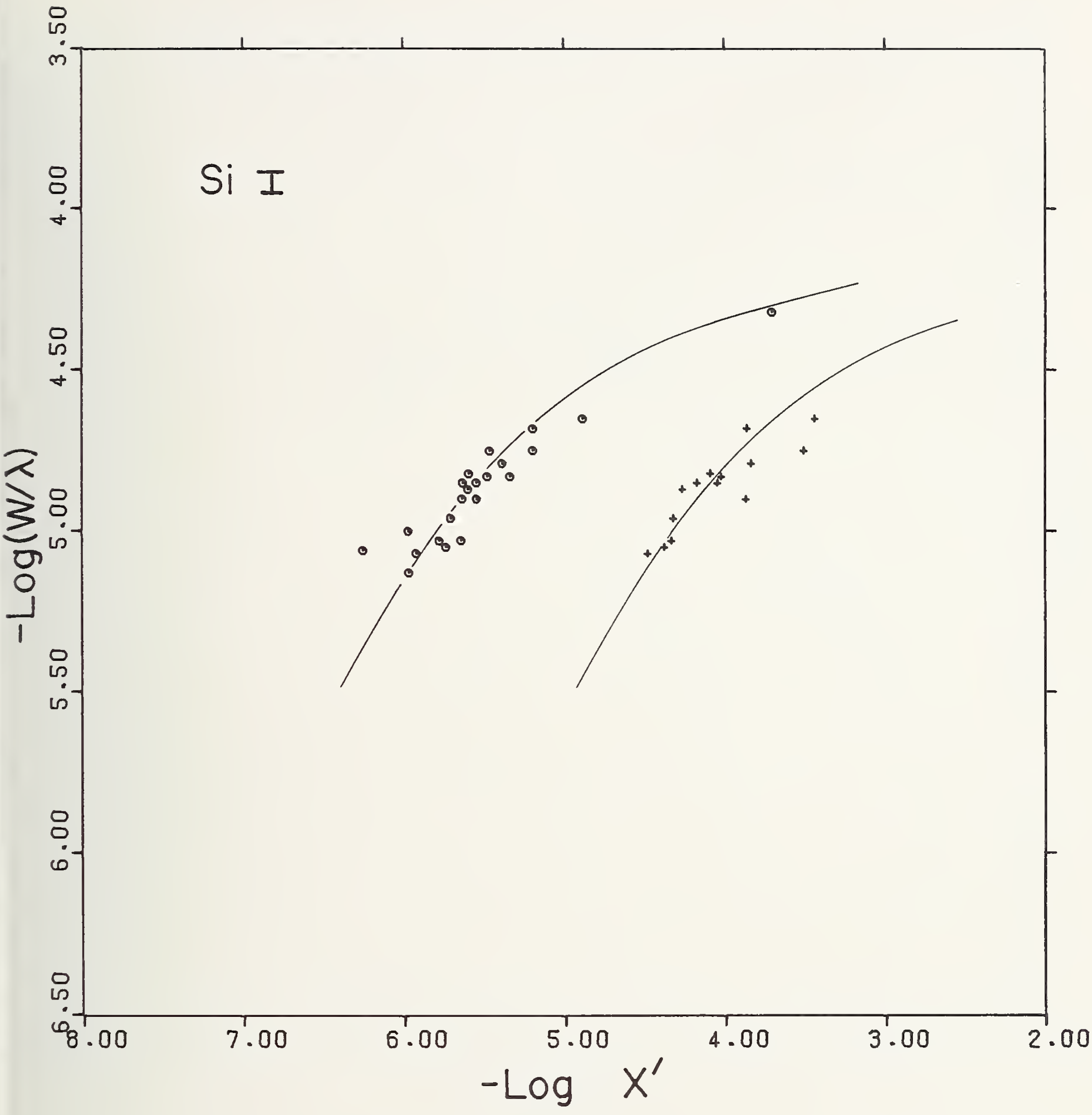

Si I
3.50
4.00
4.50
5.00
5.50
6.00
6.50
-Log(W/λ)
8.00
7.00
6.00
5.00
4.00
3.00
2.00
-Log X′

FIGURE A.1–13.

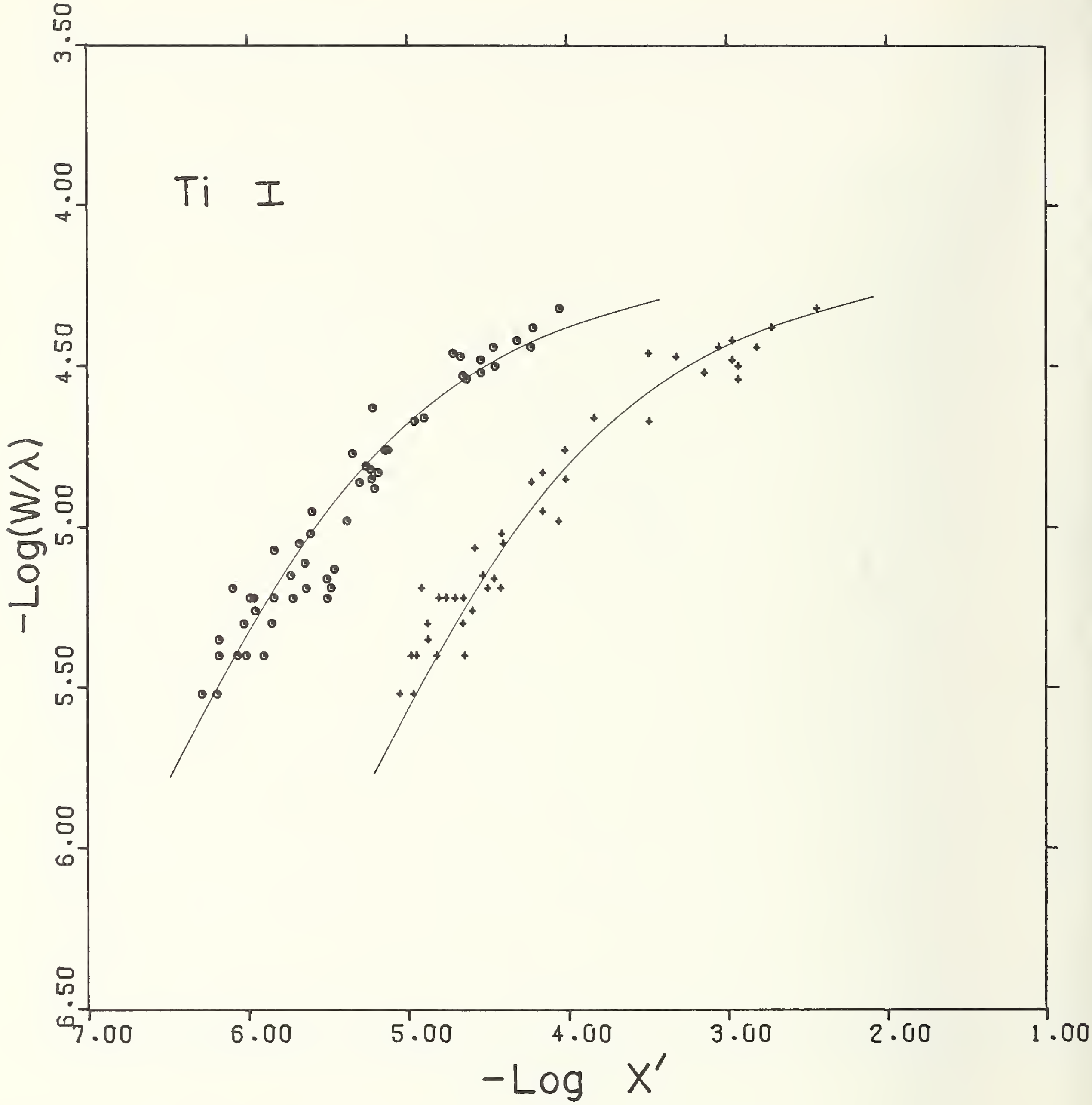

Ti I
-Log(W/λ)
3.50
4.00
4.50
5.00
5.50
6.00
6.50
7.00
6.00
5.00
4.00
3.00
2.00
1.00
-Log X′

FIGURE A.1–14.

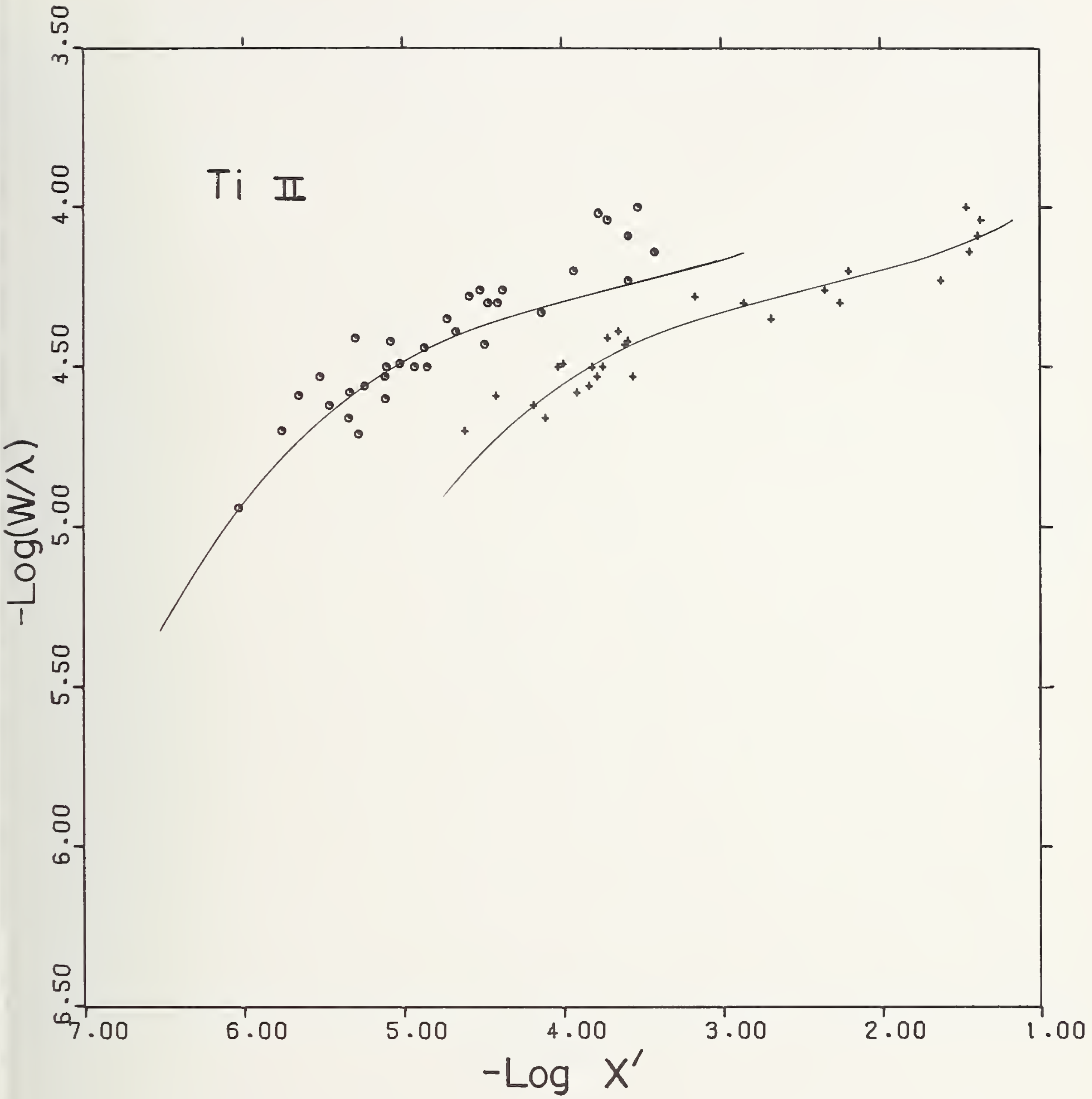
Ti II
-Log(W/λ)
3.50
4.00
4.50
5.00
5.50
6.00
6.50
7.00
6.00
5.00
4.00
3.00
2.00
1.00
-Log X′

Figure A.1–15.

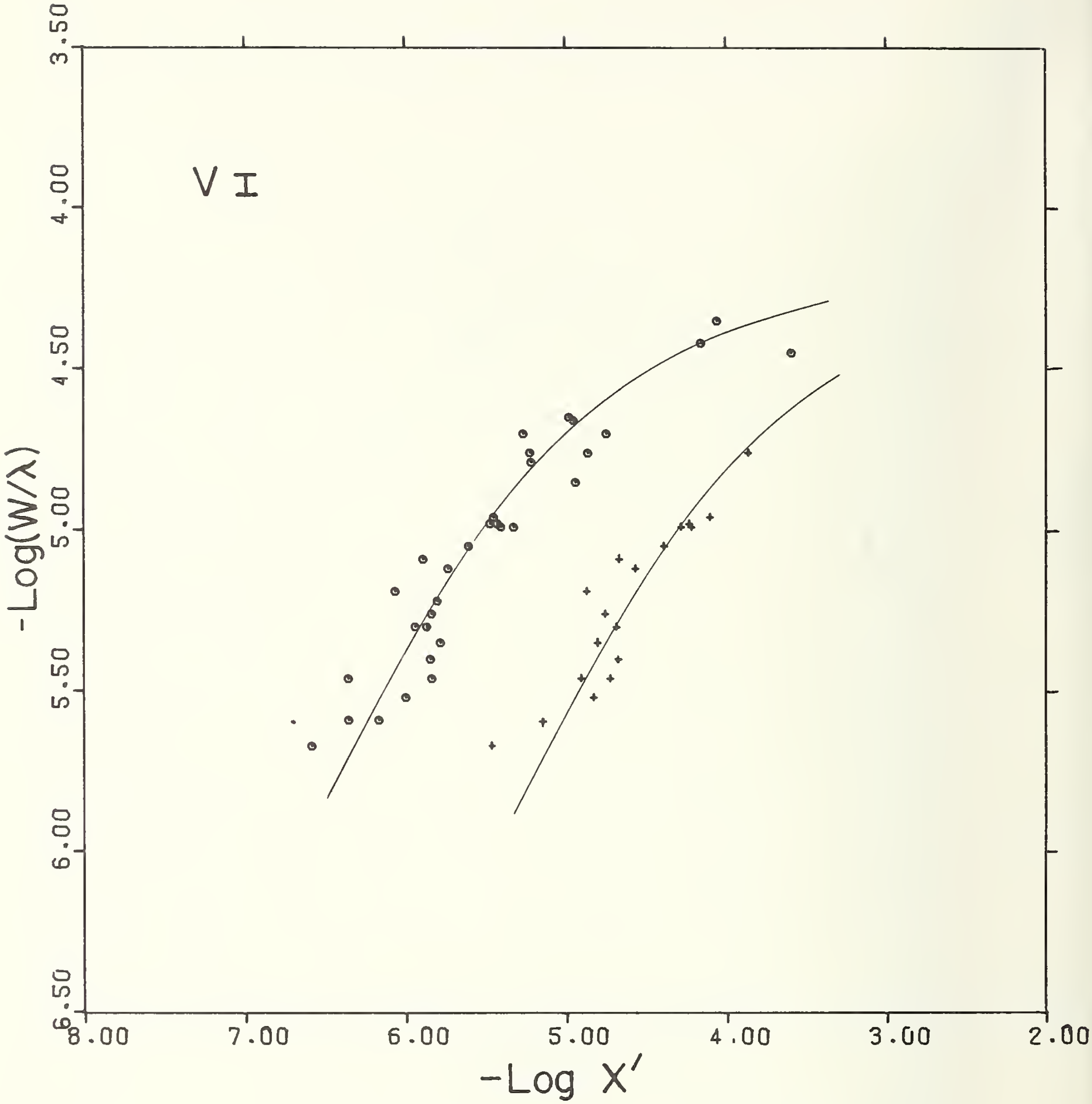

V I
-Log(W/λ)
3.50
4.00
4.50
5.00
5.50
6.00
6.50
8.00
7.00
6.00
5.00
4.00
3.00
2.00
-Log X′

FIGURE A.1–16.

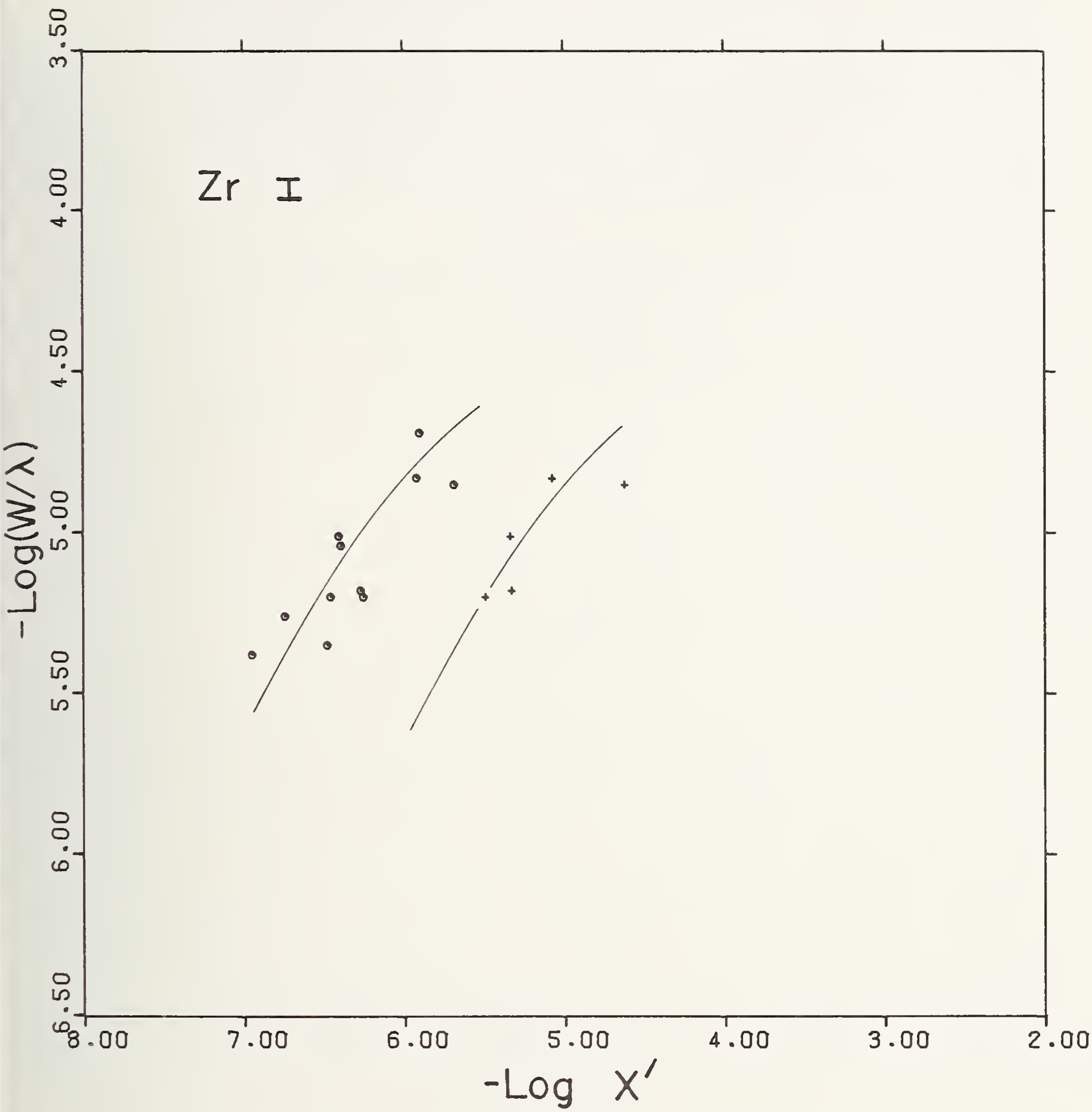
Zr I
-Log(W/λ)
-Log X′
3.50
4.00
4.50
5.00
5.50
6.00
6.50
8.00
7.00
6.00
5.00
4.00
3.00
2.00

FIGURE A.1–17.

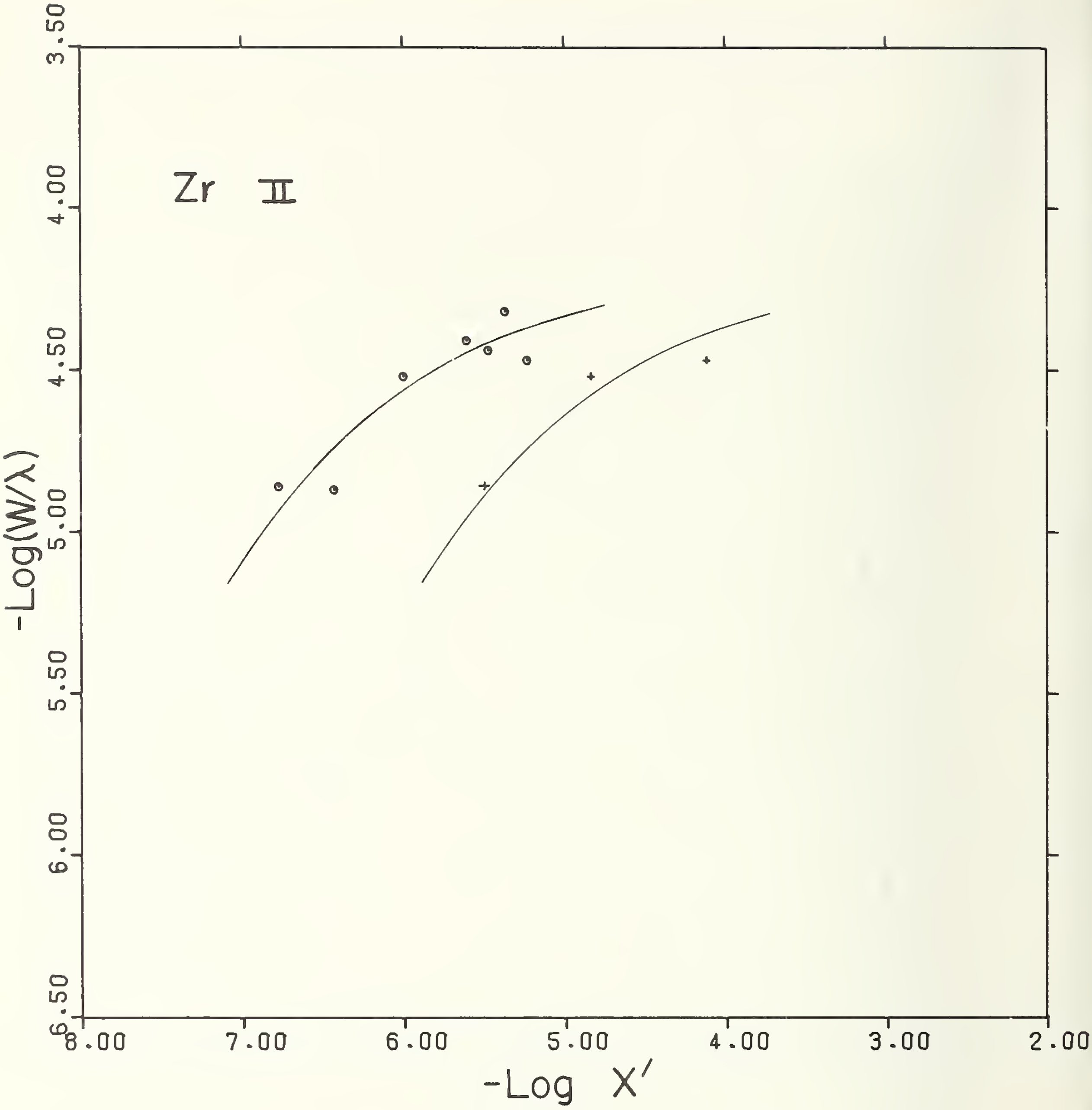

Zr II
3.50
4.00
4.50
5.00
5.50
6.00
6.50
-Log(W/λ)
8.00
7.00
6.00
5.00
4.00
3.00
2.00
-Log X′

FIGURE A.1–18.

A.2. Sample Absolute Curves of Growth

This section presents some of the absolute curves of growth constructed for the analysis of ζ Capricorni by use of the *gf*-values discussed in section 3.2. Such curves for additional spectra have already been displayed in connection with discussions in the main body of the text. The plots here are arranged in alphabetic order according to spectrum. In each plot a distinction is made between lines with wavelengths greater than 5000 Å (*crosses*) and less than 5000 Å (*circles*). The absence of systematic grouping of lines by wavelength suggests that the continuum level adopted in the measurement of equivalent widths was fairly consistent throughout the spectral range studied.

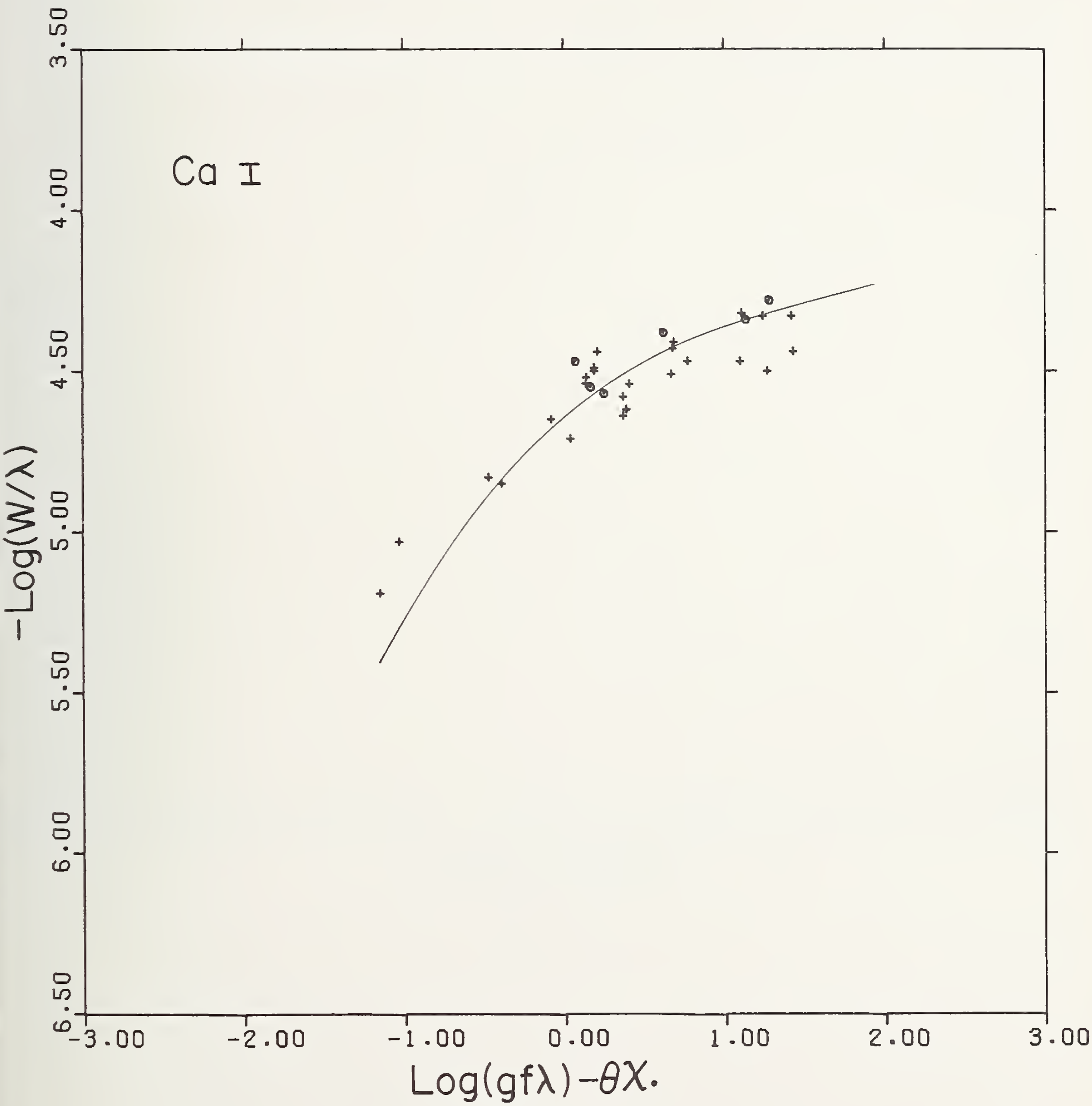

Figure A.2–1.

398-978 O - 71 - 8

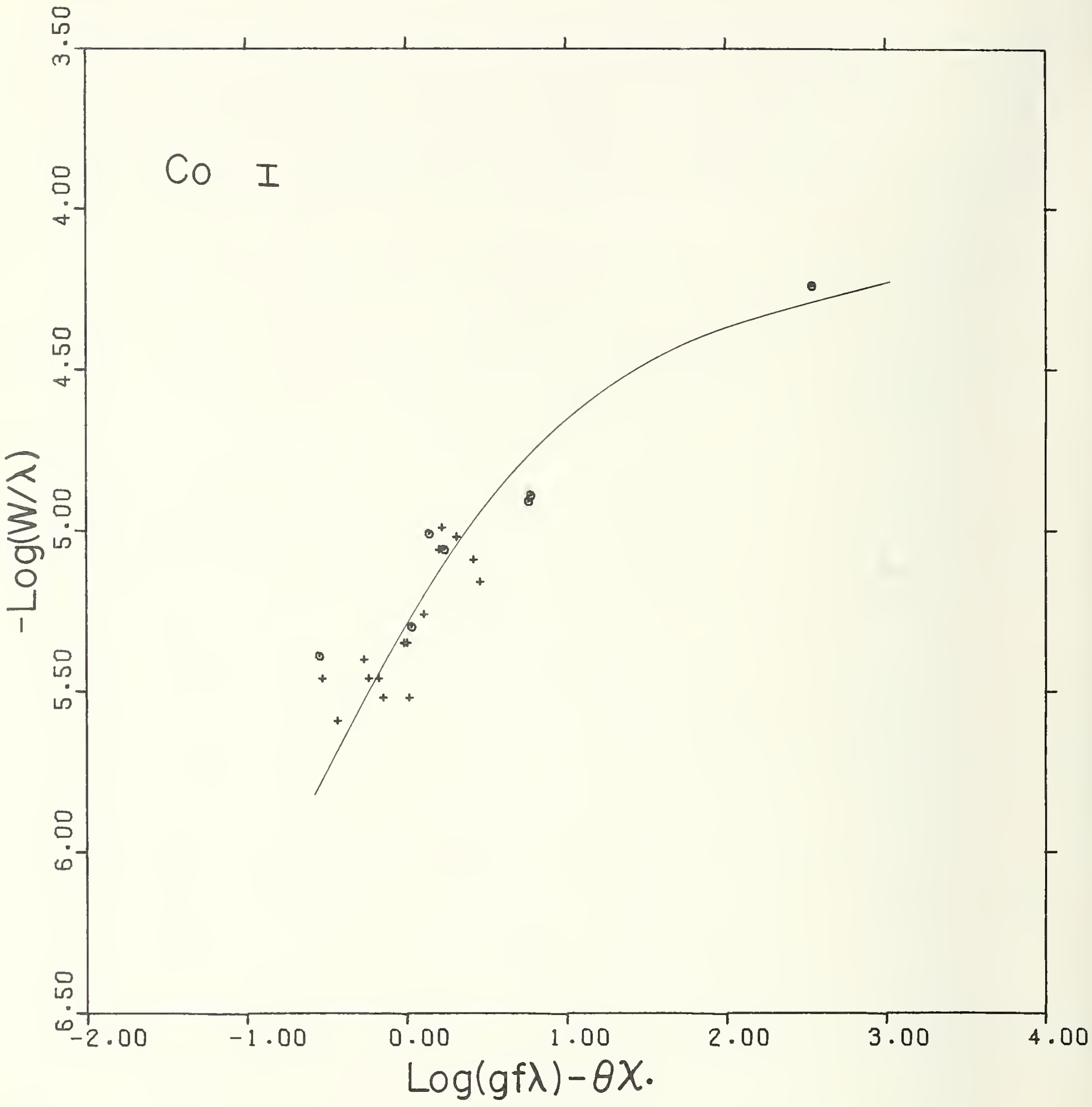
3.50
4.00
4.50
5.00
5.50
6.00
6.50
-Log(W/λ)
Co I
-2.00
-1.00
0.00
1.00
2.00
3.00
4.00
Log(gfλ)-θχ.

FIGURE A.2–2.

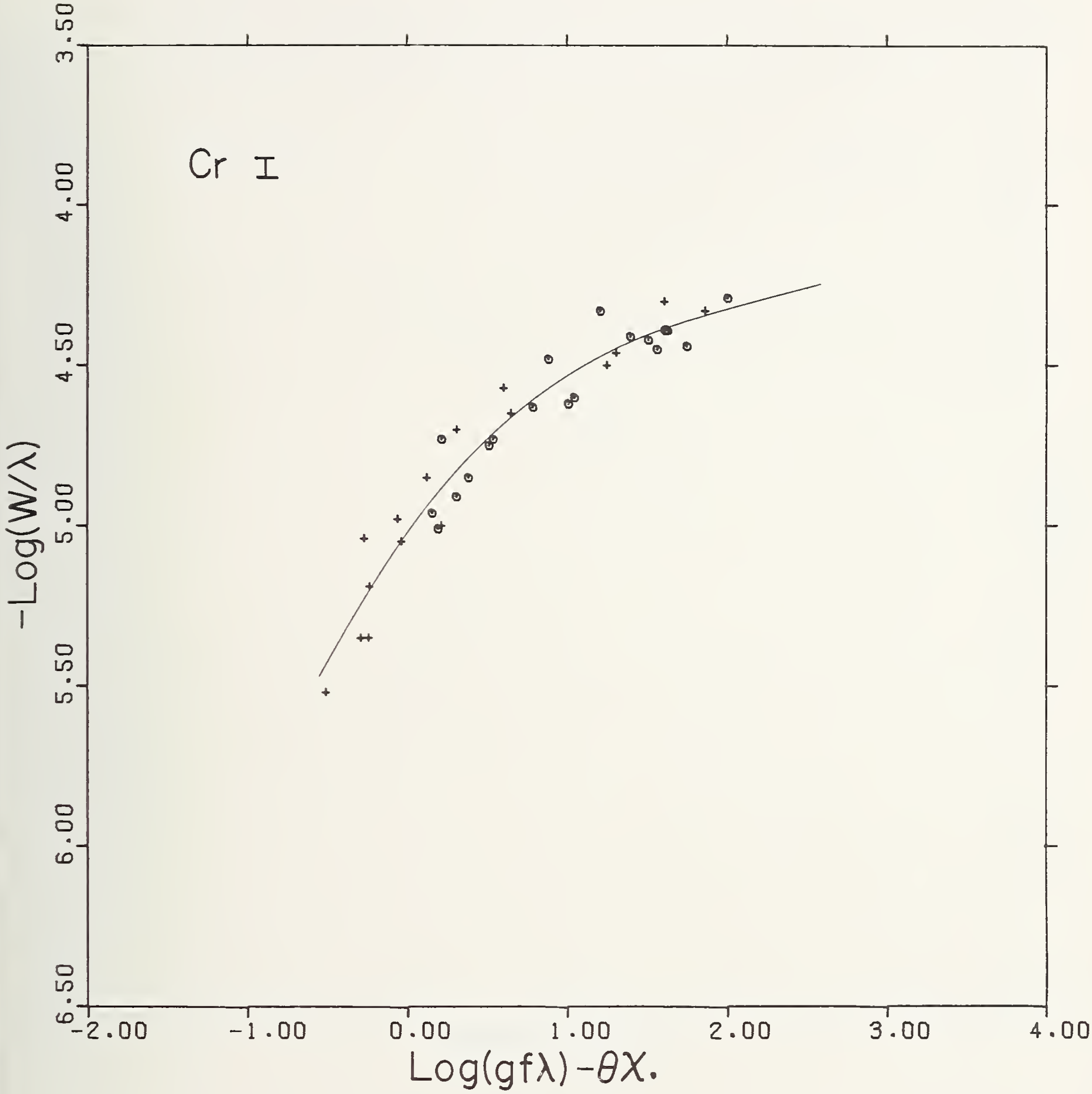

Cr I
-Log(W/λ)
Log(gfλ)-θX.
3.50
4.00
4.50
5.00
5.50
6.00
6.50
-2.00
-1.00
0.00
1.00
2.00
3.00
4.00

FIGURE A.2–3.

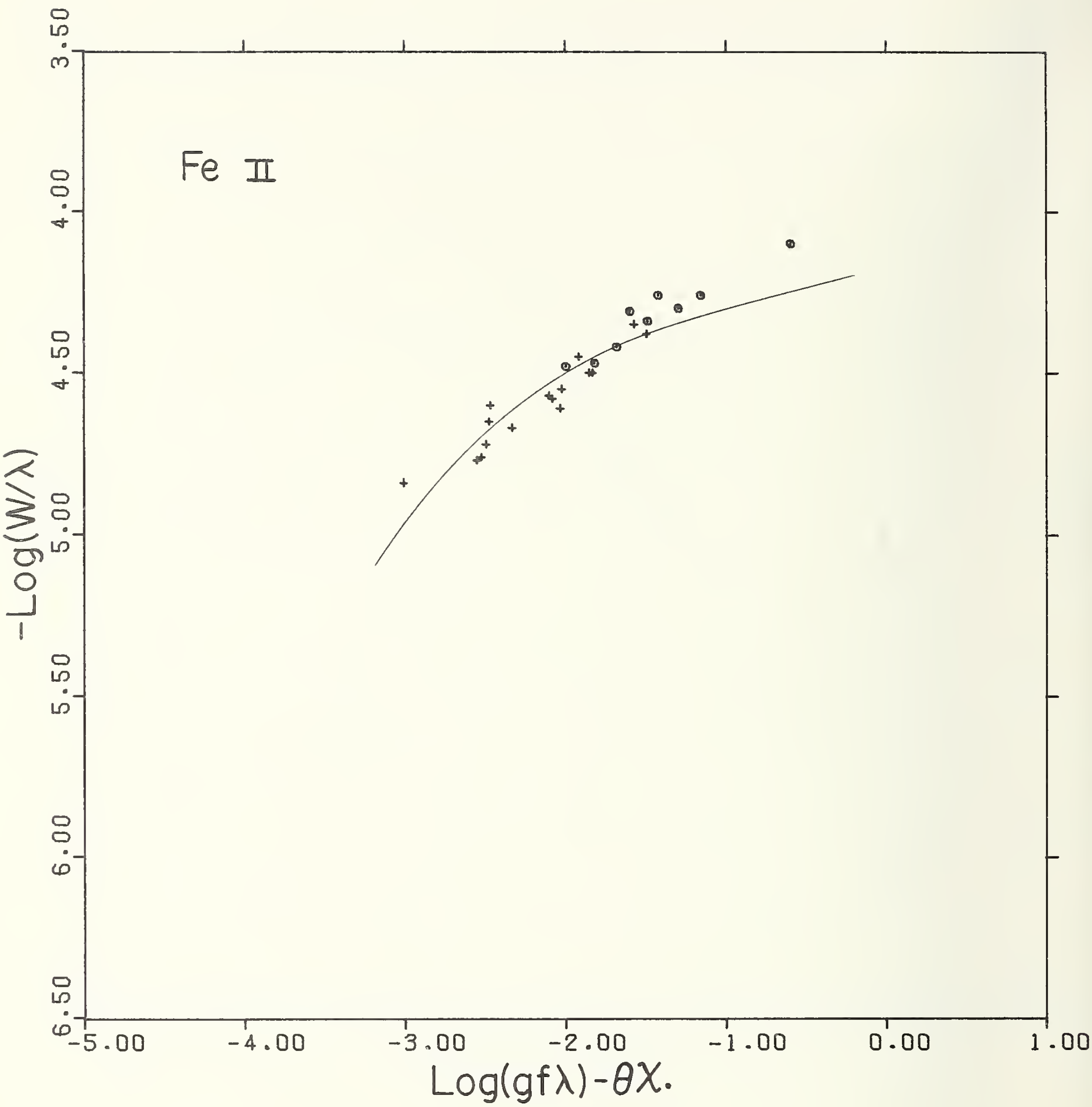
Fe II
3.50
4.00
4.50
5.00
5.50
6.00
6.50
-Log(W/λ)
-5.00
-4.00
-3.00
-2.00
-1.00
0.00
1.00
Log(gfλ)-θX.

FIGURE A.2–4.

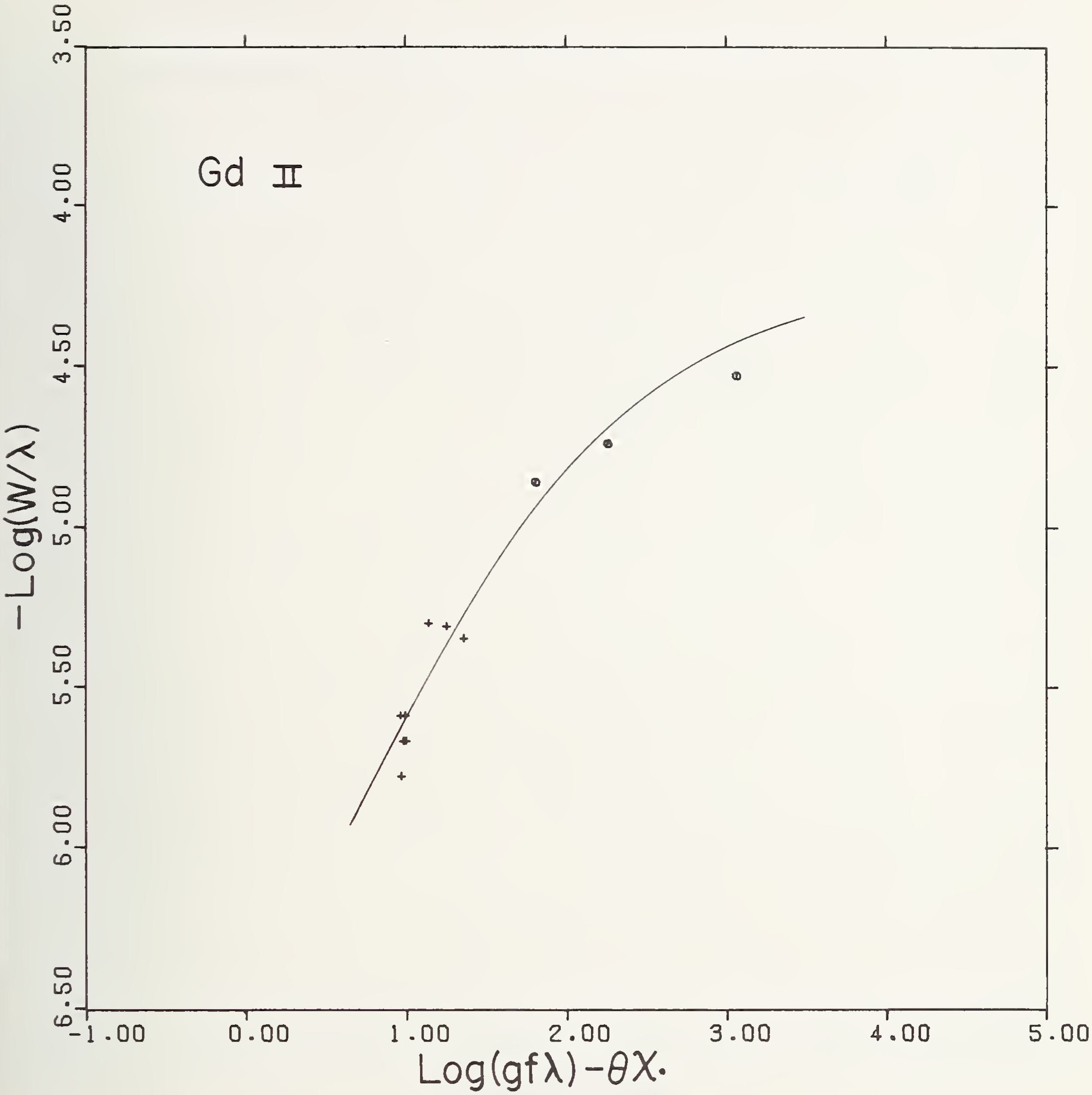
Gd II
−Log(W/λ)
3.50
4.00
4.50
5.00
5.50
6.00
6.50
−1.00
0.00
1.00
2.00
3.00
4.00
5.00
Log(gfλ)−θχ

Figure A.2–5.

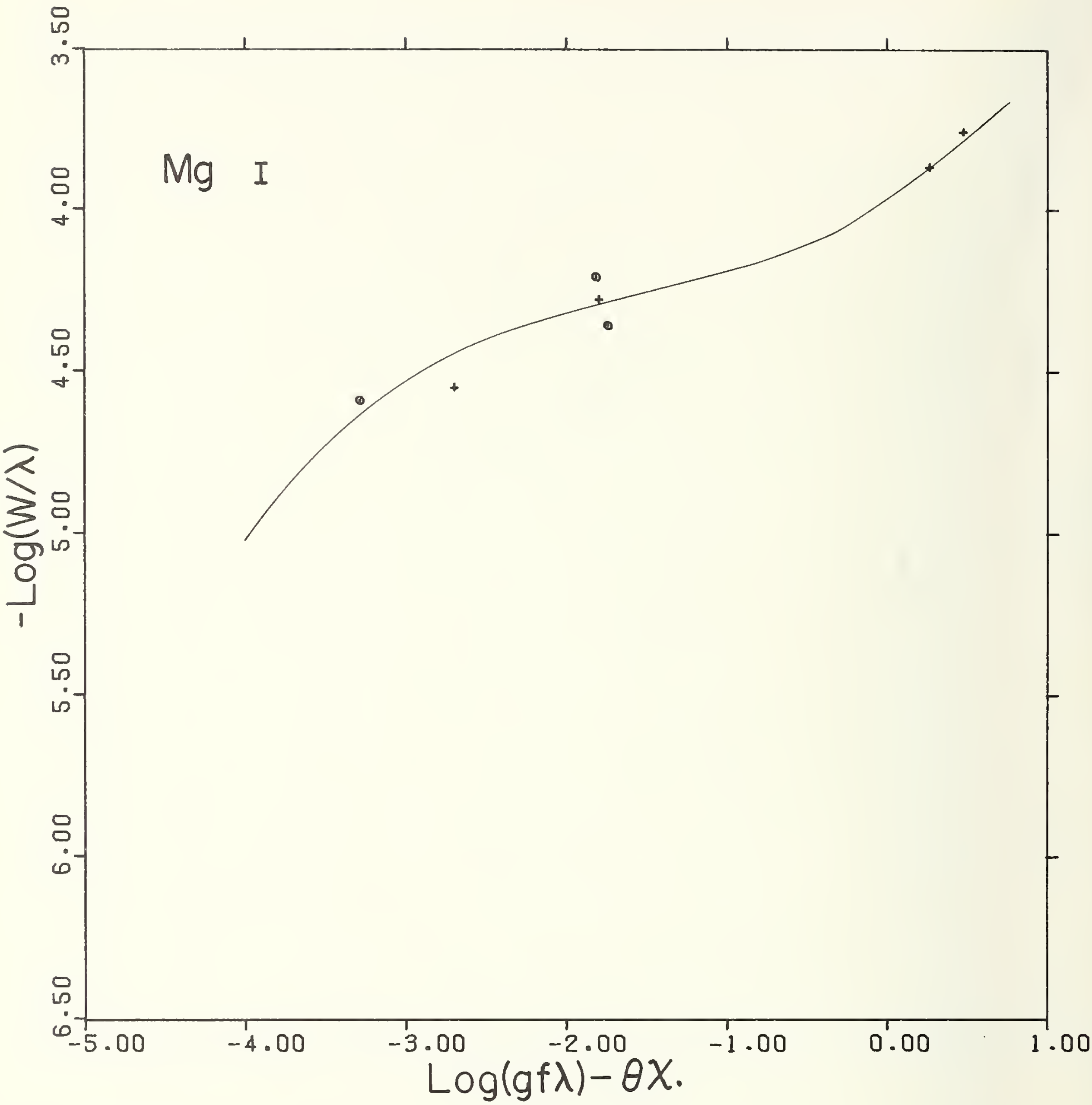
Mg I
-Log(W/λ)
3.50
4.00
4.50
5.00
5.50
6.00
6.50
-5.00
-4.00
-3.00
-2.00
-1.00
0.00
1.00
Log(gfλ)−θχ.

Figure A.2–6.

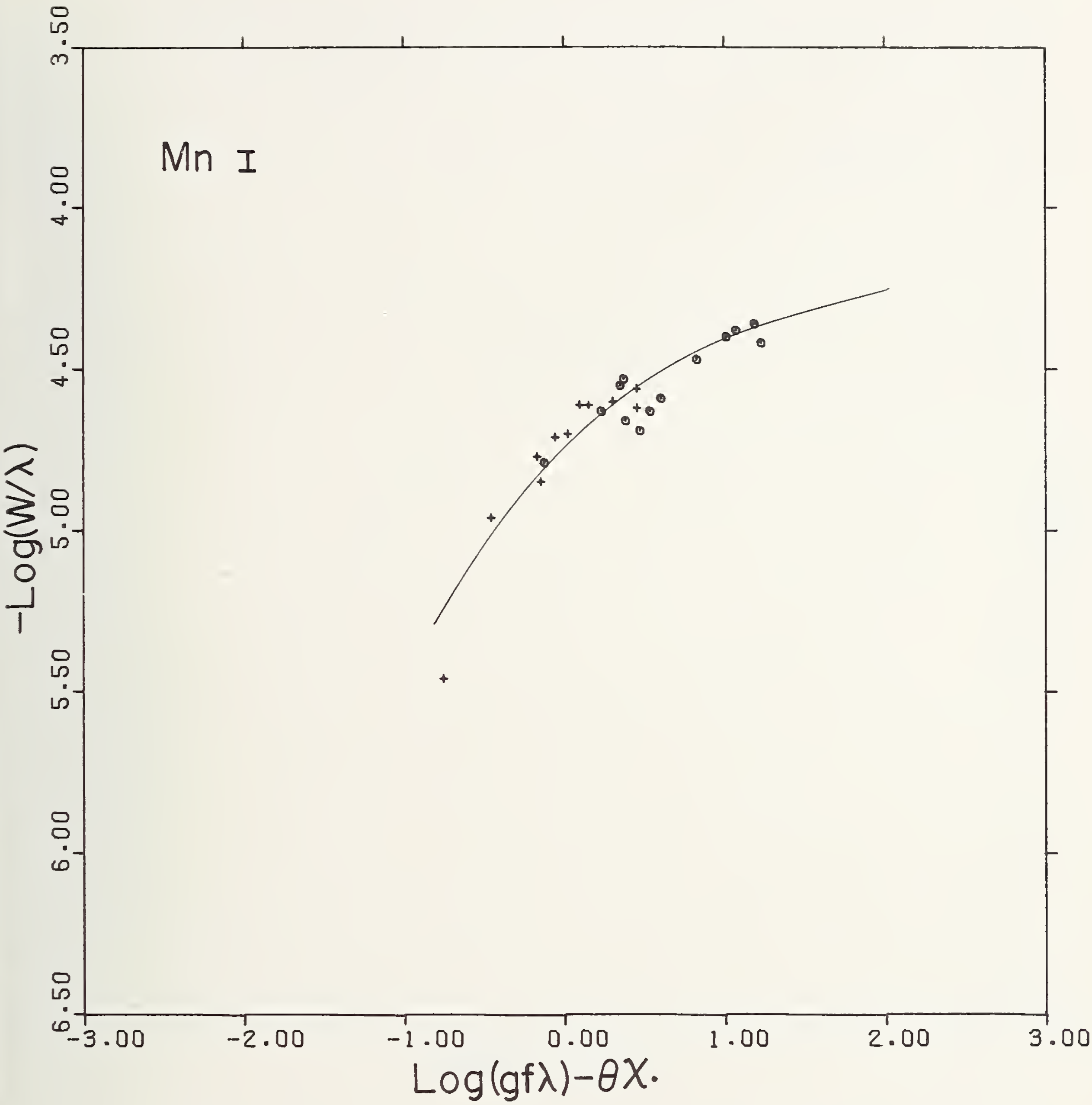
Mn I
-Log(W/λ)
3.50
4.00
4.50
5.00
5.50
6.00
6.50
-3.00
-2.00
-1.00
0.00
1.00
2.00
3.00
Log(gfλ)-θX·

FIGURE A.2–7.

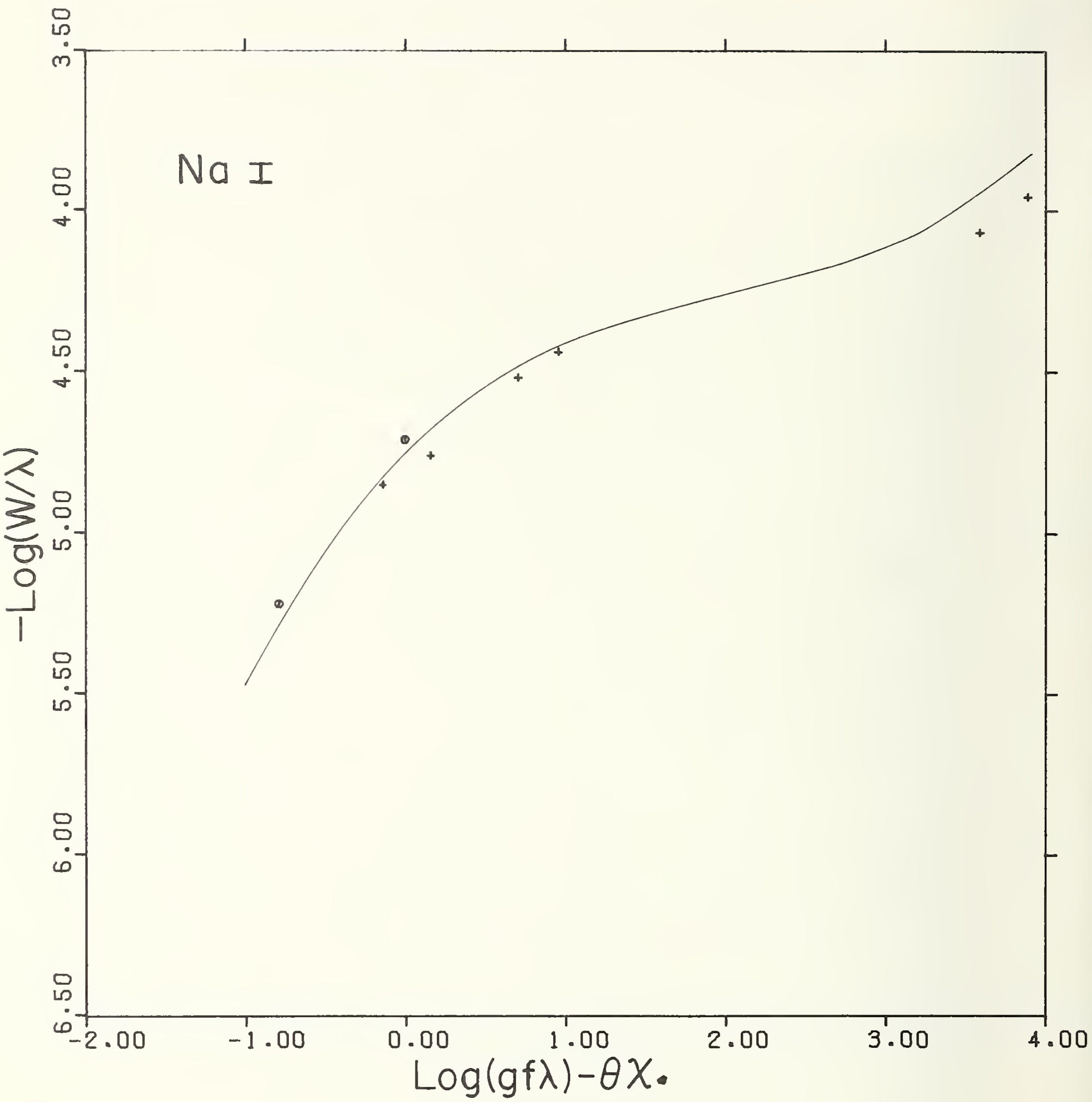

Na I
3.50
4.00
4.50
5.00
5.50
6.00
6.50
-Log(W/λ)
-2.00
-1.00
0.00
1.00
2.00
3.00
4.00
Log(gfλ)-θχ

Figure A.2–8.

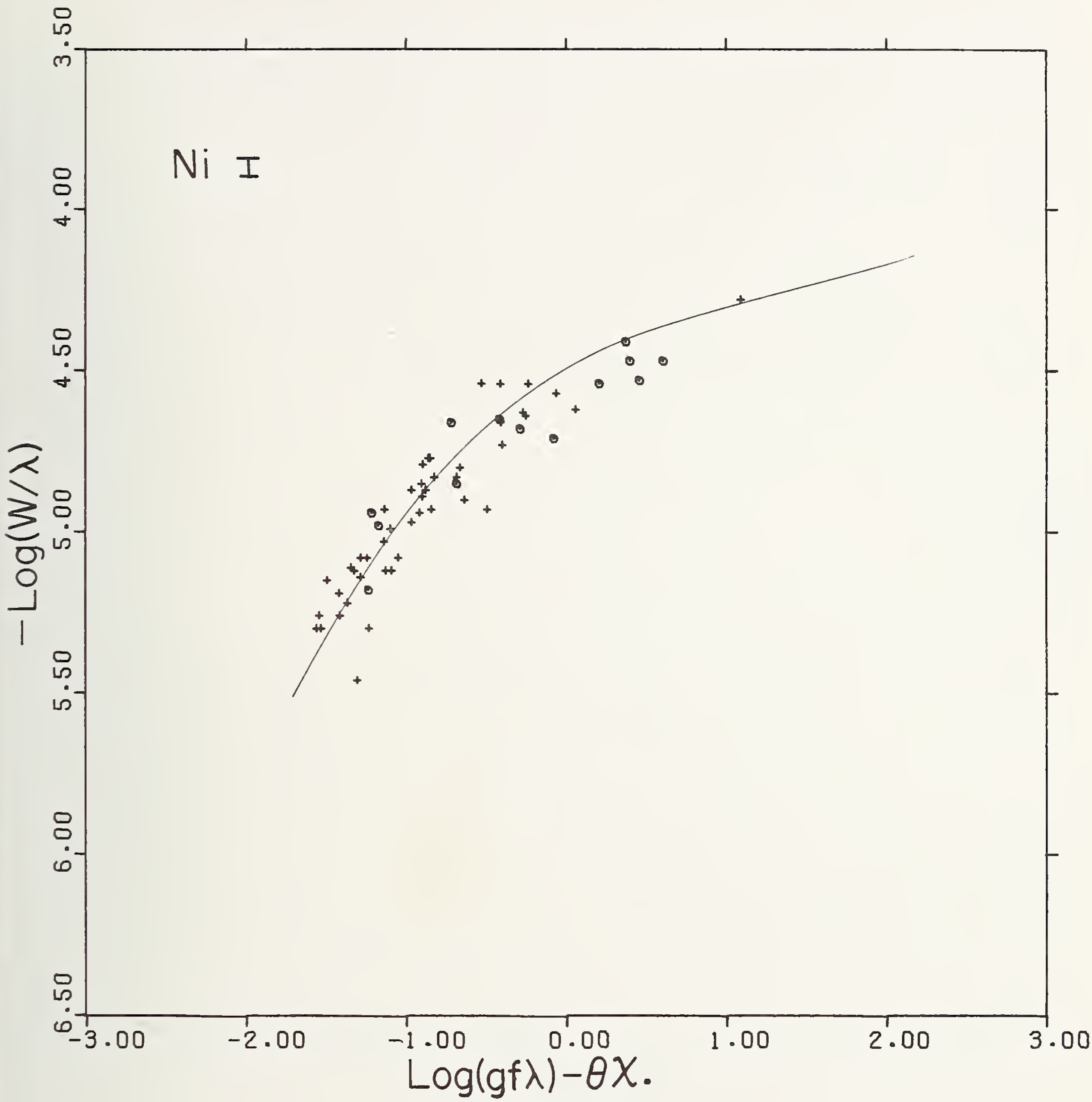

Ni I
3.50
4.00
4.50
5.00
5.50
6.00
6.50
-3.00
-2.00
-1.00
0.00
1.00
2.00
3.00
$-\text{Log}(W/\lambda)$
$\text{Log}(gf\lambda)-\theta\chi$.

Figure A.2–9.

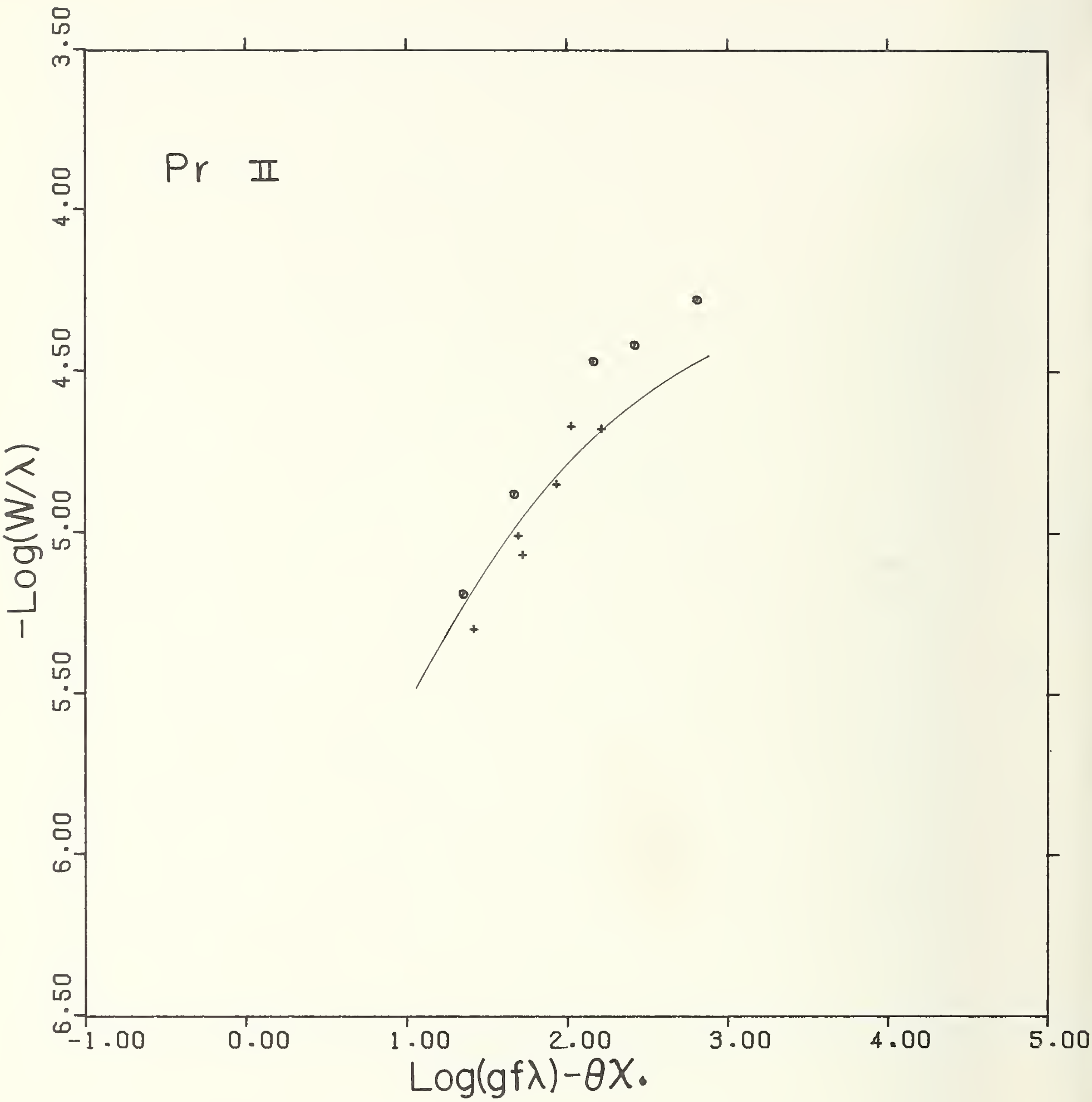

Pr II
3.50
4.00
4.50
5.00
5.50
6.00
6.50
-Log(W/λ)
-1.00
0.00
1.00
2.00
3.00
4.00
5.00
Log(gfλ)-θX.

FIGURE A.2–10.

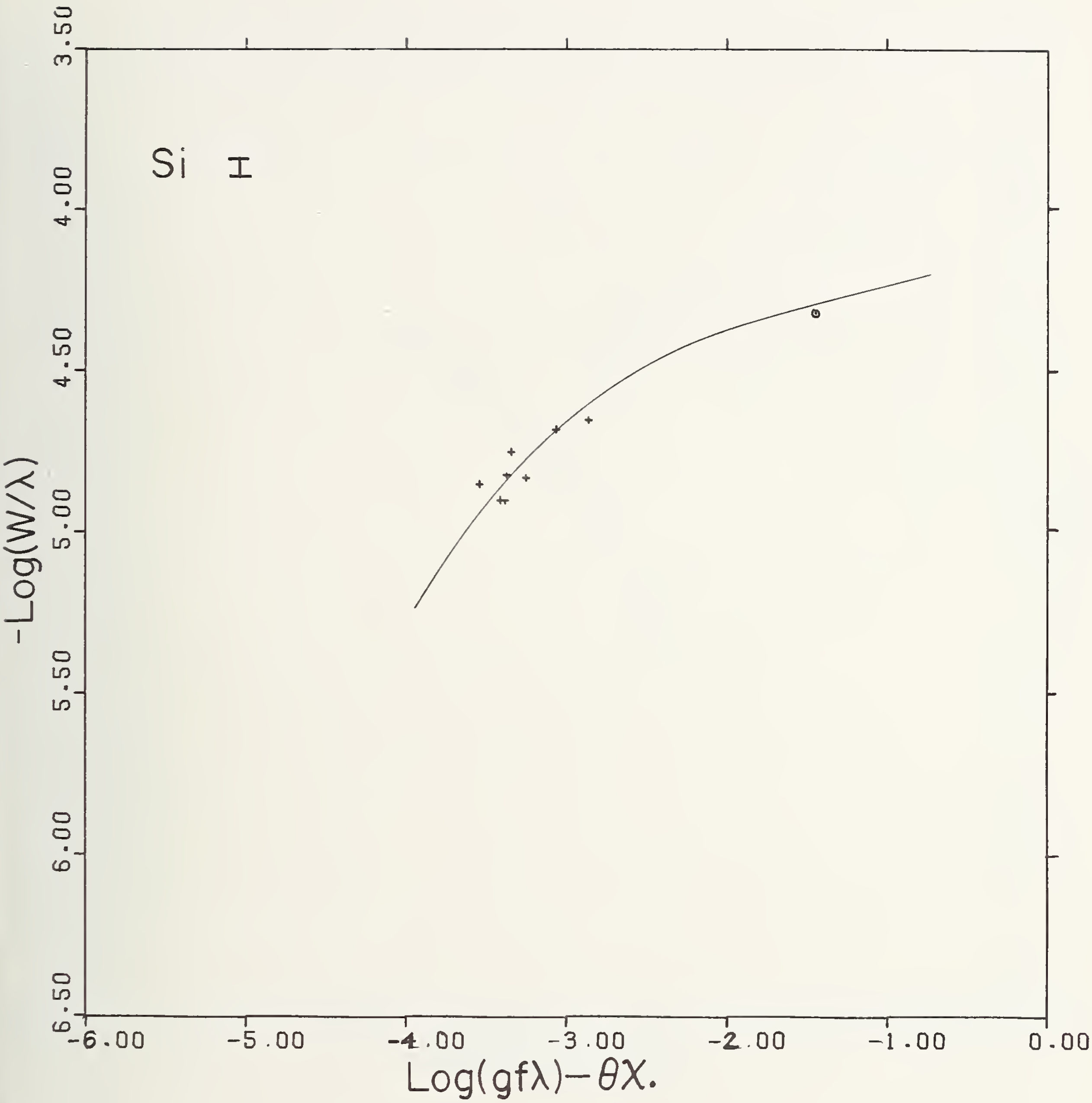
Si I
3.50
4.00
4.50
5.00
5.50
6.00
6.50
-Log(W/λ)
-6.00
-5.00
-4.00
-3.00
-2.00
-1.00
0.00
Log(gfλ)−θX.

FIGURE A.2–11.

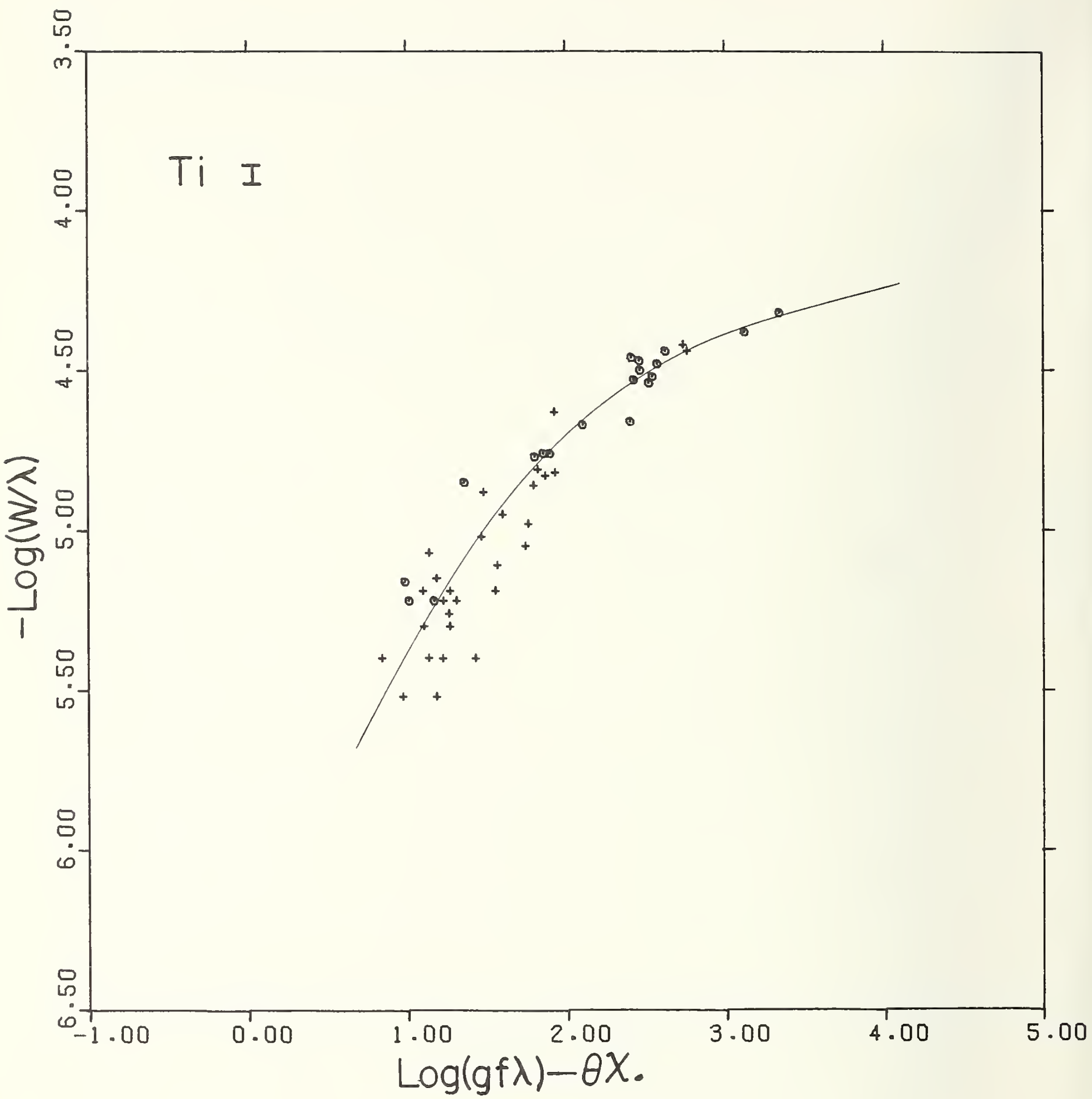

Ti I
3.50
4.00
4.50
5.00
5.50
6.00
6.50
-Log(W/λ)
-1.00
0.00
1.00
2.00
3.00
4.00
5.00
Log(gfλ)—θX.

FIGURE A.2–12.

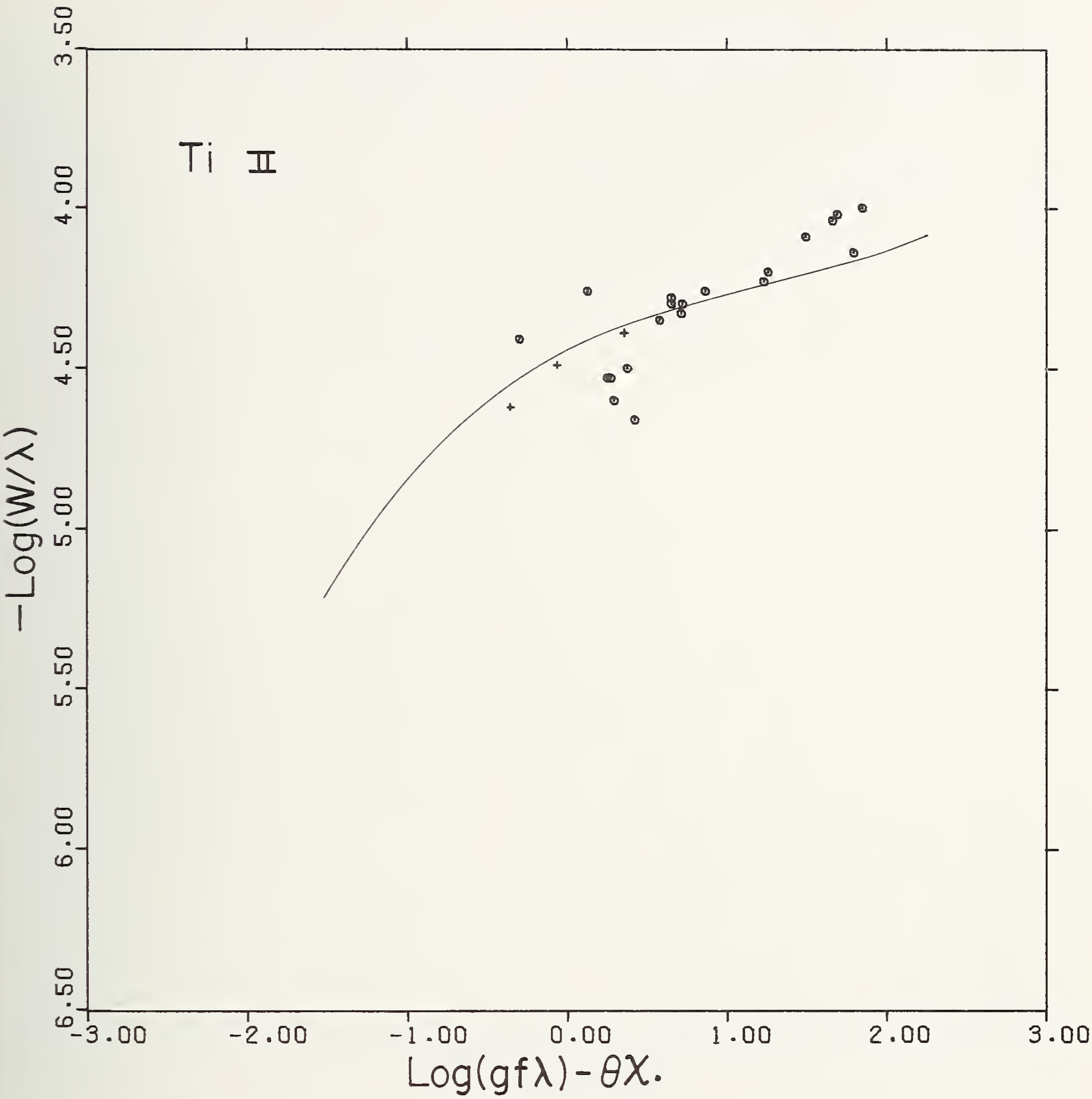
Ti II
3.50
4.00
4.50
5.00
5.50
6.00
6.50
−Log(W/λ)
-3.00
-2.00
-1.00
0.00
1.00
2.00
3.00
Log(gfλ)-θX.

Figure A.2–13.

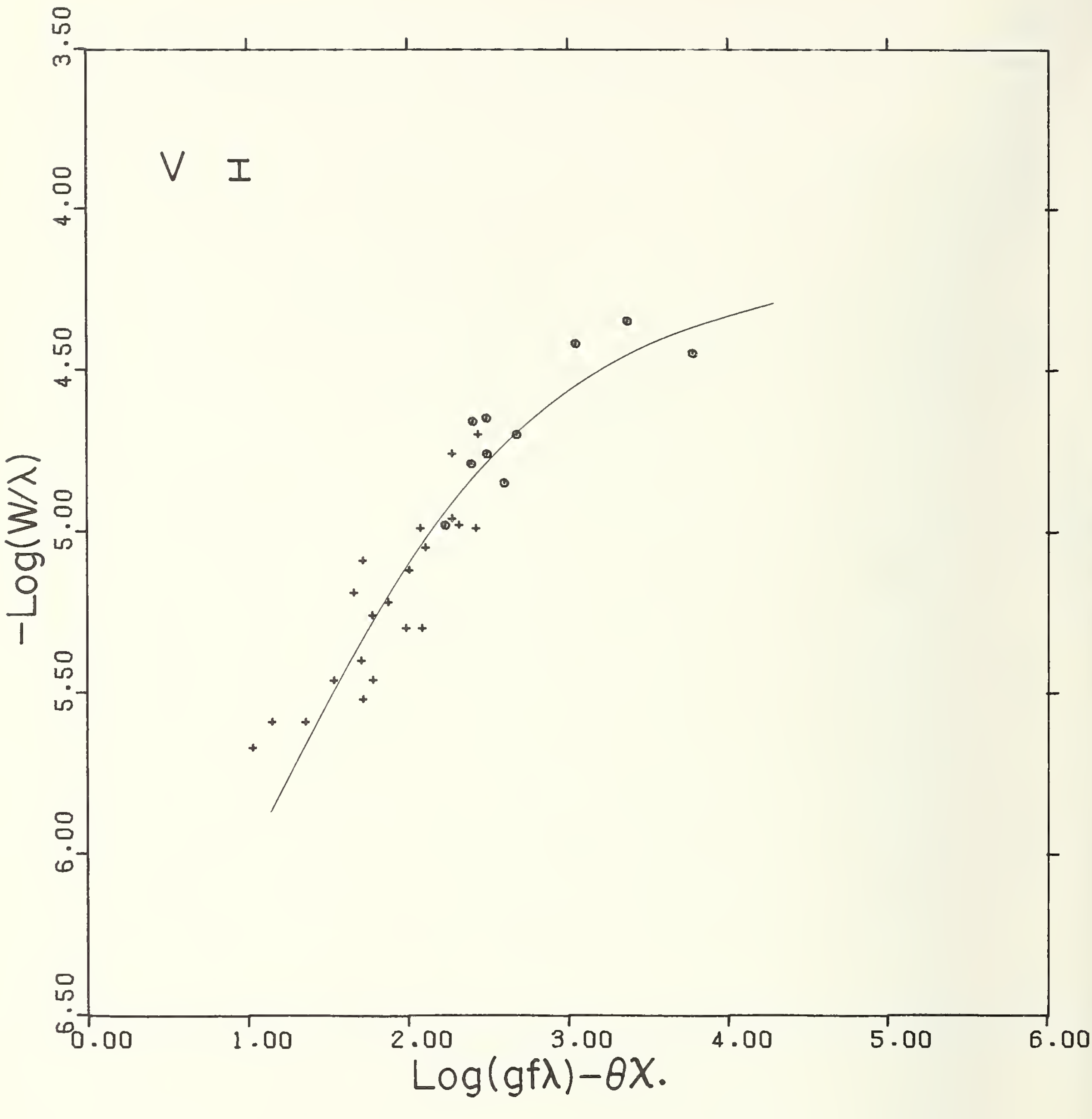

V I
-Log(W/λ)
3.50
4.00
4.50
5.00
5.50
6.00
6.50
0.00
1.00
2.00
3.00
4.00
5.00
6.00
Log(gfλ)-θX.

FIGURE A.2-14.

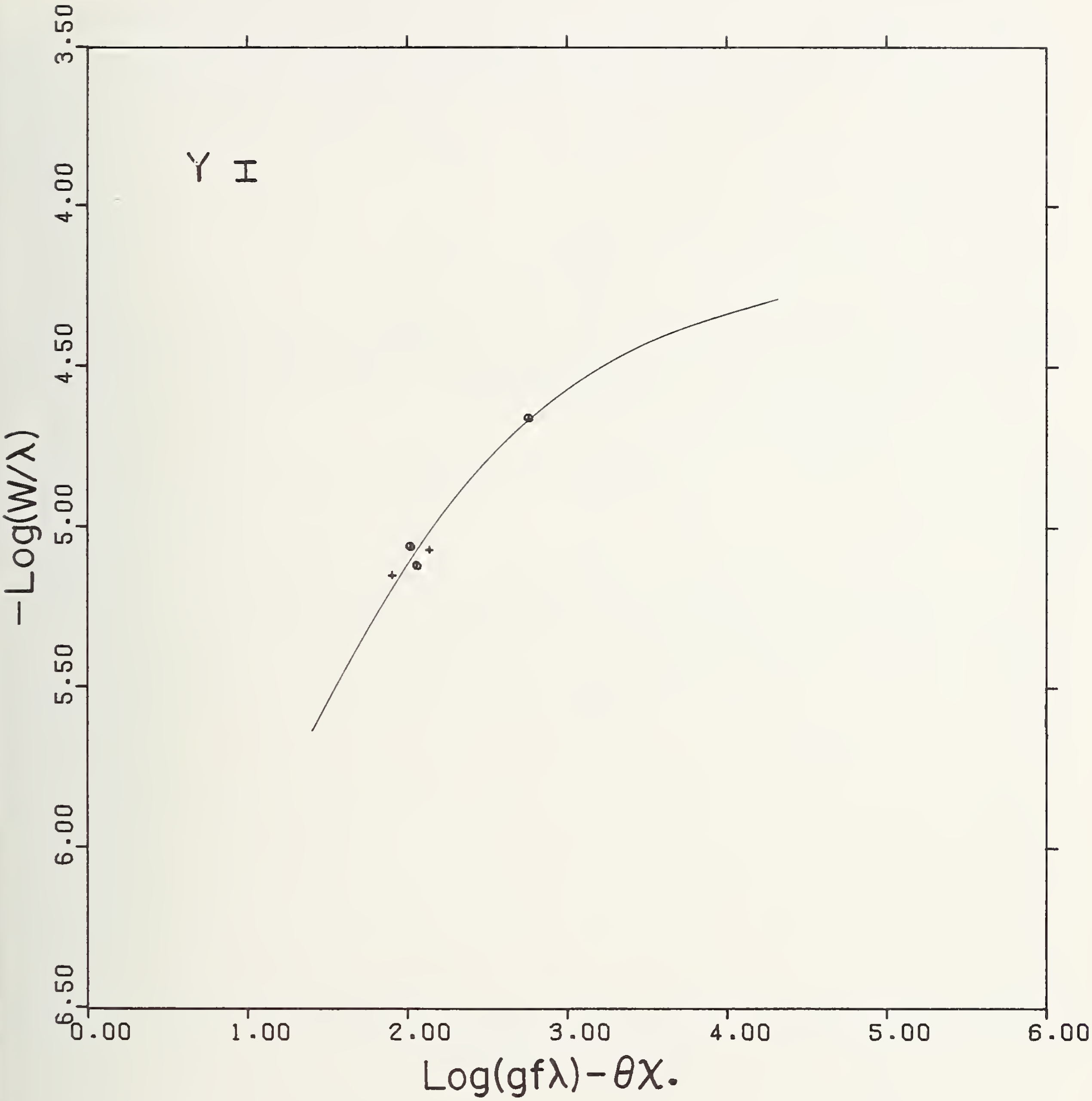

Y I
-Log(W/λ)
3.50
4.00
4.50
5.00
5.50
6.00
6.50
0.00
1.00
2.00
3.00
4.00
5.00
6.00
Log(gfλ)-θχ.

Figure A.2–15.

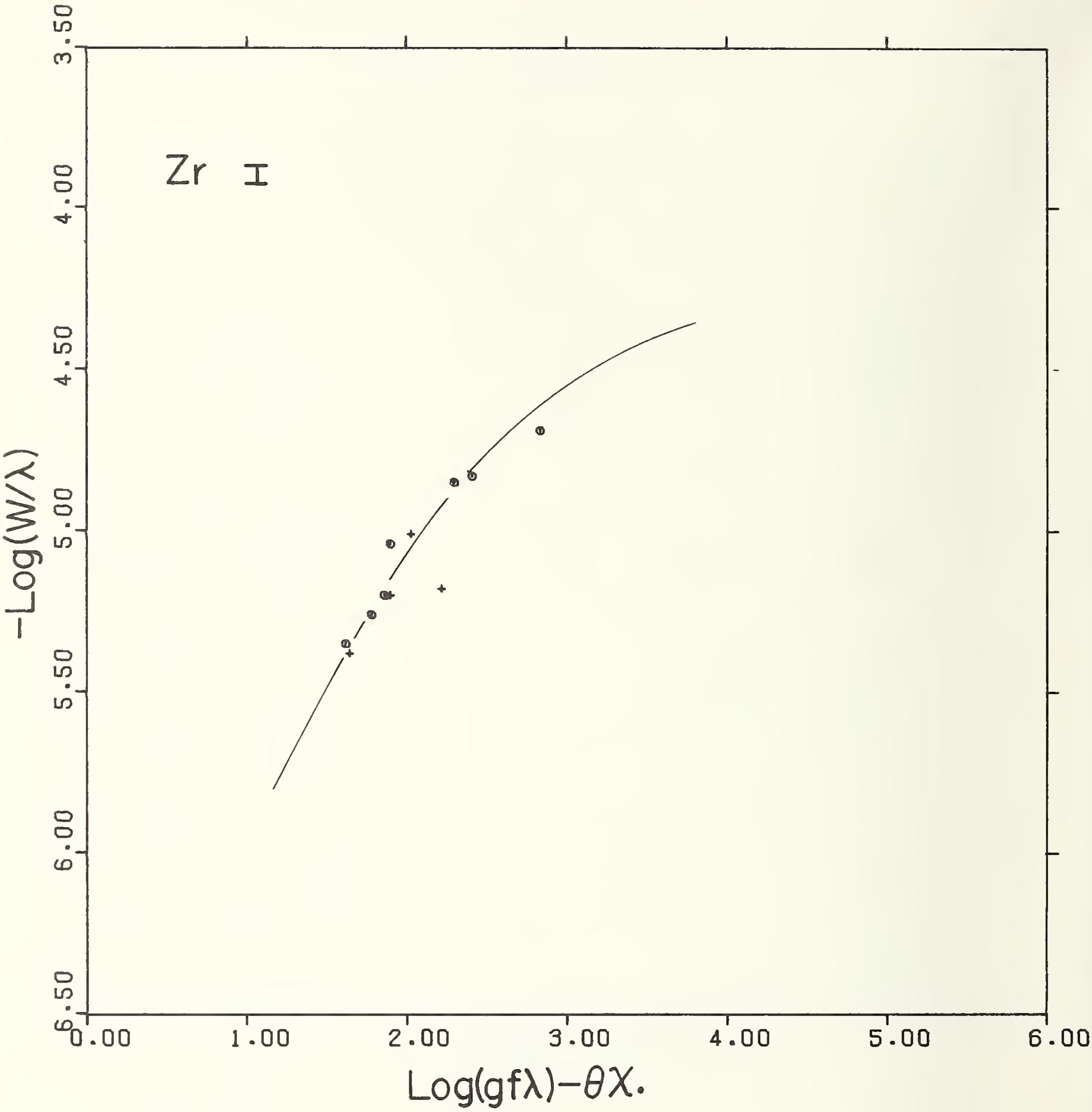

Zr I
3.50
4.00
4.50
5.00
5.50
6.00
6.50
−Log(W/λ)
0.00
1.00
2.00
3.00
4.00
5.00
6.00
Log(gfλ)−θχ.

FIGURE A.2–16.

A.3. Table A, the Line List Arranged by Wavelength

Tables A and B contain the results of measurement of 1100 atomic spectral lines in the spectrum of ζ Capricorni. Table A lists the data by increasing wavelength, whereas table B groups the lines according to spectrum. The information given in the two tables differs only in the contents of columns 5 through 7. The description of table A is given below.

Description of Table A

Column 1: the spectral identification of the measured line
Column 2: the laboratory wavelength in angstrom units
Column 3: the multiplet number of the line as listed in the Revised Multiplet Table (Moore, 1959)
Column 4: the excitation potential (in eV) of the lower level of the transition
Column 5: $-\log (W_{\odot}/\lambda)$, the solar equivalent width of the line as listed in the Second Revision of the Rowland Table (Moore et al., 1966)
Column 6: $-\log (W_{\epsilon}/\lambda)$, the equivalent width of the line as observed in ε Virginis (Cayrel and Cayrel, 1963)
Column 7: $\log (gf\lambda)$, obtained from the sources listed in table 3.1 of section 3.2.2
Column 8: the measured line width at half-intensity, in mÅ
Column 9: the central depth
Column 10: the primary equivalent width, in mÅ
Column 11: the value of $-\log (W/\lambda)$ obtained after the adjustments discussed in section 2.3.4
Column 12: an estimate of the general quality Q of the measurement on a scale of 1 (poor) to 5 (excellent). A quality $Q=0$ has been assigned to a few lines. These represent very strong blends whose primary equivalent widths have been distributed, according to estimated simple ratios, over the contributors to the absorption in the calculation of $\log (W/\lambda)$.
Column 13: the chart section on which the line was measured, as discussed in section 2.3.1

398-978 O - 71 - 9

Table A

Spect	Wave-length	Mult	EP	$-$Log ($W_{\odot}/\lambda$)	$-$Log (W_{ϵ}/λ)	Log ($gf\lambda$)	HW	R_c	W	$-$Log ($W_{\bigcirc}/\lambda$)	Q	N
Ce II	4053.51	36	.00	5.76		2.78	256	.62	194	4.32	2	0
Pb I	4057.81	1	1.32	5.40		3.96	227	.41	98	4.62	1	0
Fe I	4059.71	767	3.55	4.76		3.36	242	.52	135	4.48	2	0
Nd II	4059.97	63	.20	5.83		2.63	242	.52	135	4.48	2	0
Fe I	4067.99	559	3.21	4.49		3.96	261	.65	206	4.29	2	0
Ce II	4068.84	82	.70	6.07		3.24	253	.59	161	4.40	2	0
Nd II	4069.27	20	.06	5.68		2.60	251	.58	157	4.41	2	0
Fe I	4070.78	558	3.24	4.64		3.65	254	.60	165	4.39	2	0
Zr II	4071.09	54	1.00	5.38			247	.55	146	4.44	2	0
Ce II	4072.92		.33			2.67	243	.52	135	4.48	2	0
Dy II	4073.12		.54	5.91		3.42	233	.45	111	4.56	2	0
W I	4074.37	6	.37	5.35		2.98	225	.39	92	4.65	1	0
Fe I	4091.56	357	2.83	4.83		2.37	231	.43	105	4.59	3	0
Ce II	4093.96		.53			2.63	236	.46	115	4.55	2	0
Ca I	4094.94	25	2.52	4.61		2.92	246	.53	140	4.47	2	0
Fe I	4098.18	558	3.24	4.56		3.52	258	.61	189	4.34	2	0
Si I	4102.94	2	1.91	4.59		.71	261	.63	198	4.32	2	0
Dy II	4103.34		.10	5.53		3.18	246	.53	140	4.47	2	0
Nd II	4109.45	10	.32	5.02		3.20	277	.74	246	4.22	2	0
Ce II	4117.29		.74			2.93	227	.39	93	4.65	2	0
Ce II	4117.59		1.32			3.51	240	.48	123	4.53	2	0
Fe I	4120.21	423	2.99	4.63		3.23	256	.59	163	4.40	2	0
Ce II	4120.84	112	.32	5.50		2.88	262	.63	198	4.32	2	0
Co I	4121.33	28	.92	4.52		3.58	275	.72	237	4.24	2	0
Eu II	4129.73	1	.00	4.88		3.31	277	.73	242	4.23	2	0
Gd II	4130.37	19	.60	5.57		3.71	241	.48	123	4.53	2	0
Nd II	4133.35	19	.32	5.57		2.47	251	.55	148	4.44	2	0
Fe I	4139.94	18	.99	4.68		.78	254	.57	156	4.42	2	0
La II	4315.90	41	.40	5.98		1.28	377	.38	157	4.74	0	27
Gd II	4316.05	43	.66	5.59		2.97	377	.38	157	4.74	0	27
Ti II	4316.81	94	2.05	5.06	4.71	2.57	267	.50	135	4.50	2	27
Zr II	4317.32	40	.71	5.52		2.16	251	.61	167	4.41	2	27
Ca I	4318.65	5	1.90	4.57		3.43	283	.67	225	4.28	2	27
Sm II	4318.94	27	.28	5.64		2.86	308	.53	172	4.43	1	27
Fe I	4319.45	214	2.61	5.52		1.13	209	.20	43	5.01	1	0
Cr I	4319.64	96	2.89	5.46		3.46	210	.20	43	5.01	1	0
Ti II	4320.96	41	1.16	4.84		1.37	288	.72	237	4.26	1	0
La II	4322.51	25	.17	5.56		2.00	251	.60	167	4.40	3	27
Sc II	4325.01	15	.60	4.57		3.27	302	.81	280	4.19	3	0
Fe I	4325.76	42	1.61	3.74		4.00	628	.86	587	3.87	3	27
Ti I	4326.36	43	.83	5.29		2.74	226	.31	73	4.77	1	0
Sm II	4329.02	15	.18	5.56		2.73	282	.45	129	4.54	2	27
V I	4330.02	5	.00	5.09		2.41	237	.38	95	4.66	2	0
Ni I	4331.64	52	1.68	4.89		2.27	314	.56	179	4.41	3	27
Zr II	4333.28	132	2.41			3.53	298	.45	145	4.52	2	27
Ce II	4336.26	89	.70	6.24		3.14	232	.53	132	4.49	4	27
Fe I	4337.05	41	1.56	4.56		2.49	294	.75	251	4.24	3	0
Fe I	4343.70	517	3.05	4.79		2.55	265	.56	160	4.43	1	0
Fe I	4347.24	2	.00	5.03			246	.43	112	4.59	2	0
Fe I	4348.94	414	2.99	4.87		2.26	235	.42	108	4.60	4	27

Table A

Spect	Wave-length	Mult	EP	$-$Log ($W_\odot/\lambda$)	$-$Log (W_ϵ/λ)	Log ($gf\lambda$)	HW	R_c	W	$-$Log ($W_\odot/\lambda$)	Q	N
Ce II	4349.79	59	.70	5.76		3.22	220	.53	135	4.49	4	27
Cr I	4357.52	198	3.37	5.06			213	.27	67	4.83	3	27
Nd II	4358.17	10	.32	5.06		2.66	278	.64	202	4.33	3	0
Sm II	4362.04	45	.48	5.94		2.68	298	.52	167	4.45	2	27
Ce II	4364.66	135	.50	5.56		3.29	251	.60	172	4.40	2	27
Fe I	4365.90	415	2.99	4.96		2.21	188	.35	75	4.74	2	27
Ce II	4375.92	134	.50			3.06	301	.77	260	4.43	0	27
Fe I	4376.78	471	3.02	4.93		2.37	219	.41	90	4.65	2	27
Fe I	4377.80	645	3.27	5.05		2.31	204	.28	59	4.85	3	27
V I	4379.24	22	.30	4.60		4.12	226	.63	157	4.45	3	27
Zr II	4379.78	88	1.53			3.45	251	.63	183	4.38	3	27
Ce II	4382.17	2	.68	5.74		3.47	314	.61	195	4.35	1	27
Fe I	4383.55	41	1.48	3.64		4.15	627	.90	630	3.84	2	27
Fe I	4388.41	830	3.60	4.63		3.84	277	.62	194	4.36	3	0
Fe I	4389.24	2	.05	4.82			251	.60	165	4.41	1	28
V I	4389.97	22	.28	4.72		3.69	279	.63	198	4.35	1	0
Ti II	4391.03	61	1.23	5.11		1.61	445	.74	350	4.60	0	28
Ti II	4394.06	51	1.22	4.79	4.47	2.17	307	.71	241	4.26	3	28
Ti II	4395.85	61	1.24	4.86	4.58	1.98	290	.70	228	4.28	2	0
Y II	4398.02	5	.13	4.98		2.40	382	.81	325	4.13	2	28
Ce II	4399.20	81	.33	5.90		2.86	282	.60	181	4.39	2	28
Ti II	4399.77	51	1.24	4.58	4.39	2.56	301	.77	260	4.23	3	0
Zr II	4403.35	79	1.18			2.54	286	.67	215	4.31	2	0
Fe I	4404.75	41	1.56	3.69		3.89	643	.87	613	3.86	3	28
V I	4406.65	22	.30	4.75		3.39	282	.56	171	4.42	4	28
Pr II	4408.84	4	.00	5.64		2.81	293	.71	233	4.28	2	0
Mo I	4411.57		2.08	5.99		4.30	220	.24	54	4.91	1	0
Ce II	4413.19		1.14			3.01	282	.38	109	4.63	2	28
Pr II	4413.76	26	.22	6.10		2.40	265	.53	151	4.47	2	0
Zr II	4414.54	79	1.24	5.28		2.59	301	.63	210	4.32	2	28
Sc II	4415.56	14	.60	4.71		2.81	282	.73	238	4.27	2	28
V I	4416.47	22	.27	5.09		2.80	244	.39	100	4.65	1	0
Fe II	4416.82	27	2.78	4.76		1.55	313	.72	245	4.26	2	28
Ti II	4417.72	40	1.16	4.66	4.45	2.50	338	.77	276	4.20	3	28
Ti II	4418.35	51	1.24	4.80	4.46	1.98	301	.65	222	4.30	3	28
Ce II	4418.78	2	.86	5.41		3.68	278	.61	189	4.37	2	0
Sm II	4421.14	37	.38	5.65		2.63	263	.53	151	4.47	3	28
Fe I	4422.57	350	2.84	4.58		3.43	407	.77	333	4.32	0	28
Y II	4422.59	5	.10			2.06	407	.77	333	4.32	0	28
Sm II	4424.34	45	.48			3.22	278	.61	189	4.37	4	0
Ca I	4425.44	4	1.88	4.48		3.26	276	.67	204	4.34	4	28
Fe I	4430.62	68	2.22	4.59		2.63	329	.70	260	4.23	3	28
Sc II	4431.37	14	.61	5.17		1.51	257	.47	126	4.54	2	28
Fe I	4433.22	830	3.65	4.66		3.70	276	.59	176	4.40	2	0
Sm II	4434.32	36	.38	5.47		2.89	271	.56	163	4.43	5	0
Fe I	4436.95	516	3.05	4.77		2.27	219	.48	109	4.57	4	28
Fe I	4438.35	828	3.69	5.00		2.86	307	.41	123	4.67	0	28
Fe I	4439.89	116	2.28	4.98		1.65	266	.38	97	4.66	2	28
Fe I	4442.34	68	2.20	4.41		3.15	391	.77	307	4.16	5	28
Ti II	4443.80	19	1.08	4.55	4.36	2.95	363	.81	321	4.14	4	28

Table A

Spect	Wave-length	Mult	EP	−Log ($W_{\odot}/\lambda$)	−Log (W_{ϵ}/λ)	Log ($gf\lambda$)	HW	R_c	W	−Log ($W_{♂}/\lambda$)	Q	N
Fe I	4445.48	2	.09	5.17			244	.38	102	4.65	5	28
Nd II	4446.39	49	.20	5.72		2.35	282	.61	194	4.36	4	28
Fe I	4446.84	828	3.69	4.80		3.28	259	.48	133	4.53	3	0
Fe I	4447.13	69	2.20	4.87		1.76	261	.49	136	4.51	3	0
Fe I	4447.72	68	2.22	4.40		3.07	329	.72	259	4.23	5	28
Mn I	4451.59	22	2.89	4.69		4.34	235	.68	187	4.38	5	28
Nd II	4451.99	6	.00			1.70	250	.53	141	4.67	0	28
V I	4452.01	87	1.87	5.31		4.35	250	.53	141	4.98	0	28
Sm II	4452.73	26	.28	5.84		2.67	267	.53	152	4.47	3	0
Mn I	4453.00	22	2.94	4.99		3.71	244	.38	97	4.66	2	0
Ti I	4453.31	113	1.43	4.88		4.04	260	.48	133	4.53	1	0
Ti I	4453.71	160	1.87	5.09		4.01	250	.32	77	4.76	3	28
Fe I	4454.38	350	2.83	4.72		3.14	283	.63	198	4.35	3	0
Mn I	4457.04	28	3.07	5.07		3.35	232	.30	72	4.79	2	0
Sm II	4458.52	7	.10			2.38	260	.48	133	4.53	3	0
V I	4459.76	21	.29	4.97		3.01	211	.38	82	4.70	4	28
Fe I	4461.65	2	.09	4.59		.94	301	.74	246	4.26	2	0
Nd II	4462.99	50	.56	5.54		2.81	275	.64	201	4.35	3	29
Fe I	4466.55	350	2.83	4.55		3.83	344	.76	282	4.20	3	29
Sm II	4467.34	53	.66	5.75		3.26	270	.54	156	4.46	2	0
Ce II	4467.54	17	.61			2.82	270	.54	156	4.46	2	0
Ti II	4468.50	31	1.13	4.57	4.36	3.06	501	.85	444	4.00	3	29
Mn I	4470.14	22	2.94	4.96		3.80	242	.36	91	4.69	2	0
Ni I	4470.48	86	3.40	4.81		4.24	282	.54	147	4.47	2	29
Ti II	4470.86	40	1.16	4.92	4.51	1.82	294	.68	202	4.35	2	29
Sm II	4472.43		.18	6.11		2.12	240	.35	88	4.71	1	0
Sm II	4475.18		.10			1.23	214	.18	39	5.06	1	0
Nd II	4475.57		.06			1.07	250	.30	73	4.79	2	29
Fe I	4476.02	350	2.84	4.47		3.79	313	.73	242	4.27	5	29
Fe I	4478.04	69	2.20	5.47		.96	213	.20	44	5.01	4	29
Fe I	4480.14	515	3.05	4.92		2.64	325	.53	180	4.43	2	29
Fe I	4481.62	827	3.69	4.99		3.14	246	.38	98	4.66	2	0
Fe I	4482.17	2	.11	4.43		.80	366	.80	319	4.15	5	29
Gd II	4483.35	62	1.06	6.48		2.95	235	.27	59	4.86	2	29
Ce II	4483.90	3	.38	5.48		3.52	282	.57	185	4.40	3	29
Fe I	4484.23	828	3.60	4.77		3.88	250	.57	155	4.44	3	29
Ce II	4484.83		1.12	6.65		3.15	244	.37	95	4.67	2	29
Nd II	4485.95		.38			1.38	250	.31	94	4.98	0	29
Fe I	4485.97	825	3.65	5.40		2.34	250	.31	94	4.98	0	29
Ce II	4486.91	57	.30	5.61		3.03	263	.64	166	4.43	4	29
Fe I	4489.74	2	.12	4.74		.25	295	.69	224	4.30	3	0
Fe II	4491.40	37	2.85	4.83	4.62	1.56	289	.65	206	4.34	3	0
Ti II	4493.50	18	1.08	5.24	4.68	.86	338	.56	188	4.41	3	29
Sm II	4499.48	23	.25	6.35		2.07	243	.36	92	4.69	2	0
Ti II	4501.27	31	1.12	4.61	4.34	2.86	469	.83	409	4.04	4	29
Mn I	4502.22	22	2.92	4.96	4.66	3.84	250	.41	102	4.63	1	29
Fe I	4502.60	796	3.57	5.33	4.80	2.38	188	.24	51	4.93	1	29
Ti I	4503.76	184	2.13	5.75		3.42	244	.13	32	5.22	2	29
Fe I	4504.84	555	3.26	4.99		2.20	244	.36	92	4.69	1	0
Sm II	4505.05		.25			1.75	218	.20	44	5.01	1	0

Table A

Spect	Wave-length	Mult	EP	$-$Log $(W_{\odot}/\lambda)$	$-$Log (W_{ϵ}/λ)	Log $(gf\lambda)$	HW	R_c	W	$-$Log $(W_{\bigcirc}/\lambda)$	Q	N
Y I	4505.95	14	1.37	6.35		3.61	212	.16	34	5.12	1	0
Fe II	4508.28	38	2.85	4.78		1.89	325	.70	249	4.26	2	29
Pr II	4510.16	20	.42	6.48		2.87	313	.55	180	4.42	3	29
Ca I	4512.27	24	2.52	5.40	4.83		216	.18	39	5.06	1	0
Ti I	4512.75	42	.84	4.91	4.60	3.41	271	.53	154	4.47	3	0
Fe II	4515.34	37	2.84	4.78	4.53	1.74	298	.70	228	4.30	2	0
Fe I	4517.53	472	3.07	4.87		2.54	306	.55	166	4.44	3	29
Ti I	4518.03	42	.83	4.86	4.54	3.51	263	.54	144	4.48	2	29
Sm II	4519.63	49	.54	5.96	5.01	2.74	256	.51	141	4.50	4	29
Ce II	4523.08	2	.52	5.58	4.76	3.20	297	.69	224	4.31	2	0
Sm II	4523.91	41	.43	5.61	4.86	2.49	275	.46	122	4.56	3	29
Ti II	4524.73	60	1.23	5.40	4.70	1.59	264	.48	135	4.53	2	0
Ba II	4524.93	3	2.51	5.15	4.65	3.30	291	.65	206	4.34	2	0
Fe I	4525.15	826	3.60	4.58	4.39	3.83	297	.69	224	4.31	2	0
La II	4526.12	50	.77	5.45	4.83	2.52	306	.53	185	4.43	1	29
Cr I	4526.47	33	2.54	4.63		4.08	313	.65	213	4.33	3	29
Ca I	4526.93	36	2.71	4.78	4.58	3.23	256	.49	116	4.55	2	29
Ti I	4527.31	42	.81	4.83	4.54	3.38	306	.71	226	4.50	0	29
Ce II	4527.35	108	.32			3.05	306	.71	226	4.50	0	29
Fe I	4531.63	555	3.21	4.92		2.47	250	.47	123	4.55	2	29
Ti I	4533.27	42	.85	4.70	4.47	4.30	281	.67	215	4.32	2	29
Ti II	4533.97	50	1.24	4.62		3.02	500	.85	438	4.02	4	29
Ti I	4534.79	42	.84	4.75	4.51	4.07	281	.62	189	4.38	4	29
Cr I	4535.15	33	2.54	5.24	4.75	3.18	226	.24	56	4.91	1	0
Ce II	4536.89		1.52			3.23	225	.23	54	4.93	2	0
Sm II	4537.96	45	.48	6.00	5.19	2.58	281	.51	142	4.50	3	29
Ce II	4539.07		1.37			3.20	241	.33	83	4.74	2	0
Cr I	4540.50	33	2.54	4.90	4.55	3.88	254	.41	110	4.62	1	0
Nd II	4541.27	58	.38			2.28	276	.55	163	4.44	1	0
Ti II	4544.01	60	1.24	5.11	4.65	1.58	312	.63	214	4.53	0	29
Cr I	4545.96	10	.94	4.79		2.69	269	.64	186	4.39	5	29
Fe I	4547.85	755	3.55	4.79	4.58	3.67	244	.56	156	4.45	5	29
Ti I	4548.76	42	.83	4.86	4.57	3.48	250	.50	132	4.52	3	29
Ni I	4551.24	236	4.17	5.30	4.83	3.54	219	.52	128	4.98	0	29
Ce II	4551.30	229	.74			2.93	219	.52	128	4.68	0	29
Fe I	4551.67	972	3.94	5.30	4.87	2.66	203	.24	59	4.90	1	29
Ba II	4554.03	1	.00	4.46	4.24	3.83	843	.91	1068	3.63	3	29
Ti I	4555.49	42	.85	4.93	4.63	3.37	275	.54	160	4.46	2	0
Fe I	4558.11	894	3.64	5.38		2.31	234	.28	63	4.84	4	30
La II	4559.28	53	.77	6.48		1.94	190	.34	71	4.76	5	29
Ce II	4560.96	2	.68	6.01		2.96	271	.51	148	4.49	3	0
Ce II	4562.36	1	.48	5.43	4.85	3.59	250	.64	159	4.46	5	30
Nd II	4563.22		.18			2.08	276	.54	161	4.45	3	0
Ti II	4563.76	50	1.22	4.58	4.35	2.80	387	.79	368	4.09	3	30
Sm II	4566.21	32	.33	5.78	5.08	2.25	234	.35	83	4.72	2	30
Fe I	4566.52	641	3.30	5.10	4.74	2.37	187	.25	52	4.92	2	30
Fe I	4566.99	723	3.41	5.43		1.94	234	.32	80	5.10	0	30
Nd II	4567.61	49	.20	6.36		1.49	219	.30	68	4.81	3	30
Ti II	4568.31	60	1.22	5.26	4.78	1.73	250	.39	96	4.66	4	30
Fe I	4568.79	554	3.26	5.06		2.08	250	.37	100	4.86	0	30

Table A

Spect	Wave-length	Mult	EP	$-\text{Log}$ $(W_{\odot}/\lambda)$	$-\text{Log}$ (W_{ϵ}/λ)	Log $(gf\lambda)$	HW	R_c	W	$-\text{Log}$ $(W_{\bigcirc}/\lambda)$	Q	N
Fe I	4568.86	894	3.63	5.36		2.37	250	.37	100	4.96	0	30
Pr II	4570.61		.22	6.36		1.59	187	.14	27	5.19	1	30
Mg I	4571.10	1	.00	4.70			281	.64	199	4.36	4	30
Ce II	4572.79		1.48			3.19	250	.30	80	4.76	2	30
Nb I	4573.08		.27			2.83	203	.08	16	5.46	2	0
Fe I	4574.24	554	3.21	5.14	4.81	2.03	219	.27	61	4.86	1	30
Zr I	4575.52	5	.00	5.66	4.94	2.30	250	.27	65	4.85	3	30
Fe II	4576.33	38	2.84	4.91	4.66	1.44	343	.61	224	4.31	5	30
V I	4577.17	4	.00	5.26		2.40	234	.30	74	4.79	3	30
Sm II	4577.69	23	.25	6.06		2.26	265	.40	109	4.63	1	30
Ca I	4578.55	23	2.52	4.80	4.60	3.10	281	.45	122	4.57	1	30
Cr I	4580.06	10	.94	4.76		2.46	281	.58	178	4.41	2	30
V I	4580.39	4	.02	5.04		2.52	375	.46	183	4.76	0	30
Fe I	4580.59	827	3.65	5.06		2.51	375	.46	183	4.76	0	30
Ce II	4582.50	7	.70	6.06		3.11	343	.56	185	4.41	1	30
Fe II	4582.84	37	2.84	4.97	4.73	1.22	293	.53	157	4.47	2	30
Ti II	4583.44	39	1.16	5.26	4.73		250	.44	120	4.58	1	30
Fe II	4583.83	38	2.81	4.57		2.41	437	.77	366	4.10	4	30
Ru I	4584.44	5	1.00	6.49		3.50	206	.10	20	5.35	1	0
Ca I	4585.87	23	2.52	4.53		3.47	281	.59	199	4.38	3	30
V I	4586.36	4	.04	5.08		2.65	312	.40	145	4.85	0	30
Fe I	4587.13	795	3.57	5.00		2.87	281	.37	110	4.65	3	30
Cr II	4588.22	44	4.07	4.84		3.01	296	.58	195	4.39	5	30
Ti II	4589.96	50	1.24	4.82	4.53	2.05	306	.68	229	4.30	5	30
Sm II	4591.82	14	.18	6.49		1.89	242	.32	80	4.76	1	0
Cr II	4592.09	44	4.07	5.02		2.29	260	.43	118	4.59	2	0
Fe I	4592.66	39	1.56	4.68		1.75	337	.70	261	4.25	4	30
Fe I	4593.54	971	3.94	5.32	4.86	2.65	281	.39	106	4.83	0	30
Nd II	4594.45	52	.20			1.49	256	.32	84	4.75	1	30
Fe I	4595.36	594	3.30	4.88		2.73	312	.56	181	4.62	0	30
Ni I	4595.96	101	3.42	5.13		3.18	296	.49	151	4.85	0	30
Fe I	4596.06	820	3.60	4.88		2.92	296	.49	151	4.69	0	30
Fe I	4596.43	823	3.65	5.20	4.83	2.28	250	.23	60	4.91	1	30
Fe I	4598.12	554	3.28	4.78	4.58	2.98	271	.50	145	4.50	3	0
Fe I	4598.74	819	3.69	5.58	5.02	2.05	218	.17	39	5.08	1	30
Cr I	4600.75	21	1.00	4.76	4.52	2.64	283	.57	174	4.42	2	0
Ce II	4601.37		1.32			2.64	236	.28	68	4.83	3	0
Fe I	4602.00	39	1.61	4.88	4.55	1.16	275	.51	152	4.49	5	30
Zr I	4602.54		1.87	6.19		4.01	218	.18	44	5.04	1	30
Fe I	4602.94	39	1.48	4.68	4.34	2.20	281	.70	225	4.31	4	30
Fe I	4603.95	410	2.99	5.49		1.50	250	.27	72	4.95	0	30
Sm II	4604.18		.04			1.62	218	.29	74	4.80	1	30
Ce II	4604.21		1.03			2.16	218	.29	74	4.80	1	30
Cr I	4604.58	190	3.32	5.09	4.76		265	.28	80	4.79	2	30
Ni I	4604.99	98	3.48	4.87		4.39	265	.49	132	4.53	3	30
Ce II	4606.40		.91			3.31	286	.59	182	4.40	3	0
Nb I	4606.77		.35	5.92		3.10	217	.16	35	5.12	2	0
Sr I	4607.35	2	.00	5.11	4.71	4.00	286	.59	183	4.40	2	0
Ce II	4608.76		1.41			2.81	203	.20	47	4.99	2	30
Ti II	4609.26	39	1.18	5.62	5.00		275	.34	96	4.70	3	30

Table A

Spect	Wave-length	Mult	EP	$-\text{Log}$ $(W_{\odot}/\lambda)$	$-\text{Log}$ (W_{ϵ}/λ)	Log $(gf\lambda)$	HW	R_c	W	$-\text{Log}$ $(W_{\bigcirc}/\lambda)$	Q	N
Fe I	4611.28	826	3.65	4.64		3.68	291	.62	194	4.38	2	0
Pr II	4612.07		.00	6.12		1.67	287	.23	69	4.88	2	30
Nd II	4612.47	3	.06	6.27		.95	312	.25	74	4.84	2	30
Zr II	4613.95	67	.97	5.20	4.78		277	.53	157	4.47	2	0
Sm II	4615.69	22	.19	5.73		2.09	263	.44	122	4.58	2	0
Cr I	4616.14	21	.98	4.81	4.60	2.72	289	.60	187	4.39	3	0
Cr II	4616.63	44	4.07	5.10	4.91	2.15	306	.46	149	4.52	2	30
Ti I	4617.27	145	1.75	4.97	4.72	4.38	234	.39	99	4.66	5	30
Fe I	4619.29	821	3.60	4.82	4.65	3.40	273	.50	146	4.50	2	0
La II	4619.87	76	1.75	6.27		3.47	287	.43	126	4.58	2	30
Fe II	4620.51	38	2.83	4.99	4.78	1.03	281	.51	159	4.48	4	30
Cr I	4621.94	32	2.54	5.01		3.41	278	.32	90	4.73	3	30
Cr I	4622.49	233	3.55	5.15	4.75	4.23	265	.31	93	4.73	2	30
Ti I	4623.10	145	1.74	5.00	4.64	4.07	274	.38	98	4.67	3	30
Ce II	4624.90	27	1.12	5.89		3.52	390	.62	256	4.46	0	30
Fe I	4625.05	554	3.24	4.78	4.58	3.04	390	.62	256	4.46	0	30
Co I	4625.77	176	3.71	5.82		3.65	209	.13	29	5.39	0	30
Cr I	4625.92	244	3.85	5.59			209	.13	29	5.39	0	30
Cr I	4626.19	21	.97	4.84	4.64	2.66	281	.53	167	4.45	2	30
Ce II	4628.16	1	.52	5.52	4.86	3.52	337	.67	226	4.31	4	30
Fe I	4630.13	115	2.28	4.88	4.59	1.84	249	.56	161	4.45	2	30
Fe I	4632.92	39	1.61	4.68		1.36	291	.61	189	4.39	2	0
Fe I	4635.85	349	2.84	5.02	4.70	2.21	249	.38	91	4.68	1	30
Ti II	4636.35	38	1.16	5.52	4.90		306	.41	124	4.59	2	30
Fe I	4638.02	822	3.60	4.75		3.43	312	.53	174	4.45	3	30
Sm II	4642.24	36	.38	5.79	4.99	2.55	299	.47	152	4.51	2	30
Fe I	4643.47	820	3.65	4.87	4.57	3.21	281	.46	125	4.56	2	30
Y I	4643.70	4	.00		4.97	2.76	254	.38	101	4.66	1	0
Cr I	4646.17	21	1.03	4.78	4.47	3.17	374	.66	238	4.29	2	30
Ni I	4648.66	98	3.42	4.84	4.56	4.47	305	.52	161	4.47	2	30
Cr I	4649.46	32	2.54	5.37	4.85	3.03	218	.22	50	4.96	1	30
Cr I	4652.16	21	1.00	4.75	4.52	2.88	256	.61	170	4.44	5	30
Fe I	4653.49	17	.99	5.76			312	.27	90	5.00	0	30
Sm II	4655.13		.48			1.87	227	.21	49	4.98	2	0
Ti I	4656.47	6	.00	4.93	4.53	2.52	271	.47	135	4.54	3	30
Ti II	4657.21	59	1.24	5.09	4.66		286	.57	176	4.42	1	0
Ce II	4659.37		1.21	6.19		2.73	218	.28	69	4.83	3	30
La II	4662.51	8	.00	6.02	5.00	1.68	264	.55	150	4.47	4	30
Cr I	4664.80	186	3.12	4.95		4.04	226	.34	78	4.75	3	30
Fe I	4668.14	554	3.26	4.62		3.38	280	.60	174	4.41	3	31
Na I	4668.56	12	2.10	5.08	4.63	2.37	251	.35	92	4.71	2	0
Fe I	4672.83	40	1.61	5.18	4.81		171	.22	38	5.02	1	31
Fe I	4673.17	820	3.65	4.81		3.27	311	.53	189	4.43	4	31
Ti I	4675.12	77	1.07	5.19	4.75	2.57	218	.27	66	4.85	2	31
Sm II	4676.91	3	.04	6.13	5.08	2.13	296	.37	109	4.65	3	31
Fe I	4678.85	821	3.60	4.68	4.55	3.83	289	.58	181	4.41	3	0
Ti I	4681.91	6	.05	4.86	4.54	2.68	284	.55	168	4.44	1	0
Fe I	4683.57	346	2.83	5.01	4.72	2.12	302	.37	113	4.65	2	31
Ge I	4685.84	3	2.03	5.97		2.37	216	.13	33	5.28	2	0
Ni I	4686.22	98	3.60	4.92	4.66	3.99	234	.35	90	4.71	3	31

Table A

Spect	Wave-length	Mult	*EP*	$-$Log $(W_{\odot}/\lambda)$	$-$Log (W_{ϵ}/λ)	Log $(gf\lambda)$	*HW*	R_c	*W*	$-$Log $(W_{\bigcirc}/\lambda)$	*Q*	*N*
Ce II	4686.75		1.09	6.27		2.69	274	.29	78	4.79	3	31
Zr I	4687.80	43	.73	5.80		3.66	252	.36	95	4.69	3	31
Cr I	4689.37	186	3.12	5.18		3.91	312	.36	110	4.85	0	31
Fe I	4690.15	820	3.69	4.96	4.72	3.02	254	.36	95	4.69	1	0
Co I	4693.19	156	3.23	5.44	4.89	3.89	181	.18	41	5.06	1	31
S I	4694.13	2	6.52	5.59	5.33	1.91	226	.19	43	5.03	1	0
S I	4695.45	2	6.52	5.77	5.47	1.77	218	.14	31	5.19	1	0
S I	4696.25	2	6.52	5.77	5.56	1.52	226	.19	43	5.03	1	0
La II	4699.64		.40			1.46	265	.31	79	4.77	3	32
Fe I	4700.17	935	3.69	4.96	4.71	2.82	302	.37	105	4.66	5	32
Fe I	4701.05	820	3.69	5.09		2.58	296	.27	82	4.80	3	32
Ce II	4702.01		.81			2.41	249	.30	89	4.76	2	32
Mg I	4702.98	11	4.34	4.16	4.33	3.09	324	.69	288	4.21	4	32
Sm II	4704.40	1	.00	6.07	4.84	1.98	243	.37	88	4.70	4	32
Fe I	4704.96	821	3.69	4.91	4.69	3.13	265	.37	101	4.67	3	32
Ni I	4705.93	128	3.66	5.72	5.21	2.90	206	.13	31	5.18	2	32
Nd II	4706.54	3	.00			2.02	249	.56	136	4.48	4	32
Cr I	4708.04	186	3.17	4.96	4.70	4.37	249	.40	110	4.63	3	32
Ti II	4708.66	49	1.24	5.01	4.70		278	.50	148	4.50	2	0
Fe I	4708.98	889	3.64	5.10		2.88	280	.50	152	4.90	0	32
Fe I	4709.09	821	3.65	4.80		3.22	280	.50	152	4.70	0	32
Ru I	4709.48	14	1.13	6.13		3.47	204	.05	10	5.67	1	0
Mn I	4709.72	21	2.89	4.88	4.64	3.62	249	.47	129	4.55	3	32
La II	4716.44	52	.77			2.10	218	.34	81	4.74	4	32
Cr I	4718.43	186	3.19	4.90	4.65	4.49	330	.49	171	4.48	2	32
Zr I	4719.12	66	1.86	6.28		3.72	218	.10	21	5.35	2	32
Fe I	4721.00	409	2.99	5.00		1.98	280	.38	112	4.64	4	32
Zn I	4722.16	2	4.03	4.87	4.73	4.36	280	.55	169	4.45	5	32
Ce II	4725.09	153	.52	6.50	5.67	2.34	255	.33	87	4.74	4	32
Co I	4727.94	15	.43	5.75		.63	229	.20	47	5.01	2	0
Mg I	4730.03	10	4.34	4.86	4.67	1.62	267	.43	122	4.59	2	0
Fe II	4731.44	43	2.89	4.78	4.62	1.41	291	.57	179	4.42	3	0
Ni I	4731.81	163	3.83	5.08	4.79	3.61	259	.38	103	4.66	3	0
Mn I	4739.11	21	2.94	4.93	4.67	3.56	249	.41	108	4.63	3	32
La II	4740.28	8	.13			1.92	339	.63	226	4.52	0	32
Fe I	4740.34	409	3.02	5.11		1.99	339	.63	226	4.62	0	32
Fe I	4741.08	688	3.33	5.16		2.10	296	.34	108	4.68	4	32
Fe I	4741.53	346	2.83	4.84	4.64	2.51	311	.52	178	4.45	4	32
Sc I	4743.81	14	1.45	5.80	5.20	4.07	212	.09	19	5.40	1	0
Fe I	4745.81	821	3.65	4.84		3.24	280	.56	166	4.44	4	32
Ce II	4747.14		1.46			3.40	296	.40	128	4.60	3	32
La II	4748.73	65	.93	6.07	5.25	2.52	286	.43	122	4.59	2	32
Fe I	4749.93	1206	4.56	5.16	4.84	3.43	242	.27	67	4.85	2	0
Na I	4751.82	11	2.10	5.50	4.98	1.58	193	.13	29	5.22	1	32
Ni I	4752.43	132	3.66	4.90	4.73	3.72	262	.39	107	4.65	2	0
Ce II	4753.65		1.28			2.38	219	.13	29	5.21	2	0
Mn I	4754.04	16	2.28	4.56	4.45	3.81	249	.64	181	4.42	5	32
Cr I	4754.74	168	3.09	4.99			249	.30	84	4.77	3	32
Cr I	4756.11	145	3.10	4.90	4.69	4.55	267	.42	118	4.60	3	0
Ni I	4756.52	98	3.48	4.80	4.63	4.14	249	.47	139	4.54	2	32

Table A

Spect	Wave-length	Mult	EP	$-\mathrm{Log}$ $(W_{\odot}/\lambda)$	$-\mathrm{Log}$ (W_{ϵ}/λ)	Log $(gf\lambda)$	HW	R_c	W	$-\mathrm{Log}$ $(W_{♂}/\lambda)$	Q	N
V I	4758.74	51	1.22	5.64	5.11		196	.10	23	5.35	1	32
Ti I	4758.91	41	.84	6.08	5.13		174	.10	17	5.35	1	32
Ti I	4759.27	233	2.25	5.06	4.79	4.40	264	.32	82	4.76	3	32
Y I	4760.98	4	.07	6.28		2.10	228	.18	41	5.06	1	0
Mn I	4761.53	21	2.95	4.81	4.60	3.71	295	.46	146	4.53	4	32
Mn I	4762.38	21	2.89	4.66	4.52	4.28	296	.59	189	4.40	2	0
Ti II	4764.54	48	1.24	5.19	4.71		273	.45	130	4.56	2	0
Mn I	4765.86	21	2.94	4.83	4.62	3.93	239	.45	115	4.59	2	32
Mn I	4766.42	21	2.92	4.73	4.54	4.13	311	.52	163	4.47	2	32
Fe I	4768.32	821	3.69	4.84		3.00	299	.56	172	4.65	0	32
Fe I	4768.40	384	2.94	4.97		2.11	299	.56	172	4.65	0	32
C I	4770.03	6	7.48	5.47	5.56	1.40	230	.19	44	5.03	2	0
Ti I	4771.10	41	.83	5.38			224	.15	37	5.13	1	32
Zr I	4772.32	43	.62	5.83	5.25	3.11	218	.28	71	4.83	3	32
Fe I	4772.82	467	3.02	4.73		2.63	249	.58	161	4.44	5	32
Ce II	4773.94	17	.92	5.75	5.13	3.03	249	.41	107	4.63	2	32
Ti I	4778.26	232	2.24	5.48		3.70	187	.13	29	5.22	2	32
Fe I	4779.44	720	3.41	4.97	4.78	2.30	218	.28	65	4.85	2	32
Ti II	4780.00	92	2.05	4.80	4.68		286	.58	174	4.43	3	32
Fe I	4780.81	633	3.25	5.68	5.23	1.47	218	.10	26	5.35	1	32
Co I	4781.43	57	1.88	5.78	5.07	2.16	202	.11	26	5.30	1	32
Mn I	4783.42	16	2.30	4.48	4.44	3.79	292	.65	209	4.36	3	32
Zr I	4784.94	44	.69	6.68		2.56	187	.12	26	5.26	1	32
Fe I	4787.84	384	3.00	5.05	4.76	1.90	249	.26	69	4.86	3	32
Fe I	4788.76	588	3.24	4.82	4.70	2.75	249	.45	125	4.57	5	32
Cr I	4790.34	31	2.54	5.48	5.07		218	.13	33	5.22	1	32
Sm II	4791.58	7	.10	6.28		1.70	229	.18	42	5.06	3	0
Co I	4792.86	158	3.25	5.08	4.85	4.44	239	.24	59	4.91	2	0
Fe I	4793.96	512	3.05	5.73	5.27	1.13	218	.09	21	5.40	1	32
Ti I	4796.21	260	2.33	5.30	4.97	3.62	218	.15	32	5.16	1	32
Nd II	4797.16	60	.56	6.28		1.95	265	.39	108	4.65	2	0
Ti II	4798.54	17	1.08	4.98	4.76		283	.50	151	4.50	2	0
Fe I	4799.41	888	3.64	5.12		2.49	273	.39	111	4.84	0	32
Nd II	4799.42	2	.00			1.10	273	.39	111	4.94	0	32
Fe I	4800.65	1042	4.14	4.82	4.59	3.42	261	.37	113	4.65	2	32
Fe I	4802.88	888	3.64	4.84		2.93	249	.37	98	4.68	3	32
La II	4804.05	37	.23	6.08		1.52	280	.48	142	4.53	2	32
Ti II	4805.10	92	2.06	4.69		2.92	311	.64	223	4.33	3	32
Zr I	4805.88	43	.69	6.38		2.64	186	.15	27	5.20	2	32
Ti II	4806.33	17	1.08	5.90			271	.21	59	4.94	2	32
Ni I	4807.00	163	3.68	4.84	4.75	3.87	279	.35	106	4.68	3	32
Fe I	4807.73	688	3.37	4.90	4.74	2.32	255	.30	82	4.78	3	32
Fe I	4808.16	633	3.25	5.20	4.89	1.83	216	.17	41	5.08	2	32
Fe I	4809.94	793	3.57	5.38	4.98	1.86	201	.12	24	5.26	3	32
Zn I	4810.55	2	4.08	4.76	4.76	4.54	276	.46	141	4.54	5	32
Nd II	4811.34	3	.06	5.70	4.96	1.76	268	.50	140	4.52	5	32
Ni I	4812.00	130	3.66	5.28	4.93	2.92	233	.22	58	4.94	3	32
Cr II	4812.36	30	3.86	5.07	4.84	1.81	259	.31	90	4.75	3	33
Fe I	4813.11	630	3.27	5.30		1.73	248	.17	45	5.06	2	33
Co I	4813.48	158	3.21	4.97		4.41	226	.25	63	4.89	3	32

Table A

Spect	Wave-length	Mult	EP	$-\text{Log}$ $(W_{\odot}/\lambda)$	$-\text{Log}$ (W_{ϵ}/λ)	Log $(gf\lambda)$	HW	R_c	W	$-\text{Log}$ $(W_{\bigcirc}/\lambda)$	Q	N
Nd II	4817.20		.74	6.51		1.61	244	.26	65	4.87	2	0
C I	4817.37	5	7.48	5.71		1.15	229	.17	39	5.09	2	0
Nd II	4818.96		.47			1.16	248	.18	48	5.03	2	34
Nd II	5102.42		.68			2.18	311	.45	137	4.57	3	24
Ni I	5102.97	49	1.68	5.08	4.68	1.37	328	.44	161	4.54	2	24
Cu I	5105.55	2	1.39	4.79	4.52	2.20	319	.60	207	4.39	2	0
Fe I	5109.66	1089	4.30	4.87	4.66	3.65	282	.39	115	4.65	2	0
Fe I	5110.41	1	.00	4.61	4.34	.37	337	.70	291	4.25	3	0
Zr II	5112.28	95	1.66	5.81	5.15	2.71	278	.49	155	4.52	3	24
Y II	5119.12	20	.99	5.56	4.96	2.01	379	.56	219	4.40	2	24
Fe I	5133.70	1092	4.18	4.49		4.61	347	.62	237	4.34	5	24
Gd II	5140.84	115	1.58		5.10	2.95	177	.11	19	5.31	0	24
Fe I	5141.75	114	2.42	4.76	4.59	2.14	358	.50	189	4.47	3	24
Fe I	5143.73	65	2.20	5.35	4.94		264	.28	76	4.83	2	0
Fe I	5145.11	66	2.20	5.07	4.73	1.31	295	.45	141	4.56	2	0
Ti I	5145.47	109	1.46	5.14	4.81	3.52	264	.28	76	4.83	1	0
Fe I	5166.29	1	.00	4.65	4.32	.03	341	.66	235	4.34	4	25
Dy II	5169.71		.10	6.11		1.46	235	.10	27	5.28	1	0
Fe I	5171.61	36	1.48	4.51		2.43	347	.71	272	4.28	4	25
Mg I	5172.68	2	2.71	3.61	3.65	3.33	670	.88	693	3.87	5	25
Fe I	5180.07	1166	4.47	5.02	4.78	3.77	253	.27	78	4.84	1	25
Nd II	5181.16		.86	6.06		2.19	342	.33	122	4.68	3	25
Mg I	5183.60	2	2.72	3.51	3.56	3.55	772	.95	903	3.76	4	25
Ti II	5185.91	86	1.89	4.95			349	.53	201	4.44	3	25
Ni I	5186.59	205	3.90	5.51	5.02	2.99	190	.14	27	5.19	1	25
Ce II	5187.45	15	1.21	5.97	5.18	3.46	304	.46	151	4.54	2	25
Fe I	5187.92	1032	4.14	5.02	4.67	3.39	278	.35	109	4.69	2	25
La II	5188.24	95	2.45	6.02		3.87	291	.27	87	4.81	1	25
Fe I	5191.46	383	3.04	4.51	4.37	3.76	494	.75	381	4.25	0	25
Ti I	5192.97	4	.02	4.81	4.53	2.76	319	.57	196	4.42	3	0
Ti I	5194.04	183	2.10	5.72	5.03	3.64	228	.12	26	5.26	3	25
Fe I	5194.94	36	1.56	4.62	4.43	2.09	380	.67	263	4.30	2	25
Fe I	5195.47	1092	4.22	4.66	4.58	4.34	304	.54	182	4.46	1	25
Fe I	5196.10	1091	4.26	4.82	4.73	4.07	279	.42	120	4.62	1	25
Fe II	5197.57	49	3.23	4.81	4.65	1.88	355	.61	230	4.35	2	25
Fe I	5198.71	66	2.22	4.78	4.51	2.22	304	.57	174	4.45	5	25
Y II	5200.42	20	.99	5.15	4.69	2.67	343	.70	291	4.25	3	0
Ti I	5201.10	183	2.09	5.67	5.06	3.50	190	.09	18	5.40	3	25
Fe I	5202.34	66	2.18	4.53	4.35	2.53	342	.66	253	4.31	5	25
Cr I	5206.52	206	3.43	5.49	5.05		260	.24	64	4.91	2	0
Fe I	5207.94	880	3.63	5.44		2.52	291	.27	88	4.81	1	25
Ti I	5210.39	4	.05	4.78	4.51	2.82	304	.55	187	4.44	3	25
Ti II	5211.54	103	2.59	5.25	4.85	2.42	304	.39	135	4.62	3	25
Nd II	5212.35	44	.20	6.06		1.92	330	.46	152	4.54	3	25
Co I	5212.70	170	3.51	5.39	4.95	4.43	203	.16	33	5.16	1	25
Pr II	5219.03	37	.79	6.32		2.78	240	.28	71	4.85	3	26
Ti I	5219.70	4	.02	5.32	4.79	1.82	253	.27	70	4.86	1	26
Fe I	5223.19	880	3.63	5.30	4.91	2.51	215	.20	48	5.02	2	26
Fe I	5225.53	1	.11	4.89	4.52		354	.52	168	4.49	3	26
Fe I	5228.41	1091	4.22	4.94		3.83	316	.48	152	4.53	3	26

Table A

Spect	Wave-length	Mult	EP	$-$Log ($W_\odot/\lambda$)	$-$Log (W_ϵ/λ)	Log ($gf\lambda$)	HW	R_c	W	$-$Log ($W_\bigcirc/\lambda$)	Q	N
Fe I	5229.86	553	3.28	4.63		3.53	303	.55	180	4.45	4	26
Fe I	5232.95	383	2.94	4.18	4.20	4.11	392	.70	306	4.23	5	26
Nd II	5234.20	74	.55	5.82	5.06	2.43	392	.50	209	4.45	2	26
Fe II	5234.62	49	3.22	4.81	4.60	1.95	328	.61	219	4.38	2	26
Ti I	5238.56	37	.85	5.54		2.53	202	.17	38	5.11	2	26
Cr I	5238.97	59	2.71	5.52	5.05	2.83	151	.14	27	5.19	1	26
Sc II	5239.82	26	1.45	4.98	4.70	3.22	303	.53	179	4.47	5	26
Fe I	5253.48	553	3.28	4.85	4.65	2.92	303	.45	135	4.58	4	9
Nd II	5255.51	43	.20	5.88		1.99	354	.55	230	4.40	2	9
Fe II	5256.89	41	2.89	5.47	4.98		303	.29	89	4.79	4	9
La II	5259.38	21	.17		5.14	1.22	285	.36	107	4.69	3	0
Pr II	5259.74	35	.63	6.24	5.44	2.89	286	.37	111	4.68	3	0
Ca I	5260.39	22	2.52	5.27	4.94	1.82	291	.18	52	5.03	2	9
Ca I	5261.71	22	2.52	4.73	4.58	2.99	303	.50	155	4.52	4	9
Fe I	5263.31	553	3.26	4.64		3.53	349	.57	223	4.40	3	9
Fe II	5264.80	48	3.33	5.07	4.81	1.46	303	.44	147	4.57	1	9
Fe I	5266.56	383	3.00	4.32	4.27	3.81	384	.68	285	4.27	5	9
Fe I	5267.28	1146	4.37	5.32			265	.15	39	5.14	1	9
Fe I	5269.54	15	.86	4.04	3.96	2.37	518	.82	441	4.08	3	9
Cr I	5272.01	225	3.45	5.40	4.96	3.84	258	.21	55	4.98	2	0
Ce II	5274.24	15	1.04	5.91	5.13	3.24	286	.45	139	4.57	5	9
Nd II	5276.88	81	.86	6.55		2.24	265	.35	102	4.71	4	9
Fe I	5277.31	584	3.27	5.85			253	.11	27	5.30	1	9
S I	5278.96	4	6.86	5.91		1.62	241	.12	29	5.26	1	0
Fe I	5281.80	383	3.04	4.51	4.40	3.47	329	.60	212	4.39	5	9
Ti I	5282.38	74	1.05	5.38	4.90	2.29	278	.14	39	5.19	2	9
Fe I	5283.63	553	3.24	4.40		3.92	404	.66	283	4.27	3	9
Fe II	5284.09	41	2.89	4.90	4.74	1.24	312	.50	166	4.50	2	0
Fe I	5285.12	1166	4.43	5.33	4.95	3.40	253	.18	51	5.04	1	9
Fe I	5288.53	929	3.69	4.98		2.97	298	.35	111	4.69	4	9
Y II	5289.82	20	1.03	6.33		1.49	278	.45	136	4.58	5	9
La II	5290.83	6	.00	6.02	5.21	1.18	281	.36	114	4.68	5	9
Nd II	5293.17	75	.82	5.72		2.87	399	.53	217	4.43	2	9
Fe I	5295.32	1146	4.41	5.29			324	.18	53	5.03	1	9
Ti I	5295.78	74	1.07	5.72	5.02	2.48	253	.11	29	5.30	1	9
Cr I	5296.69	18	.98	4.75	4.53	2.36	283	.53	157	4.50	5	9
Ti I	5300.01	74	1.05	5.40	5.04		253	.13	31	5.22	1	9
Cr I	5300.75	18	.98	4.98	4.64	1.76	341	.37	127	4.65	1	9
La II	5303.54	36	.32	6.33		1.60	298	.42	130	4.61	1	9
Cr II	5305.85	24	3.83	5.33	4.99	1.72	291	.31	90	4.77	3	9
Nd II	5306.47		.86	6.73		2.11	265	.24	60	4.93	2	9
Fe I	5307.37	36	1.61	4.79	4.50	1.26	303	.54	175	4.47	5	9
Cr II	5308.44	43	4.07	5.28	4.98	1.95	253	.28	76	4.84	3	9
Cr II	5310.70	43	4.07	5.58	5.23	1.66	252	.17	43	5.09	1	0
Sm II	5312.23		.33			1.03	232	.06	14	5.59	1	0
Cr I	5312.88	225	3.45	5.45	5.04	3.66	239	.10	24	5.35	2	0
Cr II	5313.59	43	4.07	5.18	4.96	2.20	329	.40	129	4.62	3	9
Fe I	5315.07	1147	4.37	5.19	4.91	3.20	256	.19	49	5.03	1	0
Nd II	5319.82	75	.55	5.68		2.46	374	.53	187	4.46	5	9
Y II	5320.80	20	1.08	6.03		1.41	277	.30	86	4.79	1	0

Table A

Spect	Wave-length	Mult	EP	−Log $(W_{\odot}/\lambda)$	−Log (W_{ϵ}/λ)	Log $(gf\lambda)$	HW	R_c	W	−Log $(W_{\circ}/\lambda)$	Q	N
Fe I	5321.11	1165	4.43	5.09	4.87	3.62	284	.34	101	4.72	2	0
Fe I	5322.05	112	2.28	4.95	4.69	1.76	291	.41	124	4.62	4	9
Pr II	5322.78	35	.48	6.43		2.54	291	.37	113	4.67	5	9
Fe I	5324.19	553	3.21	4.20	4.21	4.20	367	.68	265	4.30	4	9
Fe II	5325.56	49	3.22	5.07	4.83	.98	283	.41	136	4.60	3	9
Fe I	5326.15	407	3.02	5.22			329	.22	73	4.91	1	9
Fe I	5326.79	1147	4.41	5.69	5.16		215	.09	17	5.40	1	9
Cr I	5329.12	94	2.91	4.83	4.65	3.60	253	.36	97	4.70	0	9
Fe I	5329.99	1028	4.07	4.95		3.49	399	.38	155	4.59	3	9
Ce II	5330.58	13	.87	6.25	5.33	2.81	303	.37	113	4.67	2	9
Co I	5331.46	39	1.78	5.55		2.33	265	.20	50	5.02	1	9
Fe I	5332.90	36	1.56	4.74		1.37	329	.58	220	4.40	1	9
Cr II	5334.88	43	4.07	5.22	4.90	2.07	253	.31	91	4.77	2	9
Ti II	5336.81	69	1.58	4.88	4.67	2.05	334	.60	216	4.39	2	0
Fe II	5337.73	48	3.23	5.18			298	.35	113	4.69	2	9
Ti I	5338.33	35	.83	5.61	5.06		316	.13	38	5.22	1	9
Fe I	5339.40	1162	4.43	5.77	5.21		240	.11	24	5.30	1	9
Fe I	5339.94	553	3.26	4.52	4.44	3.62	354	.62	230	4.37	3	9
Fe I	5341.03	37	1.61	4.47		2.14	366	.73	297	4.25	3	9
Co I	5342.70	190	4.02	5.27	4.96	4.77	324	.19	61	4.99	2	9
Cr I	5345.81	18	1.00	4.70	4.45	2.74	379	.65	267	4.30	4	9
Ce II	5347.81		.74			1.92	265	.16	42	5.11	1	9
Cr I	5348.32	18	1.00	4.76	4.54	2.44	278	.56	174	4.46	4	9
Ca I	5349.47	33	2.71	4.77	4.64		314	.49	164	4.51	1	0
Co I	5352.05	172	3.58	5.41	4.93	4.47	254	.17	44	5.09	2	0
Pr II	5352.41		.48	6.73		2.21	260	.20	53	5.01	2	0
Fe I	5353.39	1062	4.10	4.85		3.66	366	.63	249	4.50	0	9
Ce II	5353.53	15	.88			3.20	366	.63	249	4.45	0	9
Sc I	5355.73	19	1.95	6.13		3.79	239	.09	21	5.40	2	0
Nd II	5356.98	80	1.26	6.43		2.73	316	.34	114	4.70	2	9
Ce II	5359.50		1.78			2.81	278	.16	47	5.09	1	9
Nd II	5361.17	46	.56			1.43	260	.20	53	5.01	1	0
Nd II	5361.51	74	.68	5.78		2.35	341	.53	193	4.46	3	10
Fe I	5364.88	1146	4.44	4.61		4.64	316	.56	181	4.45	3	10
Fe I	5365.41	786	3.57	4.84		3.37	309	.48	163	4.52	2	10
Fe I	5367.47	1146	4.41	4.53		4.72	319	.57	205	4.42	5	10
Fe I	5369.95	1146	4.37	4.47	4.42	4.80	341	.61	231	4.37	1	10
Fe I	5371.49	15	.96	4.26	4.11	2.13	457	.80	402	4.13	4	9
Fe I	5373.70	1166	4.47	4.96		3.97	300	.34	109	4.71	5	10
La II	5377.08	95	2.30	6.13	5.33	3.41	270	.25	69	4.89	1	0
Mn I	5377.63	42	3.84	5.08	4.76	4.20	274	.27	76	4.85	2	0
Fe I	5379.58	928	3.69	4.98	4.73	2.95	311	.41	127	4.62	3	10
C I	5380.34	11	7.68	5.32		2.05	341	.25	88	4.84	1	10
Fe I	5383.37	1146	4.31	4.42	4.43	4.90	341	.63	236	4.36	2	10
Nd II	5385.89		.74	6.56		1.98	298	.34	108	4.71	1	10
Fe I	5389.46	1145	4.41	4.78	4.66	4.12	329	.46	158	4.54	2	10
Fe I	5391.49	1062	4.15	4.85		3.65	405	.47	205	4.48	5	10
Mn I	5394.67	1	.00	4.86	4.50	.46	329	.44	154	4.56	4	10
Fe I	5395.25	1143	4.44	5.43	5.09		291	.16	51	5.07	1	10
Fe I	5397.13	15	.91	4.35	4.24	1.85	392	.77	341	4.20	2	10

Table A

Spect	Wave-length	Mult	*EP*	−Log $(W_\odot/\lambda)$	−Log (W_ϵ/λ)	Log $(gf\lambda)$	*HW*	R_c	*W*	−Log $(W_\odot/\lambda)$	*Q*	*N*
Fe I	5397.60	841	3.63	5.35	4.95		256	.17	44	5.09	2	0
Fe I	5398.29	1145	4.44	4.85	4.72	4.00	341	.41	146	4.59	3	10
Mn I	5399.49	42	3.85	5.14	4.87	3.90	324	.20	64	4.96	1	10
Fe I	5400.51	1145	4.37	4.68		4.31	329	.56	209	4.42	1	10
Y II	5402.78	35	1.84	5.65		2.85	303	.53	170	4.48	4	10
Fe I	5403.82	1029	4.07	4.95	4.70	3.77	300	.40	126	4.63	1	0
Cr I	5405.00	191	3.37	5.73	5.20	3.52	243	.10	24	5.35	1	0
Fe I	5405.35	1162	4.39	5.10	4.83	3.89	275	.27	77	4.85	2	0
Fe I	5405.78	15	.99	4.31	4.31	1.98	405	.77	348	4.19	2	10
Fe I	5406.77	1148	4.37	5.16	4.93		278	.21	61	4.96	3	10
Fe I	5409.14	1147	4.37	4.98		3.42	341	.49	176	4.69	0	10
Ce II	5409.22	23	1.10			3.21	341	.49	176	4.69	0	10
Cr I	5409.79	18	1.03	4.55	4.41	3.03	329	.66	251	4.33	2	10
Fe I	5410.91	1165	4.47	4.51	4.56	4.78	331	.56	199	4.43	3	0
Fe II	5414.09	48	3.22	5.24	5.03	.95	278	.34	104	4.72	1	10
Fe I	5415.20	1165	4.39	4.41	4.48	4.94	329	.62	224	4.38	3	10
Nd II	5416.38	80	.86	6.73		1.92	266	.22	60	4.96	3	0
Fe I	5417.03	1148	4.41	5.17	4.96	3.18	298	.20	61	4.98	1	10
Ti II	5418.80	69	1.58	5.04	4.76	1.63	329	.50	179	4.49	2	10
Mn I	5420.36	4	2.14	4.84	4.50	2.52	316	.40	137	4.61	5	10
Fe II	5425.27	49	3.20	5.05	4.93	.95	299	.39	123	4.65	2	0
Ti I	5426.26	3	.02	5.99	5.13	1.25	201	.09	16	5.40	2	11
Fe I	5429.70	15	.96	4.28		1.95	556	.77	465	4.07	4	11
Nd II	5431.54	80	1.12	6.08		2.53	342	.27	98	4.79	4	11
Mn I	5432.55	1	.00	5.07	4.60	.03	330	.34	112	4.70	2	11
Fe I	5432.96	1143	4.44	4.88			355	.41	147	4.59	2	11
Fe I	5434.53	15	1.01	4.47	4.35	1.77	387	.71	294	4.27	5	11
Ni I	5435.87	70	1.99	5.07	4.71	1.85	268	.34	101	4.73	3	11
Fe I	5436.59	113	2.28	5.17	4.76	1.02	285	.31	91	4.77	1	0
Nd II	5442.27	76	.68			1.84	304	.32	100	4.75	3	12
Co I	5444.59	196	4.07	5.59	5.20	4.43	164	.08	15	5.46	1	12
Fe I	5445.05	1163	4.39	4.65	4.62	4.41	334	.53	204	4.45	4	12
Fe I	5446.92	15	.99	4.36		1.84	404	.78	360	4.18	1	12
Nd II	5447.56		1.04			1.80	290	.25	73	4.88	2	12
Ti I	5453.65	108	1.44	6.13	5.29	2.60	178	.07	13	5.52	1	13
Co I	5454.57	195	4.07	5.62	5.26	4.34	178	.09	16	5.40	1	13
Mn I	5457.47	4	2.16	5.70	5.18	1.69	178	.08	15	5.46	1	13
Ti I	5460.50	3	.05	5.81	4.97	1.37	251	.13	33	5.22	1	0
Fe I	5460.91	464	3.07	5.89	5.26		250	.12	30	5.26	1	0
Fe I	5461.54	1145	4.44	5.39	5.01	3.10	241	.20	52	5.01	2	13
Ni I	5462.49	192	3.85	5.14	4.89	3.49	329	.29	100	4.77	1	13
Fe I	5462.97	1163	4.47	4.77	4.63	4.22	304	.51	162	4.51	1	13
Fe I	5463.28	1163	4.43	4.67	4.62	4.37	279	.54	170	4.48	1	13
Fe I	5466.40	1144	4.37	4.86	4.72	3.72	304	.46	155	4.55	3	13
Fe I	5466.99	784	3.57	5.28		2.49	248	.25	64	4.91	1	13
Ce II	5468.37	24	1.40	6.19	5.42	3.20	273	.36	109	4.70	2	13
Mn I	5470.64	4	2.16	5.08	4.56	2.39	293	.33	114	4.71	2	13
Ti I	5471.20	106	1.44	5.93	5.19	2.90	252	.13	35	5.19	1	0
Ce II	5472.30	24	1.25	6.26		3.04	303	.38	133	4.64	1	13
Fe I	5473.91	1062	4.15	4.84	4.67	3.70	303	.45	160	4.55	1	13

Table A

Spect	Wave-length	Mult	EP	−Log $(W_{\odot}/\lambda)$	−Log (W_{ϵ}/λ)	Log $(gf\lambda)$	HW	R_c	W	−Log $(W_{\male}/\lambda)$	Q	N
Nd II	5474.76		.99	6.56		1.84	227	.21	54	4.99	2	13
Ni I	5476.94	59	1.83	4.52		3.16	360	.69	285	4.28	2	0
La II	5482.27	4	.00			.82	252	.29	78	4.83	1	13
Sc I	5484.62	16	1.85	6.26		4.07	235	.04	9	5.78	1	0
Nd II	5485.70	79	1.26	6.34		2.69	328	.36	119	4.68	4	13
Fe I	5487.16	1143	4.41	5.23	4.91	3.11	270	.28	81	4.83	1	13
Fe I	5487.76	1025	4.14	4.79		3.71	428	.49	222	4.45	2	13
Fe I	5488.14	1183	4.61	5.48	5.02		247	.17	45	5.15	0	13
Ti I	5488.20	265	2.40	5.48	5.02	3.90	247	.17	45	5.15	0	13
Ti I	5490.15	107	1.46	5.48	4.95	3.21	214	.14	30	5.19	1	13
Fe I	5491.84	1031	4.19	5.70	5.25		138	.08	11	5.46	1	13
La II	5493.45	4	.13			.72	332	.36	119	4.87	0	13
Fe I	5493.51	1061	4.10	5.20		2.95	332	.36	119	4.87	0	13
Fe I	5494.47	1024	4.07	5.34	4.97	2.80	201	.15	32	5.19	1	13
Ni I	5494.89	231	4.10	5.48	5.13	3.33	189	.08	14	5.46	1	13
Fe I	5496.57	1281	4.91	5.79	5.33		249	.11	27	5.30	1	0
Fe I	5497.52	15	1.01	4.63	4.41	1.25	402	.73	337	4.21	5	13
Fe I	5501.47	15	.96	4.68	4.47	1.08	389	.65	277	4.30	4	13
Cr II	5502.05	50	4.17	5.38	5.16	2.14	271	.23	62	4.94	2	13
Mo I	5506.49	4	1.33	6.00		3.69	281	.27	78	4.85	1	0
Fe I	5506.78	15	.99	4.66	4.41	1.30	404	.66	285	4.29	3	14
V I	5507.75	129	2.36	6.34	5.70	3.70	121	.05	6	5.67	1	14
Y II	5509.91	19	.99	5.46		2.05	379	.65	265	4.32	4	14
Ca I	5512.98	48	2.93	4.77	4.63	3.45	328	.45	167	4.54	2	14
Ce II	5516.08		1.61			2.70	273	.16	42	5.12	2	14
Mn I	5516.77	4	2.18	5.13	4.59	2.30	354	.28	107	4.77	2	14
Y II	5521.59	27	1.74	6.00		2.46	349	.46	180	4.52	2	14
Sc II	5526.81	31	1.77	4.86	4.67	3.77	328	.63	217	4.41	5	14
Y I	5527.54	12	1.40			3.49	258	.15	39	5.15	2	0
Mg I	5528.39	9	4.34	4.28	4.33	3.11	354	.72	292	4.28	2	14
Co I	5530.78	38	1.71	5.60	4.94	2.14	264	.18	48	5.06	2	0
Mo I	5533.01	4	1.33	5.90		3.52	280	.26	75	4.87	1	0
Fe II	5534.86	55	3.24	4.94	4.69	1.55	354	.52	208	4.45	1	14
Fe I	5543.18	926	3.69	4.96	4.66	2.99	327	.38	138	4.63	4	15
Fe I	5543.93	1062	4.22	4.94	4.77	3.49	383	.37	142	4.63	1	15
Y II	5544.61	27	1.74	5.84	5.33	2.46	318	.48	172	4.52	1	15
Y II	5546.03	27	1.75	5.93		2.34	339	.52	194	4.47	2	15
Fe I	5546.51	1145	4.37	5.02	4.81	3.52	250	.31	89	4.78	1	15
Fe I	5547.00	1061	4.22	5.28	4.92	2.89	224	.22	52	4.99	1	15
Nd II	5548.47	73	.55	6.35		1.48	345	.27	102	4.79	1	15
Fe I	5553.59	1161	4.43	5.14		3.41	315	.30	98	4.77	3	16
Fe I	5554.90	1183	4.55	4.74		4.12	306	.45	146	4.57	2	16
Ce II	5556.97		1.80			3.18	253	.17	45	5.09	1	16
Fe I	5560.23	1164	4.43	5.10		3.55	251	.28	76	4.85	2	16
Fe I	5562.71	1163	4.43	5.03		3.70	324	.38	135	4.64	1	16
Fe I	5563.60	1062	4.19	4.78	4.56	3.66	293	.49	154	4.54	5	16
Fe I	5569.63	686	3.42	4.54	4.46	3.82	378	.64	280	4.30	2	17
Mo I	5570.46	4	1.33	5.93		3.18	348	.19	66	4.98	1	17
Fe I	5572.85	686	3.40	4.43	4.36	4.03	504	.67	342	4.21	2	17
Fe I	5576.10	686	3.43	4.69	4.58	3.44	328	.59	251	4.37	4	17

Table A

Spect	Wave-length	Mult	EP	$-$Log $(W_{\odot}/\lambda)$	$-$Log (W_{ϵ}/λ)	Log $(gf\lambda)$	HW	R_c	W	$-$Log $(W_{\bigcirc}/\lambda)$	Q	N
Fe I	5577.03	1314	5.03	5.63	5.24		202	.10	22	5.35	1	17
Ni I	5578.73	47	1.68	5.08	4.70	1.49	353	.45	168	4.54	3	17
Ca I	5581.97	21	2.52	4.79	4.61	3.04	331	.51	181	4.49	3	0
Fe I	5584.77	782	3.57	5.24	4.83	2.56	296	.33	102	4.74	2	0
Fe I	5586.76	686	3.37	4.36	4.36	4.09	378	.68	286	4.29	5	17
Ca I	5588.76	21	2.52	4.60	4.49	3.96	378	.64	267	4.32	5	17
Ni I	5589.38	205	3.90	5.35	5.05	3.28	240	.17	40	5.12	2	17
Ca I	5590.12	21	2.52	4.81	4.66	3.04	353	.49	186	4.50	3	17
Fe II	5591.38	55	3.27	5.90	5.60		256	.12	31	5.26	2	0
Ni I	5592.28	69	1.95	5.05		1.97	353	.44	176	4.54	3	17
Ni I	5593.74	206	3.90	5.12	4.90	3.56	358	.30	98	4.77	2	17
Fe I	5598.30	1183	4.65	4.83		4.33	479	.64	326	4.43	0	17
Ca I	5598.49	21	2.52	4.68		3.53	479	.64	326	4.43	0	17
Ca I	5601.28	21	2.52	4.75	4.51	3.06	366	.53	218	4.44	2	17
Fe I	5607.66	1058	4.15	5.63	5.11		262	.15	39	5.15	2	0
Fe I	5608.98	1108	4.21	5.82	5.14		256	.12	31	5.26	1	0
Ce II	5610.26	26	1.05	6.05		2.56	378	.42	169	4.56	2	17
Ce II	5613.69	32	1.42			2.57	278	.19	50	5.04	1	17
Nd II	5614.30	87	1.04			1.79	353	.27	101	4.95	0	17
Ni I	5614.78	250	4.15	5.15		3.85	252	.23	68	4.93	1	17
Fe I	5618.65	1107	4.21	5.13	4.85	3.54	278	.30	91	4.79	1	17
Fe I	5619.60	1161	4.39	5.29	4.94	3.26	341	.28	101	4.79	1	17
Fe I	5624.55	686	3.42	4.60		3.57	353	.57	226	4.41	2	17
Ni I	5625.33	221	4.09	5.18	4.91	3.66	285	.26	76	4.87	2	0
Fe I	5633.97	1314	4.99	4.92	4.81	4.61	353	.39	147	4.61	1	17
Fe I	5635.85	1088	4.26	5.27	4.92	3.34	271	.19	52	5.03	1	0
Fe I	5636.71	868	3.64	5.52	5.03	2.56	264	.15	40	5.15	1	0
Fe I	5638.27	1087	4.22	4.88		3.77	325	.44	153	4.57	3	17
Sc II	5640.97	29	1.50	5.16	4.74	2.58	312	.45	155	4.56	2	17
Fe I	5641.46	1087	4.26	4.95	4.72	3.62	321	.35	117	4.69	2	17
Ni I	5641.88	234	4.10	5.37	5.05	3.39	262	.17	48	5.08	2	19
Si I	5645.61	10	4.93	5.21		2.10	280	.24	74	4.90	2	19
Co I	5647.23	112	2.28	5.71	5.06	2.69	265	.12	31	5.26	3	19
Ti I	5648.57	269	2.49	5.75	5.23	3.92	204	.11	25	5.30	2	19
Fe I	5650.01	1314	5.10	5.23	4.97	4.34	274	.20	56	5.01	2	0
Fe I	5650.71	1314	5.08	5.22	4.93	4.14	294	.23	72	4.91	4	19
Fe I	5651.47	1161	4.47	5.55	5.08		262	.14	37	5.19	1	0
Fe I	5652.32	1108	4.26	5.37	4.98	3.30	305	.17	55	5.05	2	17
Fe I	5653.89	1159	4.39	5.20	4.91	3.39	305	.21	69	4.95	2	19
Sc II	5657.87	29	1.51	4.95	4.72	3.08	306	.55	193	4.46	4	17
Fe I	5662.52	1087	4.18	4.79		4.15	297	.47	152	4.55	2	18
Cr I	5664.04	203	3.43	5.21	4.90	3.61	273	.19	51	5.04	3	18
Si I	5665.55	10	4.92	5.15	4.88	2.18	364	.24	89	4.85	3	20
Si I	5666.68		5.61	5.41			245	.16	42	5.13	2	18
Sc II	5667.16	29	1.50	5.36	4.86	2.40	297	.40	125	4.64	2	18
Sc I	5671.81	12	1.45	5.61	5.04	4.11	261	.13	34	5.22	2	0
Si I	5675.73		5.62	5.67			253	.18	49	5.06	1	21
Fe I	5679.02	1183	4.65	4.99	4.83	4.14	283	.31	90	4.79	3	21
Ni I	5682.20	232	4.10	5.04	4.85	3.95	328	.26	93	4.83	1	21
Na I	5682.63	6	2.10	4.74	4.53	3.08	303	.49	167	4.52	1	21

Table A

Spect	Wave-length	Mult	*EP*	−Log ($W_{\odot}/\lambda$)	−Log (W_{ϵ}/λ)	Log ($gf\lambda$)	*HW*	R_c	*W*	−Log ($W_{\bigcirc}/\lambda$)	*Q*	*N*
Ce II	5683.76		1.42			2.50	252	.15	36	5.17	1	21
Sc II	5684.19	29	1.51	5.19	4.85	2.67	327	.46	160	4.55	2	0
Si I	5684.48	11	4.95	4.96	4.82	2.53	310	.37	120	4.68	2	0
Fe I	5686.54	1182	4.55	4.90		4.19	353	.39	151	4.61	1	21
Sc I	5686.84	12	1.44	5.68		4.01	260	.12	31	5.26	2	0
Na I	5688.19	6	2.10	4.67	4.48	3.33	346	.55	204	4.44	2	0
Nd II	5688.52	79	.99			2.50	318	.41	137	4.62	1	0
Ti I	5689.47	249	2.30	5.71	5.18	3.83	240	.13	31	5.22	1	21
Si I	5690.42	10	4.93	5.03	4.87	2.32	366	.26	92	4.83	4	21
Fe I	5691.51	1087	4.30	5.18		3.44	278	.28	76	4.85	4	21
Ni I	5694.99	220	4.09	5.14		3.80	278	.27	87	4.83	2	21
S I	5696.63	11	7.86	6.21			246	.05	12	5.67	1	0
Fe I	5698.05	867	3.64	5.61	5.14		262	.13	34	5.22	2	0
V I	5698.53	35	1.06	5.22		3.64	434	.31	133	4.70	2	21
Sc I	5700.23	12	1.43	5.58		3.94	303	.25	78	4.88	3	21
Cu I	5700.28	2	1.64	5.58		1.42	303	.25	78	4.88	3	21
Si I	5701.10	10	4.93	5.15	4.82	2.16	303	.24	75	4.90	1	21
Fe I	5701.55	209	2.56	4.82		2.36	310	.48	178	4.52	2	21
Nd II	5702.24		.74			2.03	315	.34	115	4.71	2	21
V I	5703.56	35	1.05	5.34	4.82	3.51	279	.21	59	4.98	2	0
Fe I	5705.48	1087	4.30	5.19	4.92	3.45	273	.21	58	4.99	2	21
Fe I	5707.05	868	3.64	5.12		2.64	341	.24	90	4.85	1	21
Mg I	5711.07	8	4.34	4.73	4.64	2.21	328	.46	162	4.55	3	21
Fe I	5715.11	1061	4.19	4.89	4.77	3.48	353	.40	155	4.60	5	21
Fe I	5717.85	1107	4.28	4.96	4.76	3.75	313	.38	125	4.66	3	0
Fe I	5720.89	1178	4.55	5.61	5.19		303	.15	47	5.12	3	21
V I	5727.02	35	1.08	5.19	4.71	3.50	302	.32	100	4.76	2	0
Y II	5728.91	34	1.84	6.10		2.34	303	.42	141	4.61	4	21
Fe I	5731.77	1087	4.26	4.99		3.66	320	.35	120	4.69	3	21
Gd II	5733.86	94	1.37	7.06		2.83	258	.10	26	5.35	3	0
V I	5737.07	35	1.06	5.72	5.03	2.91	256	.09	23	5.40	1	0
Ti I	5739.46	228	2.25	5.95	5.28	3.73	252	.07	17	5.52	1	0
Nd II	5740.90		1.16			2.19	292	.27	81	4.85	2	0
Nd II	5744.77		1.35			2.17	277	.21	62	4.97	1	21
Ni I	5748.34	45	1.68	5.34	4.86	1.02	291	.26	78	4.87	1	0
Fe I	5752.04	1180	4.55	5.01	4.84	3.91	340	.29	102	4.78	3	21
Fe I	5753.14	1107	4.26	4.87	4.73	3.99	290	.43	129	4.62	1	21
Nd II	5753.53		.20			.82	328	.33	108	4.93	0	21
Si I	5753.62		5.61	5.07			328	.33	108	4.83	0	21
Ni I	5754.68	68	1.93	4.90	4.67	2.12	302	.46	151	4.57	2	21
Ni I	5760.85	231	4.10	5.31	4.92	3.72	282	.22	69	4.94	1	21
Nd II	5761.70		1.04			1.72	323	.19	65	4.99	1	21
Fe I	5762.99	1107	4.21	4.76		4.16	323	.51	187	4.49	3	21
Ti I	5766.33	309	3.29	5.83	5.36	4.56	257	.09	23	5.40	1	0
Ce II	5768.90	32	1.32	6.76		2.82	403	.43	183	4.80	0	21
La II	5769.06	70	1.26	6.36		2.41	403	.43	183	4.74	0	21
Nd II	5769.87		1.35			2.08	252	.14	35	5.19	1	21
Nd II	5770.50		1.08			1.91	302	.22	72	4.93	2	21
Si I	5772.14	17	5.08	5.09		2.40	348	.31	106	4.75	2	21
Fe I	5775.09	1087	4.22	5.08	4.83	3.60	277	.34	101	4.74	3	21

Table A

Spect	Wave-length	Mult	EP	$-\text{Log}$ $(W_{\odot}/\lambda)$	$-\text{Log}$ (W_{ϵ}/λ)	Log $(gf\lambda)$	HW	R_c	W	$-\text{Log}$ $(W_{\bigcirc}/\lambda)$	Q	N
Ba I	5777.62	9	1.68			4.48	248	.04	10	5.78	1	0
Fe I	5778.47	209	2.59	5.56	4.98		247	.19	48	5.06	2	21
Cu I	5782.13	2	1.64	4.97	4.56	1.98	335	.47	167	4.54	3	0
Cr I	5783.11	188	3.32	5.38	4.96	3.72	302	.18	53	5.05	2	21
Cr I	5787.99	188	3.32	5.21	4.84	3.88	282	.27	81	4.85	3	21
Cr I	5790.99	188	3.32	4.89		4.36	302	.45	155	4.57	3	21
Si I	5793.07	9	4.93	5.18	4.91	2.20	325	.27	92	4.82	3	21
Fe I	5793.93	1086	4.22	5.32	4.92	3.11	272	.20	64	4.98	3	21
Nd II	5804.02	79	.74			2.13	330	.38	134	4.65	3	22
Fe I	5804.46	1087	4.28	5.51			252	.14	41	5.19	1	22
Ni I	5805.23	234	4.17	5.18	4.90	3.75	290	.21	64	4.97	3	22
La II	5805.78	4	.13		5.10	1.30	290	.41	128	4.64	3	22
Fe I	5806.73	1180	4.61	5.06		3.91	303	.28	93	4.81	3	22
La II	5808.31	4	.00	7.07		.70	265	.27	80	4.86	2	22
Fe I	5809.25	982	3.88	5.07	4.77	2.96	290	.31	97	4.78	4	22
Nd II	5811.61		.86			1.94	278	.24	77	4.89	2	22
Fe I	5814.80	1086	4.28	5.44	5.02	3.13	290	.17	52	5.07	1	22
Gd II	5815.85	112	1.58	6.76		2.69	254	.06	15	5.59	2	0
Fe I	5816.36	1179	4.55	4.84	4.65	4.03	315	.38	131	4.65	3	22
Nd II	5825.87		1.08			2.11	302	.25	83	4.87	2	22
Sm II	5836.37		1.00			1.72	252	.05	12	5.67	1	0
Nd II	5842.38	86	1.28	6.59		2.36	315	.21	73	4.94	2	22
Ni I	5847.01	44	1.68	5.49	4.89	.80	297	.20	62	4.99	1	22
Fe I	5848.09	552	3.26	5.19	4.90		251	.18	48	5.07	2	22
Fe I	5852.19	1178	4.55	5.21	4.91	3.63	310	.18	58	5.03	4	22
Ba II	5853.68	2	.60	5.03	4.68	2.77	449	.71	351	4.22	5	23
Fe I	5855.13	1179	4.61	5.51	5.09	3.61	277	.13	40	5.22	4	22
Fe I	5856.08	1128	4.29	5.31	4.92	3.38	282	.19	54	5.03	1	0
Ca I	5857.45	47	2.93	4.65	4.54	4.00	366	.56	237	4.41	3	23
Fe I	5859.61	1181	4.55	4.90	4.73	4.11	350	.37	145	4.64	4	22
Fe I	5862.36	1180	4.55	4.83	4.68	4.25	272	.38	111	4.69	5	23
La II	5880.63	35	.23	6.59		1.02	308	.31	99	4.77	2	0
Fe I	5883.81	982	3.96	4.79		3.36	331	.34	125	4.70	3	1
Na I	5889.95	1	.00	3.89	3.71	3.89	685	.82	649	3.96	4	1
Ni I	5892.88	68	1.99	4.95		1.98	401	.43	191	4.63	0	1
Na I	5895.92	1	.00	4.02	3.88	3.59	590	.77	507	4.07	4	1
Gd II	5904.07	112	1.62			2.72	255	.05	12	5.67	2	0
Fe I	5905.67	1181	4.65	5.01	4.79	4.03	331	.28	93	4.82	3	1
Fe I	5909.99	552	3.21	5.29	4.83		378	.29	110	4.77	3	1
Fe I	5916.25	170	2.45	5.07	4.71	1.67	312	.32	104	4.76	3	0
Fe I	5927.80	1175	4.65	5.18	4.90	3.77	287	.20	58	5.01	1	0
Fe I	5929.70	1176	4.55	5.19	4.89	3.52	288	.20	58	5.01	1	0
Fe I	5930.19	1180	4.65	4.84	4.65	4.46	329	.40	139	4.63	3	0
Fe I	5934.66	982	3.93	4.88	4.68	3.40	330	.40	151	4.61	3	1
La II	5936.22	19	.17	7.07	5.77	.86	296	.24	73	4.91	2	0
Si I	5948.55	16	5.08	4.83	4.70	2.88	354	.38	137	4.65	4	1
Gd II	5951.60	95	1.37			2.47	257	.05	13	5.67	2	0
Fe I	5952.75	959	3.98	4.94	4.76	3.22	305	.28	88	4.83	1	0
Ti I	5953.16	154	1.89	5.24	4.79	3.90	291	.21	62	4.98	1	0
Fe I	5956.70	14	.86	5.00	4.70		307	.38	113	4.69	2	1

398-978 O - 71 - 10

Table A

Spect	Wave-length	Mult	EP	$-\mathrm{Log}$ $(W_{\odot}/\lambda)$	$-\mathrm{Log}$ (W_{ϵ}/λ)	Log $(gf\lambda)$	HW	R_c	W	$-\mathrm{Log}$ $(W_{\bigcirc}/\lambda)$	Q	N
Ce II	5959.69		1.63			2.75	283	.16	42	5.14	1	1
Ti I	5965.83	154	1.88	5.41	4.82	3.73	377	.20	76	4.95	1	1
Ba I	5971.70	7	1.14			3.67	258	.05	13	5.67	1	0
Fe I	5975.35	1260	4.83	5.13	4.82	4.13	330	.27	88	4.84	3	2
Ce II	5975.87	30	1.33	6.78		2.81	330	.20	58	5.01	2	1
Fe I	5976.80	959	3.94	4.97	4.75	3.25	306	.34	113	4.72	2	1
Ti I	5978.54	154	1.87	5.48	4.93	3.86	306	.18	55	5.05	1	2
Fe I	5983.70	1175	4.55	4.94	4.75	3.96	318	.35	121	4.70	3	1
Fe I	5984.80	1260	4.73	4.85	4.70	4.33	283	.41	140	4.62	3	2
Fe I	5987.06	1260	4.79	4.94	4.75	4.16	330	.30	108	4.77	4	2
Fe II	5991.38	46	3.15	5.32	4.93	.82	330	.30	106	4.77	1	2
Ce II	5995.35		1.49			2.81	306	.15	48	5.12	1	2
Ni I	5996.74	249	4.23	5.50	5.12	3.24	274	.12	33	5.26	1	0
Fe I	5997.81	1175	4.61	4.95		3.59	303	.26	81	4.87	1	0
Fe I	6003.03	959	3.88	4.84	4.68	3.37	283	.42	130	4.63	3	2
Gd II	6004.57	112	1.66			2.75	258	.04	10	5.78	1	0
Fe I	6005.53	207	2.59	5.46		1.07	330	.17	53	5.07	2	2
Ni I	6007.31	42	1.68	5.48	4.92	.85	306	.18	47	5.08	3	2
Fe I	6007.96	1178	4.65	5.01	4.81	3.92	330	.32	109	4.75	2	2
Fe I	6008.58	982	3.88	4.83	4.67	3.42	306	.41	132	4.64	2	2
Nd II	6009.30		.38			.71	283	.09	21	5.40	1	2
Mn I	6013.50	27	3.07	4.84	4.61	3.63	330	.40	157	4.61	4	2
C I	6014.84		8.64	6.13			269	.09	24	5.40	1	0
Fe I	6015.25	63	2.22	6.18	5.33		266	.08	21	5.46	1	0
Mn I	6016.64	27	3.07	4.82	4.61	3.78	330	.42	151	4.60	3	2
Fe I	6019.36	780	3.57	6.08	5.32		260	.05	13	5.67	1	0
Ba I	6019.47	7	1.12			3.68	260	.05	13	5.67	2	0
Fe I	6020.17	1178	4.61	4.81	4.52	4.26	377	.48	204	4.50	4	2
Mn I	6021.80	27	3.07	4.80	4.61	3.93	306	.43	132	4.62	4	2
Fe I	6024.07	1178	4.55	4.71	4.60	4.50	283	.47	166	4.55	4	2
Pr II	6025.72		1.44			2.96	259	.11	30	5.30	2	2
Fe I	6027.06	1018	4.07	4.99	4.72	3.49	306	.35	119	4.71	4	2
Mo I	6030.66	5	1.53	6.60		3.07	271	.10	27	5.35	2	0
Ce II	6034.20	30	1.46	6.78		2.58	353	.25	85	5.00	0	2
Nd II	6034.24		1.54	6.78		2.35	353	.25	85	5.00	0	2
V I	6039.69	34	1.06	5.74	5.03	3.19	306	.11	35	5.30	1	2
Ce II	6043.39	30	1.21	6.48	5.58	2.87	306	.28	88	4.83	4	2
S I	6046.04	10	7.87	5.58	5.15		276	.12	33	5.26	1	0
S I	6052.66	10	7.87	5.74	5.44	2.71	287	.17	49	5.09	2	0
Fe I	6055.99	1259	4.73	4.92	4.73	4.16	353	.35	129	4.69	2	2
Fe I	6062.89	63	2.18	5.53	4.85	.58	286	.16	46	5.12	2	0
Ti I	6064.63	69	1.05	5.94	5.11	2.62	271	.09	24	5.40	1	0
Fe I	6065.49	207	2.61	4.72	4.53	2.75	377	.57	221	4.43	4	2
La II	6067.14	48	.77			.84	236	.10	21	5.35	1	2
Fe I	6078.50	1259	4.79	4.82	4.73	4.20	283	.37	122	4.69	2	2
Fe I	6079.02	1176	4.65	5.04	4.89	3.60	330	.23	80	4.91	2	2
Gd II	6080.65	112	1.73			2.82	265	.06	16	5.59	1	0
V I	6081.42	34	1.05	5.61	4.97	3.20	286	.16	46	5.12	2	0
Fe I	6082.72	64	2.22	5.25	4.82	.86	306	.24	74	4.91	2	2
Fe II	6084.11	46	3.20	5.44	5.13	.42	306	.28	85	4.84	2	2

Table A

Spect	Wave-length	Mult	EP	$-\text{Log}$ $(W_{\odot}/\lambda)$	$-\text{Log}$ (W_{ϵ}/λ)	Log $(gf\lambda)$	HW	R_c	W	$-\text{Log}$ $(W_{\odot}/\lambda)$	Q	N
Ti I	6085.26	69	1.05	5.18		2.67	306	.25	81	4.88	3	2
Ni I	6086.29	249	4.26	5.15	4.90	3.68	353	.23	72	4.93	2	2
Fe I	6089.57	1327	5.02	5.28	4.91	4.05	377	.20	75	4.96	1	2
V I	6090.18	34	1.08	5.32	4.84	3.65	330	.21	61	4.99	1	2
Fe I	6093.66	1177	4.61	5.29	4.97	3.36	330	.13	40	5.22	1	2
Fe I	6094.42	1177	4.65	5.48	5.09		259	.13	35	5.22	1	2
Fe I	6096.69	959	3.98	5.23	4.89	2.84	353	.19	60	5.02	1	2
Ce II	6098.34		1.77			3.04	377	.23	77	4.92	1	2
Fe I	6102.18	1259	4.83	4.86	4.73	4.25	330	.35	113	4.72	2	3
Ca I	6102.72	3	1.88	4.66	4.52	2.90	330	.55	199	4.47	2	3
Fe I	6103.19	1260	4.83	4.84		3.98	388	.34	127	4.70	2	3
Zr II	6106.47	106	1.76	6.24			353	.25	88	4.87	3	3
Ni I	6108.12	45	1.68	5.01	4.69	1.49	330	.38	132	4.66	1	3
Ba I	6110.78	7	1.19			4.23	275	.10	27	5.35	1	0
Ni I	6111.06	230	4.09	5.23	4.95	3.30	288	.16	46	5.12	1	0
V I	6111.62	34	1.04	5.71	5.05	2.96	271	.08	21	5.46	2	0
Fe II	6113.33	46	3.22	5.56	5.17		296	.20	60	5.01	2	0
Zr II	6114.78	93	1.66	6.61	5.67		306	.27	83	4.86	1	3
Ni I	6116.18	218	4.09	4.97		3.73	353	.29	104	4.79	2	3
Co I	6117.00		1.78	5.88	5.32	1.87	269	.07	19	5.52	1	0
V I	6119.51	34	1.06	5.49	4.88	3.31	306	.18	56	5.05	2	3
Ca I	6122.22	3	1.89	4.44	4.40	3.38	377	.63	286	4.33	4	3
Si I	6125.02	30	5.61	5.23	5.09		259	.19	52	5.05	3	3
La II	6126.09	69	1.25			2.09	306	.23	69	5.02	0	3
Ti I	6126.22	69	1.07	5.49	4.90	2.68	306	.23	69	5.02	0	3
Zr I	6127.49	2	.15	6.24	5.41	2.39	259	.15	37	5.18	2	3
Fe I	6127.91	1017	4.14	5.11		3.19	330	.27	84	4.86	2	3
Ni I	6128.98	42	1.68	5.47	4.88	.76	306	.19	58	5.03	1	3
La II	6129.56	47	.77			1.62	330	.26	91	4.85	1	3
Si I	6131.57	30	5.61	5.37	5.15		292	.18	52	5.07	2	0
Zr I	6134.58	2	.00	6.24	5.53	1.90	235	.15	35	5.20	1	3
V I	6135.36	34	1.05	5.71	5.07	2.97	280	.12	34	5.26	2	0
Fe I	6136.62	169	2.45	4.65	4.48	2.85	381	.59	243	4.40	3	0
Fe I	6137.00	62	2.20	4.98	4.68	1.41	343	.41	148	4.62	2	0
Fe I	6137.70	207	2.59	4.68	4.44	2.84	377	.59	236	4.41	3	3
Ba II	6141.72	2	.70	4.74	4.50	3.71	683	.78	695	3.95	4	3
Si I	6142.49	30	5.62	5.26	5.06		296	.19	57	5.03	1	0
Zr I	6143.23	2	.07	6.39	5.41	2.11	298	.20	60	5.01	2	0
Ce II	6143.36		1.70			2.87	294	.18	53	5.06	1	0
Si I	6145.02	29	5.61	5.21	5.06		302	.22	67	4.96	2	0
Fe II	6149.24	74	3.89	5.24	4.95		377	.35	139	4.68	3	3
Fe I	6151.62	62	2.18	5.18	4.78	1.08	283	.33	111	4.74	3	3
Na I	6154.23	5	2.10	5.36	4.78	2.23	330	.24	100	4.85	1	3
Si I	6155.13	29	5.62	4.93	4.72		330	.33	105	4.75	3	3
Fe I	6157.73	1015	4.07	5.11		3.34	353	.44	187	4.75	0	3
Na I	6160.75	5	2.10	5.15	4.74	2.53	377	.30	117	4.76	1	3
Ca I	6161.29	20	2.52	5.07	4.73	2.77	353	.37	148	4.65	1	3
Ca I	6162.17	3	1.90	4.44	4.34	3.57	424	.66	289	4.33	3	3
Fe I	6165.37	1018	4.14	5.27		3.16	283	.24	72	4.92	1	3
Pr II	6165.95	39	.92	6.49	5.49	2.71	283	.17	54	5.07	1	3

Table A

Spect	Wave-length	Mult	*EP*	−Log $(W_\odot/\lambda)$	−Log (W_ϵ/λ)	Log $(gf\lambda)$	*HW*	R_c	*W*	−Log $(W_\odot/\lambda)$	*Q*	*N*
Ca I	6166.44	20	2.52	5.06	4.73	2.89	400	.33	126	4.71	2	3
Ca I	6169.06	20	2.52	4.86	4.62	3.24	306	.42	141	4.62	1	3
Ca I	6169.56	20	2.52	4.80	4.62	3.52	330	.49	191	4.51	1	3
Fe I	6170.52	1260	4.79	4.97		4.15	306	.39	137	4.65	2	3
La II	6172.72	4	.13	6.61		.60	330	.18	58	5.04	2	3
Fe I	6173.34	62	2.22	5.09	4.65	1.39	330	.41	152	4.61	2	3
Ni I	6175.42	217	4.09	5.23	4.86	3.72	353	.26	91	4.85	3	3
Ni I	6176.82	228	4.09	5.09	4.80	3.96	306	.30	97	4.80	4	3
Ni I	6177.26	58	1.83	5.79	4.95	.51	280	.11	31	5.30	1	0
Fe I	6180.22	269	2.73	5.19	4.77	1.71	306	.34	116	4.72	4	3
Ni I	6186.74	229	4.10	5.45	4.99	3.35	259	.17	40	5.14	2	4
Fe I	6188.00	959	3.94	5.24	4.80		282	.28	91	4.83	4	4
Co I	6189.01	37	1.71	6.01	5.06	1.94	279	.10	28	5.35	2	0
V I	6199.20	19	.29	5.89		2.42	281	.11	31	5.30	2	0
Fe I	6200.32	207	2.61	5.05	4.63	1.83	329	.41	144	4.63	4	4
Ni I	6204.64	226	4.09	5.59		3.21	294	.12	41	5.26	3	4
Sc I	6210.68	2	.00	6.49	5.29	2.22	273	.07	19	5.52	2	0
Fe I	6213.44	62	2.22	5.01	4.67	1.64	329	.49	173	4.53	4	5
V I	6213.87	20	.30	6.32	5.12	1.88	275	.08	22	5.46	1	0
Fe I	6215.15	1018	4.19	5.19		3.27	306	.33	120	4.73	2	5
V I	6216.37	19	.28	5.32	4.79	2.40	329	.20	66	4.99	2	5
Fe I	6219.29	62	2.20	4.88	4.58	1.75	329	.50	175	4.53	5	5
Fe I	6220.78	958	3.88	5.56	5.05	2.34	289	.14	40	5.19	2	0
Ni I	6223.99	228	4.10	5.41		3.29	306	.16	49	5.11	2	5
Fe I	6226.77	981	3.88	5.41	4.95	2.58	282	.16	45	5.13	2	5
Fe I	6229.23	342	2.84	5.28	4.80	1.68	353	.28	89	4.84	4	5
Fe I	6230.73	207	2.56	4.62		2.86	423	.62	285	4.34	5	5
Fe I	6232.66	816	3.65	4.91		3.07	400	.45	183	4.55	4	5
Si I	6237.32	28	5.61	5.02	4.83		353	.29	108	4.79	3	5
Fe II	6238.38	74	3.89	5.18	4.90	2.13	353	.41	155	4.61	5	5
Sc I	6239.41	2	.00	6.02	5.45	1.37	285	.12	34	5.26	2	0
Fe II	6239.95	74	3.89	5.80	5.28		296	.17	51	5.09	1	0
Fe I	6240.66	64	2.22	5.19	4.80	1.12	331	.33	114	4.74	3	0
V I	6243.11	19	.30	5.42	4.76	2.62	307	.22	69	4.96	1	0
Si I	6243.81	28	5.61	5.16	4.98		318	.27	88	4.85	2	0
Si I	6244.47	27	5.61	5.14	5.02		316	.26	85	4.87	2	0
Sc II	6245.63	28	1.51	5.32	4.87	2.74	329	.39	130	4.66	3	5
Fe I	6246.33	816	3.60	4.75	4.57	3.49	329	.49	183	4.52	3	5
Fe II	6247.56	74	3.89	5.11	4.87	2.08	376	.42	170	4.58	4	5
V I	6251.83	19	.29	5.75		2.21	288	.13	37	5.22	1	0
Fe I	6252.56	169	2.40	4.76		2.51	353	.57	212	4.45	5	5
Fe I	6254.26	111	2.28	4.74		1.82	376	.52	214	4.47	3	5
Fe I	6256.37	169	2.45	4.89		1.77	353	.51	208	4.48	3	5
V I	6256.91	19	.28	6.32		1.68	273	.06	16	5.59	2	0
Ti I	6258.11	104	1.44	5.17		3.56	282	.29	93	4.82	1	5
Ti I	6258.71	104	1.46	5.16		3.58	306	.40	144	4.63	1	5
Ti I	6261.10	104	1.43	5.19		3.44	329	.29	98	4.81	3	5
Fe I	6265.14	62	2.18	4.94		1.80	353	.50	180	4.52	5	5
Sm II	6267.28		1.17			2.23	273	.06	16	5.59	1	0
Fe I	6270.24	342	2.86	5.13	4.74	1.89	306	.36	127	4.69	2	5

Table A

Spect	Wave-length	Mult	EP	$-\text{Log}$ $(W_{\odot}/\lambda)$	$-\text{Log}$ (W_{ϵ}/λ)	Log $(gf\lambda)$	HW	R_c	W	$-\text{Log}$ $(W_{\circ}/\lambda)$	Q	N
V I	6274.67	19	.27	6.02	5.10	1.97	291	.14	41	5.19	2	0
Sc II	6279.76	28	1.50	5.44	4.98	2.29	335	.34	119	4.72	3	0
Fe I	6280.62	13	.86	5.08			306	.48	161	4.56	5	5
V I	6285.18	19	.28	5.95	5.07	2.04	276	.07	19	5.52	2	0
Fe I	6290.97	1258	4.73	4.98	4.76	3.91	306	.31	96	4.79	2	5
Sm II	6291.82		1.41			2.18	274	.06	16	5.59	1	0
V I	6292.86	19	.29	5.84	4.99	2.05	299	.17	51	5.09	2	0
Fe I	6293.92	1260	4.83	5.72	5.22		288	.12	34	5.26	1	0
Fe I	6297.80	62	2.22	4.99	4.69	1.49	329	.45	151	4.59	4	5
O I	6300.31	1	.00	6.16			288	.12	34	5.26	1	0
Fe I	6301.52	816	3.65	4.70	4.63	3.58	305	.50	182	4.52	4	5
Gd II	6305.15	94	1.31			2.55	286	.11	31	5.30	2	0
Sc I	6305.67	2	.02	6.26		2.31	286	.11	31	5.30	1	0
Sm II	6307.06		1.06			1.68	273	.05	13	5.67	1	0
Sc II	6309.90	28	1.50	5.46		2.06	310	.22	70	4.96	2	0
Fe I	6311.51	342	2.83	5.44	4.93	1.56	295	.15	44	5.15	2	0
Zr I	6313.05	65	1.58	6.80		3.43	283	.09	27	5.38	2	0
Ni I	6314.67	67	1.93	4.97		1.93	329	.41	140	4.64	5	5
Fe I	6315.32	1015	4.14	5.08	4.68	3.33	305	.39	129	4.67	3	5
Fe I	6315.81	1014	4.07	5.28	4.89	3.05	306	.20	62	5.01	1	0
Mg I	6318.72	23	5.11	5.23			304	.19	59	5.03	2	0
Mg I	6319.22	23	5.11	5.55			293	.14	41	5.19	2	0
La II	6320.39	19	.17	6.20	5.32	1.32	360	.44	168	4.58	3	0
Sc II	6320.85	28	1.50	6.02	5.22	1.84	304	.19	59	5.03	2	0
Ni I	6322.17	249	4.15	5.52	5.11	3.16	287	.11	31	5.30	2	0
Fe I	6322.69	207	2.59	4.93	4.74	1.87	305	.41	140	4.64	4	5
Ni I	6327.60	44	1.68	5.24	4.78	1.00	318	.25	81	4.89	1	0
Cr I	6330.10	6	.94	5.40	4.89	1.28	305	.21	61	5.00	2	5
Fe I	6330.86	1254	4.73	5.30	4.96	3.49	282	.19	51	5.06	2	5
Fe I	6335.34	62	2.20	4.79	4.57	1.94	305	.52	173	4.52	5	5
Fe I	6336.83	816	3.69	4.72	4.60	3.52	329	.46	171	4.56	5	5
Fe I	6344.15	169	2.43	5.05	4.73	1.48	376	.42	182	4.80	0	5
Si II	6347.10	2	8.12	5.07		4.03	322	.27	88	4.86	2	0
Fe I	6355.04	342	2.84	5.01	4.60	2.04	329	.40	147	4.63	2	5
Fe I	6358.69	13	.86	4.89	4.59		329	.45	158	4.58	2	5
Ni I	6360.80	229	4.17	5.60	5.10	3.22	297	.15	45	5.15	2	0
Zn I	6362.35	6	5.79	5.44	5.06	4.24	311	.21	66	4.98	1	0
O I	6363.79	1	.02	6.63			282	.08	22	5.46	3	0
Fe I	6364.38	1253	4.79	5.41	4.97	3.49	352	.18	61	5.04	1	6
Nd II	6365.55		.93			1.34	235	.14	29	5.19	2	6
Ni I	6366.48	230	4.17	5.39	4.95	3.43	423	.15	60	5.08	1	6
Fe II	6369.46	40	2.89	5.55			258	.25	75	4.91	1	6
Si II	6371.36	2	8.12	5.39		3.73	307	.19	59	5.03	2	0
Ni I	6378.26	247	4.15	5.37	4.99	3.60	300	.16	48	5.12	1	0
Fe I	6380.75	1015	4.19	5.20	4.81	3.41	305	.27	93	4.84	4	6
Nd II	6382.07		1.44			1.93	305	.13	41	5.22	2	6
Nd II	6385.20	85	1.16			2.10	329	.18	61	5.04	1	6
Fe I	6385.74	1253	4.73	5.90	5.34		281	.07	19	5.52	1	0
La II	6390.48	33	.32	6.50	5.44	1.50	329	.40	157	4.62	2	6
Fe I	6392.53	109	2.28	5.81	5.03	.68	292	.12	35	5.26	1	0

Table A

Spect	Wave-length	Mult	EP	$-\text{Log}$ $(W_{\odot}/\lambda)$	$-\text{Log}$ (W_{ϵ}/λ)	Log $(gf\lambda)$	HW	R_c	W	$-\text{Log}$ $(W_{\bigcirc}/\lambda)$	Q	N
Fe I	6393.61	168	2.43	4.74	4.52	2.71	376	.58	230	4.43	3	6
La II	6399.05	104	2.64			3.28	376	.11	38	5.30	2	6
Si I	6407.27		5.87	5.39			399	.19	68	5.00	1	6
Fe I	6408.03	816	3.69	4.90	4.63	3.41	376	.45	178	4.56	1	6
Sr I	6408.47	8	2.27	6.33	5.33	4.21	311	.20	63	5.01	2	0
Fe I	6411.66	816	3.65	4.70	4.57	3.80	329	.53	191	4.50	4	6
Ni I	6414.60	244	4.15	5.63	5.19	3.46	291	.11	32	5.30	1	0
Si I	6414.97		5.87	5.15			309	.19	59	5.03	2	0
Fe II	6416.91	74	3.89	5.13	4.97	1.64	329	.32	111	4.76	3	6
Ca I	6417.69		4.44	5.85			287	.09	25	5.40	1	0
Co I	6417.82	111	2.33		5.41	2.40	284	.08	22	5.46	1	0
Fe I	6419.98	1258	4.73	4.90	4.73	4.36	305	.38	140	4.66	1	6
Fe I	6421.36	111	2.28	4.87	4.50	2.27	352	.57	207	4.46	5	6
Sm II	6426.63		1.75			2.43	280	.06	16	5.59	1	0
Nd II	6428.67		.20	7.11		.61	305	.20	69	4.99	2	6
Co I	6429.91	81	2.14	6.41	5.55	1.99	280	.06	16	5.59	2	0
Fe I	6430.85	62	2.18	4.78	4.54	2.24	375	.57	230	4.43	5	6
Fe II	6432.65	40	2.89	5.23	4.98	.76	329	.38	134	4.67	4	6
Y I	6435.02	2	.07	6.63	5.60	2.22	305	.18	54	5.07	2	6
Eu II	6437.64	8	1.32	6.03		2.72	292	.11	32	5.30	2	0
Ca I	6439.07	18	2.52	4.62		4.28	352	.62	236	4.44	5	6
Fe II	6446.43	199	6.22	6.11	5.81		279	.05	14	5.67	1	0
Ca I	6449.81	19	2.52	4.82	4.65	3.26	374	.47	187	4.54	3	0
V I	6452.32	48	1.19	6.03	5.33	2.50	281	.06	17	5.59	1	0
Co I	6455.00	174	3.63	5.77	5.23	4.09	305	.10	30	5.35	1	6
Ca I	6455.60	19	2.52	5.13	4.82	2.46	352	.27	93	4.85	3	6
Fe II	6456.38	74	3.90	5.05	4.85	2.34	375	.49	206	4.50	2	6
Fe I	6456.87	1256	4.79	5.58	5.40		302	.15	45	5.15	1	0
Ca I	6462.57	18	2.52	4.66		4.12	422	.65	305	4.50	0	6
Fe I	6462.75	168	2.45	4.97		1.81	422	.65	305	4.73	0	6
Ca I	6464.68	19	2.52	5.81	5.06		258	.14	36	5.19	3	6
Ce II	6466.90		1.77			2.63	235	.13	30	5.22	1	6
Fe I	6469.21	1258	4.83	5.09	4.80	3.99	305	.27	86	4.86	2	6
Ca I	6471.66	18	2.52	4.89	4.68	3.22	328	.45	167	4.58	3	6
Sm II	6472.34		1.38			2.07	280	.05	14	5.67	1	0
Fe I	6481.88	109	2.28	5.01	4.66	1.41	355	.38	142	4.66	2	0
Ni I	6482.81	66	1.93	5.23	4.78	1.69	258	.25	70	4.93	2	6
Sm II	6484.52		1.26			1.87	278	.04	11	5.78	1	0
Ti II	6491.58	91	2.06	5.16			305	.37	117	4.71	2	6
Ca I	6493.78	18	2.52	4.69	4.57	3.95	375	.53	214	4.47	5	7
Fe I	6494.97	168	2.40	4.60	4.42	2.95	375	.61	260	4.40	3	6
Fe I	6495.78	1253	4.83	5.19	4.96	3.83	316	.21	66	4.99	2	7
Ba II	6496.90	2	.60	4.82		3.43	656	.80	586	4.04	5	6
Fe I	6498.96	13	.96	5.18	4.75		363	.34	134	4.70	4	6
Ca I	6499.65	18	2.52	4.90		3.22	293	.42	139	4.64	5	6
Cr I	6501.21	16	.98	5.86			293	.10	29	5.35	1	0
Sr I	6504.00	8	2.26	6.64		4.07	300	.13	39	5.22	2	0
Ca I	6508.85	18	2.52	5.77		1.70	302	.14	42	5.19	2	0
Fe II	6516.06	40	2.89	5.03		1.07	352	.47	178	4.55	3	7
Fe I	6518.38	342	2.83	5.03	4.77	1.88	355	.37	138	4.68	3	0

Table A

Spect	Wave-length	Mult	*EP*	−Log ($W_\odot/\lambda$)	−Log (W_ϵ/λ)	Log ($gf\lambda$)	*HW*	R_c	*W*	−Log ($W_{\bigcirc}/\lambda$)	*Q*	*N*
Fe I	6533.94	1197	4.56	5.15		3.19	258	.19	50	5.07	1	7
Nd II	6539.94		.74			0.99	294	.10	28	5.36	2	0
Sm II	6542.76		1.46			2.22	288	.07	20	5.52	1	0
Fe I	6546.25	268	2.76	4.80	4.60	2.64	352	.53	216	4.47	2	7
Nd II	6549.54		.06			.37	258	.15	32	5.22	2	7
Nd II	6550.19		.32			0.63	234	.20	54	5.04	1	7
Sr I	6550.24	12	2.69	6.42	5.52	3.99	234	.20	54	5.04	1	7
Fe I	6551.70	13	.99	5.91			234	.08	19	5.46	1	7
Ti I	6554.23	102	1.44	5.67	5.00	2.77	351	.17	58	5.07	1	7
Ca I	6572.78	1	.00	5.40	4.76		281	.30	88	4.83	1	7
Fe I	6574.24	13	.99	5.48	4.78		281	.26	82	4.89	2	7
Fe I	6575.02	206	2.59	5.01		1.58	398	.40	175	4.60	3	7
Ni I	6586.33	64	1.95	5.27	4.81	1.57	281	.26	76	4.90	1	7
C I	6587.61	22	8.53	5.50		2.48	303	.13	39	5.22	2	0
Sm II	6589.72		1.27			2.38	287	.06	17	5.59	1	0
Nd II	6591.43		.20			0.39	295	.09	27	5.39	2	0
Fe I	6592.92	268	2.73	4.73	4.57	2.72	351	.50	202	4.51	2	7
Fe I	6593.88	168	2.43	4.87	4.64	1.79	375	.44	175	4.58	5	7
Ba I	6595.33	6	1.12			3.97	301	.12	36	5.26	1	0
Co I	6595.87	174	3.71	5.97	5.37	3.67	292	.08	23	5.46	1	0
Fe I	6597.57	1253	4.79	5.18		3.54	305	.20	66	5.00	1	7
Sc II	6604.60	19	1.36	5.26	4.90	2.28	351	.36	133	4.69	4	7
Fe I	6608.03	109	2.28	5.56	5.02	.49	304	.12	39	5.26	1	7
Fe I	6609.12	206	2.56	4.94	4.70	1.54	375	.35	133	4.70	2	7
Y II	6613.75	26	1.75	6.22		2.42	351	.39	146	4.65	4	7
Fe I	6627.56	1174	4.55	5.44	5.02	3.10	292	.16	47	5.13	3	7
Cr I	6630.02	16	1.03	6.04	5.16		187	.07	15	5.52	1	8
Co I	6632.44	111	2.28	6.12	5.20	2.60	291	.07	20	5.52	1	0
Fe I	6633.76	1197	4.56	4.98	4.82	3.69	343	.29	103	4.81	2	0
Ni I	6635.15	264	4.42	5.54	5.06	3.63	351	.13	40	5.22	2	8
Fe I	6639.71	1195	4.61	5.59		2.99	308	.14	43	5.19	1	0
Ni I	6643.64	43	1.68	4.90		1.96	328	.42	154	4.62	5	8
Eu II	6645.11	8	1.38	6.22		2.84	308	.14	43	5.19	2	0
Cr I	6661.08	282	4.19	5.82	5.41	4.23	293	.07	20	5.52	1	0
Fe I	6663.45	111	2.42	4.94	4.65	1.77	444	.43	192	4.56	2	8
Ba I	6675.27	6	1.14			3.67	291	.06	17	5.59	1	0
Fe I	6677.99	268	2.69	4.74		2.90	421	.51	211	4.50	4	8
Sm II	6693.55		1.69			2.57	294	.07	20	5.52	1	0
Ba I	6693.84	6	1.19			3.81	290	.05	14	5.67	1	0
Al I	6696.02	5	3.14	5.31	4.93	2.49	327	.18	59	5.06	1	8
Al I	6698.67	5	3.14	5.50	5.11	2.18	327	.16	51	5.12	1	8
Fe I	6699.14	1228	4.59	5.98	5.39		294	.07	20	5.52	1	0
Fe I	6703.57	268	2.76	5.32	4.87	1.30	280	.21	66	4.99	1	8
Fe I	6705.12	1197	4.61	5.20	4.90	3.39	304	.24	79	4.92	1	8
Li I	6707.84	1	.00	6.53		4.01	420	.07	29	5.36	1	8
Fe I	6710.32	34	1.48	5.75	4.96		350	.16	48	5.13	3	8

A.4. Table B, the Line List Arranged Alphabetically by Spectrum

With the following exceptions, the successive columns of table B are the same as described preceding table A.

Column 5: the value of the abscissa for the line on the differential curve of growth with respect to the sun

$$\log X'_{\odot} = \log X_{\odot} - \Delta\theta\chi$$
$$\Delta\theta = +0.10$$

Column 6: the value of the abscissa for the line on the differential curve with respect to ϵ Vir

$$\log X'_{\epsilon} = \log X_{\epsilon} - \Delta\theta\chi$$
$$\Delta\theta = -0.09$$

Column 7: the value of the abscissa for the line on the absolute curves of growth

$$\theta^{n} = 1.13$$
$$\theta^{i} = 1.07$$

The stellar line strengths $\log X_{\odot}$ and $\log X_{\epsilon}$ are discussed in section 4.2.

Table B

Spect	Wave-length	Mult	EP	$-$Log $X'_\odot$	$-$Log X'_ϵ	Log $(gf\lambda)$ $-\theta\chi$	HW	R_c	W	$-$Log (W/λ)	Q	N
Al I	6696.02	5	3.14	5.60	4.32	−1.06	327	.18	59	5.06	1	8
Al I	6698.67	5	3.14	5.83	4.64	−1.37	327	.16	51	5.12	1	8
Ba I	6019.47	7	1.12			2.41	260	.05	13	5.67	2	0
Ba I	6595.33	6	1.12			2.70	301	.12	36	5.26	1	0
Ba I	5971.70	7	1.14			2.38	258	.05	13	5.67	1	0
Ba I	6675.27	6	1.14			2.38	291	.06	17	5.59	1	0
Ba I	6110.78	7	1.19			2.89	275	.10	27	5.35	1	0
Ba I	6693.84	6	1.19			2.47	290	.05	14	5.67	1	0
Ba I	5777.62	9	1.68			2.58	248	.04	10	5.78	1	0
Ba II	4554.03	1	.00	2.84	1.12	3.83	843	.91	1068	3.63	3	29
Ba II	5853.68	2	.60	4.91	3.79	2.13	449	.71	351	4.22	5	23
Ba II	6496.90	2	.60	4.41		2.79	656	.80	586	4.04	5	6
Ba II	6141.72	2	.70	4.17	2.70	2.96	683	.78	695	3.95	4	3
Ba II	4524.93	3	2.51	5.31	3.46	.61	291	.65	206	4.34	2	0
C I	4770.03	6	7.48	6.23	4.86	−7.05	230	.19	44	5.03	2	0
C I	4817.37	5	7.48	6.49		−7.30	229	.17	39	5.09	2	0
C I	5380.34	11	7.68	6.07		−6.63	341	.25	88	4.84	1	10
C I	6587.61	22	8.53	6.37		−7.16	303	.13	39	5.22	2	0
C I	6014.84		8.64	7.01			269	.09	24	5.40	1	0
Ca I	6572.78	1	.00	5.40	4.15		281	.30	88	4.83	1	7
Ca I	4425.44	4	1.88	3.14		1.14	276	.67	204	4.34	4	28
Ca I	6102.72	3	1.88	4.01	2.70	.78	330	.55	199	4.47	2	3
Ca I	6122.22	3	1.89	2.94	1.66	1.24	377	.63	286	4.33	4	3
Ca I	4318.65	5	1.90	3.61		1.28	283	.67	225	4.28	2	27
Ca I	6162.17	3	1.90	2.94	1.29	1.42	424	.66	289	4.33	3	3
Ca I	4094.94	25	2.52	3.86		.07	246	.53	140	4.47	2	0
Ca I	4512.27	24	2.52	5.65	4.14		216	.18	39	5.06	1	0
Ca I	4578.55	23	2.52	4.54	3.21	.25	281	.45	122	4.57	1	30
Ca I	4585.87	23	2.52	3.47		.62	281	.59	199	4.38	3	30
Ca I	5260.39	22	2.52	5.49	4.39	−1.03	291	.18	52	5.03	2	9
Ca I	5261.71	22	2.52	4.32	3.06	.14	303	.50	155	4.52	4	9
Ca I	5581.97	21	2.52	4.51	3.24	.19	331	.51	181	4.49	3	0
Ca I	5588.76	21	2.52	3.82	2.43	1.11	378	.64	267	4.32	5	17
Ca I	5590.12	21	2.52	4.57	3.53	.19	353	.49	186	4.50	3	17
Ca I	5598.49	21	2.52	4.15		.68	479	.64	326	4.43	0	17
Ca I	5601.28	21	2.52	4.39	2.56	.21	366	.53	218	4.44	2	17
Ca I	6161.29	20	2.52	5.18	3.79	−.08	353	.37	148	4.65	1	3
Ca I	6166.44	20	2.52	5.16	3.81	.04	400	.33	126	4.71	2	3
Ca I	6169.06	20	2.52	4.72	3.30	.39	306	.42	141	4.62	1	3
Ca I	6169.56	20	2.52	4.54	3.31	.67	330	.49	191	4.51	1	3
Ca I	6439.07	18	2.52	3.91		1.43	352	.62	236	4.44	5	6
Ca I	6449.81	19	2.52	4.60	3.45	.41	374	.47	187	4.54	3	0
Ca I	6455.60	19	2.52	5.28	4.11	−.39	352	.27	93	4.85	3	6
Ca I	6462.57	18	2.52	4.07		1.27	422	.65	305	4.50	0	6
Ca I	6464.68	19	2.52	6.09	4.61		258	.14	36	5.19	3	6
Ca I	6471.66	18	2.52	4.79	3.59	.37	328	.45	167	4.58	3	6
Ca I	6493.78	18	2.52	4.19	3.01	1.10	375	.53	214	4.47	5	7
Ca I	6499.65	18	2.52	4.82		.37	293	.42	139	4.64	5	6
Ca I	6508.85	18	2.52	6.05		−1.15	302	.14	42	5.19	2	0
Ca I	4526.93	36	2.71	4.50	3.06	.17	256	.49	116	4.55	2	29

Table B

Spect	Wave-length	Mult	EP	$-\text{Log } X'_{\odot}$	$-\text{Log } X'_{\epsilon}$	Log $(gf\lambda) - \theta\chi$	HW	R_c	W	$-\text{Log } (W/\lambda)$	Q	N
Ca I	5349.47	33	2.71	4.47	3.40		314	.49	164	4.51	1	0
Ca I	5512.98	48	2.93	4.49	3.32	.14	328	.45	167	4.54	2	14
Ca I	5857.45	47	2.93	4.07	2.76	.69	366	.56	237	4.41	3	23
Ca I	6417.69		4.44	6.32			287	.09	25	5.40	1	0
Ce II	4053.51	36	.00	5.79		2.78	256	.62	194	4.32	2	0
Ce II	4486.91	57	.30	5.67		2.71	263	.64	166	4.43	4	29
Ce II	4120.84	112	.32	5.55		2.54	262	.63	198	4.32	2	0
Ce II	4527.35	108	.32			2.71	306	.71	226	4.50	0	29
Ce II	4072.92		.33			2.32	243	.52	135	4.48	2	0
Ce II	4399.20	81	.33	5.96		2.51	282	.60	181	4.39	2	28
Ce II	4483.90	3	.38	5.53		3.11	282	.57	185	4.40	3	29
Ce II	4562.36	1	.48	5.49	4.38	3.08	250	.64	159	4.46	5	30
Ce II	4364.66	135	.50	5.63		2.75	251	.60	172	4.40	2	27
Ce II	4375.92	134	.50			2.52	301	.77	260	4.43	0	27
Ce II	4523.08	2	.52	5.66	4.09	2.64	297	.69	224	4.31	2	0
Ce II	4628.16	1	.52	5.59	4.39	2.96	337	.67	226	4.31	4	30
Ce II	4725.09	153	.52	6.56	5.61	1.78	255	.33	87	4.74	4	32
Ce II	4093.96		.53			2.06	236	.46	115	4.55	2	0
Ce II	4467.54	17	.61			2.17	270	.54	156	4.46	2	0
Ce II	4382.17	2	.68	5.84		2.74	314	.61	195	4.35	1	27
Ce II	4560.96	2	.68	6.10		2.23	271	.51	148	4.49	3	0
Ce II	4068.84	82	.70	6.16		2.49	253	.59	161	4.40	2	0
Ce II	4336.26	89	.70	6.33		2.39	232	.53	132	4.49	4	27
Ce II	4349.79	59	.70	5.86		2.47	220	.53	135	4.49	4	27
Ce II	4582.50	7	.70	6.15		2.36	343	.56	185	4.41	1	30
Ce II	4117.29		.74			2.14	227	.39	93	4.65	2	0
Ce II	4551.30	229	.74			2.14	219	.52	128	4.68	0	29
Ce II	5347.81		.74			1.13	265	.16	42	5.11	1	9
Ce II	4702.01		.81			1.54	249	.30	89	4.76	2	32
Ce II	4418.78	2	.86	5.50		2.76	278	.61	189	4.37	2	0
Ce II	5330.58	13	.87	6.35	5.16	1.88	303	.37	113	4.67	2	9
Ce II	5353.53	15	.88			2.26	366	.63	249	4.45	0	9
Ce II	4606.40		.91			2.34	286	.59	182	4.40	3	0
Ce II	4773.94	17	.92	5.87	4.88	2.05	249	.41	107	4.63	2	32
Ce II	4604.21		1.03			1.06	218	.29	74	4.80	1	30
Ce II	5274.24	15	1.04	6.04	4.86	2.13	286	.45	139	4.57	5	9
Ce II	5610.26	26	1.05	6.18		1.44	378	.42	169	4.56	2	17
Ce II	4686.75		1.09	6.39		1.52	274	.29	78	4.79	3	31
Ce II	5409.22	23	1.10			2.03	341	.49	176	4.69	0	10
Ce II	4484.83		1.12	6.76		1.95	244	.37	95	4.67	2	29
Ce II	4624.90	27	1.12	6.03		2.32	390	.62	256	4.46	0	30
Ce II	4413.19		1.14			1.79	282	.38	109	4.63	2	28
Ce II	4659.37		1.21	6.33		1.44	218	.28	69	4.83	3	30
Ce II	5187.45	15	1.21	6.12	4.93	2.17	304	.46	151	4.54	2	25
Ce II	6043.39	30	1.21	6.61	5.43	1.58	306	.28	88	4.83	4	2
Ce II	5472.30	24	1.25	6.40		1.70	303	.38	133	4.64	1	13
Ce II	4753.65		1.28			1.01	219	.13	29	5.21	2	0
Ce II	4117.59		1.32			2.10	240	.48	123	4.53	2	0
Ce II	4601.37		1.32			1.23	236	.28	68	4.83	3	0
Ce II	5768.90	32	1.32	6.89		1.41	403	.43	183	4.80	0	21

Table B

Spect	Wave-length	Mult	EP	$-\text{Log } X'_{\odot}$	$-\text{Log } X'_{\epsilon}$	Log $(gf\lambda)$ $-\theta\chi$	HW	R_c	W	$-\text{Log } (W/\lambda)$	Q	N
Ce II	5975.87	30	1.33	6.91		1.39	330	.20	58	5.01	2	1
Ce II	4539.07		1.37			1.73	241	.33	83	4.74	2	0
Ce II	5468.37	24	1.40	6.35	5.22	1.70	273	.36	109	4.70	2	13
Ce II	4608.76		1.41			1.30	203	.20	47	4.99	2	30
Ce II	5613.69	32	1.42			1.05	278	.19	50	5.04	1	17
Ce II	5683.76		1.42			.98	252	.15	36	5.17	1	21
Ce II	4747.14		1.46			1.84	296	.40	128	4.60	3	32
Ce II	6034.20	30	1.46	6.92		1.02	353	.25	85	5.00	0	2
Ce II	4572.79		1.48			1.61	250	.30	80	4.76	2	30
Ce II	5995.35		1.49			1.22	306	.15	48	5.12	1	2
Ce II	4536.89		1.52			1.60	225	.23	54	4.93	2	0
Ce II	5516.08		1.61			.98	273	.16	42	5.12	2	14
Ce II	5959.69		1.63			1.01	283	.16	42	5.14	1	1
Ce II	6143.36		1.70			1.05	294	.18	53	5.06	1	0
Ce II	6098.34		1.77			1.15	377	.23	77	4.92	1	2
Ce II	6466.90		1.77			.74	235	.13	30	5.22	1	6
Ce II	5359.50		1.78			.91	278	.16	47	5.09	1	9
Ce II	5556.97		1.80			1.25	253	.17	45	5.09	1	16
Co I	4727.94	15	.43	5.82		.14	229	.20	47	5.01	2	0
Co I	4121.33	28	.92	3.26		2.54	275	.72	237	4.24	2	0
Co I	5530.78	38	1.71	5.80	4.46	.21	264	.18	48	5.06	2	0
Co I	6189.01	37	1.71	6.20	4.68	.01	279	.10	28	5.35	2	0
Co I	5331.46	39	1.78	5.75		.32	265	.20	50	5.02	1	9
Co I	6117.00		1.78	6.08	5.07	−.14	269	.07	19	5.52	1	0
Co I	4781.43	57	1.88	6.00	4.68	.04	202	.11	26	5.30	1	32
Co I	6429.91	81	2.14	6.63	5.32	−.43	280	.06	16	5.59	2	0
Co I	5647.23	112	2.28	5.97	4.63	.11	265	.12	31	5.26	3	19
Co I	6632.44	111	2.28	6.37	4.85	.02	291	.07	20	5.52	1	0
Co I	6417.82	111	2.33		5.13	−.23	284	.08	22	5.46	1	0
Co I	4813.48	158	3.21	5.05		.78	226	.25	63	4.89	3	32
Co I	4693.19	156	3.23	5.77	4.22	.24	181	.18	41	5.06	1	31
Co I	4792.86	158	3.25	5.27	4.13	.77	239	.24	59	4.91	2	0
Co I	5212.70	170	3.51	5.74	4.32	.46	203	.16	33	5.16	1	25
Co I	5352.05	172	3.58	5.77	4.27	.42	254	.17	44	5.09	2	0
Co I	6455.00	174	3.63	6.16	4.78	−.01	305	.10	30	5.35	1	6
Co I	4625.77	176	3.71	6.22		−.54	209	.13	29	5.39	0	30
Co I	6595.87	174	3.71	6.37	4.96	−.52	292	.08	23	5.46	1	0
Co I	5342.70	190	4.02	5.64	4.30	.23	324	.19	61	4.99	2	9
Co I	5444.59	196	4.07	6.02	4.70	−.17	164	.08	15	5.46	1	12
Co I	5454.57	195	4.07	6.05	4.78	−.26	178	.09	16	5.40	1	13
Cr I	4545.96	10	.94	4.35		1.63	269	.64	186	4.39	5	29
Cr I	4580.06	10	.94	4.26		1.40	281	.58	178	4.41	2	30
Cr I	6330.10	6	.94	5.50	4.43	.22	305	.21	61	5.00	2	5
Cr I	4626.19	21	.97	4.51	3.56	1.56	281	.53	167	4.45	2	30
Cr I	4616.14	21	.98	4.42	3.33	1.61	289	.60	187	4.39	3	0
Cr I	5296.69	18	.98	4.23	2.89	1.25	283	.53	157	4.50	5	9
Cr I	5300.75	18	.98	4.85	3.53	.65	341	.37	127	4.65	1	9
Cr I	6501.21	16	.98	5.98			293	.10	29	5.35	1	0
Cr I	4600.75	21	1.00	4.27	2.83	1.51	283	.57	174	4.42	2	0
Cr I	4652.16	21	1.00	4.24	2.84	1.75	256	.61	170	4.44	5	30

Table B

Spect	Wave-length	Mult	EP	$-\mathrm{Log}$ $X'_{\odot}$	$-\mathrm{Log}$ X'_{ϵ}	Log $(gf\lambda)$ $-\theta\chi$	HW	R_c	W	$-\mathrm{Log}$ (W/λ)	Q	N
Cr I	5345.81	18	1.00	4.07	2.16	1.61	379	.65	267	4.30	4	9
Cr I	5348.32	18	1.00	4.27	2.96	1.31	278	.56	174	4.46	4	9
Cr I	4646.17	21	1.03	4.33	2.39	2.01	374	.66	238	4.29	2	30
Cr I	5409.79	18	1.03	3.42	1.79	1.87	329	.66	251	4.33	2	10
Cr I	6630.02	16	1.03	6.17	4.90		187	.07	15	5.52	1	8
Cr I	4526.47	33	2.54	3.95		1.21	313	.65	213	4.33	3	29
Cr I	4535.15	33	2.54	5.45	3.89	.31	226	.24	56	4.91	1	0
Cr I	4540.50	33	2.54	4.82	2.90	1.01	254	.41	110	4.62	1	0
Cr I	4621.94	32	2.54	5.06		.54	278	.32	90	4.73	3	30
Cr I	4649.46	32	2.54	5.62	4.20	.16	218	.22	50	4.96	1	30
Cr I	4790.34	31	2.54	5.75	4.62		218	.13	33	5.22	1	32
Cr I	5238.97	59	2.71	5.81	4.57	−.23	151	.14	27	5.19	1	26
Cr I	4319.64	96	2.89	5.76		.19	210	.20	43	5.01	1	0
Cr I	5329.12	94	2.91	4.67	3.43	.31	253	.36	97	4.70	0	9
Cr I	4754.74	168	3.09	5.08			249	.30	84	4.77	3	32
Cr I	4756.11	145	3.10	4.88	3.61	1.05	267	.42	118	4.60	3	0
Cr I	4664.80	186	3.12	4.99		.51	226	.34	78	4.75	3	30
Cr I	4689.37	186	3.12	5.42		.38	312	.36	110	4.85	0	31
Cr I	4708.04	186	3.17	5.02	3.63	.79	249	.40	110	4.63	3	32
Cr I	4718.43	186	3.19	4.89	3.41	.89	330	.49	171	4.48	2	32
Cr I	4604.58	190	3.32	5.29	3.85		265	.28	80	4.79	2	30
Cr I	5783.11	188	3.32	5.71	4.36	−.03	302	.18	53	5.05	2	21
Cr I	5787.99	188	3.32	5.48	4.08	.13	282	.27	81	4.85	3	21
Cr I	5790.99	188	3.32	4.87		.61	302	.45	155	4.57	3	21
Cr I	4357.52	198	3.37	5.24			213	.27	67	4.83	3	27
Cr I	5405.00	191	3.37	6.09	4.76	−.29	243	.10	24	5.35	1	0
Cr I	5206.52	206	3.43	5.85	4.52		260	.24	64	4.91	2	0
Cr I	5664.04	203	3.43	5.50	4.21	−.27	273	.19	51	5.04	3	18
Cr I	5272.01	225	3.45	5.75	4.34	−.06	258	.21	55	4.98	2	0
Cr I	5312.88	225	3.45	5.81	4.48	−.24	239	.10	24	5.35	2	0
Cr I	4622.49	233	3.55	5.42	3.78	.22	265	.31	93	4.73	2	30
Cr I	4625.92	244	3.85	6.00			209	.13	29	5.39	0	30
Cr I	6661.08	282	4.19	6.27	4.96	−.50	293	.07	20	5.52	1	0
Cr II	5305.85	24	3.83	5.70	4.37	−2.38	291	.31	90	4.77	3	9
Cr II	4812.36	30	3.86	5.31	4.03	−2.32	259	.31	90	4.75	3	33
Cr II	4588.22	44	4.07	4.82		−1.34	296	.58	195	4.39	5	30
Cr II	4592.09	44	4.07	5.24		−2.06	260	.43	118	4.59	2	0
Cr II	4616.63	44	4.07	5.38	4.18	−2.20	306	.46	149	4.52	2	30
Cr II	5308.44	43	4.07	5.66	4.32	−2.40	253	.28	76	4.84	3	9
Cr II	5310.70	43	4.07	6.01	4.74	−2.69	252	.17	43	5.09	1	0
Cr II	5313.59	43	4.07	5.51	4.29	−2.15	329	.40	129	4.62	3	9
Cr II	5334.88	43	4.07	5.57	4.16	−2.28	253	.31	91	4.77	2	9
Cr II	5502.05	50	4.17	5.80	4.63	−2.32	271	.23	62	4.94	2	13
Cu I	5105.55	2	1.39	4.40	2.78	.63	319	.60	207	4.39	2	0
Cu I	5700.28	2	1.64	5.77		−.43	303	.25	78	4.88	3	21
Cu I	5782.13	2	1.64	4.89	3.01	.13	335	.47	167	4.54	3	0
Dy II	4103.34		.10	5.56		3.07	246	.53	140	4.47	2	0
Dy II	5169.71		.10	6.14		1.35	235	.10	27	5.28	1	0
Dy II	4073.12		.54	5.99		2.84	233	.45	111	4.56	2	0
Eu II	4129.73	1	.00	4.52		3.31	277	.73	242	4.23	2	0

Table B

Spect	Wave-length	Mult	*EP*	$-\text{Log}$ $X'_{\odot}$	$-\text{Log}$ X'_{ϵ}	Log $(gf\lambda)$ $-\theta\chi$	*HW*	R_c	*W*	$-\text{Log}$ (W/λ)	*Q*	*N*
Eu II	6437.64	8	1.32	6.18		1.31	292	.11	32	5.30	2	0
Eu II	6645.11	8	1.38	6.37		1.36	308	.14	43	5.19	2	0
Fe I	4347.24	2	.00	4.85			246	.43	112	4.59	2	0
Fe I	5110.41	1	.00	3.61	1.46	.37	337	.70	291	4.25	3	0
Fe I	5166.29	1	.00	3.78	1.40	.03	341	.66	235	4.34	4	25
Fe I	4389.24	2	.05	4.36			251	.60	165	4.41	1	28
Fe I	4445.48	2	.09	5.10			244	.38	102	4.65	5	28
Fe I	4461.65	2	.09	3.53		.84	301	.74	246	4.26	2	0
Fe I	4482.17	2	.11	2.71		.68	366	.80	319	4.15	5	29
Fe I	5225.53	1	.11	4.55	2.91		354	.52	168	4.49	3	26
Fe I	4489.74	2	.12	4.12		.11	295	.69	224	4.30	3	0
Fe I	5269.54	15	.86	1.86	.47	1.40	518	.82	441	4.08	3	9
Fe I	5956.70	14	.86	4.88	3.83		307	.38	113	4.69	2	1
Fe I	6280.62	13	.86	5.03			306	.48	161	4.56	5	5
Fe I	6358.69	13	.86	4.63	3.29		329	.45	158	4.58	2	5
Fe I	5397.13	15	.91	2.52	1.04	.82	392	.77	341	4.20	2	10
Fe I	5371.49	15	.96	2.30	.76	1.05	457	.80	402	4.13	4	9
Fe I	5429.70	15	.96	2.35		.87	556	.77	465	4.07	4	11
Fe I	5501.47	15	.96	3.99	2.35	−.00	389	.65	277	4.30	4	13
Fe I	6498.96	13	.96	5.20	4.02		363	.34	134	4.70	4	6
Fe I	4139.94	18	.99	4.00		−.34	254	.57	156	4.42	2	0
Fe I	4653.49	17	.99	5.89			312	.27	90	5.00	0	30
Fe I	5405.78	15	.99	2.42	1.27	.86	405	.77	348	4.19	2	10
Fe I	5446.92	15	.99	2.56		.72	404	.78	360	4.18	1	12
Fe I	5506.78	15	.99	3.92	1.80	.18	404	.66	285	4.29	3	14
Fe I	6551.70	13	.99	6.03			234	.08	19	5.46	1	7
Fe I	6574.24	13	.99	5.59	4.11		281	.26	82	4.89	2	7
Fe I	5434.53	15	1.01	3.00	1.43	.63	387	.71	294	4.27	5	11
Fe I	5497.52	15	1.01	3.80	1.80	.11	402	.73	337	4.21	5	13
Fe I	4383.55	41	1.48	1.31		2.48	627	.90	630	3.84	2	27
Fe I	4602.94	39	1.48	4.05	1.36	.53	281	.70	225	4.31	4	30
Fe I	5171.61	36	1.48	3.26		.76	347	.71	272	4.28	4	25
Fe I	6710.32	34	1.48	5.93	4.52		350	.16	48	5.13	3	8
Fe I	4337.05	41	1.56	3.53		.73	294	.75	251	4.24	3	0
Fe I	4404.75	41	1.56	1.40		2.13	643	.87	613	3.86	3	28
Fe I	4592.66	39	1.56	4.05		−.01	337	.70	261	4.25	4	30
Fe I	5194.94	36	1.56	3.81	1.95	.33	380	.67	263	4.30	2	25
Fe I	5332.90	36	1.56	4.26		−.39	329	.58	220	4.40	1	9
Fe I	4325.76	42	1.61	1.48		2.18	628	.86	587	3.87	3	27
Fe I	4602.00	39	1.61	4.68	2.98	−.66	275	.51	152	4.49	5	30
Fe I	4632.92	39	1.61	4.06		−.46	291	.61	189	4.39	2	0
Fe I	4672.83	40	1.61	5.27	4.14		171	.22	38	5.02	1	31
Fe I	5307.37	36	1.61	4.42	2.64	−.56	303	.54	175	4.47	5	9
Fe I	5341.03	37	1.61	3.06		.32	366	.73	297	4.25	3	9
Fe I	5202.34	66	2.18	3.43	1.32	.07	342	.66	253	4.31	5	25
Fe I	6062.89	63	2.18	5.77	4.21	−1.88	286	.16	46	5.12	2	0
Fe I	6151.62	62	2.18	5.33	4.01	−1.38	283	.33	111	4.74	3	3
Fe I	6265.14	62	2.18	4.88		−.66	353	.50	180	4.52	5	5
Fe I	6430.85	62	2.18	4.45	2.87	−.22	375	.57	230	4.43	5	6
Fe I	4442.34	68	2.20	2.84		.66	391	.77	307	4.16	5	28

Table B

Spect	Wave-length	Mult	EP	$-\text{Log } X'_{\odot}$	$-\text{Log } X'_{\epsilon}$	$\text{Log } (gf\lambda) - \theta\chi$	HW	R_c	W	$-\text{Log } (W/\lambda)$	Q	N
Fe I	4447.13	69	2.20	4.71		−.73	261	.49	136	4.51	3	0
Fe I	4478.04	69	2.20	5.70		−1.53	213	.20	44	5.01	4	29
Fe I	5143.73	65	2.20	5.56	4.41		264	.28	76	4.83	2	0
Fe I	5145.11	66	2.20	5.14	3.83	−1.18	295	.45	141	4.56	2	0
Fe I	6137.00	62	2.20	4.97	3.65	−1.08	343	.41	148	4.62	2	0
Fe I	6219.29	62	2.20	4.74	3.09	−.74	329	.50	175	4.53	5	5
Fe I	6335.34	62	2.20	4.48	3.06	−.55	305	.52	173	4.52	5	5
Fe I	4430.62	68	2.22	3.74		.12	329	.70	260	4.23	3	28
Fe I	4447.72	68	2.22	2.81		.56	329	.72	259	4.23	5	28
Fe I	5198.71	66	2.22	4.45	2.64	−.29	304	.57	174	4.45	5	25
Fe I	6015.25	63	2.22	6.42	5.04		266	.08	21	5.46	1	0
Fe I	6082.72	64	2.22	5.43	4.13	−1.65	306	.24	74	4.91	2	2
Fe I	6173.34	62	2.22	5.18	3.47	−1.12	330	.41	152	4.61	2	3
Fe I	6213.44	62	2.22	5.03	3.59	−.87	329	.49	173	4.53	4	5
Fe I	6240.66	64	2.22	5.34	4.07	−1.39	331	.33	114	4.74	3	0
Fe I	6297.80	62	2.22	4.99	3.65	−1.02	329	.45	151	4.59	4	5
Fe I	4439.89	116	2.28	4.98		−.93	266	.38	97	4.66	2	28
Fe I	4630.13	115	2.28	4.74	3.17	−.74	249	.56	161	4.45	2	30
Fe I	5322.05	112	2.28	4.91	3.66	−.82	291	.41	124	4.62	4	9
Fe I	5436.59	113	2.28	5.32	3.93	−1.56	285	.31	91	4.77	1	0
Fe I	6254.26	111	2.28	4.33		−.76	376	.52	214	4.47	3	5
Fe I	6392.53	109	2.28	6.07	4.59	−1.90	292	.12	35	5.26	1	0
Fe I	6421.36	111	2.28	4.72	2.57	−.31	352	.57	207	4.46	5	6
Fe I	6481.88	109	2.28	5.04	3.51	−1.17	355	.38	142	4.66	2	0
Fe I	6608.03	109	2.28	5.81	4.56	−2.09	304	.12	39	5.26	1	7
Fe I	6252.56	169	2.40	4.41		−.20	353	.57	212	4.45	5	5
Fe I	6494.97	168	2.40	3.81	1.74	.24	375	.61	260	4.40	3	6
Fe I	5141.75	114	2.42	4.41	3.16	−.59	358	.50	189	4.47	3	24
Fe I	6663.45	111	2.42	4.90	3.45	−.96	444	.43	192	4.56	2	8
Fe I	6344.15	169	2.43	5.13	3.82	−1.27	376	.42	182	4.80	0	5
Fe I	6393.61	168	2.43	4.35	2.72	−.04	376	.58	230	4.43	3	6
Fe I	6593.88	168	2.43	4.73	3.41	−.96	375	.44	175	4.58	5	7
Fe I	5916.25	170	2.45	5.17	3.74	−1.10	312	.32	104	4.76	3	0
Fe I	6136.62	169	2.45	4.03	2.35	.08	381	.59	243	4.40	3	0
Fe I	6256.37	169	2.45	4.79		−1.00	353	.51	208	4.48	3	5
Fe I	6462.75	168	2.45	4.97		−.96	422	.65	305	4.73	0	6
Fe I	5701.55	209	2.56	4.61		−.53	310	.48	178	4.52	2	21
Fe I	6230.73	207	2.56	3.91		−.03	423	.62	285	4.34	5	5
Fe I	6609.12	206	2.56	4.92	3.67	−1.35	375	.35	133	4.70	2	7
Fe I	5778.47	209	2.59	5.84	4.46		247	.19	48	5.06	2	21
Fe I	6005.53	207	2.59	5.73		−1.86	330	.17	53	5.07	2	2
Fe I	6137.70	207	2.59	4.16	1.89	−.09	377	.59	236	4.41	3	3
Fe I	6322.69	207	2.59	4.90	3.83	−1.06	305	.41	140	4.64	4	5
Fe I	6575.02	206	2.59	5.07		−1.35	398	.40	175	4.60	3	7
Fe I	4319.45	214	2.61	5.80		−1.82	209	.20	43	5.01	1	0
Fe I	6065.49	207	2.61	4.30	2.70	−.20	377	.57	221	4.43	4	2
Fe I	6200.32	207	2.61	5.15	3.33	−1.12	329	.41	144	4.63	4	4
Fe I	6677.99	268	2.69	4.37		−.14	421	.51	211	4.50	4	8
Fe I	6180.22	269	2.73	5.40	3.92	−1.37	306	.34	116	4.72	4	3
Fe I	6592.92	268	2.73	4.34	3.01	−.36	351	.50	202	4.51	2	7

Table B

Spect	Wave-length	Mult	EP	$-\mathrm{Log}\ X'_{\odot}$	$-\mathrm{Log}\ X'_{\epsilon}$	$\mathrm{Log}\ (gf\lambda) - \theta\chi$	HW	R_c	W	$-\mathrm{Log}\ (W/\lambda)$	Q	N
Fe I	6546.25	268	2.76	4.57	3.14	−.48	352	.53	216	4.47	2	7
Fe I	6703.57	268	2.76	5.58	4.21	−1.82	280	.21	66	4.99	1	8
Fe I	4091.56	357	2.83	4.66		−.83	231	.43	105	4.59	3	0
Fe I	4454.38	350	2.83	4.32		−.06	283	.63	198	4.35	3	0
Fe I	4466.55	350	2.83	3.60		.63	344	.76	282	4.20	3	29
Fe I	4683.57	346	2.83	5.09	3.73	−1.08	302	.37	113	4.65	2	31
Fe I	4741.53	346	2.83	4.69	3.39	−.69	311	.52	178	4.45	4	32
Fe I	6311.51	342	2.83	5.73	4.33	−1.64	295	.15	44	5.15	2	0
Fe I	6518.38	342	2.83	5.13	3.92	−1.32	355	.37	138	4.68	3	0
Fe I	4422.57	350	2.84	3.76		.22	407	.77	333	4.32	0	28
Fe I	4476.02	350	2.84	3.18		.58	313	.73	242	4.27	5	29
Fe I	4635.85	349	2.84	5.11	3.65	−1.00	249	.38	91	4.68	1	30
Fe I	6229.23	342	2.84	5.53	4.02	−1.53	353	.28	89	4.84	4	5
Fe I	6355.04	342	2.84	5.09	3.14	−1.17	329	.40	147	4.63	2	5
Fe I	6270.24	342	2.86	5.31	3.82	−1.34	306	.36	127	4.69	2	5
Fe I	4768.40	384	2.94	5.02		−1.21	299	.56	172	4.65	0	32
Fe I	5232.95	383	2.94	2.33	.75	.79	392	.70	306	4.23	5	26
Fe I	4120.21	423	2.99	4.00		−.15	256	.59	163	4.40	2	0
Fe I	4348.94	414	2.99	4.79		−1.12	235	.42	108	4.60	4	27
Fe I	4365.90	415	2.99	5.00		−1.17	188	.35	75	4.74	2	27
Fe I	4603.95	410	2.99	5.81		−1.88	250	.27	72	4.95	0	30
Fe I	4721.00	409	2.99	5.09		−1.40	280	.38	112	4.64	4	32
Fe I	4787.84	384	3.00	5.19	3.86	−1.49	249	.26	69	4.86	3	32
Fe I	5266.56	383	3.00	2.65	.93	.42	384	.68	285	4.27	5	9
Fe I	4376.78	471	3.02	4.94		−1.04	219	.41	90	4.65	2	27
Fe I	4740.34	409	3.02	5.30		−1.42	339	.63	226	4.62	0	32
Fe I	4772.82	467	3.02	4.37		−.78	249	.58	161	4.44	5	32
Fe I	5326.15	407	3.02	5.47			329	.22	73	4.91	1	9
Fe I	5191.46	383	3.04	3.41	1.39	.32	494	.75	381	4.25	0	25
Fe I	5281.80	383	3.04	3.41	1.53	.03	329	.60	212	4.39	5	9
Fe I	4343.70	517	3.05	4.57		−.90	265	.56	160	4.43	1	0
Fe I	4436.95	516	3.05	4.50		−1.18	219	.48	109	4.57	4	28
Fe I	4480.14	515	3.05	4.92		−.81	325	.53	180	4.43	2	29
Fe I	4793.96	512	3.05	6.06	4.88	−2.32	218	.09	21	5.40	1	32
Fe I	4517.53	472	3.07	4.80		−.93	306	.55	166	4.44	3	29
Fe I	5460.91	464	3.07	6.22	4.87		250	.12	30	5.26	1	0
Fe I	4067.99	559	3.21	3.32		.33	261	.65	206	4.29	2	0
Fe I	4531.63	555	3.21	4.94		−1.16	250	.47	123	4.55	2	29
Fe I	4574.24	554	3.21	5.36	4.01	−1.60	219	.27	61	4.86	1	30
Fe I	5324.19	553	3.21	2.40	.75	.57	367	.68	265	4.30	4	9
Fe I	5909.99	552	3.21	5.59	4.06		378	.29	110	4.77	3	1
Fe I	4070.78	558	3.24	4.07		−.01	254	.60	165	4.39	2	0
Fe I	4098.18	558	3.24	3.70		−.14	258	.61	189	4.34	2	0
Fe I	4625.05	554	3.24	4.55	2.98	−.62	390	.62	256	4.46	0	30
Fe I	4788.76	588	3.24	4.67	3.61	−.91	249	.45	125	4.57	5	32
Fe I	5283.63	553	3.24	2.91		.26	404	.66	283	4.27	3	9
Fe I	4780.81	633	3.25	6.03	4.81	−2.20	218	.10	26	5.35	1	32
Fe I	4808.16	633	3.25	5.46	4.21	−1.84	216	.17	41	5.08	2	32
Fe I	4504.84	555	3.26	5.09		−1.48	244	.36	92	4.69	1	0
Fe I	4568.79	554	3.26	5.23		−1.60	250	.37	100	4.86	0	30

Table B

Spect	Wave-length	Mult	EP	$-\text{Log } X'_{\odot}$	$-\text{Log } X'_{\epsilon}$	$\text{Log } (gf\lambda) - \theta\chi$	HW	R_c	W	$-\text{Log } (W/\lambda)$	Q	N
Fe I	4668.14	554	3.26	3.98		−.30	280	.60	174	4.41	3	31
Fe I	5263.31	553	3.26	4.07		−.15	349	.57	223	4.40	3	9
Fe I	5339.94	553	3.26	3.49	1.91	−.06	354	.62	230	4.37	3	9
Fe I	5848.09	552	3.26	5.45	4.24		251	.18	48	5.07	2	22
Fe I	4377.80	645	3.27	5.21		−1.39	204	.28	59	4.85	3	27
Fe I	4813.11	630	3.27	5.60		−1.97	248	.17	45	5.06	2	33
Fe I	5277.31	584	3.27	6.20			253	.11	27	5.30	1	9
Fe I	4598.12	554	3.28	4.56	2.98	−.73	271	.50	145	4.50	3	0
Fe I	5229.86	553	3.28	4.03		−.18	303	.55	180	4.45	4	26
Fe I	5253.48	553	3.28	4.77	3.38	−.79	303	.45	135	4.58	4	9
Fe I	4566.52	641	3.30	5.31	3.76	−1.36	187	.25	52	4.92	2	30
Fe I	4595.36	594	3.30	4.85		−1.00	312	.56	181	4.62	0	30
Fe I	4741.08	688	3.33	5.41		−1.66	296	.34	108	4.68	4	32
Fe I	4807.73	688	3.37	4.90	3.78	−1.49	255	.30	82	4.78	3	32
Fe I	5586.76	686	3.37	2.80	1.28	.28	378	.68	286	4.29	5	17
Fe I	5572.85	686	3.40	3.04	1.27	.19	504	.67	342	4.21	2	17
Fe I	4566.99	723	3.41	5.78		−1.91	234	.32	80	5.10	0	30
Fe I	4779.44	720	3.41	5.07	3.91	−1.55	218	.28	65	4.85	2	32
Fe I	5569.63	686	3.42	3.61	2.11	−.04	378	.64	280	4.30	2	17
Fe I	5624.55	686	3.42	3.91		−.29	353	.57	226	4.41	2	17
Fe I	5576.10	686	3.43	4.28	2.97	−.44	328	.59	251	4.37	4	17
Fe I	4059.71	767	3.55	4.52		−.65	242	.52	135	4.48	2	0
Fe I	4547.85	755	3.55	4.62	2.99	−.34	244	.56	156	4.45	5	29
Fe I	4502.60	796	3.57	5.67	3.95	−1.65	188	.24	51	4.93	1	29
Fe I	4587.13	795	3.57	5.15		−1.16	281	.37	110	4.65	3	30
Fe I	4809.94	793	3.57	5.74	4.37	−2.17	201	.12	24	5.26	3	32
Fe I	5365.41	786	3.57	4.77		−.66	309	.48	163	4.52	2	10
Fe I	5466.99	784	3.57	5.61		−1.54	248	.25	64	4.91	1	13
Fe I	5584.77	782	3.57	5.55	4.03	−1.47	296	.33	102	4.74	2	0
Fe I	6019.36	780	3.57	6.46	4.90		260	.05	13	5.67	1	0
Fe I	4388.41	830	3.60	4.06		−.23	277	.62	194	4.36	3	0
Fe I	4484.23	828	3.60	4.56		−.19	250	.57	155	4.44	3	29
Fe I	4525.15	826	3.60	3.83	1.46	−.24	297	.69	224	4.31	2	0
Fe I	4596.06	820	3.60	4.88		−1.15	296	.49	151	4.69	0	30
Fe I	4619.29	821	3.60	4.71	3.37	−.67	273	.50	146	4.50	2	0
Fe I	4638.02	822	3.60	4.50		−.64	312	.53	174	4.45	3	30
Fe I	4678.85	821	3.60	4.26	2.80	−.24	289	.58	181	4.41	3	0
Fe I	6246.33	816	3.60	4.50	2.90	−.58	329	.49	183	4.52	3	5
Fe I	4568.86	894	3.63	5.72		−1.73	250	.37	100	4.96	0	30
Fe I	5207.94	880	3.63	5.81		−1.58	291	.27	88	4.81	1	25
Fe I	5223.19	880	3.63	5.64	4.23	−1.59	215	.20	48	5.02	2	26
Fe I	5397.60	841	3.63	5.70	4.30		256	.17	44	5.09	2	0
Fe I	4558.11	894	3.64	5.74		−1.80	234	.28	63	4.84	4	30
Fe I	4708.98	889	3.64	5.34		−1.23	280	.50	152	4.90	0	32
Fe I	4799.41	888	3.64	5.37		−1.62	273	.39	111	4.84	0	32
Fe I	4802.88	888	3.64	4.77		−1.18	249	.37	98	4.68	3	32
Fe I	5636.71	868	3.64	5.90	4.45	−1.55	264	.15	40	5.15	1	0
Fe I	5698.05	867	3.64	6.00	4.65		262	.13	34	5.22	2	0
Fe I	5707.05	868	3.64	5.37		−1.47	341	.24	90	4.85	1	21
Fe I	4433.22	830	3.65	4.19		−.42	276	.59	176	4.40	2	0

Table B

Spect	Wave-length	Mult	EP	$-\text{Log } X'_{\odot}$	$-\text{Log } X'_{\epsilon}$	$\text{Log } (gf\lambda) - \theta\chi$	HW	R_c	W	$-\text{Log } (W/\lambda)$	Q	N
Fe I	4485.97	825	3.65	5.77		−1.78	250	.31	94	4.98	0	29
Fe I	4580.59	827	3.65	5.27		−1.61	375	.46	183	4.76	0	30
Fe I	4596.43	823	3.65	5.50	4.03	−1.84	250	.23	60	4.91	1	30
Fe I	4611.28	826	3.65	4.11		−.44	291	.62	194	4.38	2	0
Fe I	4643.47	820	3.65	4.86	2.93	−.91	281	.46	125	4.56	2	30
Fe I	4673.17	820	3.65	4.69		−.85	311	.53	189	4.43	4	31
Fe I	4709.09	821	3.65	4.66		−.90	280	.50	152	4.70	0	32
Fe I	4745.81	821	3.65	4.77		−.88	280	.56	166	4.44	4	32
Fe I	6232.66	816	3.65	4.96		−1.05	400	.45	183	4.55	4	5
Fe I	6301.52	816	3.65	4.33	3.23	−.54	305	.50	182	4.52	4	5
Fe I	6411.66	816	3.65	4.33	2.93	−.32	329	.53	191	4.50	4	6
Fe I	4438.35	828	3.69	5.16		−1.31	307	.41	123	4.67	0	28
Fe I	4446.84	828	3.69	4.66		−.89	259	.48	133	4.53	3	0
Fe I	4481.62	827	3.69	5.14		−1.03	246	.38	98	4.66	2	0
Fe I	4598.74	819	3.69	5.97	4.43	−2.12	218	.17	39	5.08	1	30
Fe I	4690.15	820	3.69	5.07	3.65	−1.15	254	.36	95	4.69	1	0
Fe I	4700.17	935	3.69	5.07	3.62	−1.35	302	.37	105	4.66	5	32
Fe I	4701.05	820	3.69	5.33		−1.59	296	.27	82	4.80	3	32
Fe I	4704.96	821	3.69	4.96	3.54	−1.04	265	.37	101	4.67	3	32
Fe I	4768.32	821	3.69	4.78		−1.17	299	.56	172	4.65	0	32
Fe I	5288.53	929	3.69	5.12		−1.20	298	.35	111	4.69	4	9
Fe I	5379.58	928	3.69	5.12	3.69	−1.22	311	.41	127	4.62	3	10
Fe I	5543.18	926	3.69	5.07	3.40	−1.18	327	.38	138	4.63	4	15
Fe I	6336.83	816	3.69	4.41	3.10	−.65	329	.46	171	4.56	5	5
Fe I	6408.03	816	3.69	4.94	3.27	−.76	376	.45	178	4.56	1	6
Fe I	5809.25	982	3.88	5.31	3.84	−1.42	290	.31	97	4.78	4	22
Fe I	6003.03	959	3.88	4.80	3.50	−1.01	283	.42	130	4.63	3	2
Fe I	6008.58	982	3.88	4.77	3.42	−.96	306	.41	132	4.64	2	2
Fe I	6220.78	958	3.88	5.97	4.46	−2.04	289	.14	40	5.19	2	0
Fe I	6226.77	981	3.88	5.80	4.28	−1.80	282	.16	45	5.13	2	5
Fe I	5934.66	982	3.93	4.91	3.46	−1.04	330	.40	151	4.61	3	1
Fe I	4551.67	972	3.94	5.67	4.11	−1.79	203	.24	59	4.90	1	29
Fe I	4593.54	971	3.94	5.70	4.09	−1.80	281	.39	106	4.83	0	30
Fe I	5976.80	959	3.94	5.12	3.74	−1.20	306	.34	113	4.72	2	1
Fe I	6188.00	959	3.94	5.59	3.92		282	.28	91	4.83	4	4
Fe I	5883.81	982	3.96	4.66		−1.11	331	.34	125	4.70	3	1
Fe I	5952.75	959	3.98	5.06	3.79	−1.28	305	.28	88	4.83	1	0
Fe I	6096.69	959	3.98	5.58	4.14	−1.66	353	.19	60	5.02	1	2
Fe I	5329.99	1028	4.07	5.09		−1.11	399	.38	155	4.59	3	9
Fe I	5403.82	1029	4.07	5.09	3.55	−.83	300	.40	126	4.63	1	0
Fe I	5494.47	1024	4.07	5.74	4.30	−1.80	201	.15	32	5.19	1	13
Fe I	6027.06	1018	4.07	5.18	3.64	−1.11	306	.35	119	4.71	4	2
Fe I	6157.73	1015	4.07	5.40		−1.26	353	.44	187	4.75	0	3
Fe I	6315.81	1014	4.07	5.66	4.13	−1.55	306	.20	62	5.01	1	0
Fe I	5353.39	1062	4.10	4.85		−.97	366	.63	249	4.50	0	9
Fe I	5493.51	1061	4.10	5.55		−1.68	332	.36	119	4.87	0	13
Fe I	4800.65	1042	4.14	4.76	2.97	−1.26	261	.37	113	4.65	2	32
Fe I	5187.92	1032	4.14	5.24	3.41	−1.29	278	.35	109	4.69	2	25
Fe I	5487.76	1025	4.14	4.67		−.97	428	.49	222	4.45	2	13
Fe I	6127.91	1017	4.14	5.41		−1.49	330	.27	84	4.86	2	3

398-978 O - 71 - 11

Table B

Spect	Wave-length	Mult	EP	$-\text{Log } X'_{\odot}$	$-\text{Log } X'_{\epsilon}$	$\text{Log } (gf\lambda) - \theta\chi$	HW	R_c	W	$-\text{Log } (W/\lambda)$	Q	N
Fe I	6165.37	1018	4.14	5.65		−1.52	283	.24	72	4.92	1	3
Fe I	6315.32	1015	4.14	5.36	3.47	−1.35	305	.39	129	4.67	3	5
Fe I	5391.49	1062	4.15	4.85		−1.04	405	.47	205	4.48	5	10
Fe I	5473.91	1062	4.15	4.82	3.41	−.99	303	.45	160	4.55	1	13
Fe I	5607.66	1058	4.15	6.07	4.54		262	.15	39	5.15	2	0
Fe I	5133.70	1092	4.18	3.42		−.11	347	.62	237	4.34	5	24
Fe I	5662.52	1087	4.18	4.68		−.57	297	.47	152	4.55	2	18
Fe I	5491.84	1031	4.19	6.15	4.75		138	.08	11	5.46	1	13
Fe I	5563.60	1062	4.19	4.65	2.78	−1.07	293	.49	154	4.54	5	16
Fe I	5715.11	1061	4.19	4.96	3.80	−1.25	353	.40	155	4.60	5	21
Fe I	6215.15	1018	4.19	5.54		−1.46	306	.33	120	4.73	2	5
Fe I	6380.75	1015	4.19	5.56	3.93	−1.32	305	.27	93	4.84	4	6
Fe I	5608.98	1108	4.21	6.27	4.58		256	.12	31	5.26	1	0
Fe I	5618.65	1107	4.21	5.45	4.03	−1.22	278	.30	91	4.79	1	17
Fe I	5762.99	1107	4.21	4.59		−.60	323	.51	187	4.49	3	21
Fe I	5195.47	1092	4.22	4.24	2.91	−.43	304	.54	182	4.46	1	25
Fe I	5228.41	1091	4.22	5.08		−.94	316	.48	152	4.53	3	26
Fe I	5543.93	1062	4.22	5.08	3.78	−1.28	383	.37	142	4.63	1	15
Fe I	5547.00	1061	4.22	5.67	4.20	−1.88	224	.22	52	4.99	1	15
Fe I	5638.27	1087	4.22	4.94		−1.00	325	.44	153	4.57	3	17
Fe I	5775.09	1087	4.22	5.36	3.97	−1.17	277	.34	101	4.74	3	21
Fe I	5793.93	1086	4.22	5.73	4.19	−1.66	272	.20	64	4.98	3	21
Fe I	5196.10	1091	4.26	4.78	3.65	−.74	279	.42	120	4.62	1	25
Fe I	5635.85	1088	4.26	5.66	4.18	−1.47	271	.19	52	5.03	1	0
Fe I	5641.46	1087	4.26	5.11	3.62	−1.19	321	.35	117	4.69	2	17
Fe I	5652.32	1108	4.26	5.79	4.31	−1.51	305	.17	55	5.05	2	17
Fe I	5731.77	1087	4.26	5.19		−1.15	320	.35	120	4.69	3	21
Fe I	5753.14	1107	4.26	4.92	3.64	−.82	290	.43	129	4.62	1	21
Fe I	5717.85	1107	4.28	5.13	3.75	−1.09	313	.38	125	4.66	3	0
Fe I	5804.46	1087	4.28	5.96			252	.14	41	5.19	1	22
Fe I	5814.80	1086	4.28	5.88	4.37	−1.71	290	.17	52	5.07	1	22
Fe I	5856.08	1128	4.29	5.72	4.19	−1.47	282	.19	54	5.03	1	0
Fe I	5109.66	1089	4.30	4.92	3.36	−1.21	282	.39	115	4.65	2	0
Fe I	5691.51	1087	4.30	5.54		−1.42	278	.28	76	4.85	4	21
Fe I	5705.48	1087	4.30	5.55	4.19	−1.41	273	.21	58	4.99	2	21
Fe I	5383.37	1146	4.31	3.09	1.70	.03	341	.63	236	4.36	2	10
Fe I	5267.28	1146	4.37	5.74			265	.15	39	5.14	1	9
Fe I	5315.07	1147	4.37	5.56	4.15	−1.74	256	.19	49	5.03	1	0
Fe I	5369.95	1146	4.37	3.33	1.61	−.14	341	.61	231	4.37	1	10
Fe I	5400.51	1145	4.37	4.33		−.63	329	.56	209	4.42	1	10
Fe I	5406.77	1148	4.37	5.51	4.19		278	.21	61	4.96	3	10
Fe I	5409.14	1147	4.37	5.18		−1.52	341	.49	176	4.69	0	10
Fe I	5466.40	1144	4.37	4.90	3.62	−1.22	304	.46	155	4.55	3	13
Fe I	5546.51	1145	4.37	5.27	3.90	−1.42	250	.31	89	4.78	1	15
Fe I	5405.35	1162	4.39	5.42	3.96	−1.07	275	.27	77	4.85	2	0
Fe I	5415.20	1165	4.39	3.06	2.14	−.02	329	.62	224	4.38	3	10
Fe I	5445.05	1163	4.39	4.22	3.14	−.55	334	.53	204	4.45	4	12
Fe I	5619.60	1161	4.39	5.70	4.22	−1.70	341	.28	101	4.79	1	17
Fe I	5653.89	1159	4.39	5.58	4.15	−1.57	305	.21	69	4.95	2	19
Fe I	5295.32	1146	4.41	5.71			324	.18	53	5.03	1	9

Table B

Spect	Wave-length	Mult	EP	$-\mathrm{Log}\ X'_{\odot}$	$-\mathrm{Log}\ X'_{\epsilon}$	$\mathrm{Log}\ (gf\lambda) - \theta\chi$	HW	R_c	W	$-\mathrm{Log}\ (W/\lambda)$	Q	N
Fe I	5326.79	1147	4.41	6.16	4.60		215	.09	17	5.40	1	9
Fe I	5367.47	1146	4.41	3.66		−.26	319	.57	205	4.42	5	10
Fe I	5389.46	1145	4.41	4.67	3.33	−.86	329	.46	158	4.54	2	10
Fe I	5417.03	1148	4.41	5.53	4.25	−1.80	298	.20	61	4.98	1	10
Fe I	5487.16	1143	4.41	5.62	4.14	−1.87	270	.28	81	4.83	1	13
Fe I	5285.12	1166	4.43	5.76	4.24	−1.61	253	.18	51	5.04	1	9
Fe I	5321.11	1165	4.43	5.40	4.06	−1.39	284	.34	101	4.72	2	0
Fe I	5339.40	1162	4.43	6.24	4.67		240	.11	24	5.30	1	9
Fe I	5463.28	1163	4.43	4.30	3.11	−.64	279	.54	170	4.48	1	13
Fe I	5553.59	1161	4.43	5.49		−1.60	315	.30	98	4.77	3	16
Fe I	5560.23	1164	4.43	5.42		−1.46	251	.28	76	4.85	2	16
Fe I	5562.71	1163	4.43	5.29		−1.31	324	.38	135	4.64	1	16
Fe I	5364.88	1146	4.44	4.06		−.38	316	.56	181	4.45	3	10
Fe I	5395.25	1143	4.44	5.88	4.49		291	.16	51	5.07	1	10
Fe I	5398.29	1145	4.44	4.88	3.58	−1.02	341	.41	146	4.59	3	10
Fe I	5432.96	1143	4.44	4.96			355	.41	147	4.59	2	11
Fe I	5461.54	1145	4.44	5.83	4.35	−1.92	241	.20	52	5.01	2	13
Fe I	5180.07	1166	4.47	5.28	3.81	−1.28	253	.27	78	4.84	1	25
Fe I	5373.70	1166	4.47	5.15		−1.08	300	.34	109	4.71	5	10
Fe I	5410.91	1165	4.47	3.56	2.77	−.27	331	.56	199	4.43	3	0
Fe I	5462.97	1163	4.47	4.65	3.16	−.83	304	.51	162	4.51	1	13
Fe I	5651.47	1161	4.47	6.02	4.47		262	.14	37	5.19	1	0
Fe I	5554.90	1183	4.55	4.56		−1.02	306	.45	146	4.57	2	16
Fe I	5686.54	1182	4.55	5.02		−.95	353	.39	151	4.61	1	21
Fe I	5720.89	1178	4.55	6.09	4.63		303	.15	47	5.12	3	21
Fe I	5752.04	1180	4.55	5.26	3.96	−1.23	340	.29	102	4.78	3	21
Fe I	5816.36	1179	4.55	4.86	3.26	−1.11	315	.38	131	4.65	3	22
Fe I	5852.19	1178	4.55	5.61	4.14	−1.51	310	.18	58	5.03	4	22
Fe I	5859.61	1181	4.55	5.02	3.61	−1.03	350	.37	145	4.64	4	22
Fe I	5862.36	1180	4.55	4.83	3.41	−.89	272	.38	111	4.69	5	23
Fe I	5929.70	1176	4.55	5.58	4.10	−1.62	288	.20	58	5.01	1	0
Fe I	5983.70	1175	4.55	5.12	3.69	−1.18	318	.35	121	4.70	3	1
Fe I	6024.07	1178	4.55	4.46	2.98	−.64	283	.47	166	4.55	4	2
Fe I	6627.56	1174	4.55	5.90	4.36	−2.04	292	.16	47	5.13	3	7
Fe I	4749.93	1206	4.56	5.53	3.97	−1.72	242	.27	67	4.85	2	0
Fe I	6533.94	1197	4.56	5.52		−1.96	258	.19	50	5.07	1	7
Fe I	6633.76	1197	4.56	5.20	3.92	−1.46	343	.29	103	4.81	2	0
Fe I	6699.14	1228	4.59	6.46	4.91		294	.07	20	5.52	1	0
Fe I	5488.14	1183	4.61	5.96	4.34		247	.17	45	5.15	0	13
Fe I	5806.73	1180	4.61	5.37		−1.30	303	.28	93	4.81	3	22
Fe I	5855.13	1179	4.61	5.99	4.47	−1.60	277	.13	40	5.22	4	22
Fe I	5997.81	1175	4.61	5.14		−1.62	303	.26	81	4.87	1	0
Fe I	6020.17	1178	4.61	4.78	2.52	−.95	377	.48	204	4.50	4	2
Fe I	6093.66	1177	4.61	5.73	4.26	−1.85	330	.13	40	5.22	1	2
Fe I	6639.71	1195	4.61	6.08		−2.22	308	.14	43	5.19	1	0
Fe I	6705.12	1197	4.61	5.60	4.11	−1.82	304	.24	79	4.92	1	8
Fe I	5598.30	1183	4.65	4.84		−.92	479	.64	326	4.43	0	17
Fe I	5679.02	1183	4.65	5.23	3.94	−1.11	283	.31	90	4.79	3	21
Fe I	5905.67	1181	4.65	5.27	3.83	−1.22	331	.28	93	4.82	3	1
Fe I	5927.80	1175	4.65	5.57	4.10	−1.48	287	.20	58	5.01	1	0

Table B

Spect	Wave-length	Mult	EP	$-$Log $X'_{\odot}$	$-$Log X'_{ϵ}	Log $(gf\lambda)$ $-\theta\chi$	HW	R_c	W	$-$Log (W/λ)	Q	N
Fe I	5930.19	1180	4.65	4.87	3.26	−.79	329	.40	139	4.63	3	0
Fe I	6007.96	1178	4.65	5.27	3.87	−1.33	330	.32	109	4.75	2	2
Fe I	6079.02	1176	4.65	5.33	4.09	−1.65	330	.23	80	4.91	2	2
Fe I	6094.42	1177	4.65	5.96	4.48		259	.13	35	5.22	1	2
Fe I	5984.80	1260	4.73	4.91	3.48	−1.01	283	.41	140	4.62	3	2
Fe I	6055.99	1259	4.73	5.09	3.61	−1.18	353	.35	129	4.69	2	2
Fe I	6290.97	1258	4.73	5.22	3.72	−1.43	306	.31	96	4.79	2	5
Fe I	6330.86	1254	4.73	5.75	4.23	−1.85	282	.19	51	5.06	2	5
Fe I	6385.74	1253	4.73	6.40	4.83		281	.07	19	5.52	1	0
Fe I	6419.98	1258	4.73	5.04	3.60	−.98	305	.38	140	4.66	1	6
Fe I	5987.06	1260	4.79	5.14	3.67	−1.25	330	.30	108	4.77	4	2
Fe I	6078.50	1259	4.79	4.83	3.62	−1.21	283	.37	122	4.69	2	2
Fe I	6170.52	1260	4.79	5.21		−1.26	306	.39	137	4.65	2	3
Fe I	6364.38	1253	4.79	5.89	4.24	−1.92	352	.18	61	5.04	1	6
Fe I	6456.87	1256	4.79	6.08	4.89		302	.15	45	5.15	1	0
Fe I	6597.57	1253	4.79	5.59		−1.87	305	.20	66	5.00	1	7
Fe I	5975.35	1260	4.83	5.51	3.90	−1.33	330	.27	88	4.84	3	2
Fe I	6102.18	1259	4.83	4.95	3.60	−1.21	330	.35	113	4.72	2	3
Fe I	6103.19	1260	4.83	4.89		−1.48	388	.34	127	4.70	2	3
Fe I	6293.92	1260	4.83	6.23	4.65		288	.12	34	5.26	1	0
Fe I	6469.21	1258	4.83	5.44	3.83	−1.47	305	.27	86	4.86	2	6
Fe I	6495.78	1253	4.83	5.61	4.22	−1.63	316	.21	66	4.99	2	7
Fe I	5496.57	1281	4.91	6.31	4.79		249	.11	27	5.30	1	0
Fe I	5633.97	1314	4.99	5.11	3.85	−1.03	353	.39	147	4.61	1	17
Fe I	6089.57	1327	5.02	5.75	4.10	−1.62	377	.20	75	4.96	1	2
Fe I	5577.03	1314	5.03	6.16	4.67		202	.10	22	5.35	1	17
Fe I	5650.71	1314	5.08	5.67	4.14	−1.60	294	.23	72	4.91	4	19
Fe I	5650.01	1314	5.10	5.69	4.21	−1.42	274	.20	56	5.01	2	0
Fe II	4416.82	27	2.78	4.45		−1.42	313	.72	245	4.26	2	28
Fe II	4583.83	38	2.81	3.70		−.60	437	.77	366	4.10	4	30
Fe II	4620.51	38	2.83	5.05	3.97	−2.00	281	.51	159	4.48	4	30
Fe II	4515.34	37	2.84	4.51	2.72	−1.30	298	.70	228	4.30	2	0
Fe II	4576.33	38	2.84	4.87	3.46	−1.60	343	.61	224	4.31	5	30
Fe II	4582.84	37	2.84	5.01	3.79	−1.82	293	.53	157	4.47	2	30
Fe II	4491.40	37	2.85	4.66	3.29	−1.49	289	.65	206	4.34	3	0
Fe II	4508.28	38	2.85	4.51		−1.16	325	.70	249	4.26	2	29
Fe II	4731.44	43	2.89	4.52	3.26	−1.68	291	.57	179	4.42	3	0
Fe II	5256.89	41	2.89	5.77	4.43		303	.29	89	4.79	4	9
Fe II	5284.09	41	2.89	4.86	3.82	−1.85	312	.50	166	4.50	2	0
Fe II	6369.46	40	2.89	5.86			258	.25	75	4.91	1	6
Fe II	6432.65	40	2.89	5.47	4.42	−2.33	329	.38	134	4.67	4	6
Fe II	6516.06	40	2.89	5.14		−2.02	352	.47	178	4.55	3	7
Fe II	5991.38	46	3.15	5.62	4.31	−2.55	330	.30	106	4.77	1	2
Fe II	5425.27	49	3.20	5.21	4.30	−2.47	299	.39	123	4.65	2	0
Fe II	6084.11	46	3.20	5.77	4.67	−3.00	306	.28	85	4.84	2	2
Fe II	5234.62	49	3.22	4.64	3.15	−1.50	328	.61	219	4.38	2	26
Fe II	5325.56	49	3.22	5.25	4.08	−2.47	283	.41	136	4.60	3	9
Fe II	5414.09	48	3.22	5.52	4.49	−2.50	278	.34	104	4.72	1	10
Fe II	6113.33	46	3.22	5.90	4.73		296	.20	60	5.01	2	0
Fe II	5197.57	49	3.23	4.64	3.40	−1.58	355	.61	230	4.35	2	25

Table B

Spect	Wave-length	Mult	*EP*	−Log $X'_{\odot}$	−Log X'_{ϵ}	Log $(gf\lambda)$ $-\theta\chi$	*HW*	R_c	*W*	−Log (W/λ)	*Q*	*N*
Fe II	5337.73	48	3.23	5.43			298	.35	113	4.69	2	9
Fe II	5534.86	55	3.24	4.98	3.56	−1.92	354	.52	208	4.45	1	14
Fe II	5591.38	55	3.27	6.25	5.28		256	.12	31	5.26	2	0
Fe II	5264.80	48	3.33	5.26	3.99	−2.10	303	.44	147	4.57	1	9
Fe II	6149.24	74	3.89	5.58	4.28		377	.35	139	4.68	3	3
Fe II	6238.38	74	3.89	5.50	4.18	−2.03	353	.41	155	4.61	5	5
Fe II	6239.95	74	3.89	6.22	4.82		296	.17	51	5.09	1	0
Fe II	6247.56	74	3.89	5.38	4.10	−2.08	376	.42	170	4.58	4	5
Fe II	6416.91	74	3.89	5.42	4.33	−2.52	329	.32	111	4.76	3	6
Fe II	6456.38	74	3.90	5.28	4.05	−1.83	375	.49	206	4.50	2	6
Fe II	6446.43	199	6.22	6.75	5.24		279	.05	14	5.67	1	0
Gd II	4130.37	19	.60	5.65		3.07	241	.48	123	4.53	2	0
Gd II	4316.05	43	.66	5.68		2.26	377	.38	157	4.74	0	27
Gd II	4483.35	62	1.06	6.59		1.82	235	.27	59	4.86	2	29
Gd II	6305.15	94	1.31			1.15	286	.11	31	5.30	2	0
Gd II	5733.86	94	1.37	7.20		1.36	258	.10	26	5.35	3	0
Gd II	5951.60	95	1.37			1.00	257	.05	13	5.67	2	0
Gd II	5140.84	115	1.58		4.76	1.26	177	.11	19	5.31	0	24
Gd II	5815.85	112	1.58	6.91		1.00	254	.06	15	5.59	2	0
Gd II	5904.07	112	1.62			.99	255	.05	12	5.67	2	0
Gd II	6004.57	112	1.66			.97	258	.04	10	5.78	1	0
Gd II	6080.65	112	1.73			.97	265	.06	16	5.59	1	0
Ge I	4685.84	3	2.03	6.20		.08	216	.13	33	5.28	2	0
La II	4662.51	8	.00	6.04	4.72	1.68	264	.55	150	4.47	4	30
La II	5290.83	6	.00	6.04	5.07	1.18	281	.36	114	4.68	5	9
La II	5482.27	4	.00			.82	252	.29	78	4.83	1	13
La II	5808.31	4	.00	7.08		.70	265	.27	80	4.86	2	22
La II	4740.28	8	.13			1.78	339	.63	226	4.52	0	32
La II	5493.45	4	.13			.58	332	.36	119	4.87	0	13
La II	5805.78	4	.13		4.89	1.16	290	.41	128	4.64	3	22
La II	6172.72	4	.13	6.62		.46	330	.18	58	5.04	2	3
La II	4322.51	25	.17	5.60		1.82	251	.60	167	4.40	3	27
La II	5259.38	21	.17		4.95	1.04	285	.36	107	4.69	3	0
La II	5936.22	19	.17	7.09	5.75	.68	296	.24	73	4.91	2	0
La II	6320.39	19	.17	6.23	5.22	1.14	360	.44	168	4.58	3	0
La II	4804.05	37	.23	6.12		1.27	280	.48	142	4.53	2	32
La II	5880.63	35	.23	6.61		.77	308	.31	99	4.77	2	0
La II	5303.54	36	.32	6.37		1.26	298	.42	130	4.61	1	9
La II	6390.48	33	.32	6.54	5.36	1.16	329	.40	157	4.62	2	6
La II	4315.90	41	.40	6.04		.85	377	.38	157	4.74	0	27
La II	4699.64		.40			1.03	265	.31	79	4.77	3	32
La II	4526.12	50	.77	5.54	4.29	1.70	306	.53	185	4.43	1	29
La II	4559.28	53	.77	6.56		1.12	190	.34	71	4.76	5	29
La II	4716.44	52	.77			1.28	218	.34	81	4.74	4	32
La II	6067.14	48	.77			.02	236	.10	21	5.35	1	2
La II	6129.56	47	.77			.80	330	.26	91	4.85	1	3
La II	4748.73	65	.93	6.18	5.04	1.52	286	.43	122	4.59	2	32
La II	6126.09	69	1.25			.75	306	.23	69	5.02	0	3
La II	5769.06	70	1.26	6.50		1.06	403	.43	183	4.74	0	21
La II	4619.87	76	1.75	6.46		1.60	287	.43	126	4.58	2	30

Table B

Spect	Wave-length	Mult	EP	$-\text{Log } X'_{\odot}$	$-\text{Log } X'_{\epsilon}$	$\text{Log } (gf\lambda) - \theta\chi$	HW	R_c	W	$-\text{Log } (W/\lambda)$	Q	N
La II	5377.08	95	2.30	6.38	5.04	.95	270	.25	69	4.89	1	0
La II	5188.24	95	2.45	6.29		1.25	291	.27	87	4.81	1	25
La II	6399.05	104	2.64			.46	376	.11	38	5.30	2	6
Li I	6707.84	1	.00	6.53		4.01	420	.07	29	5.36	1	8
Mg I	4571.10	1	.00	3.97			281	.64	199	4.36	4	30
Mg I	5172.68	2	2.71	1.37	−.32	.27	670	.88	693	3.87	5	25
Mg I	5183.60	2	2.72	1.03	−.50	.48	772	.95	903	3.76	4	25
Mg I	4702.98	11	4.34	2.43	1.02	−1.81	324	.69	288	4.21	4	32
Mg I	4730.03	10	4.34	4.90	3.39	−3.28	267	.43	122	4.59	2	0
Mg I	5528.39	9	4.34	2.68	1.03	−1.79	354	.72	292	4.28	2	14
Mg I	5711.07	8	4.34	4.51	3.22	−2.69	328	.46	162	4.55	3	21
Mg I	6318.72	23	5.11	5.69			304	.19	59	5.03	2	0
Mg I	6319.22	23	5.11	6.08			293	.14	41	5.19	2	0
Mn I	5394.67	1	.00	4.47	2.78	.46	329	.44	154	4.56	4	10
Mn I	5432.55	1	.00	4.92	3.39	.03	330	.34	112	4.70	2	11
Mn I	5420.36	4	2.14	4.62	2.58	.10	316	.40	137	4.61	5	10
Mn I	5457.47	4	2.16	5.94	4.84	−.75	178	.08	15	5.46	1	13
Mn I	5470.64	4	2.16	5.16	2.99	−.05	293	.33	114	4.71	2	13
Mn I	5516.77	4	2.18	5.25	3.14	−.16	354	.28	107	4.77	2	14
Mn I	4754.04	16	2.28	3.60	2.05	1.23	249	.64	181	4.42	5	32
Mn I	4783.42	16	2.30	3.18	1.95	1.19	292	.65	209	4.36	3	32
Mn I	4451.59	22	2.89	4.22		1.07	235	.68	187	4.38	5	28
Mn I	4709.72	21	2.89	4.81	3.37	.35	249	.47	129	4.55	3	32
Mn I	4762.38	21	2.89	4.11	2.64	1.01	296	.59	189	4.40	2	0
Mn I	4502.22	22	2.92	5.00	3.48	.54	250	.41	102	4.63	1	29
Mn I	4766.42	21	2.92	4.36	2.77	.83	311	.52	163	4.47	2	32
Mn I	4453.00	22	2.94	5.06		.39	244	.38	97	4.66	2	0
Mn I	4470.14	22	2.94	5.00		.48	242	.36	91	4.69	2	0
Mn I	4739.11	21	2.94	4.93	3.52	.24	249	.41	108	4.63	3	32
Mn I	4765.86	21	2.94	4.67	3.27	.61	239	.45	115	4.59	2	32
Mn I	4761.53	21	2.95	4.62	3.14	.38	295	.46	146	4.53	4	32
Mn I	4457.04	28	3.07	5.23		−.12	232	.30	72	4.79	2	0
Mn I	6013.50	27	3.07	4.72	3.19	.16	330	.40	157	4.61	4	2
Mn I	6016.64	27	3.07	4.66	3.19	.31	330	.42	151	4.60	3	2
Mn I	6021.80	27	3.07	4.60	3.19	.46	306	.43	132	4.62	4	2
Mn I	5377.63	42	3.84	5.33	3.81	−.14	274	.27	76	4.85	2	0
Mn I	5399.49	42	3.85	5.43	4.11	−.45	324	.20	64	4.96	1	10
Mo I	5506.49	4	1.33	6.16		2.19	281	.27	78	4.85	1	0
Mo I	5533.01	4	1.33	6.06		2.02	280	.26	75	4.87	1	0
Mo I	5570.46	4	1.33	6.09		1.68	348	.19	66	4.98	1	17
Mo I	6030.66	5	1.53	6.75		1.34	271	.10	27	5.35	2	0
Mo I	4411.57		2.08	6.22		1.95	220	.24	54	4.91	1	0
Na I	5889.95	1	.00	1.52	.04	3.89	685	.82	649	3.96	4	1
Na I	5895.92	1	.00	1.73	.38	3.59	590	.77	507	4.07	4	1
Na I	4668.56	12	2.10	5.15	3.38	−.00	251	.35	92	4.71	2	0
Na I	4751.82	11	2.10	5.73	4.50	−.79	193	.13	29	5.22	1	32
Na I	5682.63	6	2.10	4.31	2.80	.71	303	.49	167	4.52	1	21
Na I	5688.19	6	2.10	4.07	2.41	.96	346	.55	204	4.44	2	0
Na I	6154.23	5	2.10	5.56	4.02	−.14	330	.24	100	4.85	1	3
Na I	6160.75	5	2.10	5.27	3.89	.16	377	.30	117	4.76	1	3

Table B

Spect	Wave-length	Mult	*EP*	$-\mathrm{Log}\ X'_{\odot}$	$-\mathrm{Log}\ X'_{\epsilon}$	$\mathrm{Log}\ (gf\lambda) - \theta\chi$	*HW*	R_c	*W*	$-\mathrm{Log}\ (W/\lambda)$	*Q*	*N*
Nb I	4573.08		.27			2.52	203	.08	16	5.46	2	0
Nb I	4606.77		.35	5.98		2.70	217	.16	35	5.12	2	0
Nd II	4451.99	6	.00			1.70	250	.53	141	4.67	0	28
Nd II	4706.54	3	.00			2.02	249	.56	136	4.48	4	32
Nd II	4799.42	2	.00			1.10	273	.39	111	4.94	0	32
Nd II	4069.27	20	.06	5.71		2.54	251	.58	157	4.41	2	0
Nd II	4475.57		.06			1.01	250	.30	73	4.79	2	29
Nd II	4612.47	3	.06	6.29		.89	312	.25	74	4.84	2	30
Nd II	4811.34	3	.06	5.73	4.64	1.70	268	.50	140	4.52	5	32
Nd II	6549.54		.06			.31	258	.15	32	5.22	2	7
Nd II	4563.22		.18			1.89	276	.54	161	4.45	3	0
Nd II	4059.97	63	.20	5.88		2.42	242	.52	135	4.48	2	0
Nd II	4446.39	49	.20	5.77		2.14	282	.61	194	4.36	4	28
Nd II	4567.61	49	.20	6.39		1.28	219	.30	68	4.81	3	30
Nd II	4594.45	52	.20			1.28	256	.32	84	4.75	1	30
Nd II	5212.35	44	.20	6.10		1.71	330	.46	152	4.54	3	25
Nd II	5255.51	43	.20	5.93		1.78	354	.55	230	4.40	2	9
Nd II	5753.53		.20			.61	328	.33	108	4.93	0	21
Nd II	6428.67		.20	7.14		.40	305	.20	69	4.99	2	6
Nd II	6591.43		.20			0.18	295	.09	27	5.39	2	0
Nd II	4109.45	10	.32	4.86		2.86	277	.74	246	4.22	2	0
Nd II	4133.35	19	.32	5.63		2.13	251	.55	148	4.44	2	0
Nd II	4358.17	10	.32	4.94		2.32	278	.64	202	4.33	3	0
Nd II	6550.19		.32			0.29	234	.20	54	5.04	1	7
Nd II	4485.95		.38			.97	250	.31	94	4.98	0	29
Nd II	4541.27	58	.38			1.87	276	.55	163	4.44	1	0
Nd II	6009.30		.38			.30	283	.09	21	5.40	1	2
Nd II	4818.96		.47			.66	248	.18	48	5.03	2	34
Nd II	5234.20	74	.55	5.90	4.78	1.84	392	.50	209	4.45	2	26
Nd II	5319.82	75	.55	5.76		1.87	374	.53	187	4.46	5	9
Nd II	5548.47	73	.55	6.42		.89	345	.27	102	4.79	1	15
Nd II	4462.99	50	.56	5.62		2.21	275	.64	201	4.35	3	29
Nd II	4797.16	60	.56	6.35		1.35	265	.39	108	4.65	2	0
Nd II	5361.17	46	.56			.83	260	.20	53	5.01	1	0
Nd II	5102.42		.68			1.45	311	.45	137	4.57	3	24
Nd II	5361.51	74	.68	5.88		1.62	341	.53	193	4.46	3	10
Nd II	5442.27	76	.68			1.11	304	.32	100	4.75	3	12
Nd II	4817.20		.74	6.59		.82	244	.26	65	4.87	2	0
Nd II	5385.89		.74	6.64		1.19	298	.34	108	4.71	1	10
Nd II	5702.24		.74			1.24	315	.34	115	4.71	2	21
Nd II	5804.02	79	.74			1.34	330	.38	134	4.65	3	22
Nd II	6539.94		.74			0.20	294	.10	28	5.36	2	0
Nd II	5293.17	75	.82	5.83		1.99	399	.53	217	4.43	2	9
Nd II	5181.16		.86	6.17		1.27	342	.33	122	4.68	3	25
Nd II	5276.88	81	.86	6.64		1.32	265	.35	102	4.71	4	9
Nd II	5306.47		.86	6.81		1.19	265	.24	60	4.93	2	9
Nd II	5416.38	80	.86	6.81		1.00	266	.22	60	4.96	3	0
Nd II	5811.61		.86			1.02	278	.24	77	4.89	2	22
Nd II	6365.55		.93			.34	235	.14	29	5.19	2	6
Nd II	5474.76		.99	6.66		.78	227	.21	54	4.99	2	13

Table B

Spect	Wave-length	Mult	EP	$-\text{Log } X'_{\odot}$	$-\text{Log } X'_{\epsilon}$	Log $(gf\lambda) - \theta\chi$	HW	R_c	W	$-\text{Log } (W/\lambda)$	Q	N
Nd II	5688.52	79	.99			1.44	318	.41	137	4.62	1	0
Nd II	5447.56		1.04			.69	290	.25	73	4.88	2	12
Nd II	5614.30	87	1.04			.68	353	.27	101	4.95	0	17
Nd II	5761.70		1.04			.61	323	.19	65	4.99	1	21
Nd II	5770.50		1.08			.75	302	.22	72	4.93	2	21
Nd II	5825.87		1.08			.95	302	.25	83	4.87	2	22
Nd II	5431.54	80	1.12	6.21		1.33	342	.27	98	4.79	4	11
Nd II	5740.90		1.16			.95	292	.27	81	4.85	2	0
Nd II	6385.20	85	1.16			.86	329	.18	61	5.04	1	6
Nd II	5356.98	80	1.26	6.56		1.38	316	.34	114	4.70	2	9
Nd II	5485.70	79	1.26	6.48		1.34	328	.36	119	4.68	4	13
Nd II	5842.38	86	1.28	6.72		.99	315	.21	73	4.94	2	22
Nd II	5744.77		1.35			.73	277	.21	62	4.97	1	21
Nd II	5769.87		1.35			.64	252	.14	35	5.19	1	21
Nd II	6382.07		1.44			.39	305	.13	41	5.22	2	6
Nd II	6034.24		1.54	6.93		.70	353	.25	85	5.00	0	2
Ni I	4331.64	52	1.68	4.71		.37	314	.56	179	4.41	3	27
Ni I	5102.97	49	1.68	5.11	3.69	−.53	328	.44	161	4.54	2	24
Ni I	5578.73	47	1.68	5.11	3.75	−.41	353	.45	168	4.54	3	17
Ni I	5748.34	45	1.68	5.50	4.29	−.88	291	.26	78	4.87	1	0
Ni I	5847.01	44	1.68	5.67	4.35	−1.10	297	.20	62	4.99	1	22
Ni I	6007.31	42	1.68	5.66	4.41	−1.05	306	.18	47	5.08	3	2
Ni I	6108.12	45	1.68	4.98	3.70	−.41	330	.38	132	4.66	1	3
Ni I	6128.98	42	1.68	5.65	4.34	−1.14	306	.19	58	5.03	1	3
Ni I	6327.60	44	1.68	5.36	4.07	−.90	318	.25	81	4.89	1	0
Ni I	6643.64	43	1.68	4.73		.06	328	.42	154	4.62	5	8
Ni I	5476.94	59	1.83	3.35		1.09	360	.69	285	4.28	2	0
Ni I	6177.26	58	1.83	6.00	4.47	−1.56	280	.11	31	5.30	1	0
Ni I	5754.68	68	1.93	4.76	3.62	−.06	302	.46	151	4.57	2	21
Ni I	6314.67	67	1.93	4.92		−.25	329	.41	140	4.64	5	5
Ni I	6482.81	66	1.93	5.37	4.04	−.49	258	.25	70	4.93	2	6
Ni I	5592.28	69	1.95	5.08		−.23	353	.44	176	4.54	3	17
Ni I	6586.33	64	1.95	5.43	4.12	−.63	281	.26	76	4.90	1	7
Ni I	5435.87	70	1.99	5.12	3.79	−.40	268	.34	101	4.73	3	11
Ni I	5892.88	68	1.99	4.88		−.27	401	.43	191	4.63	0	1
Ni I	4470.48	86	3.40	4.66		.40	282	.54	147	4.47	2	29
Ni I	4595.96	101	3.42	5.37		−.68	296	.49	151	4.85	0	30
Ni I	4648.66	98	3.42	4.75	2.87	.61	305	.52	161	4.47	2	30
Ni I	4604.99	98	3.48	4.84		.46	265	.49	132	4.53	3	30
Ni I	4756.52	98	3.48	4.64	3.26	.21	249	.47	139	4.54	2	32
Ni I	4686.22	98	3.60	4.97	3.40	−.08	234	.35	90	4.71	3	31
Ni I	4705.93	128	3.66	6.11	4.75	−1.24	206	.13	31	5.18	2	32
Ni I	4752.43	132	3.66	4.93	3.70	−.42	262	.39	107	4.65	2	0
Ni I	4812.00	130	3.66	5.62	4.27	−1.22	233	.22	58	4.94	3	32
Ni I	4807.00	163	3.68	4.78	3.79	−.29	279	.35	106	4.68	3	32
Ni I	4731.81	163	3.83	5.32	3.91	−.72	259	.38	103	4.66	3	0
Ni I	5462.49	192	3.85	5.43	4.15	−.86	329	.29	100	4.77	1	13
Ni I	5186.59	205	3.90	5.92	4.42	−1.42	190	.14	27	5.19	1	25
Ni I	5589.38	205	3.90	5.73	4.47	−1.13	240	.17	40	5.12	2	17
Ni I	5593.74	206	3.90	5.40	4.17	−.85	358	.30	98	4.77	2	17

Table B

Spect	Wave-length	Mult	EP	$-\text{Log } X'_{\odot}$	$-\text{Log } X'_{\epsilon}$	Log $(gf\lambda) - \theta\chi$	HW	R_c	W	$-\text{Log } (W/\lambda)$	Q	N
Ni I	5625.33	221	4.09	5.52	4.17	−.96	285	.26	76	4.87	2	0
Ni I	5694.99	220	4.09	5.45		−.82	278	.27	87	4.83	2	21
Ni I	6111.06	230	4.09	5.59	4.27	−1.32	288	.16	46	5.12	1	0
Ni I	6116.18	218	4.09	5.14		−.89	353	.29	104	4.79	2	3
Ni I	6175.42	217	4.09	5.59	4.07	−.90	353	.26	91	4.85	3	3
Ni I	6176.82	228	4.09	5.37	3.91	−.66	306	.30	97	4.80	4	3
Ni I	6204.64	226	4.09	6.02		−1.41	294	.12	41	5.26	3	4
Ni I	5494.89	231	4.10	5.91	4.58	−1.30	189	.08	14	5.46	1	13
Ni I	5641.88	234	4.10	5.78	4.45	−1.24	262	.17	48	5.08	2	19
Ni I	5682.20	232	4.10	5.28	4.03	−.68	328	.26	93	4.83	1	21
Ni I	5760.85	231	4.10	5.70	4.20	−.91	282	.22	69	4.94	1	21
Ni I	6186.74	229	4.10	5.87	4.33	−1.28	259	.17	40	5.14	2	4
Ni I	6223.99	228	4.10	5.82		−1.34	306	.16	49	5.11	2	5
Ni I	5614.78	250	4.15	5.48		−.84	252	.23	68	4.93	1	17
Ni I	6322.17	249	4.15	5.95	4.55	−1.53	287	.11	31	5.30	2	0
Ni I	6378.26	247	4.15	5.78	4.33	−1.09	300	.16	48	5.12	1	0
Ni I	6414.60	244	4.15	6.07	4.68	−1.23	291	.11	32	5.30	1	0
Ni I	4551.24	236	4.17	5.69	3.97	−1.17	219	.52	128	4.98	0	29
Ni I	5805.23	234	4.17	5.52	4.15	−.96	290	.21	64	4.97	3	22
Ni I	6360.80	229	4.17	6.04	4.52	−1.49	297	.15	45	5.15	2	0
Ni I	6366.48	230	4.17	5.81	4.25	−1.28	423	.15	60	5.08	1	6
Ni I	5996.74	249	4.23	5.94	4.55	−1.54	274	.12	33	5.26	1	0
Ni I	6086.29	249	4.26	5.49	4.15	−1.13	353	.23	72	4.93	2	2
Ni I	6635.15	264	4.42	6.00	4.44	−1.36	351	.13	40	5.22	2	8
O I	6300.31	1	.00	6.18			288	.12	34	5.26	1	0
O I	6363.79	1	.02	6.63			282	.08	22	5.46	3	0
Pb I	4057.81	1	1.32	5.53		2.47	227	.41	98	4.62	1	0
Pr II	4408.84	4	.00	5.67		2.81	293	.71	233	4.28	2	0
Pr II	4612.07		.00	6.14		1.67	287	.23	69	4.88	2	30
Pr II	4413.76	26	.22	6.14		2.16	265	.53	151	4.47	2	0
Pr II	4570.61		.22	6.39		1.35	187	.14	27	5.19	1	30
Pr II	4510.16	20	.42	6.53		2.42	313	.55	180	4.42	3	29
Pr II	5322.78	35	.48	6.49		2.03	291	.37	113	4.67	5	9
Pr II	5352.41		.48	6.77		1.70	260	.20	53	5.01	2	0
Pr II	5259.74	35	.63	6.32	5.33	2.22	286	.37	111	4.68	3	0
Pr II	5219.03	37	.79	6.41		1.93	240	.28	71	4.85	3	26
Pr II	6165.95	39	.92	6.59	5.36	1.73	283	.17	54	5.07	1	3
Pr II	6025.72		1.44			1.42	259	.11	30	5.30	2	2
Ru I	4584.44	5	1.00	6.60		2.37	206	.10	20	5.35	1	0
Ru I	4709.48	14	1.13	6.26		2.19	204	.05	10	5.67	1	0
S I	4694.13	2	6.52	6.27	4.65	−5.46	226	.19	43	5.03	1	0
S I	4695.45	2	6.52	6.45	4.83	−5.60	218	.14	31	5.19	1	0
S I	4696.25	2	6.52	6.45	4.93	−5.85	226	.19	43	5.03	1	0
S I	5278.96	4	6.86	6.62		−6.13	241	.12	29	5.26	1	0
S I	5696.63	11	7.86	7.01			246	.05	12	5.67	1	0
S I	6046.04	10	7.87	6.39	4.27		276	.12	33	5.26	1	0
S I	6052.66	10	7.87	6.55	4.67	−6.18	287	.17	49	5.09	2	0
Sc I	6210.68	2	.00	6.50	5.18	2.22	273	.07	19	5.52	2	0
Sc I	6239.41	2	.00	6.04	5.40	1.37	285	.12	34	5.26	2	0
Sc I	6305.67	2	.02	6.28		2.29	286	.11	31	5.30	1	0

Table B

Spect	Wave-length	Mult	EP	$-\text{Log } X'_{\odot}$	$-\text{Log } X'_{\epsilon}$	Log $(gf\lambda) - \theta\chi$	HW	R_c	W	$-\text{Log } (W/\lambda)$	Q	N
Sc I	5700.23	12	1.43	5.75		2.32	303	.25	78	4.88	3	21
Sc I	5686.84	12	1.44	5.85		2.38	260	.12	31	5.26	2	0
Sc I	4743.81	14	1.45	5.97	4.93	2.43	212	.09	19	5.40	1	0
Sc I	5671.81	12	1.45	5.78	4.67	2.47	261	.13	34	5.22	2	0
Sc I	5484.62	16	1.85	6.46		1.98	235	.04	9	5.78	1	0
Sc I	5355.73	19	1.95	6.34		1.59	239	.09	21	5.40	2	0
Sc II	4325.01	15	.60	3.48		2.63	302	.81	280	4.19	3	0
Sc II	4415.56	14	.60	4.06		2.17	282	.73	238	4.27	2	28
Sc II	4431.37	14	.61	5.15		.86	257	.47	126	4.54	2	28
Sc II	6604.60	19	1.36	5.36	4.39	.82	351	.36	133	4.69	4	7
Sc II	5239.82	26	1.45	4.89	3.78	1.67	303	.53	179	4.47	5	26
Sc II	5640.97	29	1.50	5.23	3.93	.97	312	.45	155	4.56	2	17
Sc II	5667.16	29	1.50	5.50	4.31	.79	297	.40	125	4.64	2	18
Sc II	6279.76	28	1.50	5.60	4.55	.69	335	.34	119	4.72	3	0
Sc II	6309.90	28	1.50	5.62		.45	310	.22	70	4.96	2	0
Sc II	6320.85	28	1.50	6.19	4.96	.23	304	.19	59	5.03	2	0
Sc II	5657.87	29	1.51	4.83	3.86	1.46	306	.55	193	4.46	4	17
Sc II	5684.19	29	1.51	5.27	4.28	1.05	327	.46	160	4.55	2	0
Sc II	6245.63	28	1.51	5.45	4.32	1.12	329	.39	130	4.66	3	5
Sc II	5526.81	31	1.77	4.64	3.64	1.88	328	.63	217	4.41	5	14
Si I	4102.94	2	1.91	3.71		−1.45	261	.63	198	4.32	2	0
Si I	5665.55	10	4.92	5.55	4.05	−3.38	364	.24	89	4.85	3	20
Si I	5645.61	10	4.93	5.65		−3.47	280	.24	74	4.90	2	19
Si I	5690.42	10	4.93	5.34	4.03	−3.25	366	.26	92	4.83	4	21
Si I	5701.10	10	4.93	5.55	3.87	−3.41	303	.24	75	4.90	1	21
Si I	5793.07	9	4.93	5.60	4.10	−3.37	325	.27	92	4.82	3	21
Si I	5684.48	11	4.95	5.20	3.87	−3.06	310	.37	120	4.68	2	0
Si I	5772.14	17	5.08	5.47		−3.34	348	.31	106	4.75	2	21
Si I	5948.55	16	5.08	4.89	3.44	−2.86	354	.38	137	4.65	4	1
Si I	5666.68		5.61	5.98			245	.16	42	5.13	2	18
Si I	5753.62		5.61	5.48			328	.33	108	4.83	0	21
Si I	6125.02	30	5.61	5.74	4.38		259	.19	52	5.05	3	3
Si I	6131.57	30	5.61	5.93	4.49		292	.18	52	5.07	2	0
Si I	6145.02	29	5.61	5.71	4.32		302	.22	67	4.96	2	0
Si I	6237.32	28	5.61	5.39	3.84		353	.29	108	4.79	3	5
Si I	6243.81	28	5.61	5.64	4.18		318	.27	88	4.85	2	0
Si I	6244.47	27	5.61	5.60	4.27		316	.26	85	4.87	2	0
Si I	5675.73		5.62	6.26			253	.18	49	5.06	1	21
Si I	6142.49	30	5.62	5.79	4.34		296	.19	57	5.03	1	0
Si I	6155.13	29	5.62	5.20	3.51		330	.33	105	4.75	3	3
Si I	6407.27		5.87	5.98			399	.19	68	5.00	1	6
Si I	6414.97		5.87	5.65			309	.19	59	5.03	2	0
Si II	6347.10	2	8.12	5.74		−4.66	322	.27	88	4.86	2	0
Si II	6371.36	2	8.12	6.20		−4.96	307	.19	59	5.03	2	0
Sm II	4704.40	1	.00	6.09	4.39	1.98	243	.37	88	4.70	4	32
Sm II	4604.18		.04			1.58	218	.29	74	4.80	1	30
Sm II	4676.91	3	.04	6.15	4.87	2.09	296	.37	109	4.65	3	31
Sm II	4458.52	7	.10			2.27	260	.48	133	4.53	3	0
Sm II	4475.18		.10			1.12	214	.18	39	5.06	1	0
Sm II	4791.58	7	.10	6.30		1.59	229	.18	42	5.06	3	0

Table B

Spect	Wave-length	Mult	*EP*	−Log $X'_{\odot}$	−Log X'_{ϵ}	Log $(gf\lambda)$ $-\theta\chi$	*HW*	R_c	*W*	−Log (W/λ)	*Q*	*N*
Sm II	4329.02	15	.18	5.60		2.54	282	.45	129	4.54	2	27
Sm II	4472.43		.18	6.15		1.93	240	.35	88	4.71	1	0
Sm II	4591.82	14	.18	6.51		1.70	242	.32	80	4.76	1	0
Sm II	4615.69	22	.19	5.78		1.89	263	.44	122	4.58	2	0
Sm II	4499.48	23	.25	6.39		1.80	243	.36	92	4.69	2	0
Sm II	4505.05		.25			1.48	218	.20	44	5.01	1	0
Sm II	4577.69	23	.25	6.11		1.99	265	.40	109	4.63	1	30
Sm II	4318.94	27	.28	5.69		2.56	308	.53	172	4.43	1	27
Sm II	4452.73	26	.28	5.89		2.37	267	.53	152	4.47	3	0
Sm II	4566.21	32	.33	5.84	4.84	1.90	234	.35	83	4.72	2	30
Sm II	5312.23		.33			.68	232	.06	14	5.59	1	0
Sm II	4421.14	37	.38	5.71		2.22	263	.53	151	4.47	3	28
Sm II	4434.32	36	.38	5.52		2.48	271	.56	163	4.43	5	0
Sm II	4642.24	36	.38	5.86	4.68	2.14	299	.47	152	4.51	2	30
Sm II	4523.91	41	.43	5.68	4.39	2.03	275	.46	122	4.56	3	29
Sm II	4362.04	45	.48	6.01		2.17	298	.52	167	4.45	2	27
Sm II	4424.34	45	.48			2.71	278	.61	189	4.37	4	0
Sm II	4537.96	45	.48	6.07	5.01	2.07	281	.51	142	4.50	3	29
Sm II	4655.13		.48			1.36	227	.21	49	4.98	2	0
Sm II	4519.63	49	.54	6.04	4.70	2.16	256	.51	141	4.50	4	29
Sm II	4467.34	53	.66	5.84		2.55	270	.54	156	4.46	2	0
Sm II	5836.37		1.00			.65	252	.05	12	5.67	1	0
Sm II	6307.06		1.06			.55	273	.05	13	5.67	1	0
Sm II	6267.28		1.17			.98	273	.06	16	5.59	1	0
Sm II	6484.52		1.26			.52	278	.04	11	5.78	1	0
Sm II	6589.72		1.27			1.02	287	.06	17	5.59	1	0
Sm II	6472.34		1.38			.59	280	.05	14	5.67	1	0
Sm II	6291.82		1.41			.67	274	.06	16	5.59	1	0
Sm II	6542.76		1.46			.66	288	.07	20	5.52	1	0
Sm II	6693.55		1.69			.76	294	.07	20	5.52	1	0
Sm II	6426.63		1.75			.56	280	.06	16	5.59	1	0
Sr I	4607.35	2	.00	4.99	3.97	4.00	286	.59	183	4.40	2	0
Sr I	6504.00	8	2.26	6.86		1.52	300	.13	39	5.22	2	0
Sr I	6408.47	8	2.27	6.57	5.04	1.64	311	.20	63	5.01	2	0
Sr I	6550.24	12	2.69	6.70	5.23	.95	234	.20	54	5.04	1	7
Ti I	4656.47	6	.00	4.64	2.94	2.52	271	.47	135	4.54	3	30
Ti I	5192.97	4	.02	4.32	2.98	2.74	319	.57	196	4.42	3	0
Ti I	5219.70	4	.02	5.31	4.23	1.80	253	.27	70	4.86	1	26
Ti I	5426.26	3	.02	6.02	4.95	1.23	201	.09	16	5.40	2	11
Ti I	4681.91	6	.05	4.47	3.06	2.62	284	.55	168	4.44	1	0
Ti I	5210.39	4	.05	4.23	2.82	2.76	304	.55	187	4.44	3	25
Ti I	5460.50	3	.05	5.84	4.66	1.31	251	.13	33	5.22	1	0
Ti I	4527.31	42	.81	4.46	2.94	2.46	306	.71	226	4.50	0	29
Ti I	4326.36	43	.83	5.35		1.80	226	.31	73	4.77	1	0
Ti I	4518.03	42	.83	4.55	2.97	2.57	263	.54	144	4.48	2	29
Ti I	4548.76	42	.83	4.55	3.15	2.54	250	.50	132	4.52	3	29
Ti I	4771.10	41	.83	5.46			224	.15	37	5.13	1	32
Ti I	5338.33	35	.83	5.72	4.77		316	.13	38	5.22	1	9
Ti I	4512.75	42	.84	4.67	3.33	2.46	271	.53	154	4.47	3	0
Ti I	4534.79	42	.84	4.22	2.73	3.12	281	.62	189	4.38	4	29

Table B

Spect	Wave-length	Mult	EP	$-$Log $X'_{\odot}$	$-$Log X'_{ϵ}	Log $(gf\lambda)$ $-\theta\chi$	HW	R_c	W	$-$Log (W/λ)	Q	N
Ti I	4758.91	41	.84	6.19	4.88		174	.10	17	5.35	1	32
Ti I	4533.27	42	.85	4.05	2.44	3.34	281	.67	215	4.32	2	29
Ti I	4555.49	42	.85	4.72	3.50	2.41	275	.54	160	4.46	2	0
Ti I	5238.56	37	.85	5.65		1.57	202	.17	38	5.11	2	26
Ti I	5282.38	74	1.05	5.48	4.43	1.10	278	.14	39	5.19	2	9
Ti I	5300.01	74	1.05	5.51	4.71		253	.13	31	5.22	1	9
Ti I	6064.63	69	1.05	6.07	4.83	1.43	271	.09	24	5.40	1	0
Ti I	6085.26	69	1.05	5.21		1.48	306	.25	81	4.88	3	2
Ti I	4675.12	77	1.07	5.23	4.02	1.36	218	.27	66	4.85	2	31
Ti I	5295.78	74	1.07	5.85	4.66	1.27	253	.11	29	5.30	1	9
Ti I	6126.22	69	1.07	5.61	4.42	1.47	306	.23	69	5.02	0	3
Ti I	4453.31	113	1.43	4.66		2.42	260	.48	133	4.53	1	0
Ti I	6261.10	104	1.43	5.27		1.82	329	.29	98	4.81	3	5
Ti I	5453.65	108	1.44	6.29	5.06	.97	178	.07	13	5.52	1	13
Ti I	5471.20	106	1.44	6.10	4.92	1.27	252	.13	35	5.19	1	0
Ti I	6258.11	104	1.44	5.24		1.93	282	.29	93	4.82	1	5
Ti I	6554.23	102	1.44	5.84	4.59	1.14	351	.17	58	5.07	1	7
Ti I	5145.47	109	1.46	5.19	4.16	1.87	264	.28	76	4.83	1	0
Ti I	5490.15	107	1.46	5.64	4.51	1.56	214	.14	30	5.19	1	13
Ti I	6258.71	104	1.46	5.22		1.93	306	.40	144	4.63	1	5
Ti I	4623.10	145	1.74	4.96	3.49	2.10	274	.38	98	4.67	3	30
Ti I	4617.27	145	1.75	4.90	3.84	2.40	234	.39	99	4.66	5	30
Ti I	4453.71	160	1.87	5.15		1.90	250	.32	77	4.76	3	28
Ti I	5978.54	154	1.87	5.68	4.41	1.75	306	.18	55	5.05	1	2
Ti I	5965.83	154	1.88	5.60	4.16	1.61	377	.20	76	4.95	1	1
Ti I	5953.16	154	1.89	5.38	4.06	1.76	291	.21	62	4.98	1	0
Ti I	5201.10	183	2.09	5.91	4.65	1.14	190	.09	18	5.40	3	25
Ti I	5194.04	183	2.10	5.96	4.60	1.27	228	.12	26	5.26	3	25
Ti I	4503.76	184	2.13	5.99		1.01	244	.13	32	5.22	2	29
Ti I	4778.26	232	2.24	5.72		1.17	187	.13	29	5.22	2	32
Ti I	4759.27	233	2.25	5.13	4.02	1.86	264	.32	82	4.76	3	32
Ti I	5739.46	228	2.25	6.20	4.97	1.19	252	.07	17	5.52	1	0
Ti I	5689.47	249	2.30	5.97	4.82	1.23	240	.13	31	5.22	1	21
Ti I	4796.21	260	2.33	5.51	4.47	.99	218	.15	32	5.16	1	32
Ti I	5488.20	265	2.40	5.74	4.54	1.19	247	.17	45	5.15	0	13
Ti I	5648.57	269	2.49	6.03	4.88	1.11	204	.11	25	5.30	2	19
Ti I	5766.33	309	3.29	6.19	4.99	.84	257	.09	23	5.40	1	0
Ti II	4443.80	19	1.08	3.43	1.45	1.79	363	.81	321	4.14	4	28
Ti II	4493.50	18	1.08	5.30	3.73	$-.30$	338	.56	188	4.41	3	29
Ti II	4798.54	17	1.08	4.86	4.04		283	.50	151	4.50	2	0
Ti II	4806.33	17	1.08	6.03			271	.21	59	4.94	2	32
Ti II	4501.27	31	1.12	3.72	1.38	1.66	469	.83	409	4.04	4	29
Ti II	4468.50	31	1.13	3.54	1.47	1.85	501	.85	444	4.00	3	29
Ti II	4320.96	41	1.16	4.52		.13	288	.72	237	4.26	1	0
Ti II	4417.72	40	1.16	3.94	2.21	1.26	338	.77	276	4.20	3	28
Ti II	4470.86	40	1.16	4.73	2.70	.58	294	.68	202	4.35	2	29
Ti II	4583.44	39	1.16	5.34	3.92		250	.44	120	4.58	1	30
Ti II	4636.35	38	1.16	5.66	4.43		306	.41	124	4.59	2	30
Ti II	4609.26	39	1.18	5.76	4.62		275	.34	96	4.70	3	30
Ti II	4394.06	51	1.22	4.38	2.36	.86	307	.71	241	4.26	3	28

Table B

Spect	Wave-length	Mult	EP	$-\text{Log } X'_{\odot}$	$-\text{Log } X'_{\epsilon}$	Log $(gf\lambda) - \theta\chi$	HW	R_c	W	$-\text{Log } (W/\lambda)$	Q	N
Ti II	4563.76	50	1.22	3.59	1.40	1.49	387	.79	368	4.09	3	30
Ti II	4568.31	60	1.22	5.35	4.11	.42	250	.39	96	4.66	4	30
Ti II	4391.03	61	1.23	5.12		.29	445	.74	350	4.60	0	28
Ti II	4524.73	60	1.23	5.53	3.79	.27	264	.48	135	4.53	2	0
Ti II	4395.85	61	1.24	4.59	3.18	.65	290	.70	228	4.28	2	0
Ti II	4399.77	51	1.24	3.60	1.63	1.23	301	.77	260	4.23	3	0
Ti II	4418.35	51	1.24	4.41	2.27	.65	301	.65	222	4.30	3	28
Ti II	4533.97	50	1.24	3.78		1.69	500	.85	438	4.02	4	29
Ti II	4544.01	60	1.24	5.12	3.56	.25	312	.63	214	4.53	0	29
Ti II	4589.96	50	1.24	4.47	2.87	.72	306	.68	229	4.30	5	30
Ti II	4657.21	59	1.24	5.08	3.60		286	.57	176	4.42	1	0
Ti II	4708.66	49	1.24	4.93	3.82		278	.50	148	4.50	2	0
Ti II	4764.54	48	1.24	5.25	3.84		273	.45	130	4.56	2	0
Ti II	5336.81	69	1.58	4.67	3.66	.36	334	.60	216	4.39	2	0
Ti II	5418.80	69	1.58	5.03	4.00	−.06	329	.50	179	4.49	2	10
Ti II	5185.91	86	1.89	4.87			349	.53	201	4.44	3	25
Ti II	4316.81	94	2.05	5.11	3.75	.38	267	.50	135	4.50	2	27
Ti II	4780.00	92	2.05	4.50	3.62		286	.58	174	4.43	3	32
Ti II	4805.10	92	2.06	4.14		.72	311	.64	223	4.33	3	32
Ti II	6491.58	91	2.06	5.28			305	.37	117	4.71	2	6
Ti II	5211.54	103	2.59	5.47	4.19	−.35	304	.39	135	4.62	3	25
V I	4330.02	5	.00	4.96		2.41	237	.38	95	4.66	2	0
V I	4577.17	4	.00	5.22		2.40	234	.30	74	4.79	3	30
V I	4580.39	4	.02	4.87		2.50	375	.46	183	4.76	0	30
V I	4586.36	4	.04	4.95		2.60	312	.40	145	4.85	0	30
V I	4416.47	22	.27	4.99		2.49	244	.39	100	4.65	1	0
V I	6274.67	19	.27	6.07	4.88	1.66	291	.14	41	5.19	2	0
V I	4389.97	22	.28	4.07		3.37	279	.63	198	4.35	1	0
V I	6216.37	19	.28	5.33	4.23	2.08	329	.20	66	4.99	2	5
V I	6256.91	19	.28	6.36		1.36	273	.06	16	5.59	2	0
V I	6285.18	19	.28	6.00	4.84	1.72	276	.07	19	5.52	2	0
V I	4459.76	21	.29	4.76		2.68	211	.38	82	4.70	4	28
V I	6199.20	19	.29	5.95		2.09	281	.11	31	5.30	2	0
V I	6251.83	19	.29	5.81		1.88	288	.13	37	5.22	1	0
V I	6292.86	19	.29	5.90	4.68	1.72	299	.17	51	5.09	2	0
V I	4379.24	22	.30	3.60		3.78	226	.63	157	4.45	3	27
V I	4406.65	22	.30	4.17		3.05	282	.56	171	4.42	4	28
V I	6213.87	20	.30	6.36	4.91	1.54	275	.08	22	5.46	1	0
V I	6243.11	19	.30	5.46	4.11	2.28	307	.22	69	4.96	1	0
V I	6111.62	34	1.04	5.84	4.73	1.78	271	.08	21	5.46	2	0
V I	5703.56	35	1.05	5.43	4.24	2.32	279	.21	59	4.98	2	0
V I	6081.42	34	1.05	5.74	4.58	2.01	286	.16	46	5.12	2	0
V I	6135.36	34	1.05	5.84	4.76	1.78	280	.12	34	5.26	2	0
V I	5698.53	35	1.06	5.27		2.44	434	.31	133	4.70	2	21
V I	5737.07	35	1.06	5.85	4.68	1.71	256	.09	23	5.40	1	0
V I	6039.69	34	1.06	5.87	4.69	1.99	306	.11	35	5.30	1	2
V I	6119.51	34	1.06	5.61	4.40	2.11	306	.18	56	5.05	2	3
V I	5727.02	35	1.08	5.23	3.87	2.28	302	.32	100	4.76	2	0
V I	6090.18	34	1.08	5.41	4.29	2.43	330	.21	61	4.99	1	2
V I	6452.32	48	1.19	6.17	5.14	1.16	281	.06	17	5.59	1	0

Table B

Spect	Wave-length	Mult	EP	$-\text{Log } X'_{\odot}$	$-\text{Log } X'_{\epsilon}$	Log $(gf\lambda)$ $-\theta\chi$	HW	R_c	W	$-\text{Log } (W/\lambda)$	Q	N
V I	4758.74	51	1.22	5.79	4.81		196	.10	23	5.35	1	32
V I	4452.01	87	1.87	5.48		2.24	250	.53	141	4.98	0	28
V I	5507.75	129	2.36	6.59	5.47	1.03	121	.05	6	5.67	1	14
W I	4074.37	6	.37	5.38		2.56	225	.39	92	4.65	1	0
Y I	4643.70	4	.00		4.67	2.76	254	.38	101	4.66	1	0
Y I	4760.98	4	.07	6.30		2.02	228	.18	41	5.06	1	0
Y I	6435.02	2	.07	6.64	5.57	2.14	305	.18	54	5.07	2	6
Y I	4505.95	14	1.37	6.50		2.06	212	.16	34	5.12	1	0
Y I	5527.54	12	1.40			1.91	258	.15	39	5.15	2	0
Y II	4422.59	5	.10			1.95	407	.77	333	4.32	0	28
Y II	4398.02	5	.13	4.76		2.26	382	.81	325	4.13	2	28
Y II	5119.12	20	.99	5.68	4.56	.95	379	.56	219	4.40	2	24
Y II	5200.42	20	.99	5.16	3.79	1.61	343	.70	291	4.25	3	0
Y II	5509.91	19	.99	5.57		.99	379	.65	265	4.32	4	14
Y II	5289.82	20	1.03	6.45		.39	278	.45	136	4.58	5	9
Y II	5320.80	20	1.08	6.16		.25	277	.30	86	4.79	1	0
Y II	5521.59	27	1.74	6.20		.60	349	.46	180	4.52	2	14
Y II	5544.61	27	1.74	6.04	5.08	.60	318	.48	172	4.52	1	15
Y II	5546.03	27	1.75	6.13		.47	339	.52	194	4.47	2	15
Y II	6613.75	26	1.75	6.41		.55	351	.39	146	4.65	4	7
Y II	5402.78	35	1.84	5.86		.88	303	.53	170	4.48	4	10
Y II	5728.91	34	1.84	6.30		.37	303	.42	141	4.61	4	21
Zn I	4722.16	2	4.03	4.89	3.69	−.19	280	.55	169	4.45	5	32
Zn I	4810.55	2	4.08	4.58	3.77	−.07	276	.46	141	4.54	5	32
Zn I	6362.35	6	5.79	6.03	4.31	−2.30	311	.21	66	4.98	1	0
Zr I	4575.52	5	.00	5.69	4.62	2.30	250	.27	65	4.85	3	30
Zr I	6134.58	2	.00	6.26	5.49	1.90	235	.15	35	5.20	1	3
Zr I	6143.23	2	.07	6.41	5.34	2.03	298	.20	60	5.01	2	0
Zr I	6127.49	2	.15	6.27	5.33	2.22	259	.15	37	5.18	2	3
Zr I	4772.32	43	.62	5.92	5.07	2.41	218	.28	71	4.83	3	32
Zr I	4784.94	44	.69	6.75		1.78	187	.12	26	5.26	1	32
Zr I	4805.88	43	.69	6.46		1.86	186	.15	27	5.20	2	32
Zr I	4687.80	43	.73	5.90		2.84	252	.36	95	4.69	3	31
Zr I	6313.05	65	1.58	6.95		1.64	283	.09	27	5.38	2	0
Zr I	4719.12	66	1.86	6.48		1.62	218	.10	21	5.35	2	32
Zr I	4602.54		1.87	6.39		1.90	218	.18	44	5.04	1	30
Zr II	4317.32	40	.71	5.61		1.40	251	.61	167	4.41	2	27
Zr II	4613.95	67	.97	5.23	4.11		277	.53	157	4.47	2	0
Zr II	4071.09	54	1.00	5.48			247	.55	146	4.44	2	0
Zr II	4403.35	79	1.18			1.28	286	.67	215	4.31	2	0
Zr II	4414.54	79	1.24	5.37		1.26	301	.63	210	4.32	2	28
Zr II	4379.78	88	1.53			1.81	251	.63	183	4.38	3	27
Zr II	5112.28	95	1.66	6.00	4.84	.93	278	.49	155	4.52	3	24
Zr II	6114.78	93	1.66	6.78	5.50		306	.27	83	4.86	1	3
Zr II	6106.47	106	1.76	6.43			353	.25	88	4.87	3	3
Zr II	4333.28	132	2.41			.95	298	.45	145	4.52	2	27

A.5. References

ADAMS, W. S., and RUSSELL, H. N.
1928 Astrophys. J. **68,** 9
ALLER, L. A.
1963 Astrophysics, 2d ed. (Ronald Press Co., New York)
ALLER, L. H., and GREENSTEIN, J. L.
1960 Astrophys. J. Suppl. **5,** No. 46, 139
ALLER, L. H., and PIERCE, A. K.
1952 Astrophys. J. **116,** 176
BIDELMAN, W. P., and KEENAN, P. C.
1951 Astrophys. J. **114,** 473
BOND, H. E., and NEFF, J. S.
1969 Astrophys. J. **158,** 1235
BONSACK, W. K.
1959 Astrophys. J. **130,** 843
BOZMAN, W. R., CORLISS, C. H., and TECH, J. L.
1968 J. Res. Nat. Bur. Stand. (U.S.), **72A** (Phys. and Chem.), 559
BURBIDGE, E. M., and BURBIDGE, G. R.
1957 Astrophys. J. **126,** 357
1958 Handbuch der Physik, Vol. II (Springer Verlag, Berlin), p. 134
BURBIDGE, E. M., BURBIDGE, G. R., FOWLER, W. A., and HOYLE, F.
1957 Rev. Mod. Phys. **29,** 547
CAMERON, R. C., ed.
1967 The Magnetic and Related Stars (Mono Book Corporation, Baltimore)
CARTER, W. W.
1949 Phys. Rev. **76,** 962
CAYREL, G., and CAYREL, R.
1963 Astrophys. J. **137,** 431
CAYREL, R., and CAYREL DE STROBEL, G.
1966 Ann. Rev. Astron. and Astrophys. **4,** 1
CAYREL, R., and JUGAKU, J.
1963 Ann. d'Astrophys. **26,** 495
CHROMEY, F. R., FABER, S. M., WOOD, A., and DANZIGER, I. J.
1969 Astrophys. J. **158,** 599
CORLISS, C. H., and BOZMAN, W. R.
1962 Experimental Transition Probabilities for Spectral Lines of Seventy Elements. (Nat. Bur. Stand. (U.S.), Monogr. 53)
CORLISS, C. H., and TECH, J. L.
1968 Oscillator Strengths and Transition Probabilities for 3288 Lines of Fe I (Nat. Bur. Stand. (U.S.), Monogr. 108)
COWLEY, C. R.
1968 Astrophys. J. **153,** 169
COWLEY, C. R., and COWLEY, A. P.
1964 Astrophys. J. **140,** 713
DANZIGER, I. J.
1965 Mon. Not. Roy. Astron. Soc. **131,** 51
DE GALAN, L.
1968 (private communication) Cf. Spectrochim. Acta **23B,** 521 (1968)
GARSTANG, R. H.
1952 Publ. Astron. Soc. Pac. **64,** 227
GOLDSCHMIDT, Z.
1968 Unpublished energy levels for Ce II (private communication)
GOLDBERG, L., MÜLLER, E. A., and ALLER, L. A.
1960 Astrophys. J. Suppl. **5,** No. 45, 1
GORDON, C. P.
1968 Astrophys. J. **153,** 915
GREENSTEIN, J. L.
1948 Astrophys. J. **107,** 151
1949 Astrophys. J. **109,** 121
1954 Mem. in 8° Soc. Roy. Sci. Liege (4) **14,** 307
GREENSTEIN, J. L., and RICHARDSON, R. S.
1951 Astrophys. J. **113,** 536
GRIFFIN, R., and GRIFFIN, R.
1967 Mon. Not. Roy. Astron. Soc. **137,** 253
GROTH, H. G.
1961 Zeit. für Astrophys. **51,** 231
HARRISON, G. R.
1939 MIT Wavelength Tables (John Wiley & Sons, New York)
VAN DER HELD, E. F. M.
1931 Zeit. für Physik **70,** 508
HELFER, H. L., WALLERSTEIN, G., and GREENSTEIN, J. L.
1959 Astrophys. J. **129,** 700
HUNGER, K.
1956 Zeit. für Astrophys. **39,** 36
KING, A. S.
1933 Astrophys. J. **78,** 9
KOELBLOED, D.
1953 Publ. Astron. Inst. Amst., No. 10
1967 Astrophys. J. **149,** 299
KULI-ZADE, D. M.
1968 Astronomicheskii Zhurnal **45,** 69
MAURY, A. C.
1897 Harvard Ann. **28,** 97, remark **111**
MEGGERS, W. F., CORLISS, C. H., and SCRIBNER, B. F.
1961 Tables of Spectral Line Intensities (Nat. Bur. Stand. (U.S.), Monogr. 32)
MERRILL, P. W.
1952 Astrophys. J. **116,** 21
MILES, B. M., and WIESE, W. L.
1969 Critically Evaluated Transition Probabilities for Ba I and II (Nat. Bur. Stand. (U.S.), Tech. Note 474)
MINNAERT, M., MULDERS, G. F. W., and HOUTGAST, J.
1940 Photometric Atlas of the Solar Spectrum (Sterrewacht "Sonnenborgh," Utrecht)
MOORE, C. E.
1959 A Multiplet Table of Astrophysical Interest (Nat. Bur. Stand. (U.S.), Note 36)
MOORE, C. E., MINNAERT, M. G. J., and HOUTGAST, J.
1966 The Solar Spectrum 2935 Å to 8770 Å (Nat. Bur. Stand. (U.S.), Monogr. 61)
NISHIMURA, S.
1967 in Colloquim on Late-Type Stars, Margherita Hack, ed. (Osservatorio Astronomico di Trieste, Trieste)
PAGEL, B. E. J.
1964 Roy. Obs. Bull. **87,** 227
PRESTON, G. W.
1961 Astrophys. J. **134,** 633
REEVES, H.
1966 Astrophys. J. **146,** 447

Rodgers, A. W., and Bell, R. A.
1968 Mon. Not. Roy. Astron. Soc. **138**, 23
Russell, H. N.
1925 Proc. Natl. Acad. Sci. **11**, 314
Sandage, A. R., and Hill, A. J.
1951 Astrophys. J. **113**, 525
Seeger, P. A., Fowler, W. A., and Clayton, D. D.
1965 Astrophys. J. Suppl. **11**, No. 97, 121
Unsöld, A. O.
1955 Physik der Sternatmosphären (Springer-Verlag, Berlin)
1969 Science **163**, 1015
Wallerstein, G.
1966 Icarus **5**, No. 1, 75
Wallerstein, G., and Greenstein, J.
1964 Astrophys. J. **139**, 1163
Warner, B.
1964a J. Quant. Spectrosc. Radiat. Transfer **4**, 415
1964b Comm. Univ. London Obs., No. 65
1965a Mon. Not. Roy. Astron. Soc. **129**, 263
1965b J. Quant. Spectrosc. Radiat. Transfer **5**, 639
1967 Mem. Roy. Astron. Soc. **70**, 165
Warner, B., and Cowley, C. R.
1967 J. Quant. Spectrosc. Radiat. Transfer **7**, 751
Wright, K. O.
1948 Publ. Dom. Astrophys. Obs. **8**, No. 1, 1
Wrubel, M. H.
1949 Astrophys. J. **109**, 66
Wyart, J. F.
1968 Thesis (Univ. d'Orsay, France)
Yamashita, Y.
1967 Publ. Domin. Astrophys. Obs. **12**, 455

U.S. GOVERNMENT PRINTING OFFICE : 1971 OL—398-978

Latest developments in the subject area of this publication, as well as in other areas where the National Bureau of Standards is active, are reported in the NBS Technical News Bulletin. See following page.

HOW TO KEEP ABREAST OF NBS ACTIVITIES

Your purchase of this publication indicates an interest in the research, development, technology, or service activities of the National Bureau of Standards.

The best source of current awareness in your specific area, as well as in other NBS programs of possible interest, is the TECHNICAL NEWS BULLETIN, a monthly magazine designed for engineers, chemists, physicists, research and product development managers, librarians, and company executives.

If you do not now receive the TECHNICAL NEWS BULLETIN and would like to subscribe, and/or to review some recent issues, please fill out and return the form below.

(cut here)

Mail to: Office of Technical Information and Publications
National Bureau of Standards
Washington, D. C. 20234

Name ____________________

Affiliation ____________________

Address ____________________

City ____________ State ________ Zip ________

☐ Please send complimentary past issues of the Technical News Bulletin.

☐ Please enter my 1–yr subscription. Enclosed is my check or money order for $3.00 (additional $1.00 for foreign mailing).
Check is made payable to: SUPERINTENDENT OF DOCUMENTS.

Monogr. 119